AD_____

Award Number: DAMD17-01-1-0172

TITLE: A Novel Molecular Target for Breast Cancer Prevention and Treatment

PRINCIPAL INVESTIGATOR: Xiao-kun Zhang, Ph.D.

CONTRACTING ORGANIZATION: The Burnham Institute
La Jolla, California 92027

REPORT DATE: June 2004

TYPE OF REPORT: Final

PREPARED FOR: U.S. Army Medical Research and Materiel Command
Fort Detrick, Maryland 21702-5012

REPORT DOCUMENTATION PAGE

Form Approved
OMB No. 074-0188

1. AGENCY USE ONLY (Leave blank)	2. REPORT DATE	3. REPORT TYPE AND DATES COVERED
	June 2004	Final (1 Jun 2001 - 31 May 2004)

4. TITLE AND SUBTITLE
A Novel Molecular Target for Breast Cancer Prevention and Treatment

5. FUNDING NUMBERS
DAMD17-01-1-0172

6. AUTHOR(S)
Xiao-kun Zhang, Ph.D.

7. PERFORMING ORGANIZATION NAME(S) AND ADDRESS(ES)
The Burnham Institute
La Jolla, California 92027

E-Mail: xzhang@burnham.org

8. PERFORMING ORGANIZATION REPORT NUMBER

9. SPONSORING / MONITORING AGENCY NAME(S) AND ADDRESS(ES)
U.S. Army Medical Research and Materiel Command
Fort Detrick, Maryland 21702-5012

10. SPONSORING / MONITORING AGENCY REPORT NUMBER

11. SUPPLEMENTARY NOTES
Original contains color; all DTIC reproductions will be in black and white.

12a. DISTRIBUTION / AVAILABILITY STATEMENT
Approved for Public Release; Distribution Unlimited

12b. DISTRIBUTION CODE

13. Abstract *(Maximum 200 Words)* *(abstract should contain no proprietary or confidential information)*

We have investigated the mechanism by which retinoids induce apoptosis in breast cancer cells. Our results reveal a new apoptosis paradigm involving translocation of orphan receptor TR3 from the nucleus to the cytoplasm, where it targets mitochondria to induce cytochrome c release and apoptosis. The translocation of TR3 requires its unique heterodimerization with retinoid X receptor (RXRα). A putative nuclear export sequence (NES) in RXRα mediates nuclear export of TR3/RXRα heterodimer. The RXRα NES activities are regulated by RXRα dimerization and ligand-binding. In studying how TR3 targets mitochondria, we have discovered that TR3 targets mitochondria through its interaction with Bcl-2. Bcl-2 acts as a mitochondrial receptor of TR3. It mediates the pro-apoptotic effects of TR3 by undergoing a conformational change upon TR3 binding. Such a conformational change converts Bcl-2 from a protector to killer. Together, our studies reveal a novel apoptotic pathway involving TR3, RXRα and Bcl-2 in breast cancer cells and our results provide various new strategies for developing agents against breast cancer.

14. SUBJECT TERMS
apoptosis, TR3, RXRα, Bcl-2, mitochondria

15. NUMBER OF PAGES
108

16. PRICE CODE

17. SECURITY CLASSIFICATION OF REPORT	18. SECURITY CLASSIFICATION OF THIS PAGE	19. SECURITY CLASSIFICATION OF ABSTRACT	20. LIMITATION OF ABSTRACT
Unclassified	Unclassified	Unclassified	Unlimited

Table of Contents

INTRODUCTION

Although anti-estrogen tamoxifen shows activities in preventing development of breast cancer, there are no effective therapies for malignant estrogen-independent breast cancer, which is also often resistant to chemotherapy and g-radiation therapy. Lack of such therapies has contributed to the high mortality for U.S. women. Novel therapies are therefore urgently needed.

Retinoids, natural and synthetic vitamin A derivatives, exert profound effects on many biological processes, including cell proliferation and differentiation, reproduction, morphogenesis and pattern formation (1). Epidemiological, *in vitro*, and animal data have suggested retinoids as novel agents for the treatment of breast cancer. The effects of retinoids are mainly mediated by two classes of nuclear receptors, the retinoic acid receptor (RAR) and retinoid X receptor (RXR) (2). Ligands of RXR are more effective than RAR-selective ligands in the prevention of mammary carcinogenesis and the inhibition of the growth of established mammary tumors (3, 4). Recently, a new class of synthetic retinoids related to 6-[3-(1-adamantyl)-4-hydroxyphenyl]-2-naphthalene carboxylic acid (AHPN/CD437) were found to potently induce apoptosis of both hormone-dependent and –independent breast cancers (5), indicating that it may be representative of a novel class of compounds suitable for treatment of estrogen-independent breast cancers. We subsequently showed that TR3, an orphan member of the steroid/thyroid/retinoid receptor superfamily, is required for induction of apoptosis by AHPN/CD437 and other apoptotic stimuli (6, 7). Moreover, we discovered that TR3, in response to apoptosis stimuli, translocated from the nucleus to the cytoplasm, where it targets mitochondria to induce cytochrome c release and apoptosis (7).

The objective of this application was to develop evidence that TR3 is a suitable molecular target for developing novel drugs against breast cancer. With the support of USAMRMC, we have demonstrated that AHPN analogs SR11453 and MM002 potently induce TR3 expression and apoptosis in breast cancer cells (8). They effectively induce migration of TR3 from the nucleus to mitochondria. Importantly, we show that migration of TR3 from the nucleus to the cytoplasm required RXRa through their unique heterodimerization (9). This finding reveals a new retinoid signaling pathway for apoptosis induction. Furthermore, we demonstrate that Bcl-2, a potent anti-apoptotic protein that is overexpressed in more than half of all human cancers, including breast cancer (10), is required for TR3 mitochondrial targeting and TR3-dpendent apoptosis through its interaction with TR3. The interaction induces a Bcl-2 conformational change, resulting in conversion of Bcl-2 from a protector to a killer (11). Together, our results demonstrate that TR3, RXRa, and Bcl-2 are excellent molecular targets suitable for developing new agents against breast cancer.

KEY RESEARCH ACCOMPLISHMENTS

1. **The TR3-dependent apoptotic pathway in breast cancer** (*Cancer Res.* 61, 4723-4730, 2001; *J. Med. Chem.* 47, 3518-3536, 2004).

AHPN analogs induce TR3 expression and mitochondrial membrane potential change in breast cancer cells. Synthetic retinoids, related to AHPN/CD437 effectively induced apoptosis of both estrogen-dependent and -independent breast cancer cells (5), suggesting that these retinoids may represent a new class of drugs that have therapeutic value for the treatment of estrogen-independent breast cancer. Several AHPN analogs were evaluated for their regulation of TR3 expression. The AHPN analogs SR11453 and SR11384 were used to treat MDA-MB-231 breast cancer cells (7). TR3 expression in the cells was analyzed by Northern blotting. Figure 1A shows that upon treatment with SR11453 and SR11384, TR3 expression in MDA-MB-231 cells was significantly induced. Consistent with our previous observation (12),

TR3 expression was also induced by TPA, and the mitogenic agent epidermal growth factor (EGF). We also studied mitochondrial membrane potential change in breast cancer cells treated with or without SR11453 using Rh123. As shown in Figure 1B, SR11453 induced significant increases in the percentage of cells experiencing $\Delta\psi m$ loss. Disruption of $\Delta\psi m$ was observed in both estrogen-dependent MCF-7 and independent MDA-MB-231 cells. Thus, induction of apoptosis by AHPN/CD437 analogs in breast cancer cells involves mitochondrial-mediated apoptotic pathway.

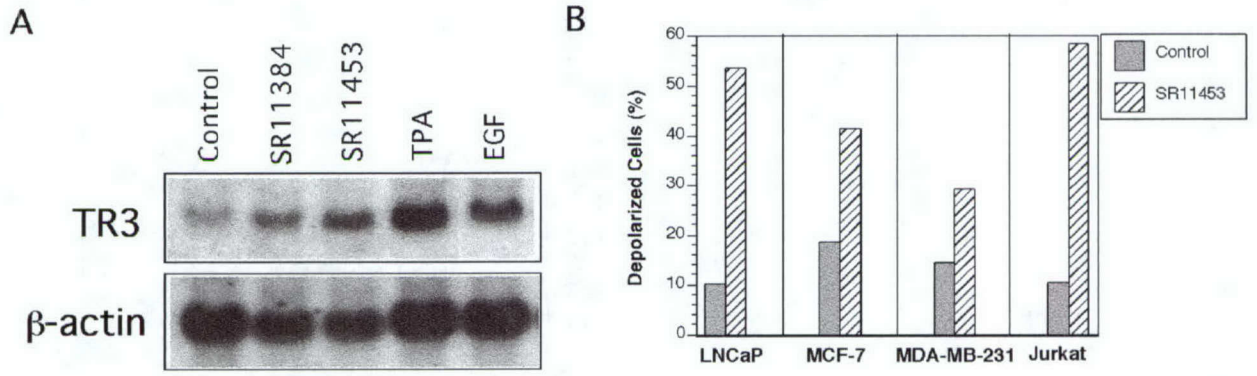

Figure 1. AHPN analogs induce TR3 expression and disrupt mitochondrial membrane potential of breast cancer cells. A. Induction of TR3 expression by AHPN analogs. Total RNAs were prepared from MDA-MB-231 cells treated with SR1153 (10^{-6} M), SR11384 (10^{-6} M), TPA (100 ng/ml) or EGF (200 ng/ml) for 3 h and analyzed by Northern blotting. **B.** AHPN analog SR11453 disrupts $\Delta\psi m$. The indicated cells were treated with or without 10^{-6} M SR11453 for 18 h. Cells were then incubated with Rh123 for 30 min and analyzed by a FACScalibur cytometery. The percent of cells fluorescencing within the range of Rh123 were considered as depolarized.

Mitochondrial localization of TR3 in breast cancer cells. To study whether the TR3 nuclear-to-mitochondrial targeting pathway occurs in breast cancer cells, GFP–TR3/ΔDBD (a mutant that lacks the DNA-binding domain) (7) was transfected into MDA-MB-231 and ZR-75-1 breast cancer cells. Confocal microscopy analysis revealed that it targeted mitochondria (Figure 2A). Mitochondrial targeting of TR3/ΔDBD resulted in cytochrome c release as cytochrome c was diffused distributed in cells expressing TR3/ΔDBD (Figure 2A). We also studied cellular localization of TR3 expressed in mammary tumors derived from transgenic mice bearing polyomavirus middle T antigen (kindly provided by Dr. W. Muller). The tissue sample was also analyzed by the TdT assay for apoptosis. TR3 was localized in the cytoplasm in cells undergoing extensive apoptosis, while it was found in the nucleus in nonapoptotic cells (Figure 2B). Furthermore, we transfected a green fluorescent protein (GFP)–TR3 fusion construct into MDA-MB-231 cells. The GFP–TR3 fusion protein was predominately present in the nucleus in nonstimulated cells. However, upon treatment with AHPN analogs SR11453 and SR11384, GFP–TR3 translocated to mitochondria (Figure 2C). Thus, subcellular localization of TR3 plays a role in regulating apoptosis of breast cancer cells.

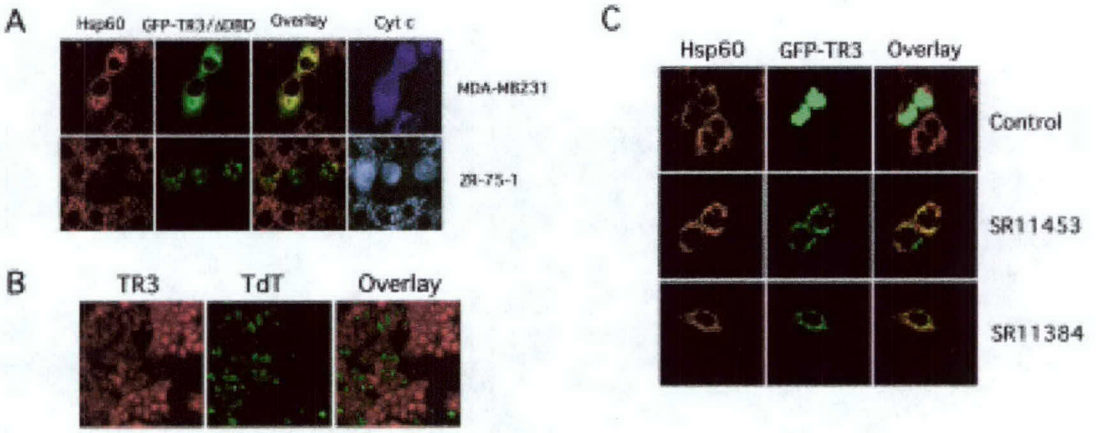

Figure 2. Apoptotic stimuli induce mitochondrial targeting of TR3. A. Mitochondrial targeting of TR3/DDBD is associated with cytochrome c release. GFP–TR3/ΔDBD was transiently transfected into ZR-75-1 or MDA-MB-231 cells, which were stained for mitochondria (Hsp60) and cytochrome c (Cyt c), and analyzed by confocal microscopy. **B.** TR3 is targeted to mitochondria in MDA-MB-231 cells in response to an apoptosis inducer. GFP–TR3-transfected MDA-MB-231 cells were treated with or without SR11453 (10^{-6} M) or SR11384 (10^{-6} M) for 1 h, then immunostained with anti-Hsp60 antibody (Sigma), followed by Cy3-conjugated secondary antibody (Sigma) to detect mitochondria. GFP–TR3 and mitochondria (Hsp60) were visualized using confocal microscopy, and the two images were overlaid (see Overlay). **C.** Correlation between TR3 subcellular localization and apoptosis in a mammary tumor. Mammary tumor tissue from transgenic mice bearing polyomavirus middle T antigen was stained with anti-TR3 antibody followed by Cy3-conjugated secondary antibody to detect TR3 expression and subcellular localization by confocal microscopy. The tissue was also analyzed by the fluorescein-conjugated TdT enzyme (Oncogene) to detect DNA fragmentation (TdT-labeled cells are indicated by green color). The two images were overlaid (overlay) to assess the correlation between apoptosis and TR3 subcellular localization.

A New AHPN analog 3-Cl-AHPC induces mitochondrial localization of endogenous TR3 in breast cancer cells. AHPN analog 3-Cl-AHPC effectively induces apoptosis in breast cancer cells and retarded breast tumor growth (8, 13). To determine whether this new AHPN analog functioned through TR3, MDA-MB-231 cells were treated with 3-Cl-AHPC and cellular localization of endogenous TR3 was analyzed by confocal microscopy. Figure 3 shows that the endogenous TR3 was found exclusively in the cytoplasm and colocalized with mitochondria in 3-Cl-AHPC-treated cells. This result further establishes the TR3-dependent apoptotic pathway in breast cancer cells and suggests that AHPN analogs are promising agents for breast cancer.

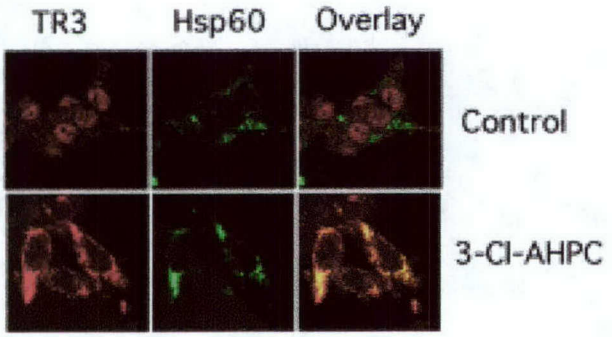

Figure 3. A new AHPN analog 3-Cl-AHPC induces mitochondrial localization of endogenous TR3 in MDA-MB-231 cells. MDA-MB-231 cells were treated with or without 3-Cl-

AHPC (10^{-6} M) for 1 h, then immunostained with anti-TR3 antibody (Geneka) followed by Cy3-conjugated secondary antibody to detect endogenous TR3, or with anti-Hsp60 antibody followed by Cy5-conjugated secondary antibody (Sigma) to detect mitochondria. TR3 and mitochondria (Hsp60) were visualized using confocal microscopy, and the two images were overlaid (overlay).

Antagonist Analogue of AHPN Family of Apoptosis Inducers That Effectively Blocks AHPN-Induced Apoptosis but Not Cell-Cycle Arrest. We have also identified a new retinoid (3-A-AHPC) that antagonizes the effect of AHPN on inducing TR3 expression and apoptosis of breast cancer cells (8). In both MDA-MB468 and MDA-MB231 breast cancer cell lines, the antagonist 3-A- AHPC alone had no effects on cell-cycle arrest and apoptosis induction, whereas both processes were readily induced by AHPN and its apoptotic analogues such as 5-Cl-AHPN and 3-Cl-AHPC. Alone, 3-A-AHPC had no detectable effect on p21WAF1/CIP1 protein levels and did not block the induction of p21WAF1/CIP1 by 3-Cl-AHPC. However, 3-A-AHPC markedly inhibited MDA-MB-468 cell apoptosis induced by 3-Cl-AHPC or AHPN. Antagonist 3-A-AHPC also inhibited apoptosis induced by AHPN in retinoid-resistant MDA-MB-231 breast cancer cells (8). The identification of 3-A-AHPC provides an excellent opportunity to dissect TR3-dependent-signaling pathways in breast cancer cells.

2. Role of RXRα and RXRα ligands in the regulation of TR3-dependent apoptotic pathway (*Mol. Cell. Biol.* In press, 2004)

RXRα is required for TR3 nuclear export and mitochondrial targeting. RXRα plays a central role in the regulation of intracellular receptor signaling pathways by acting as a ubiquitous heterodimerization partner of many nuclear receptors, including the orphan receptor TR3. We studied whether TR3 and RXRα targeted mitochondria as a heterodimer. When expression vectors for RXRα and TR3 were transfected into LNCaP cells, the expressed RXRα and TR3 resided in the nucleus. However, when cells were treated with 3-Cl-AHPC, a apoptosis-inducing retinoid (8, 9) both RXRα and TR3 were found in the cytoplasm and their distributions overlaid (Figure 1A). To study whether TR3 mitochondrial targeting required RXRα, we used the siRNA approach to inhibit RXRα expression in LNCaP cells, then examined the subcellular localization of TR3. Transfection of LNCaP cells with RXRα siRNA strongly reduced RXRα protein levels (Figure 1B). In cells transfected with RXRα siRNA, TR3 was mainly confined in the nucleus despite TPA treatment (Figure 1C). Thus, cytoplasmic localization of TR3 requires RXRα (Fgure 5).

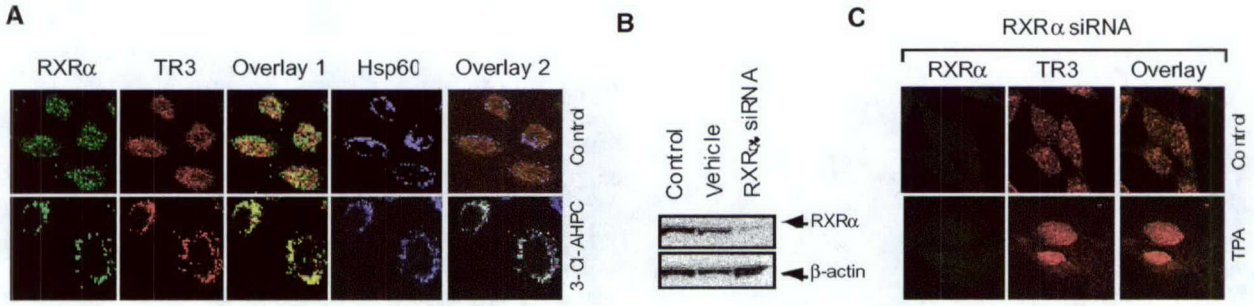

Figure 4. RXR is required for translocation of TR3 from the nucleus to the cytoplasm. A. 3-Cl-AHPC induces mitochondrial localization of transfected RXRα and TR3. Expression vectors for myc-TR3 and RXRα were transfected into LNCaP cells. Cells were then treated with 3-Cl-AHPC for 3 hr, then immunostained with anti-myc antibody (9E10, Santa Cruz Biotechnology, Inc) followed by FITC-conjugated secondary antibody, anti-RXRα antibody followed by Cy3-conjugated secondary antibody or anti-Hsp60 antibody followed by Cy5-conjugated secondary antibody (Tackson Immuno Res.). Myc-TR3, RXRα, and Hsp60 were visualized and the images were overlaid. Overlay1 is the merge of myc-TR3 and RXRα images, and Overlay 2 is the merge of myc-TR3, RXRα, and Hsp60 images. **B**. LNCaP cells were transfected with or without RXRα siRNA or control

siRNA for 72 hr. Cell extracts were prepared and analyzed for RXRα expression by Western blotting. C. Effect of RXR siRNA on RXRα levels and TR3 localization. LNCaP cells were transfected with or without RXRα siRNA or control siRNA for 72 hr. Cells were analyzed for subcellular localization of RXRα and TR3 by confocal microscopy.

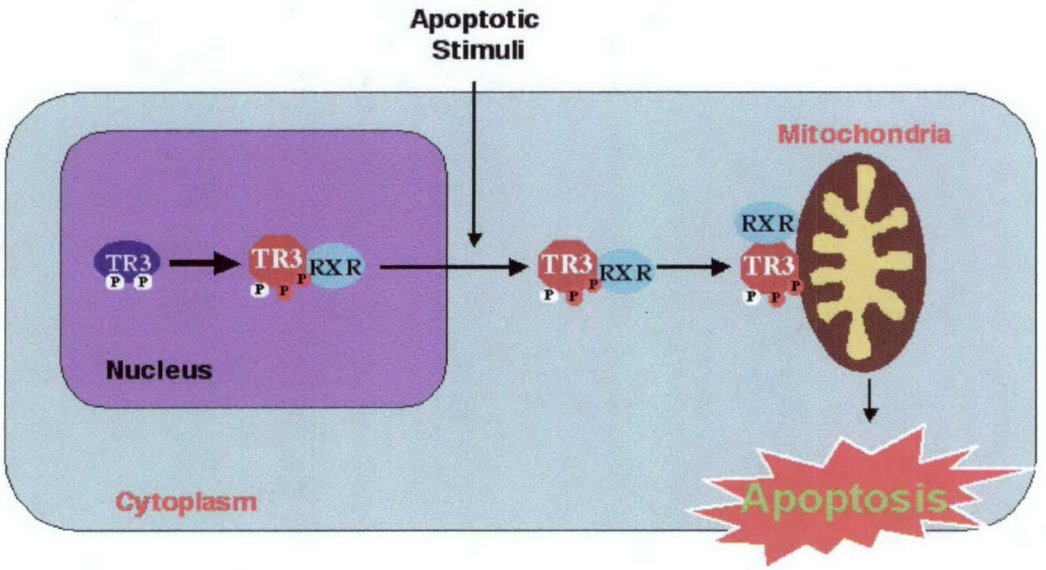

Figure 5. Schematic representation of the role of RXRα in TR3 nuclear export and mitochondrial targeting (9). RXRα heterodimerizes with TR3 in the nucleus. In response to apoptotic stimuli, such as retinoid AHPN, TR3/RXRα heterodimer undergoes a protein modification, such as phosphorylation, then translocates to the cytoplasm, where it targets mitochondria.

Identification of a putative nuclear export sequence in RXRα. To study how RXRα/TR3 heterodimer translocates from the nucleus to the cytoplasm, we have constructed a number of TR3 and RXRα mutants and analyzed their subcellular distribution. Our results (9) revealed the presence of a putative nuclear export sequence (NES) in RXRα (Figure 6A). The DNA sequences representing RXRα residues 348-368 were fused to green fluorescent protein (GFP), and the fusion was transfected into HEK293T embryonic kidney cells. The GFP-NES fusion was found exclusively in the cytoplasm, while LMB treatment prevented its nuclear export. Mutations of Met357 and Met360 to Ala (GFP-NESm-RXRα) largely abolished nuclear export activity. Consistently, TPA-induced cytoplasmic localization of TR3 and RXRα was prevented by leptomycin B (LMB), an inhibitor of CRM1-dependent nuclear export. Thus, RXRα amino acids 348-368 represent a putative NES.

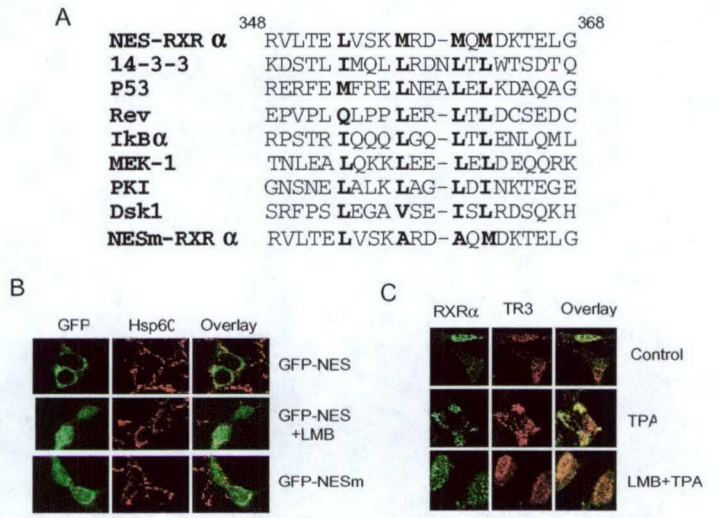

Figure 6. Identification of a nuclear export sequence in RXRα. **A.** Schematic representation of the RXRα NES. The identified RXRα NES is compared with known NESs identified in the indicated genes. The bold letters indicate conserved amino acid residues. **B.** The RXRα NES is capable of directing GFP to the cytoplasm. The putative RXRα NES (RVLTELVSKMRDMQMDKTELG) or its mutant (RVLTELVSKARDAQMDKTELG) (NESm) was fused to GFP, and the expression vectors were transfected into HEK293T embryonic kidney cells. Cells were treated with or without LMB for 6 hr, then stained for Hsp60 and analyzed by confocal microscopy. **C.** Cytoplasmic localization of RXRα/TR3 is mediated by CRM1-dependent nuclear export. LNCaP cells were treated with TPA in the absence (control) or presence of leptomycin B (LMB, 2.5 ng/ml) (Sigma) and analyzed by confocal microscopy.

Unique TR3/RXRα heterodimerization. We have studied the regulation of the RXRα NES and found that it is highly regulated by RXRα homodimerization and heterodimerization. Indeed, subcellular localization of RXRα is highly regulated by its dimerization. The RXRα NES is active in the RXRα monomer but is silenced by RXRα homodimerization and certain heterodimerizations, such as RXRα heterodimerization with VDR or RAR. Our results demonstrate that nuclear export of the RXRα/Nur77 heterodimer is due to its unique heterodimerization in solution (9). RXRα possesses two dimerization interfaces, which are located in the DBD and the ligand-binding domain (LBD) (14, 15). The strong dimerization interface in the LBD enables RXRα homodimerization and heterodimerization with certain receptors, such as RAR and vitamin D receptor (VDR) in solution. In contrast, the weak dimerization interface in the DBD does not allow the formation of the RXR homodimer or heterodimer with RAR in the absence of a specific response element. Our data indicate that deletion of the major dimerization interface from the RXRα LBD did not impair the interaction of RXRα with TR3 in solution, although the deletion completely abolished RXRα interaction with RAR (9). Our observation that the RXRα DBD alone was sufficient to interact with TR3 (9) demonstrated that the formation of the RXRα/TR3 heterodimer in solution is mediated by dimerization interfaces in their DBD. Given the fact that the RXRα NES is active in the RXRα monomer conformation, we envision that the unique RXRα/Nur77 heterodimer formed in solution through their DBD dimerization interfaces will ensure that the RXRα NES is situated is its active conformation, resulting in their nuclear export (Figure 7).

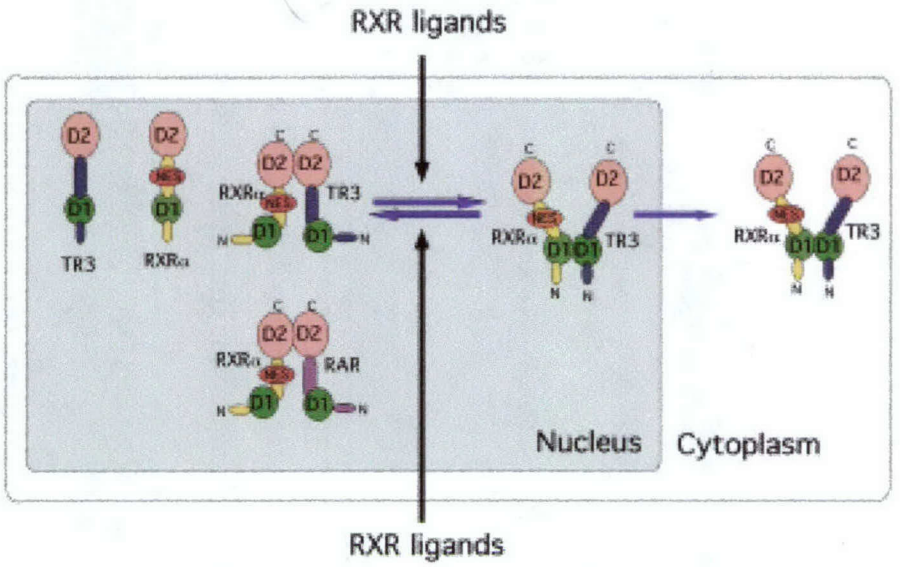

Figure 7. Regulation of TR3-dependent apoptotic pthway by RXRα, its heterodimerization and RXRα ligands. Our results demonstrate that migration of TR3 from the nucleus to the cytoplasm requires its unique heterodimerization with RXRa, that is mediated by their dimerization interfaces in their DNA-binding domain interfaces (D1). Such a unique dimerization results in activation of the RXRα NES. In contrast, In contrast, binding of RXR ligand 9-*cis*-RA to the RXRα/TR3 heterodimer induces an RXRα conformation that allows heterodimerization with TR3 through their ligand-binding domain interfaces (D2). Such a heterodimer suppresses the RXRα NES, resulting nuclear localization of TR3/RXRα heterodimer and their DNA binding. It is expected that certain RXRα ligands may bind to RXRα and promote D1-mediated heterodimerization. Such RXRα ligands may be effective apoptosis inducers of breast cancer cells.

Modulation of RXRα/TR3 heterodimerization, their mitochondrial targeting and apoptosis induction by RXR ligands. In contrast to their heterodimerization in solution, the C-terminal sequences of TR3 and RXRα are required for the efficient binding of RXRα/TR3 heterodimer to their specific response element βRARE and transactivation, as is found for the RXR/RAR heterodimer (16, 17). By using various biochemical approaches, we observed that RXR ligand can promote RXRα/TR3 heterodimer binding to the βRARE (9). The induction of RXRα/TR3 heterodimer DNA binding and transactivation by 9-*cis*-RA is associated with its inhibition of their DBD-mediated dimerization. RXRα ligand binding allows RXRα to interact with TR3 through their LBD dimerization interfaces, which may silence the RXRα NES, as does RXR/VDR or RXR/RAR heterodimerization (9). Thus, the nuclear export of the RXRα/TR3 heterodimer may be suppressed by 9-*cis*-RA through its induction RXRα homodimerization or modulation of RXRα/TR3 heterodimerization interfaces. Consistently, we found that RXR ligands 9-*cis*-RA and SR11237 effectively inhibited the release of cytochrome *c* induced by TPA or SR11453 in LNCaP cells (9). As the inhibition was accompanied by the prevention of TR3 and RXRα mitochondrial targetin, we suggest that RXR ligands suppress apoptosis by inhibiting mitochondrial targeting of RXRα/TR3 heterodimer.

Different RXRα/TR3 heterodimers may exist in a dynamic equilibrium depending on their cellular environment. Under normal conditions, both the DBD and LBD dimerization interfaces may participate in RXRα/TR3 heterodimer formation, so that the dimers exist in both the nucleus and cytoplasm. In response to apoptotic stimuli, RXRα and TR3 may preferentially heterodimerize through their DBD dimerization interfaces to activate the RXRα NES, resulting in their cytoplasmic localization. In contrast, binding by RXR ligands may induce a dimerization interface switch that silences the RXRα NES to ensure RXRα/TR3 nuclear localization and efficient transcriptional regulation. Our observation that RXR ligands regulate apoptosis by

modulating RXRα/TR3 heterodimer nuclear export provides a novel approach for developing RXRα-based apoptosis regulators (Figure 7).

3. The mechanism by which TR3 targets mitochondria and induces apoptosis (*Cell*, 116,527-540, 2004).

Identification of TR3 mitochondrial receptor. TR3 exerts its apoptotic effect by targeting mitochondria. TR3 does not have a classical mitochondrial targeting sequences. We examined the possibility that it might target mitochondria through its interaction with a mitochondrial protein. Members of the Bcl-2 family are important regulators of cell death and survival (18). Many of which, such as Bcl-2, are located predominantly in the mitochondrial outer membrane. By using a variety of approaches, including GST-pull-down, mammalian two-hybrid studies, reported gene assay, and immunoprecipitation assays, we found that TR3 physically interacts with Bcl-2 and that the interaction promotes TR3 mitochondrial targeting (11). Thus, Bcl-2 acts as a TR3 mitochondrial receptor (Figure 8).

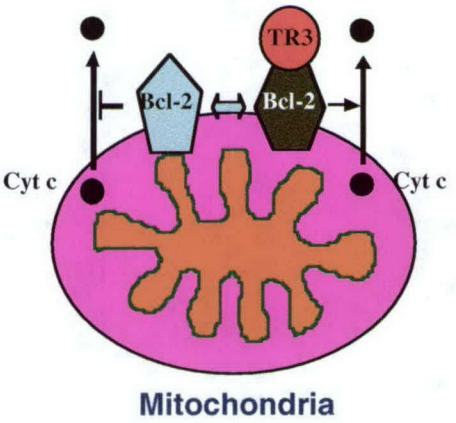

Figure 8. TR3 interaction with Bcl-2 induces cytochrome c release. Bcl-2 expression suppresses cytochrome c release. In contrast, interaction of Bcl-2 with TR3 results in extensive cytochrome c release and apoptosis.

Bcl-2 is required for TR3 induction of cytochrome c release and apoptosis. TR3 mitochondrial targeting is essential for TR3 induction of cytochrome c release and apoptosis. Our observation that Bcl-2, a potent apoptosis inhibitor, was required for mitochondrial targeting by TR3 suggested that Bcl-2 was needed for apoptosis. Indeed, we found that Bcl-2 expression was required for induction of cytochrome c release and apoptosis by TR3, whereas inhibition of Bcl-2 expression by Bcl-2 siRNA or Bcl-2 dominant-negative mutant abolished TR3-dependent apoptosis (11). The pro-apoptotic effect of Bcl-2 seen upon co-expression was specific to TR3, because Bax-induced apoptosis was effectively prevented by Bcl-2 co-expression. Thus, Bcl-2 can manifest a pro-apoptotic phenotype in settings where TR3 is expressed and targets to mitochondria. In contrast, Bcl-2 suppresses apoptosis when co-expressed with Bax.

Bcl-2 undergoes a conformational change upon TR3 binding. Bcl-2 promotes apoptosis when co-expressed with TR3 but suppresses apoptosis when co-expressed with Bax. Bcl-2 has a hydrophobic crevice (BH3-binding pocket) on its surfaces that bind the BH3 domains of other family members. The BH3-binding pocket is essential for anti-apoptotic function of Bcl-2. Our analysis of structure–function relationships for the pro-apoptotic effect of Bcl-2 in TR3-induced apoptosis showed that an intact hydrophobic groove in Bcl-2 is required for its anti-apoptotic activity but not for its pro-apoptotic activity, demonstrating a structural distinction between these two opposing phenotypes of Bcl-2. We explored whether a conformational change

might be involved in converting Bcl-2 function from anti-apoptotic to pro-apoptotic. By comparing the effects of TR3 on binding of Bcl-2 to various anti-Bcl-2 antibodies that recognize different epitopes using flow cytometry and immunoprecipitation, we found that TR3 binding induces a Bcl-2 conformational change that exposes its BH3 domain (11). Further analysis showed that such a conformational change was responsible for its pro-apoptotic effects.

4. Regulation of RARβ expression by RXR ligands (*Cancer Res.* 63, 3531-3538, 2003).

We previously reported that RXR ligands could effectively induce RARβ expression in breast cancer cells (17). In studying how RXR ligands induce RARβ expression, we have reported that TR3/RXR heterodimer could bind effectively to the βRARE in the RARβ promoter and induced RARβ expression in response to RXR ligands. Interestingly, we also observed that RXR could bind to the βRARE as an RXR/PPARγ heterodimer (Figure 9A). Moreover, Western analysis showed that the RXR and PPARγ ligands were capable of inducing RARβ protein expression in ZR-75-1 and T-47D breast cancer cells (Figure 9B). Together, these data demonstrate that RXR ligands can induce RARβ expression through its activation of either RXR/TR3 or RXR/PPARγ heterodimer (19).

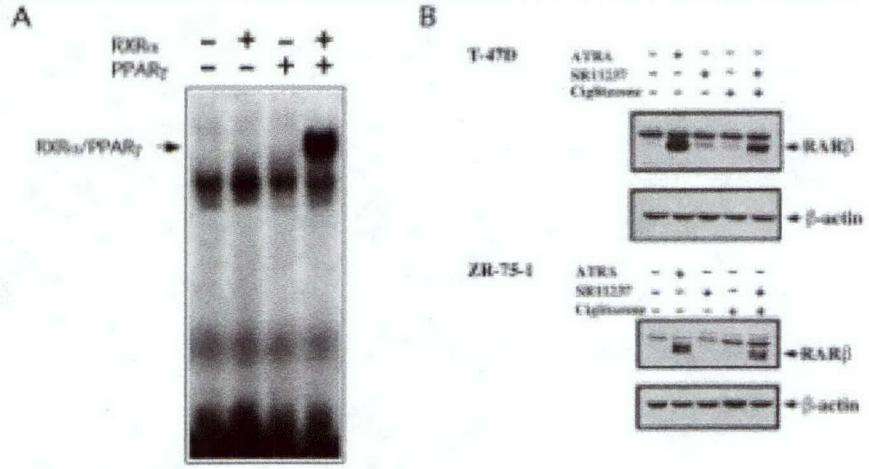

Figure 9. Regulation of RARβ expression by RXR and its ligands. A. RXR and PPARγ bind to βRARE as a heterodimeric complex. *In vitro* translated RXR and PPARγ were incubated with ^{32}P-radiolabelled βRARE either alone or in combination. The resulting reactions were then analyzed by EMSA. **B. Regulation of RARβ protein expression by RXR and PPARγ ligands in T-47D and ZR-75-1 breast cancer cells.** T-47D and ZR-75-1 cells were treated for 24 h with SR11237 (1 μM) in the absence or presence of ciglitazone (10 μM). Cell lysates were prepared and Western analysis performed as described in Materials and Methods.

REPORTABLE OUTCOMES

Publications

1. Dawson, M.I., Hobbs, P., Peterson, V., Leid, M., Lange, C., Feng, K., Chen, G., Gu, J., Li, H., Kolluri, S., Zhang, X-k., Zhang, Y., and Fontana, J. Induction of apoptosis in cancer cells by a novel analog of 6-[3- (1-Adamantyl) –4- hydroxyphenyl} –2-naphthalenecarboxylic acid (AHPN) lacking retinoid receptor transcriptional activation activity. Cancer Research. 61: 4723-4730, 2001.

2. Lin, F., Kolluri, S., Chen, G.-q.and Zhang, X.-k. Regulation of Retinoic Acid-induced Inhibition of AP-1 Activity by Orphan Receptor COUP-TF. J. Biol. Chem. 277: 21414-22, 2002.
3. Dawson MI, Zhang X-k. Discovery and design of retinoic acid receptor and retinoid X receptor class- and subtype-selective synthetic analogs of all-trans-retinoic acid and 9-cis-retinoic acid. Curr. Med. Chem. 9: 623-37. 2002.
4. James, S., Lin, F., Kolluri, S., Dawson, M.I., and Zhang, X.-k. Regulation of retinoic acid receptor β expression by peroxisome proliferator-activated receptor γ ligands in cancer cells. *Cancer Res.* 63: 3531-3538. 2003.
5. Lin, B., Kolluri, S., Cao, X., Li, H., Han, Y.-h., Lin, F., Reed, J.C., and Zhang, X.-k. Conversion of Bcl-2 from Protector to Killer by Interaction with Nuclear Orphan Receptor Nur77/TR3. *Cell.* 116: 1-20. 2004.
6. Dawson, M.I., Harris, D., Liu, G., Hobbs, P., Lange, C., Jong, L., Bruey-Sedano, N., James, S., Zhang, X.k., Peterson, V., Leid, M., Farhana, L., Rishi, A., and Fontana, J. Antagonist Analogue of 6-[3'-(1-Adamantyl)-4'–hydroxyphenyl]-2-naphthalenecarboxylic Acid (AHPN) Family of Apoptosis Inducers That Effectively Blocks AHPN-Induced Apoptosis but Not Cell-Cycle Arrest. *J. Med. Chem.* 47: 3518-3536. 2004.
7. Cavasotto, C.N., Liu, G., James, S.Y., Hobbs, P.D., Peterson, V.J., Bobkov, A., Bhattacharya, A.A., Kolluri, S.K., Abagyan, R., Zhang, X.-k., Leid, M., Liddington, R.C., and Dawson,.M.I. Determinants of Retinoid X Receptor Transcriptional Antagonism. *J. Med. Chem.* 47: 4360-4372. 2004.
8. Cao, X., Li, H., Liu, W., Lin, F., Kolluri, S., and Zhang, X.-k. Mitochondrial targeting of retinoid X receptor and its regulation by ligands and dimerization. *Mol. Cell. Biol.* In Press. 2004.

Meetings

1. Kolluri, S., Lin, B., Cao, X., Li, H., Lin, F., James, S., and Zhang, X-k. Nuclear orphan receptor TR3 induces apoptosis and proliferation by distinct pathways. The Keystone Symposium on Nuclear Receptor Superfamily. Snowbird, Utah, April 13-29, 2002
2. Zhang, X-k., Kolluri, S., Cao, X., Li, H., Lin, B., and Dawson, M.I. Subcellular Localization of Orphan Receptor TR3 Defines its Biological Activities. The FASEB Summer Conference on Retinoids. Tucson, Arizona, June 22-27, 2002.
3. Lin, B., Kolluri, S., Lin, F., Liu, W., Han, Y-h., Cao, X., Dawson, M.I., Reed, J.C., Zhang, X-k. Nuclear orphan receptor TR3 targets mitochondria and induces apoptosis through interaction with Bcl-2. The Keystone Symposium on Nuclear Receptors: Orphan Receptors. Keystone, Co., Feb. 28-March 4, 2004.
4. Lin, B., Kolluri, S., Lin, F., Liu, W., Han, Y-h., Cao, X., Dawson, M.I., Reed, J.C., Zhang, X-k. Conversion of Bcl-2 from a protector to a killer by orphan nuclear receptor TR3. 95th Annual Meeting, American Association for Cancer Res. Orlando, Fl., March 27-31, 2004.
5. Lin, B., Kolluri, S., Lin, F., Liu, W., Han, Y-h., Cao, X., Dawson, M.I., Reed, J.C., Zhang, X-k. Regulation of TR3-dependent apoptotic pathway by retinoids. The FASEB Summer Conference on Retinoids. Pine Mountain, Georgia, June 12-17, 2004.

Patents

03/002/001
Conversion of Apoptotic Proteins
Reed, John C., Zhang, Xiao-kun, Gao, Bing, Lin, Bingzhen, Kolluri, Siva K.

8014-005
Cytoplasmic Activity of Retinoid X Receptor and its Regulation by Ligands and Dimerization.
Zhang, Xiao-kun, Cao, Xihua, Liu, Wen

CONCLUSIONS

We have investigated the mechanism by which retinoids induce apoptosis in breast cancer cells. Our results reveal a new apoptosis paradigm involving translocation of orphan receptor TR3 from the nucleus to the cytoplasm, where it targets mitochondria to induce cytochrome c release and apoptosis. The migration of TR3 from the nucleus to the cytoplasm requires its heterodimerization with retinoid X receptor (RXRα). Unlike other RXRα heterodimerizations, RXRα heterodimerization with TR3 can be mediated by dimerization interfaces either in their DNA-binding domain or ligand-binding domain. TR3 heterodimerization with RXRα through its DNA-binding domain activates a nuclear export sequence (NES) in RXRα, resulting in their cytoplasmic localization. In contrast, heterodimerization through their ligand-binding domain suppress the RXRα NES. Binding of RXRα with its agonists promotes its heterodimerization with TR3 via their ligand-binding domain, leading to their nuclear localization, DNA binding and transactivation. In studying how TR3 targets mitochondria, we have discovered that TR3 can physically interacts with Bcl-2 and that Bcl-2 acts as a mitochondrial receptor of TR3 and is required for apoptotic effect of TR3 in breast cancer cells. Upon TR3 biding, Bcl-2 undergoes a conformational change, resulting in conversion of Bcl-2 from a protector to killer. Together, our studies reveal a novel apoptotic pathway involving TR3, RXRα and Bcl-2 in breast cancer cells. Our results provide various new strategies for develop agents against breast cancer.

REFERENCES

1. Yang, L. M., Tin, U. C., Wu, K., and Brown, P. Role of retinoid receptors in the prevention and treatment of breast cancer. J Mammary Gland Biol Neoplasia, *4:* 377-388, 1999.
2. Mangelsdorf, D. J. and Evans, R. M. The RXR heterodimers and orphan receptors. Cell, *83:* 841-850, 1995.
3. Bischoff, E. D., Gottardis, M. M., Moon, T. E., Heyman, R. A., and Lamph, W. W. Beyond tamoxifen: the retinoid X receptor-selective ligand LGD1069 (TARGRETIN) causes complete regression of mammary carcinoma. Cancer Res, *58:* 479-484, 1998.
4. Gottardis, M. M., Bischoff, E. D., Shirley, M. A., Wagoner, M. A., Lamph, W. W., and Heyman, R. A. Chemoprevention of mammary carcinoma by LGD1069 (Targretin): an RXR-selective ligand. Cancer Res, *56:* 5566-5570, 1996.
5. Shao, Z. M., Dawson, M. I., Li, X. S., Rishi, A. K., Sheikh, M. S., Han, Q. X., Ordonez, J. V., Shroot, B., and Fontana, J. A. p53 independent G0/G1 arrest and apoptosis induced by a novel retinoid in human breast cancer cells. Oncogene, *11:* 493-504, 1995.
6. Li, Y., Lin, B., Agadir, A., Liu, R., Dawson, M. I., Reed, J. C., Fontana, J. A., Bost, F., Hobbs, P. D., Zheng, Y., Chen, G. Q., Shroot, B., Mercola, D., and Zhang, X. K. Molecular determinants of AHPN (CD437)-induced growth arrest and apoptosis in human lung cancer cell lines. Mol Cell Biol, *18:* 4719-4731, 1998.
7. Li, H., Kolluri, S. K., Gu, J., Dawson, M. I., Cao, X., Hobbs, P. D., Lin, B., Chen, G., Lu, J., Lin, F., Xie, Z., Fontana, J. A., Reed, J. C., and Zhang, X. Cytochrome c release and apoptosis induced by mitochondrial targeting of nuclear orphan receptor TR3 [see comments] [comment]. Science, *289:* 1159-1164, 2000.
8. Dawson, M. I., Harris, D. L., Liu, G., Hobbs, P. D., Lange, C. W., Jong, L., Bruey-Sedano, N., James, S. Y., Zhang, X. K., Peterson, V. J., Leid, M., Farhana, L., Rishi, A. K., and Fontana, J. A. Antagonist analogue of 6-[3'-(1-adamantyl)-4'-hydroxyphenyl]-2-naphthalenecarboxylic acid (AHPN) family of apoptosis inducers that effectively blocks AHPN-induced apoptosis but not cell-cycle arrest. J Med Chem, *47:* 3518-3536, 2004.
9. Cao, X., Liu, W., Lin, F., Kolluri, S. K., Lin, B., Han, Y.-h., Dawson, M. I., and Zhang, X. K. Nuclear export and mitochondrial targeting of Nur77/TR3 are regulated by retinoid X receptor. Mol. Cell. Biol., 2004.

10. Reed, J. C. Bcl-2 family proteins: regulators of apoptosis and chemoresistance in hematologic malignancies. Semin Hematol, *34:* 9-19, 1997.
11. Lin, B., Kolluri, S., Lin, F., Liu, W., Han, Y.H., Cao, X., Dawson, M.I., Reed, J.C., and Zhang, X.K. Conversion of Bcl-2 from Protector to Killer by Interaction with Nuclear Orphan Receptor Nur77/TR3. Cell, *116:* 527-540, 2004.
12. Kolluri, S. K., Cao, X., Bruey-Sedano, N., Lin, B., Lin, F., Han, Y., Dawson, M. I., and Zhang, X. Mitogenic effect of orphan receptor TR3 and its regulation by MEKK1 in lung cancer cells. Mol Cell Biol, *23:* 8651-8667, 2003.
13. Farhana, L., Dawson, M. I., Huang, Y., Zhang, Y., Rishi, A. K., Reddy, K. B., Freeman, R. S., and Fontana, J. A. Apoptosis signaling by the novel compound 3-Cl-AHPC involves increased EGFR proteolysis and accompanying decreased phosphatidylinositol 3-kinase and AKT kinase activities. Oncogene, *23:* 1874-1884, 2004.
14. Lee, M. S., Kliewer, S. A., Provencal, J., Wright, P. E., and Evans, R. M. Structure of the retinoid X receptor alpha DNA binding domain: a helix required for homodimeric DNA binding. Science, *260:* 1117-1121., 1993.
15. Zhang, X. K., Salbert, G., Lee, M. O., and Pfahl, M. Mutations that alter ligand-induced switches and dimerization activities in the retinoid X receptor. Mol Cell Biol, *14:* 4311-4323, 1994.
16. Zhang, X. K., Hoffmann, B., Tran, P. B., Graupner, G., and Pfahl, M. Retinoid X receptor is an auxiliary protein for thyroid hormone and retinoic acid receptors. Nature, *355:* 441-446, 1992.
17. Wu, Q., Dawson, M. I., Zheng, Y., Hobbs, P. D., Agadir, A., Jong, L., Li, Y., Liu, R., Lin, B., and Zhang, X. K. Inhibition of trans-retinoic acid-resistant human breast cancer cell growth by retinoid X receptor-selective retinoids. Mol Cell Biol, *17:* 6598-6608, 1997.
18. Reed, J. C. Bcl-2 family proteins. Oncogene, *17:* 3225-3236, 1998.
19. James, S. Y., Lin, F., Kolluri, S. K., Dawson, M. I., and Zhang, X. K. Regulation of retinoic acid receptor beta expression by peroxisome proliferator-activated receptor gamma ligands in cancer cells. Cancer Res, *63:* 3531-3538, 2003.

APPENDICES

1. Lin, B., Kolluri, S., Cao, X., Li, H., Han, Y.-h., Lin, F., Reed, J.C., and Zhang, X.-k. Conversion of Bcl-2 from Protector to Killer by Interaction with Nuclear Orphan Receptor Nur77/TR3. *Cell.* 116: 1-20. 2004.
2. Cao, X., Li, H., Liu, W., Lin, F., Kolluri, S., and Zhang, X.-k. Mitochondrial targeting of retinoid X receptor and its regulation by ligands and dimerization. *Mol. Cell. Biol.* In Press. 2004.
3. James, S., Lin, F., Kolluri, S., Dawson, M.I., and Zhang, X.-k. Regulation of retinoic acid receptor β expression by peroxisome proliferator-activated receptor γ ligands in cancer cells. *Cancer Res.* 63: 3531-3538. 2003.
4. Lin, F., Kolluri, S., Chen, G.-q.and Zhang, X.-k. Regulation of Retinoic Acid-induced Inhibition of AP-1 Activity by Orphan Receptor COUP-TF. J. Biol. Chem. 277: 21414-22, 2002.
5. Dawson, M.I., Harris, D., Liu, G., Hobbs, P., Lange, C., Jong, L., Bruey-Sedano, N., James, S., Zhang, X.k., Peterson, V., Leid, M., Farhana, L., Rishi, A., and Fontana, J. Antagonist Analogue of 6-[3'-(1-Adamantyl)-4'–hydroxyphenyl]-2-naphthalenecarboxylic Acid (AHPN) Family of Apoptosis Inducers That Effectively Blocks AHPN-Induced Apoptosis but Not Cell-Cycle Arrest. *J. Med. Chem.* 47: 3518-3536. 2004.

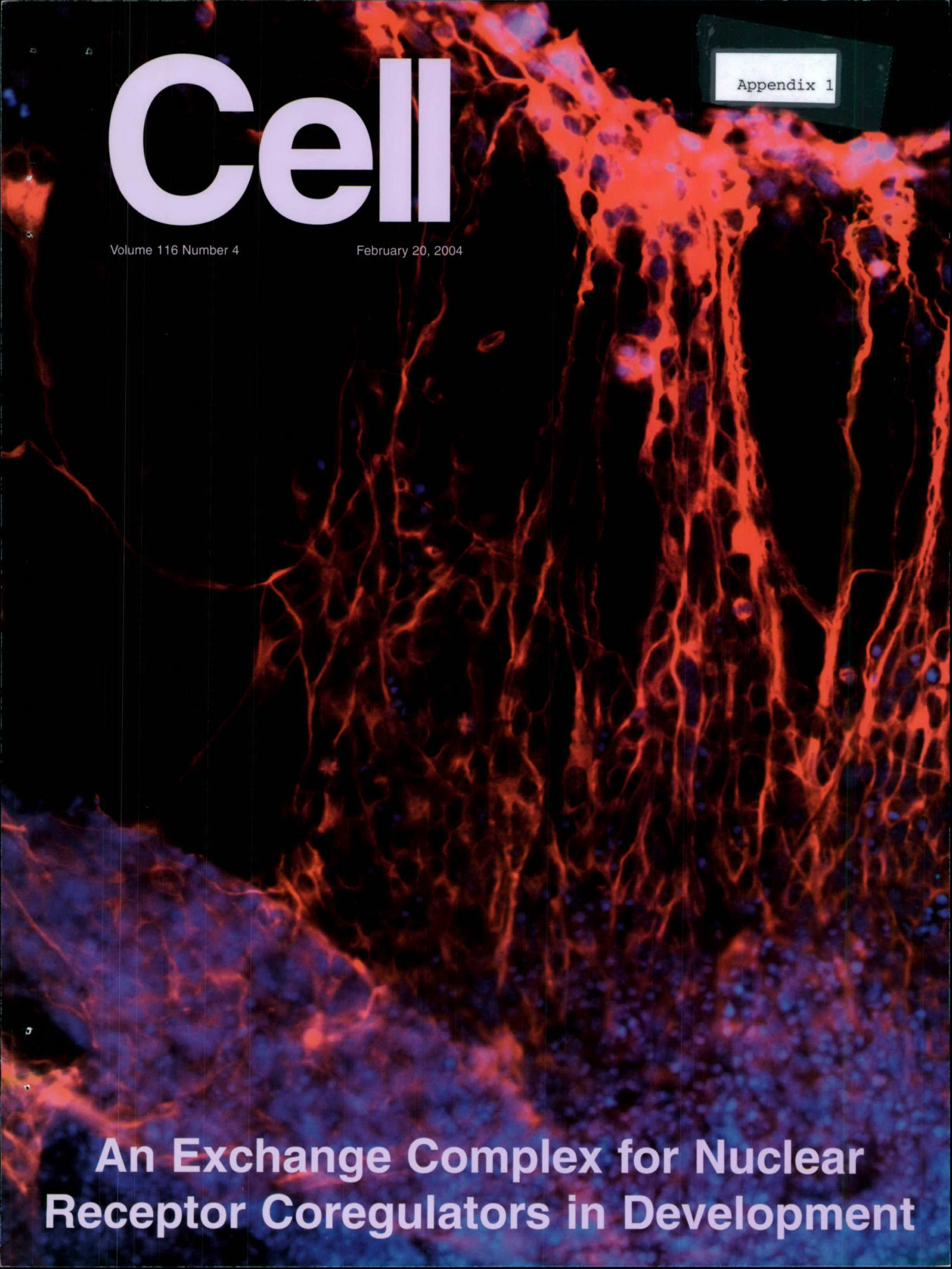

Cell

Volume 116 Number 4 February 20, 2004

An Exchange Complex for Nuclear Receptor Coregulators in Development

Cell, Vol. 116, 527–540, February 20, 2004, Copyright ©2004 by Cell Press

Conversion of Bcl-2 from Protector to Killer by Interaction with Nuclear Orphan Receptor Nur77/TR3

Bingzhen Lin, Siva Kumar Kolluri, Feng Lin, Wen Liu, Young-Hoon Han, Xihua Cao, Marcia I. Dawson, John C. Reed,* and Xiao-kun Zhang*
The Burnham Institute
Cancer Center
10901 North Torrey Pines Road
La Jolla, California 92037

Summary

The Bcl-2 family proteins are key regulators of apoptosis in human diseases and cancers. Though known to block apoptosis, Bcl-2 promotes cell death through an undefined mechanism. Here, we show that Bcl-2 interacts with orphan nuclear receptor Nur77 (also known as TR3), which is required for cancer cell apoptosis induced by many antineoplastic agents. The interaction is mediated by the N-terminal loop region of Bcl-2 and is required for Nur77 mitochondrial localization and apoptosis. Nur77 binding induces a Bcl-2 conformational change that exposes its BH3 domain, resulting in conversion of Bcl-2 from a protector to a killer. These findings establish the coupling of Nur77 nuclear receptor with the Bcl-2 apoptotic machinery and demonstrate that Bcl-2 can manifest opposing phenotypes, induced by interactions with proteins such as Nur77, suggesting novel strategies for regulating apoptosis in cancer and other diseases.

Introduction

Bcl-2-family proteins are evolutionarily conserved regulators of apoptosis (Adams and Cory, 1998; Gross et al., 1999; Reed, 1998; Vander Heiden and Thompson, 1999). All members possess at least one of the four conserved motifs called Bcl-2 homology (BH) domains. Antiapoptotic members, such as Bcl-2 and Bcl-X_L, contain all four BH domains. Some proapoptotic members, such as Bax and Bak, contain BH1, BH2, and BH3 domains, while others, such as Bad and Bid, share sequence homology only at the BH3 domain. The Bcl-2 family proteins primarily act at mitochondria to regulate apoptosis, possibly by forming channels in mitochondrial membranes (Green and Reed, 1998).

One curious and as yet unexplained aspect of some Bcl-2-family proteins is that their phenotypes can be reversed in some cellular contexts. Overexpression of Bcl-2 or Bcl-X_L in some cells promotes rather than prevents apoptosis, whereas Bax and Bak prevent apoptosis under some circumstances (Chen et al., 1996; Fannjiang et al., 2003; Grandgirard et al., 1998; Lewis et al., 1999; Subramanian and Chinnadurai, 2003; Uhlmann et al., 1998). *Drosophila* Bcl-2 homologs exhibit either pro- or antiapoptotic activity (Colussi et al., 2000; Igaki et al., 2000). Similarly, mutants of the Bcl-2-homolog, Ced-9, appear to promote rather than prevent programmed cell death in *C. elegans* (Xue and Horvitz, 1997). Given that the *C. elegans* genome contains no Bax-homologs, Ced-9 may perform the functions of both Bcl-2 and Bax by adopting different conformations to exert opposing effects on cell life and death.

Nur77 (TR3 or NGFI-B), an orphan member of the steroid/thyroid/retinoid nuclear receptor superfamily (Kastner et al., 1995; Mangelsdorf and Evans, 1995; Zhang, 2002), plays roles in regulating growth and apoptosis (Winoto and Littman, 2002; Zamzami and Kroemer, 2001; Zhang, 2002). Nur77 expression is rapidly induced during apoptosis in immature thymocytes and T cell hybridomas (Liu et al., 1994; Woronicz et al., 1994), and cancer cells of lung (Li et al., 1998; Kolluri et al., 2003), prostate (Li et al., 2000; Uemura and Chang, 1998), ovary (Holmes et al., 2002, 2003), colon (Wilson et al., 2003), and stomach (Liu et al., 2002; Wu et al., 2002). High levels of Nor1, a Nur77-family member, are associated with favorable responses to several chemotherapeutic agents in patients with diffuse large B-cell lymphoma (Shipp et al., 2002).

Recently, we discovered a paradigm in cellular apoptosis (Li et al., 2000), wherein Nur77 translocates from the nucleus to the cytoplasm, targeting to mitochondria and inducing cyt *c* release. Nur77 mitochondrial-targeting occurs during apoptosis of different types of cancer cells (Holmes et al., 2003; Kolluri et al., 2003; Liu et al., 2002; Wilson et al., 2003; Wu et al., 2002). Sindbis virus-induced apoptosis also involves Nur77 translocation to mitochondria (Lee et al., 2002). How Nur77 targets mitochondria and induces apoptosis however has been unclear.

In this study, we investigated the mechanism by which Nur77 targets mitochondria and induces apoptosis. Our results demonstrate that Nur77 interacts with Bcl-2 through its ligand binding domain (LBD) and that the interaction is required for Nur77 mitochondrial targeting and Nur77-dependent apoptosis. Interestingly, Nur77 binds to the Bcl-2 N-terminal loop region, located between its BH4 and BH3 domains, resulting in a conformational change in Bcl-2, which converts it from a protector to a killer protein.

Results

Nur77 Interacts with Bcl-2

We investigated whether Nur77 targets to mitochondria by binding Bcl-2. In vitro protein binding assays showed that similar proportions of ^{35}S-labeled Bcl-2 or RXRα, a known Nur77 heterodimerization partner, were selectively pulled-down by GST-Nur77 but not by GST (Figure 1A). Conversely, ^{35}S-labeled Nur77 and Bax, a known heterodimerization partner of Bcl-2, bound equally to GST-Bcl-2 but not to GST (Figure 1A). In mammalian two-hybrid studies, Bcl-2/ΔTM, a Bcl-2 mutant lacking its C-terminal transmembrane domain, strongly inter-

*Correspondence: xzhang@burnham.org (X.-k.Z.), jreed@burnham.org (J.C.R.)

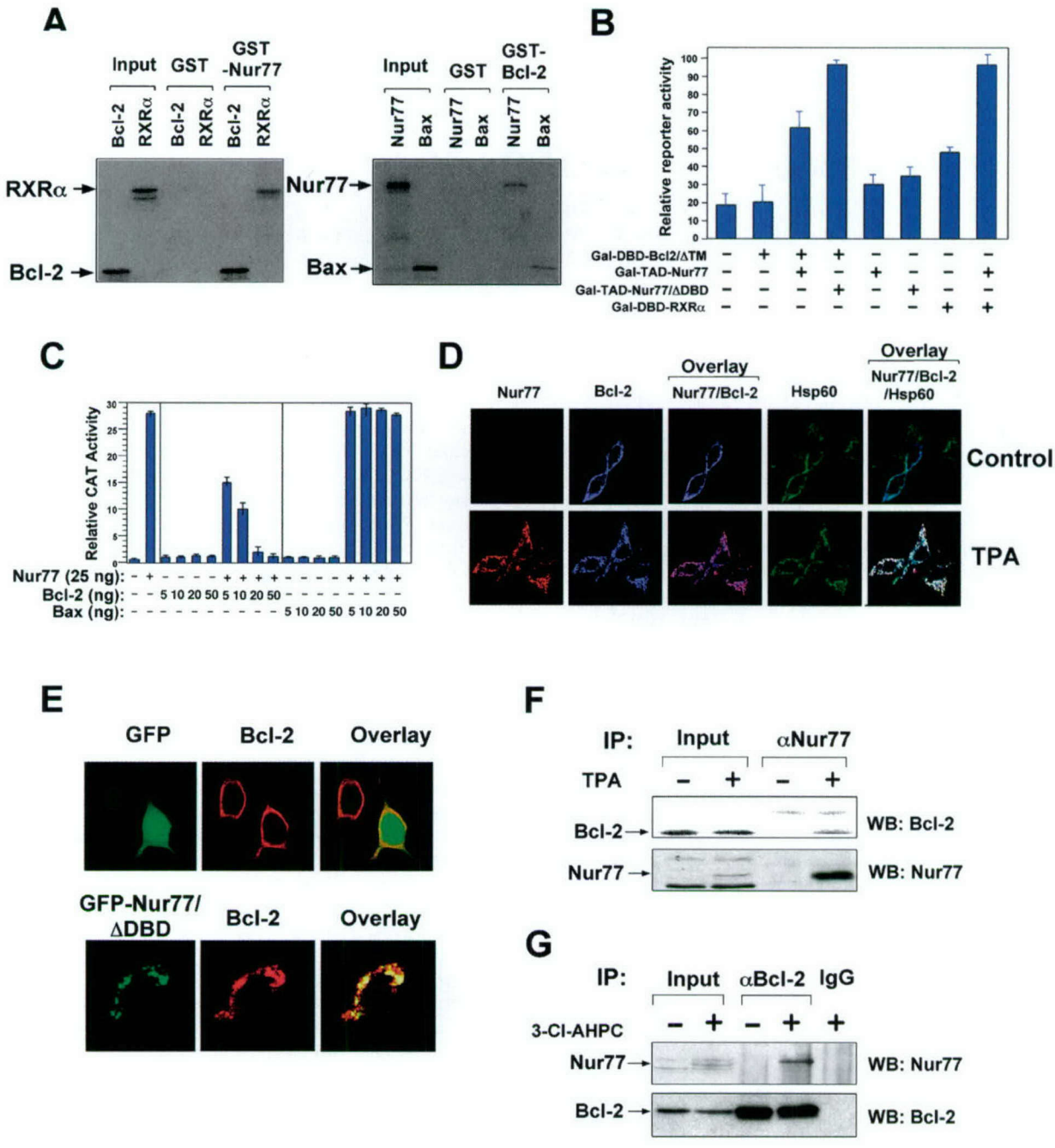

Figure 1. Interaction of Nur77 with Bcl-2

(A) GST-pull down. GST-Nur77, GST-Bcl-2, or GST control protein immobilized on glutathione-Sepharose was incubated with in vitro synthesized ^{35}S-labeled Bcl-2, RXRα, Nur77, or Bax as indicated. Bound proteins were analyzed by SDS-PAGE autoradiography. Input represents 5% of protein used in the pull down assays

(B) Mammalian two-hybrid assay. Gal4 reporter gene $(Gal4)_2$-*tk*-Luc) was transfected into CV-1 cells with the Bcl-2/ΔTM (TM was deleted to prevent Bcl-2 membrane association) or RXRα fused with the Gal-DBD alone or with the Nur77 or Nur77/ΔDBD fused with the Gal-transactivation domain (TAD). Reporter gene activity was determined 48 hr later.

(C) Inhibition of Nur77-dependent transactivation by Bcl-2. CV-1 cells were transfected with the NurRE-*tk*-CAT reporter (Li et al., 2000) with or without Nur77 expression vector together with or without the Bcl-2 or Bax. CAT activity was then determined. The bars in (B) and (C) are means ± SD from three and six experiments, respectively.

(D) Colocalization of endogenous Nur77 and transfected Bcl-2. LNCaP cells were transfected with Bcl-2, treated with or without TPA (100 ng/ml) for 3 hr, then immunostained with polyclonal rabbit anti-Bcl-2, mouse monoclonal anti-Nur77, or anti-Hsp60 antibody. Nur77, Bcl-2, and Hsp60 were visualized using confocal microscopy and images were overlaid (overlay). Approximately 80% of TPA-treated cells demonstrated colocalization.

(E) Colocalization of transfected GFP-Nur77/ΔDBD and Bcl-2. GFP–Nur77/ΔDBD (3 μg) and Bcl-2 (1 μg) were cotransfected into LNCaP cells. After 20 hr, cells were immunostained with anti-Bcl-2 antibody. GFP–fusion and Bcl-2 were visualized as in (D). For control, distribution of transfected GFP empty vector is shown. Approximately 30% of transfected cells exhibited colocalization shown.

(F) In vivo Co-IP assay in LNCaP cells. Lysates from LNCaP cells treated with or without TPA for 3 hr were incubated with mouse monoclonal anti-Nur77 antibody (Abgent, San Diego, CA). For immunoblotting of immunoprecipitates, anti-Bcl-2 or rabbit polyclonal anti-Nur77 antibody (Active Motif, Carlsbad, CA) were used.

(G) In vivo Co-IP in H460 cells. Lysates from H460 cells treated with or without 3-Cl-AHPC (10^{-6} M) for 3 hr were incubated with anti-Bcl-2 antibody. Immunoblotting of immunoprecipitates was conducted as in (F).

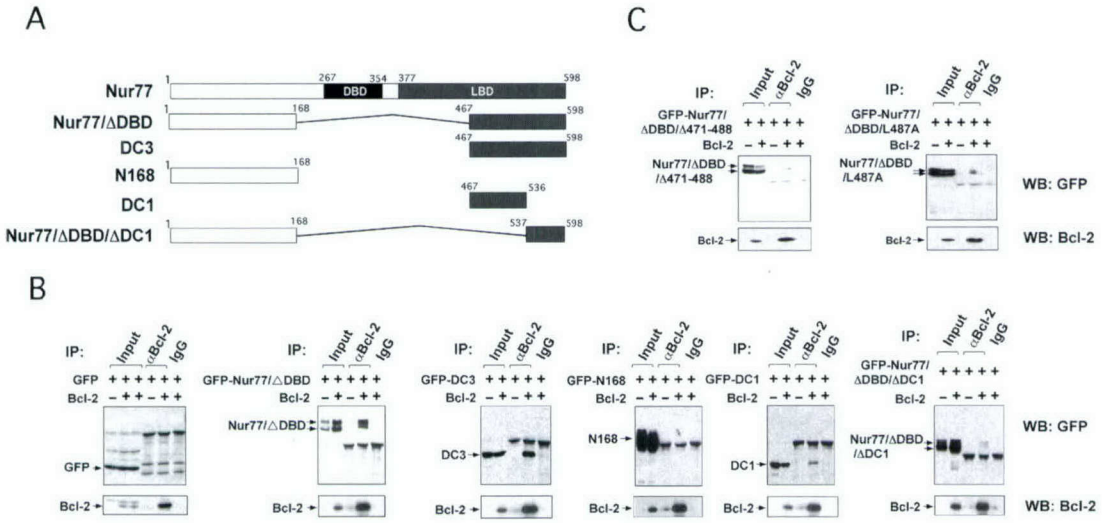

Figure 2. Ligand binding Domain of Nur77 Interacts with Bcl-2

(A) Schematic representation of Nur77 mutants. The Nur77 DBD and LBD are indicated.

(B-C) In vivo Co-IP of Nur77 mutants and Bcl-2. The indicated Nur77 mutant fused with GFP or the empty GFP vector (6 μg) was cotransfected with the empty vector (pRC/CMV) or Bcl-2 expression vector (2 μg) into HEK293T cells. Lysates were immunoprecipitated by using either polyclonal rabbit anti-Bcl-2 antibody (against whole Bcl-2 protein) or control IgG. Cell lysates and immunoprecipitates were examined by immunoblotting using anti-GFP antibody. The same membranes were also blotted with anti-Bcl-2 antibody to determine IP specificity and efficiency. Input represents 5% of cell lysates used in the Co-IP assays.

acted with Nur77 or Nur77/ΔDBD, a Nur77 mutant lacking its DNA binding domain (DBD), comparable to the interaction of Nur77 with RXRα (Figure 1B). Bcl-2 but not Bax potently inhibited Nur77 transactivation (Figure 1C), again suggesting an interaction between Nur77 and Bcl-2.

We next determined whether endogenous Nur77 and transfected Bcl-2 colocalized in cells. The phorbol ester 12-*0*-tetradecanoyl phorbol-13-acetate (TPA) induces the expression of endogenous Nur77 and its mitochondrial localization in LNCaP prostate cancer cells (Li et al., 2000). In TPA-stimulated cells, the distribution patterns of TPA-induced endogenous Nur77 and transfected Bcl-2 overlapped extensively in the cytoplasm and colocalized with Hsp60, a mitochondria-specific protein (Figure 1D). Transfected Nur77/ΔDBD and Bcl-2 also colocalized in cells. The green fluorescent protein (GFP) tagged Nur77/ΔDBD, which constitutively resides on mitochondria in LNCaP cells (Li et al., 2000), displayed a distribution pattern that overlapped extensively with coexpressed Bcl-2, while control GFP protein distributed diffusely in cells (Figure 1E).

The interaction between Nur77 and Bcl-2 was further confirmed by coimmunoprecipitation (Co-IP) assays. As shown in Figure 1F, Bcl-2 was specifically coimmunoprecipitated by anti-Nur77 antibody in TPA-treated cells but not in nontreated cells. Co-IP using lysates from H460 lung cancer cells treated with AHPN analog 3-Cl-AHPC, which potently induces Nur77 expression, mitochondrial targeting and apoptosis (Kolluri et al., 2003), also demonstrated a strong interaction between endogenous Nur77 and Bcl-2 (Figure 1G).

The Nur77 LBD Is Required for Binding Bcl-2

To identify the Nur77 domain responsible for interaction with Bcl-2, we constructed several Nur77 mutants (Figure 2A) as GFP fusions. When GFP-Nur77/ΔDBD and Bcl-2 were cotransfected into HEK293T cells, a significant amount of GFP-Nur77/ΔDBD was coprecipitated with Bcl-2 by anti-Bcl-2 antibody but not by control IgG (Figure 2B). This Co-IP was specific because Bcl-2 coexpression was required and the GFP control protein did not interact with Bcl-2. Analysis of other Nur77 mutants revealed that the C-terminal domain (DC3), but not the N-terminal domain (N168), of Nur77/ΔDBD was responsible for binding Bcl-2. The C-terminal fragment DC1 (467–536 aa) strongly interacted with Bcl-2, while its deletion from Nur77/ΔDBD (Nur77/ΔDBD/ΔDC1) largely abolished the interaction. Furthermore, deletion of a putative amphipathic α-helix (471–488 aa) from Nur77/ΔDBD (Nur77/ΔDBD/Δ471–488) or mutation of Leu487 in the region to Ala (Nur77/ΔDBD/L487A) significantly impaired the interaction between Nur77/ΔDBD and Bcl-2 (Figure 2C). Thus, the DC1 region in the Nur77 LBD is crucial for Bcl-2 interaction.

The Bcl-2 Loop Region, but Not Its Hydrophobic Groove, Is Responsible for Nur77 Binding

Bcl-2 and Bcl-X_L have hydrophobic crevices on their surfaces that bind the BH3 domains of other family members (Sattler et al., 1997). To examine whether Nur77 binds to the Bcl-2 hydrophobic groove, we analyzed the interaction of Nur77/ΔDBD with several deletion or point mutants of Bcl-2 (Figure 3A), which are defective in forming the hydrophobic groove (Petros et al., 2001; Sattler et al., 1997). Deletion (data not shown) or point mutations (Y108K, L137A, G145A, or R146Q) in Bcl-2 abolished or reduced the interaction with Bax (Figure 3B). In contrast, these mutants retained the ability to bind Nur77/ΔDBD (Figure 3C). We also analyzed whether Bax or Bcl-Gs, a BH3-only Bcl-2-family protein (Guo et al., 2001), could compete with Nur77 for binding Bcl-2. Our results

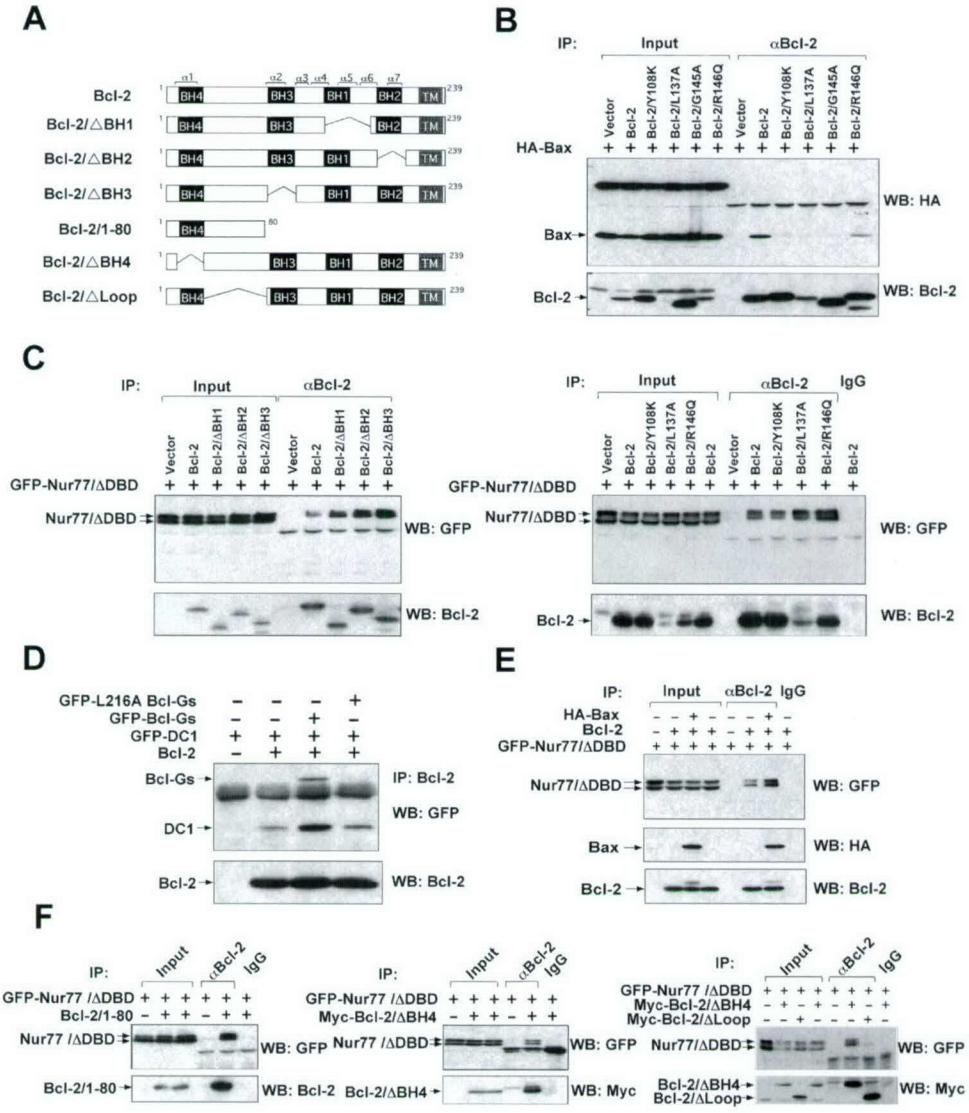

Figure 3. The Bcl-2 Loop Region Interacts with Nur77

(A) Schematic representation of Bcl-2 and its mutants. BH and loop domains and α-helical regions are indicated.

(B) Mutations in the Bcl-2 hydrophobic groove abolish Bcl-2 interaction with Bax.

(C) The Bcl-2 hydrophobic groove is not required for Bcl-2 binding to Nur77/ΔDBD. Co-IP assays (B and C) were performed as in Figure 2B using lysates from HEK293T cells transfected with GFP-Nur77/ΔDBD and the empty vector or the indicated Bcl-2 plasmid. Immunoprecipitates and lysates were examined by immunoblotting using the indicated antibodies.

(D) BH3-only protein Bcl-Gs does not compete with DC1 for binding to Bcl-2. GFP-DC1 (4 μg) was expressed in HEK293T cells with or without Bcl-2 (2 μg) in the presence or absence of GFP-Bcl-Gs or GFP-Bcl-Gs/L216E (4 μg). Lysates were immunoprecipitated by anti-Bcl-2 antibody, followed by immunoblotting with anti-GFP or anti-Bcl-2 antibody.

(E) Bax does not compete with Nur77/ΔDBD for binding to Bcl-2. GFP-Nur77/ΔDBD (6 μg) was expressed in HEK293T cells with or without Bcl-2 (2 μg) in the presence or absence of Bax (2 μg). Lysates were immunoprecipitated by anti-Bcl-2 antibody. Immunoprecipitates and lysates were examined by immunoblotting using anti-GFP, anti-Bcl-2, or anti-HA antibody.

(F) The Bcl-2 N-terminal loop region is essential for Nur77/Bcl-2 interaction. GFP-Nur77/ΔDBD was cotransfected with the indicated Bcl-2 mutant plasmid into HEK293T cells. Lysates were immunoprecipitated by anti-myc or Bcl-2 antibody as indicated. Immunoprecipitates were analyzed by immunoblotting with anti-GFP, anti-Bcl-2, or anti-myc antibody.

showed that neither Bcl-Gs (Figure 3D) nor Bax (Figure 3E) interfered with DC1 or Nur77/ΔDBD binding to Bcl-2. Rather, these proteins consistently enhanced their interaction with Bcl-2. Thus, binding of Bcl-2 to Nur77 is distinct for its binding to Bcl-Gs and Bax and does not require the BH3 binding hydrophobic groove in Bcl-2.

The above observations suggested that the N-terminal portion of Bcl-2 was responsible for binding Nur77. Indeed, the first 80 amino acid residues of Bcl-2 (Bcl-2/1-80), like the full-length Bcl-2, strongly interacted with Nur77/ΔDBD (Figure 3F). The Bcl-2/1-80 encompasses the BH4 domain and an unstructured loop domain. To determine whether the BH4 domain or the loop region was responsible for binding to Nur77/ΔDBD, we investigated Nur77/ΔDBD interaction with Bcl-2 mutants lacking the BH4 domain (Bcl-2/ΔBH4) or the loop region

(Bcl-2/ΔLoop) (Figure 3F). Co-IP assays demonstrated that the Bcl-2/ΔBH4 retained the ability to interact with Nur77/ΔDBD, whereas Bcl-2/ΔLoop did not (Figure 3F). Thus, the loop region of Bcl-2 is required for binding to Nur77.

Interaction with Bcl-2 Mediates Nur77 Mitochondrial Targeting

To determine whether interaction with Bcl-2 mediated Nur77 mitochondrial targeting, we transfected GFP-Nur77/ΔDBD alone or with Bcl-2 into HEK293T cells, which lack detectable levels of endogenous Bcl-2. GFP-Nur77/ΔDBD was diffusely distributed in the cytosol (Figure 4A), indicating that it failed to target mitochondria. However, when coexpressed with Bcl-2, GFP-Nur77/ΔDBD displayed a distribution pattern overlapping with mitochondrial Hsp60. Thus, Bcl-2 expression conferred mitochondrial targeting to Nur77/ΔDBD. The colocalization of Nur77/ΔDBD and Hsp60 was dependent on Nur77/ΔDBD binding to Bcl-2, because mutants of GFP-Nur77/ΔDBD (Nur77/ΔDBD/L487A and Nur77/ΔDBD/Δ471–488) that failed to bind Bcl-2 (Figure 2) did not colocalize with mitochondria.

The role of Bcl-2 in mitochondrial targeting of Nur77 was further studied by examining the accumulation of Bcl-2 binding Nur77/ΔDBD and nonbinding Nur77/ΔDBD/Δ471–488 in mitochondria-enriched heavy membrane (HM) fractions of HEK293T cells (Figure 4B). HM preparation purity was established by assessing levels of mitochondrial Hsp60, nuclear protein PARP, and cytosolic/nuclear protein Jun N-terminal kinase (JNK). Nur77/ΔDBD accumulated in the HM fraction when Bcl-2 was coexpressed, whereas Nur77/ΔDBD/Δ471-488 did not accumulate irrespective of Bcl-2 coexpression.

To complement these gene transfection experiments, small interfering (si)RNA was used to determine whether suppressing endogenous Bcl-2 expression affected Nur77 mitochondrial targeting. In MGC80-3 gastric cancer cells, in which Nur77 was reported to target mitochondria in response to specific apoptotic stimuli (Liu et al., 2002), Bcl-2 expression was almost completely inhibited by Bcl-2-specific siRNA but not by GFP siRNA control (Figure 4C). Both confocal microscopy (Figure 4D) and immunoblotting of HM fractions (Figure 4E) revealed that endogenous Nur77 targeted mitochondria in MGC80-3 cells treated with 3-Cl-AHPC. However, Bcl-2 siRNA, but not control GFP siRNA, largely abolished mitochondrial targeting of Nur77. Similarly, inhibition of endogenous Bcl-2 expression using Bcl-2 antisense oligonucleotides impaired Nur77 mitochondrial targeting in H460 lung cancer cells (Supplemental Figure S1 available at http://www.cell.com/cgi/content/full/116/4/527/DC1).

We next studied whether the Bcl-2 loop region could act in a dominant-negative fashion to inhibit Nur77 mitochondrial targeting. In LNCaP cells transfected with GFP-Bcl-2/1-90, a Bcl-2 mutant comprised of the first 90 N-terminal amino acids, TPA-induced Nur77 failed to target mitochondria, displaying a diffuse cytosolic distribution pattern, in contrast to nontransfected cells, which exhibited colocalization of Nur77 and Hsp60 (Figure 4F). Thus, Bcl-2/1-90 inhibits Nur77 mitochondrial targeting, probably by competing with endogenous Bcl-2 for binding to Nur77. Together, these results demonstrate that Bcl-2 acts as a receptor for Nur77 and is responsible for Nur77 mitochondrial targeting.

Nur77 Interaction with Bcl-2 Triggers cyt *c* Release and Apoptosis

Next, we determined the requirement of Nur77 interaction with Bcl-2 for Nur77-induced cyt *c* release and apoptosis. Transient expression of Nur77/ΔDBD or Bcl-2 alone did not cause release of cyt *c* from mitochondria in HEK293T cells, as confocal microscopy analysis showed punctate cyt *c* staining, indicative of mitochondrial cyt *c* (Figure 5A). However, their coexpression resulted in their colocalization and release of cyt *c* from mitochondria (Figure 5A). Cyt *c* release required mitochondrial localization of Nur77/ΔDBD and Bcl-2, because it did not occur upon coexpression of Nur77/ΔDBD with Bcl-2/ΔTM, a Bcl-2 mutant unable to target mitochondria (Figure 5A). Interestingly, coexpression of Nur77/ΔDBD and Bcl-2/Y108K did not induce cyt *c* release, although they colocalized (Figure 5A). These results suggest that the interaction between Nur77/ΔDBD and Bcl-2 is insufficient for inducing cyt *c* release.

Expression of either Nur77/ΔDBD or Bcl-2 alone did not induce apoptosis, as revealed by the absence of nuclear fragmentation and chromatin condensation in HEK293T cells (Figure 5B). However, when coexpressed, Bcl-2 and Nur77/ΔDBD induced striking apoptosis. The proapoptotic effect of Bcl-2 was specific to Nur77, because Bax-induced apoptosis was effectively prevented by Bcl-2 coexpression (see below). Thus, Bcl-2 promotes apoptosis when coexpressed with Nur77 but suppresses apoptosis when coexpressed with Bax.

We next examined the role of endogenous Bcl-2 on Nur77-dependent apoptosis in MGC80-3 cells. Treatment of control GFP-siRNA-transfected cells with 3-Cl-AHPC resulted in apoptosis (Figures 5C and 5D). However, transfection of Bcl-2 siRNA suppressed 3-Cl-AHPC-induced apoptosis by about 60%. Similar results were obtained in H460 cells (Supplemental Figure S1 available on *Cell* website). Moreover, expression of Bcl-2/1-90 protein also suppressed Nur77-dependent apoptosis induced by TPA and 3-Cl-AHPC in LNCaP cells (Figure 5E). Thus, Bcl-2 can manifest a proapoptotic phenotype in settings where Nur77 is expressed and targets to mitochondria.

To extend the above findings to primary cells, we performed experiments using primary cultures of peripheral blood lymphocytes (PBLs). Freshly isolated PBLs were transfected with GFP-Nur77, then treated with TPA plus calcium ionophore ionomycin, which induce Nur77-dependent apoptosis of T-lymphocytes (Woronicz et al., 1994). The treatment caused translocation of GFP-Nur77 from the nucleus to the cytoplasm, colocalizing with cotransfected DsRed2-Mito, a red fluorescent protein (RFP) fused with a mitochondria-targeting sequence (Figure 6A). Subcellular fractionation revealed that the treatment induced accumulation of endogenous Nur77 in HM fractions (Figure 6B). Interestingly, this treatment also altered the migration of Nur77 protein, suggesting a possible posttranslational modification. Thus, both transfected and endogenous Nur77 targets mitochondria in primary lymphocytes.

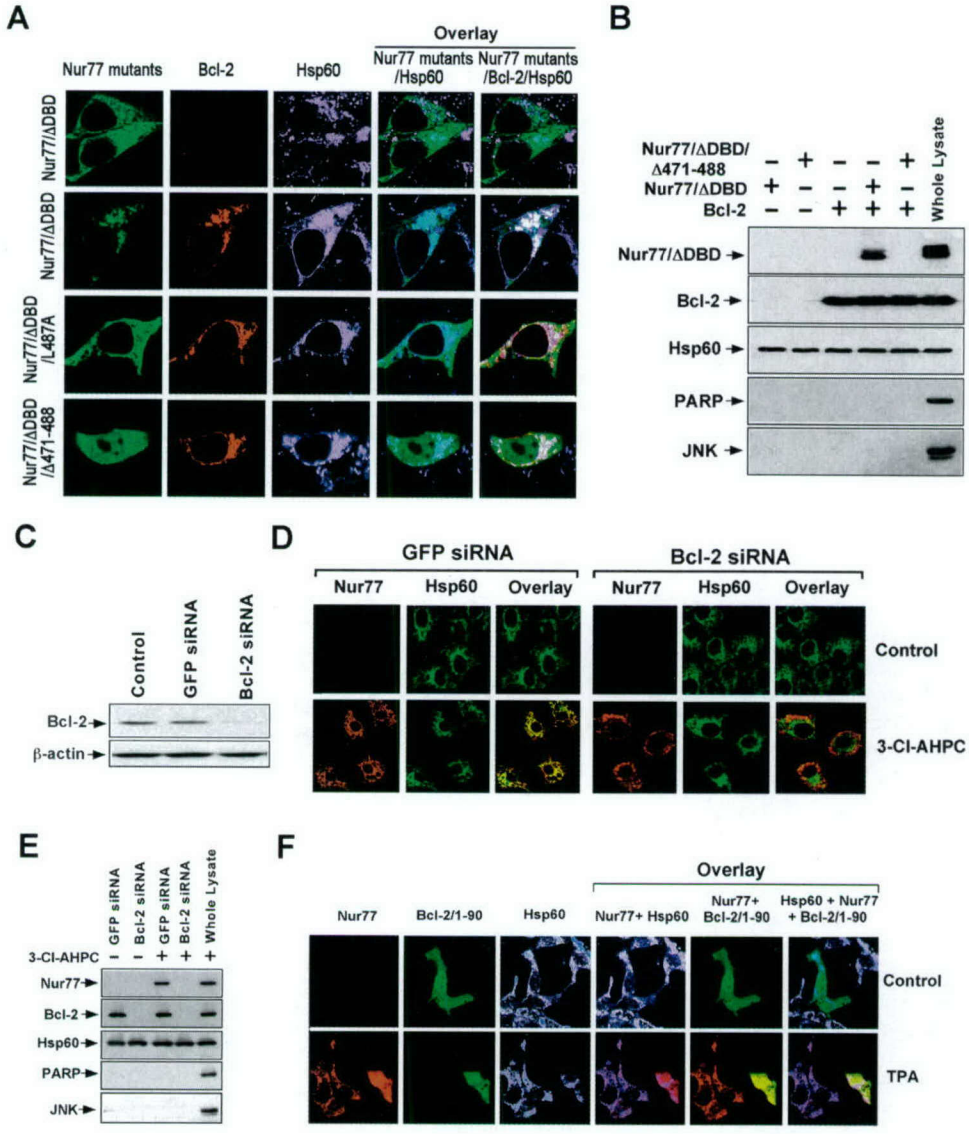

Figure 4. Nur77/Bcl-2 Interaction Mediates Nur77 Mitochondrial Localization

(A) Bcl-2 expression promotes Nur77/ΔDBD mitochondrial localization. The indicated GFP-Nur77 mutant (3 μg) and Bcl-2 (1 μg) were expressed in HEK293T cells alone or together. Cells were immunostained with anti-Bcl-2 or anti-Hsp60 antibody. Bcl-2, Nur77/ΔDBD, its mutants, and mitochondria (Hsp60) were visualized using confocal microscopy and the images were overlaid (overlay). Approximately 30% of cells showed Nur77/ΔDBD colocalization with Bcl-2 and Hsp60, while less than 5% of cells transfected with Nur77/ΔDBD mutants were similarly colocalized. In the absence of Bcl-2, Nur77/ΔDBD did not colocalize with Hsp60.

(B) Immunoblotting analysis of the effect of Bcl-2 expression. GFP-Nur77/ΔDBD or GFP-Nur77/ΔDBD/Δ471-488 (6 μg) and Bcl-2 (2 μg) were transfected into HEK293T cells alone or together. HM fractions were prepared and analyzed for accumulation of Nur77/ΔDBD in mitochondria by immunoblotting using anti-GFP antibody. The same membrane was also blotted with anti-Bcl-2, anti-Hsp60, anti-PARP, or anti-JNK antibody. Whole lysate was prepared from cells transfected with Nur77/ΔDBD and Bcl-2.

(C) Inhibition of Bcl-2 expression by Bcl-2 siRNA. MGC80-3 cells were transfected with Bcl-2 siRNA SMARTpool or control GFP siRNA or left alone. After 48 hr, lysates were prepared and assayed by immunoblotting using anti-Bcl-2 and anti-β-actin antibodies.

(D–E) Inhibition of endogenous Bcl-2 expression abrogates 3-Cl-AHPC-induced Nur77 mitochondrial targeting. MGC80-3 cells transfected with siRNA as described in (C) were treated with 3-Cl-AHPC (10^{-6} M) for 5 hr. Cells were immunostained with anti-Nur77 and anti-Hsp60 antibodies for confocal microscopy analysis (D) or subjected to HM fractionation and analysis (E) as described in (B).

(F) Bcl-2/1-90 inhibits Nur77 mitochondrial targeting. LNCaP cells were transfected with GFP-Bcl-2/1-90 (4 μg). After 24 hr, cells were treated with TPA (100 ng/ml) for 3 hr and immunostained with anti-Nur77 and anti-Hsp60 antibodies, followed by confocal microscopy analysis. Approximately 77% of transfected cells showed the effect presented.

We also studied the role of Bcl-2 in Nur77-dependent apoptosis in PBLs. Treatment with TPA/ionomycin induced extensive apoptosis of PBLs, which was partially inhibited by Bcl-2 antisense oligonucleotides or Nur77 siRNA (Figure 6C). In addition, GFP-Nur77/ΔDBD also colocalized extensively with DsRed2-Mito (Figure 6D) and potently induced PBL apoptosis (Figure 6E), which was almost completely suppressed by Bcl-2 antisense

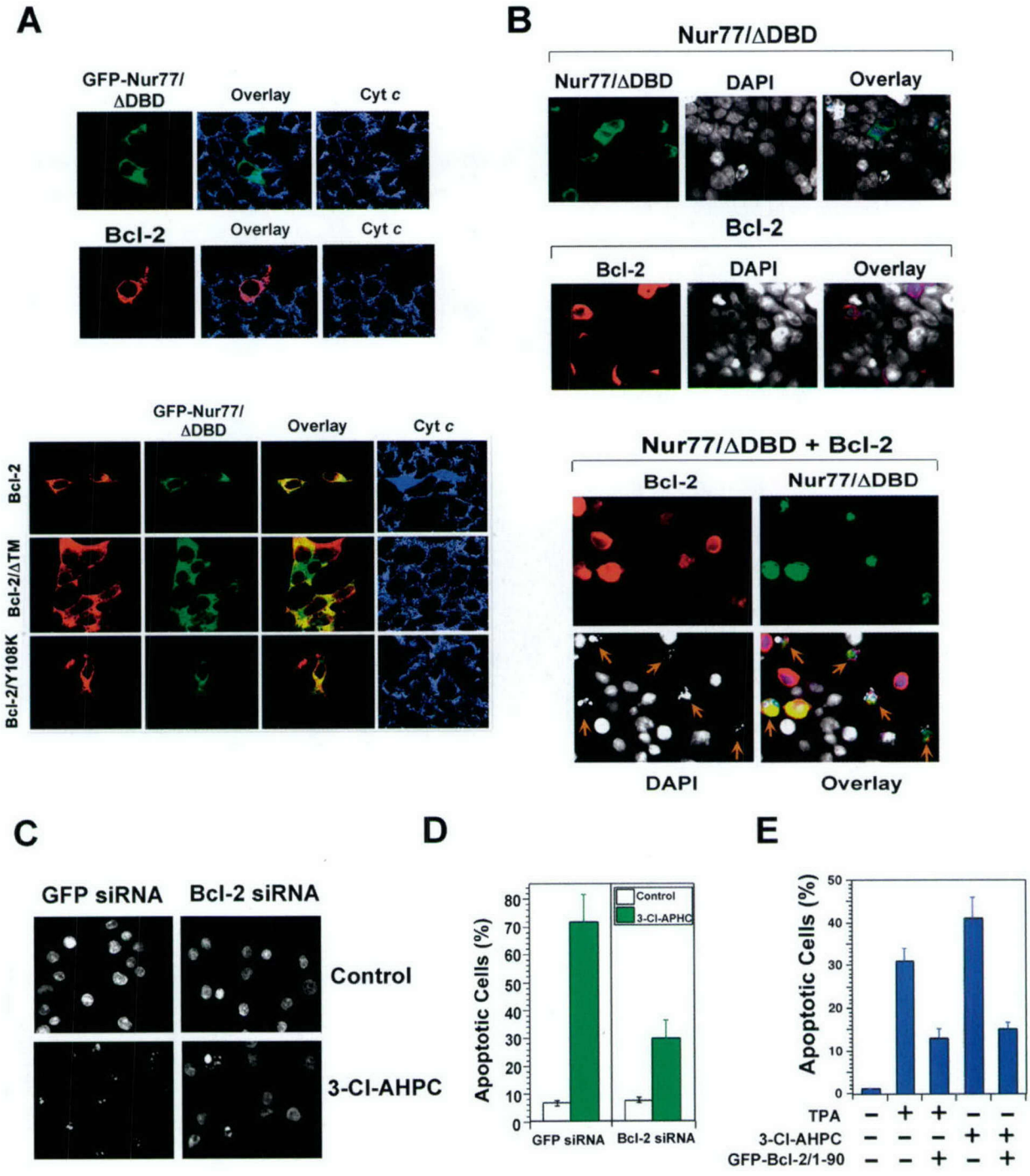

Figure 5. Interaction of Nur77 with Bcl-2 Results in cyt *c* Release and Apoptosis

(A) Induction of cyt *c* release by coexpression of Bcl-2 and Nur77/ΔDBD. GFP-Nur77/ΔDBD (6 μg) and Bcl-2 (2 μg) were expressed in HEK293T cells alone and together. GFP-Nur77/ΔDBD was also coexpressed with Bcl-2/ΔTM or Bcl-2/Y108K (2 μg). Cells were immunostained with anti-Bcl-2 or anti-cyt *c* antibody. Nur77/ΔDBD, Bcl-2 and cyt *c* were visualized using confocal microscopy, and images for Nur77/ΔDBD and Bcl-2 were overlaid (overlay). Approximately 75% of the Nur77/ΔDBD and Bcl-2 colocalized cells displayed various levels of diffuse cyt *c* staining.

(B) Induction of apoptosis by coexpression of Bcl-2 and Nur77/ΔDBD. Bcl-2 and GFP-Nur77/ΔDBD were expressed alone or together in HEK293T cells. After 36 hr, cells were stained by anti-Bcl-2 antibody, followed by TRITC-conjugated secondary antibody (Sigma) and the nucleus was stained by DAPI. Expression of Bcl-2 and GFP-Nur77/ΔDBD, as well as nuclear morphology, were visualized by fluorescence microscopy, and the three images were overlaid. Arrows indicate cells expressing Bcl-2 and GFP-Nur77/ΔDBD. One of four similar experiments is shown.

(C–D) Inhibition of endogenous Bcl-2 expression suppresses 3-Cl-AHPC-induced apoptosis. MGC80-3 cells were transfected with Bcl-2 siRNA SMARTpool or control GFP siRNA. After 36 hr, cells were treated with 3-Cl-AHPC (10^{-6} M) for 48 hr. Apoptosis was determined by DAPI staining as shown in (C) and scored by examining 300 cells for nuclear fragmentation and/or chromatin condensation (D).

(E) Bcl-2/1-90 inhibits TPA and 3-Cl-AHPC-induced apoptosis. LNCaP cells were transfected with GFP or GFP-Bcl-2/1-90. After 24 hr, cells were treated with TPA (100 ng/ml) or 3-Cl-AHPC (10^{-6} M) for 24 hr. Apoptosis was studied as in D.

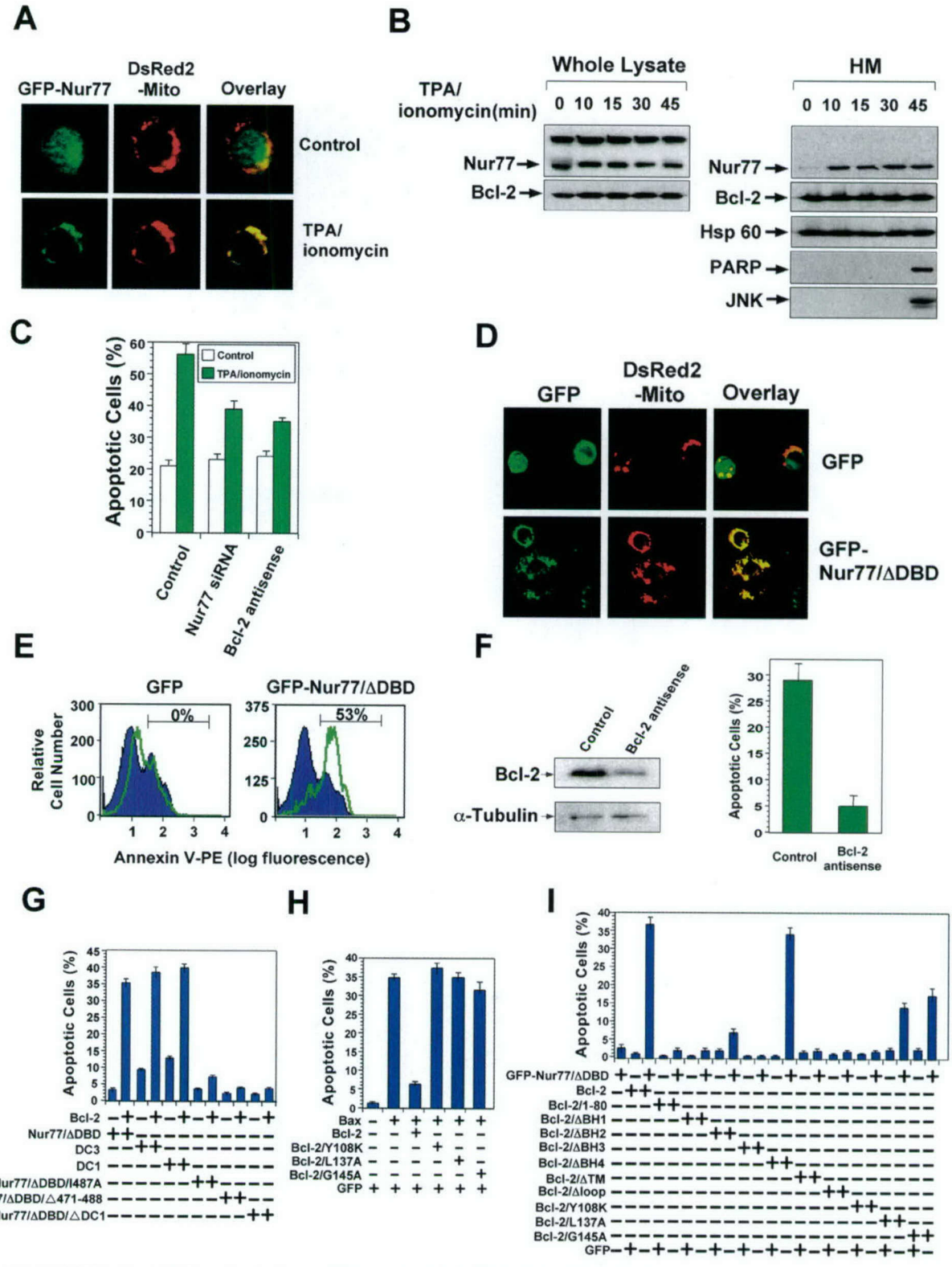

Figure 6. Nur77 Mitochondrial Targeting in Human PBLs and Apoptotic Effects of Nur77 and Bcl-2 Mutants

(A) Mitochondrial targeting of Nur77 in PBLs. GFP-Nur77 (1 μg) and pDsRed2-Mito (1 μg) were transfected into freshly isolated human PBLs. The cells were then treated with TPA (10 ng/ml) and ionomycin (0.5 μM) for 30 min after 10 hr of transfection. GFP-Nur77 and mitochondria (pDsRed2-Mito) were visualized using confocal microscopy. Approximately 20% of the cells showed the pattern presented.

(B) Endogenous Nur77 accumulates in the PBL HM fraction. PBLs were treated with TPA and ionomycin as in (A) for the indicated times and HM fractions were isolated. Total cell lysates and HM fractions were subjected to immunoblotting as described in Figure 4B.

(C) Nur77 and Bcl-2 are required for apoptosis in PBLs. PBLs were transfected with control GFP siRNA, Nur77 siRNA, or Bcl-2 antisense oligonucleotides (2 μg). After 40 hr, cells were treated with TPA and ionomycin for 7 hr and apoptotic cells (Annexin-V positive) were determined by flow cytometry. Bars represent average ± means from two experiments.

oligonucleotides (Figure 6F). Thus, endogenous Bcl-2 contributes to Nur77-dependent apoptosis in primary lymphocytes.

Analysis of Bcl-2 Domain Required for Apoptosis Induction by Nur77

To characterize the proapoptotic mechanism of Bcl-2 in Nur77-induced apoptosis, various Nur77 and Bcl-2 mutants were coexpressed in HEK293T cells. Similar to Nur77/ΔDBD, coexpression of either DC3 or DC1 with Bcl-2 strongly induced apoptosis (Figure 6G). Thus, the minimal C-terminal domain of Nur77, capable of binding Bcl-2, was sufficient to induce apoptosis when coexpressed with Bcl-2. The requirement of Nur77 interaction with Bcl-2 for apoptosis was further illustrated by the failure of Nur77 mutants (Nur77/ΔDBD/ΔDC1, Nur77/ΔDBD/Δ471-488, and Nur77/ΔDBD/L487A) that failed to bind Bcl-2 (Figure 2) to induce apoptosis when coexpressed with Bcl-2 (Figure 6G).

Bcl-2 effectively suppressed apoptosis induced by Bax expression in HEK293T cells (Figure 6H). Bcl-2 mutations (Y108K, L137A, G145A) that impaired its interaction with Bax (Figure 3B) abolished its inhibitory effect on Bax-induced apoptosis (Figure 6H), consistent with previous observations that the Bcl-2 hydrophobic cleft is essential for its antiapoptotic effect.

We then performed experiments to delineate the structure-function relationships for the proapoptotic effect of Bcl-2 in Nur77-induced apoptosis (Figure 6I). Coexpression of Nur77/ΔDBD with Bcl-2/ΔLoop did not induce cell death, consistent with the inability of this Bcl-2 mutant to bind Nur77 (Figure 3). Though capable of binding Nur77/ΔDBD, mutants of Bcl-2 lacking the membrane-anchoring TM domain, the BH1 domain, BH2 domain, or BH3 domain were incapable of inducing apoptosis when coexpressed with Nur77/ΔDBD. Similarly, although binding Nur77, a BH3 domain mutant of Bcl-2 (Y108K) also failed to induce apoptosis when coexpressed with Nur77/ΔDBD. Moreover, mutations of the BH3 binding pocket of Bcl-2, L137A, and G145A, which abrogated the ability of Bcl-2 to suppress Bax-induced apoptosis (Figure 6H), retained the ability to promote apoptosis when coexpressed with Nur77/ΔDBD. Thus, an intact hydrophobic groove in Bcl-2 is required for its antiapoptotic activity but not for its proapoptotic activity, demonstrating a structural distinction between these two opposing phenotypes of Bcl-2.

Bcl-2 Undergoes a Conformational Change upon Nur77 Binding

Bax and Bak undergo conformational changes in association with their conversion from latent to active killer proteins (Griffiths et al., 1999; Nechushtan et al., 1999). We therefore explored whether a conformational change might be involved in converting Bcl-2 function from antiapoptotic to proapoptotic. To this end, we compared the effects of Nur77 on binding of Bcl-2 to various anti-Bcl-2 antibodies that recognize different epitopes. Antibody binding to Bcl-2 was measured by immunofluorescence using flow cytometry or by immunoprecipitation.

First, Bcl-2 was coexpressed with GFP-Nur77/ΔDBD or the control GFP in HEK293T cells, and immunostaining was performed on fixed and permeabilized cells using rabbit polyclonal antibody against the whole Bcl-2 protein (αBcl-2), mouse monoclonal antibody against the Bcl-2 BH3 binding pocket (αBcl-2/BH3-pocket), or polyclonal antibody against the Bcl-2 BH3 domain (αBcl-2/BH3-domain) (Figure 7A). Bcl-2 immunofluorescence was undetectable in control GFP-coexpressing cells stained with the αBcl-2/BH3-domain antibody but dramatically increased in GFP-Nur77/ΔDBD-coexpressing cells, suggesting increased availability of the BH3-domain epitope upon Nur77/ΔDBD coexpression (Figure 7A). In contrast, immunofluorescence obtained by staining with the αBcl-2/BH3-pocket antibody was reduced by coexpression of GFP-Nur77/ΔDBD, suggesting decreased availability of this epitope. Alterations in binding of epitope-specific antibodies to Bcl-2 in response to GFP-Nur77/ΔDBD coexpression were not due to changes in Bcl-2 levels, because GFP-Nur77/ΔDBD coexpression did not alter Bcl-2 immunofluorescence when stained with αBcl-2 antibody. In addition, both immunoblotting analysis (Figure 7A) and BD cytometric bead assays (Supplemental Figure S2 available on *Cell* website) revealed equivalent Bcl-2 levels with GFP or GFP-Nur77/ΔDBD coexpression. Nur77/ΔDBD coexpression also did not modify binding of these epitope-specific antibodies to Bcl-2/ΔLoop (Supplemental Figure S3 available on *Cell* website). The Nur77/ΔDBD-induced change in Bcl-2 conformation was also observed in PBLs (Figure 7B and Supplemental Figure S4 available on *Cell* website).

Second, the effects of Nur77/ΔDBD on Bcl-2 conformation were studied using immunoprecipitation assays. These experiments showed that coexpression of Nur77/ΔDBD reduced binding of Bcl-2 to the αBcl-2/BH3-

(D) Nur77/ΔDBD targets mitochondria in PBLs. pDsRed2-Mito and GFP or GFP-Nur77/ΔDBD (1 μg each) were cotransfected into PBLs. GFP-Nur77/ΔDBD and pDsRed2-Mito were visualized as described in (A). Approximately 30% of the transfected cells showed the pattern presented.
(E) Nur77/ΔDBD induces apoptosis of PBLs. GFP or GFP-Nur77/ΔDBD (2 μg) was transfected into PBLs for 18 hr. The transfected (GFP-positive) cell subpopulation was identified by flow cytometry (Kolluri et al., 1999). The apoptotic cells in the transfected (green histogram) and nontransfected (purple histogram) cells were identified by Annexin-V-PE staining. The numbers represent % of transfected cells showing Annexin-V staining compared to nontransfected cells from the same culture dish.
(F) Bcl-2 is required for Nur77/ΔDBD-induced apoptosis. GFP-Nur77/ΔDBD (1 μg) was cotransfected into PBLs with control oligonucleotides or Bcl-2 antisense oligonucleotides (2 μg). After 48 hr, apoptotic cells were determined as described for (E). Bars represent average ± means from two measurements.
(G) Interaction of Nur77 with Bcl-2 is required for apoptotic effect of Nur77/Bcl-2 coexpression. The indicated Nur77 mutant (6 μg) was transfected with empty or Bcl-2 expression vector (2 μg) into HEK293T cells. After 36 hr, apoptotic cells were determined by DAPI staining.
(H) Effect of Bcl-2 mutations on the apoptotic effect of Bax. HEK293T cells were transfected with the indicated expression vectors and apoptotic cells were determined by DAPI staining.
(I) Effect of Bcl-2 mutations on the apoptotic effect of Nur77/Bcl-2 coexpression. Bcl-2 or a mutant was transfected with GFP or GFP-Nur77/ΔDBD into HEK293T cells. Apoptosis wan then determined by DAPI staining. Bars in (G)–(I) are means ± SD from three independent experiments.

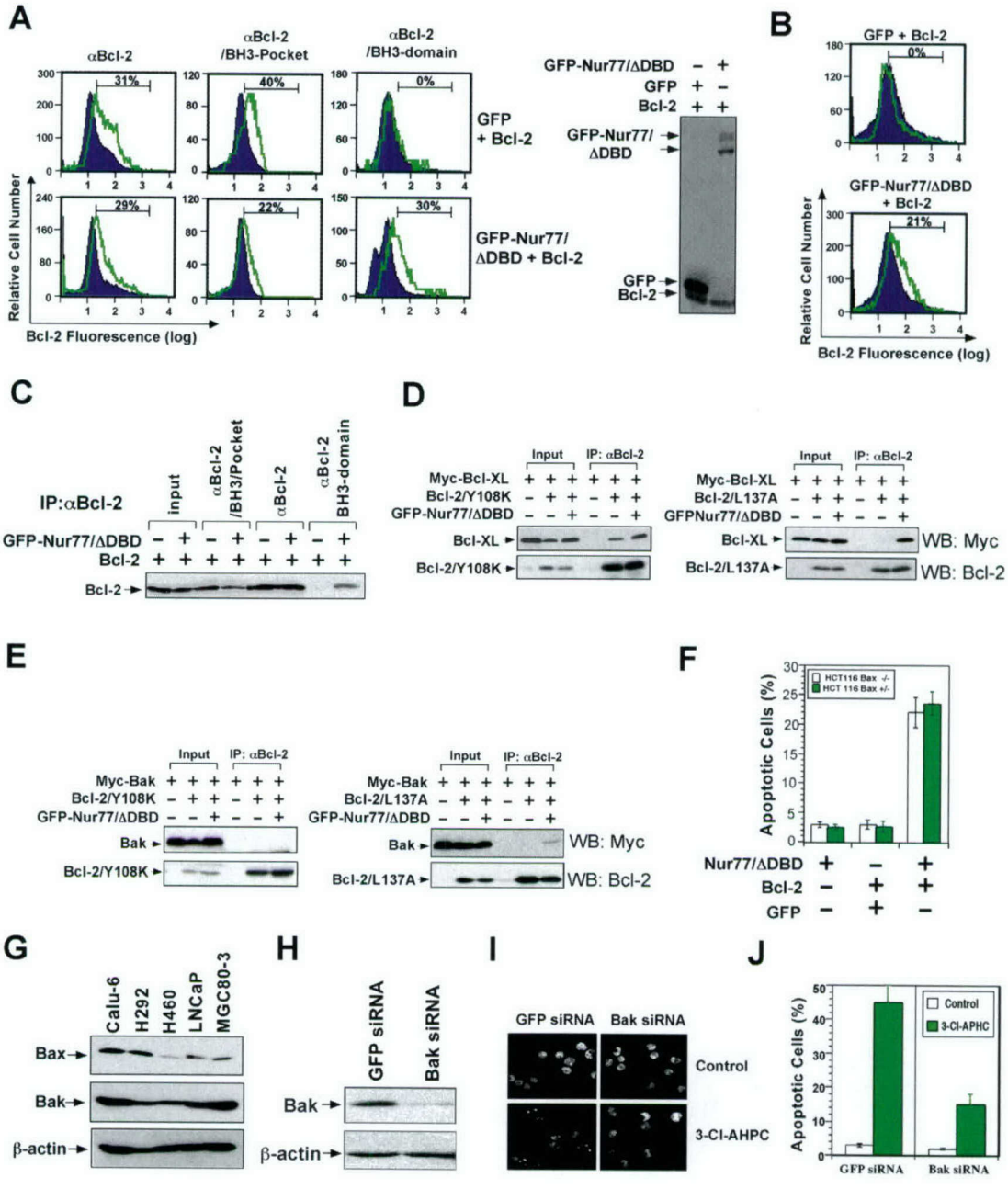

Figure 7. Interaction of Nur77 with Bcl-2 Induces Bcl-2 Conformational Change

(A) Nur77 induces change in Bcl-2 conformation. Bcl-2 (5 μg) was cotransfected into HEK293T cells with GFP or GFP-Nur77/ΔDBD (5 μg) for 14 hr. Portion of the transfected cells were subjected to immunoblotting to confirm similar expression of Bcl-2 in the two samples (right). The remaining cells were divided into three different pools, which were immunostained with three different anti-Bcl-2 antibodies: αBcl-2, αBcl-2/BH3-pocket (BD Transduction Labs), and αBcl-2/BH3 domain (Abgent), followed by SRPD-conjugated secondary antibody (Southern Biotech). Transfected (GFP-positive) cells were identified by flow cytometry. Bcl-2 fluorescence from the transfected cells (green histogram) was compared to that from the nontransfected cells (purple histogram). Similarly fluorescing cells were gated to compare Bcl-2 immunofluorescence after GFP or GFP-Nur77/ΔDBD coexpression. Numbers represent % of transfected cells showing Bcl-2 immunofluorescence compared to the autofluorescence of the nontransfected cells from the same transfection.

(B) Change of Bcl-2 conformation by Nur77/ΔDBD in PBLs. Bcl-2 (1 μg) was cotransfected into PBLs with GFP or GFP-Nur77/ΔDBD (1 μg). A portion of the cells were subjected to immunoblotting (Supplemental Figure S4 available on *Cell* website). The remaining cells were immunostained with αBcl-2/BH3-domain antibody 10 hr after transfection as described in (A).

(C) Nur77/ΔDBD modulates immunoprecipitation of Bcl-2 by epitope-specific anti-Bcl-2 antibodies. HEK293T cells were transfected with the indicated expression vector. After 18 hr, cells lysates were prepared and incubated with the indicated anti-Bcl-2 antibody for immunoprecipitation. Immunoprecipitates were subjected to immunoblotting using anti-Bcl-2 antibody (Santa Cruz).

(D) Alteration of Bcl-2 interaction with Bcl-X_L by Nur77/ΔDBD. The indicated Bcl-2 mutant and Bcl-X_L were coexpressed with or without GFP-Nur77/ΔDBD in HEK293T cells. Lysates were immunoprecipitated by anti-Bcl-2 antibody, and immunoprecipitates examined by immunoblotting using anti-Myc or anti-Bcl-2 antibody.

(E) Alteration of Bcl-2 interaction with Bak by Nur77/ΔDBD. The indicated Bcl-2 mutant and Bak were coexpressed with or without GFP-

pocket antibody, but enhanced binding of Bcl-2 to the αBcl-2/BH3-domain antibody. In contrast, Nur77/ΔDBD did not affect the immunoprecipitation efficiency of the αBcl-2 antibody (Figure 7C). Together, these results demonstrate that Nur77 binding induces a Bcl-2 conformational change that exposes its BH3 domain.

Proapoptotic BH3-only members of the Bcl-2 family induce apoptosis by binding to other Bcl-2 family members through their BH3 domains (Huang and Strasser, 2000; Kelekar and Thompson, 1998). We therefore examined whether Nur77 binding alters the ability of Bcl-2 to bind Bcl-X_L or Bak (Figures 7D-7E). At least when assessed in detergent containing cell lysates by Co-IP, Bcl-2 bound Bcl-X_L and Bak independently of Nur77 (data not shown). To address whether Bcl-2 bound differently to Bcl-X_L and Bak in the presence of Nur77/ΔDBD, two Bcl-2 mutants were analyzed. Bcl-2/L137A, a BH3 binding pocket mutant that retained killing activity in the presence of Nur77/ΔDBD, interacted with Bcl-X_L and Bak only when Nur77/ΔDBD was coexpressed. In contrast, binding of Bcl-X_L and Bak to the Bcl-2/Y108K BH3 domain mutant was unaffected by coexpression of Nur77 (Figures 7D and 7E). Thus, Nur77 binding may result in altered association of Bcl-2 with other Bcl-2 family members. Moreover, the observation that Bcl-2/L137A, but not Bcl-2/Y108K, was capable of killing cells in collaboration with Nur77/ΔDBD (Figure 6I) suggests that exposure of the BH3 domain of Bcl-2 may be responsible for the conversion of Bcl-2 to a proapoptotic molecule.

The above data suggest that Bcl-2, upon Nur77 binding, induces apoptosis through its BH3 domain. BH3-only proteins exert their apoptotic effects through either Bax or Bak. We therefore examined the involvement of Bax and Bak in Bcl-2-dependent apoptosis induced by Nur77. Coexpression of Nur77/ΔDBD and Bcl-2 resulted in a similar degree of apoptosis in HCT116 cells and HCT116 cells lacking Bax (HCT116 $Bax^{-/-}$) (Figure 7F), suggesting that expression of Bax is not crucial. This was also supported by the observation that H460 cells, which underwent extensive apoptosis in response to 3-Cl-AHPC (Supplemental Figure S1 available on *Cell* website), expressed only trace levels of Bax (Figure 7G).

To determine whether Bak, which was highly expressed in H460 cells (Figure 7G), plays a role in Bcl-2-dependent apoptosis induced by Nur77, we examined the effects of suppressing endogenous Bak expression. Significant reductions of Bak protein were observed when H460 cells were transfected with Bak siRNA but not control siRNA (Figure 7H), correlating with significant repression of Nur77-dependent 3-Cl-AHPC-induced apoptosis (Figures 7I–7J). Thus, Bcl-2-mediated apoptosis induced by Nur77 depends on multidomain proapoptotic Bcl-2-family proteins such as Bak.

Discussion

Despite lacking classical mitochondria-targeting sequences, Nur77 translocates from the nucleus to mitochondria, in response to specific cell death stimuli, to trigger cyt *c* release and apoptosis. The results presented here provide evidence that Nur77 targets mitochondria through its interaction with Bcl-2, revealing a crosstalk between Nur77 nuclear receptor and the Bcl-2 signalings. Furthermore, our results demonstrate that the interaction provokes a proapoptotic phenotype of Bcl-2 by inducing a conformational change in Bcl-2 that results in exposure of its BH3 domain. Given that Bcl-2 has been shown to have proapoptotic phenotypes in a variety of contexts, it will be interesting to explore in the future whether Nur77 serves as the mediator of this phenotypic conversion versus other Bcl-2 binding proteins that may await discovery.

Our mutagenesis studies indicate that the loop region located between the BH4 and BH3 domains of Bcl-2 is required for Nur77 binding. Previous studies (Chang et al., 1997) demonstrated that the loop regions of Bcl-2 and Bcl-X_L act as an autoinhibitory domain that reduces the antiapoptotic function of Bcl-2 and Bcl-X_L. Our data suggest that this conserved loop segment found in the vertebrate orthologs of Bcl-2 and Bcl-X_L may also participate in converting the phenotype of Bcl-2 from a protector to a killer of cells. Intriguingly, deletion of the loop region of Bcl-2 blocks paclitaxel-induced apoptosis (Srivastava et al., 1999), thereby suggesting the requirement of the loop region for the apoptotic effect of certain anticancer drugs. Though controversial, paclitaxel may also bind directly to the Bcl-2 loop domain to exert its apoptotic effect (Rodi et al., 1999). For Bcl-X_L, deamidation of residues in its loop region is associated with down regulation of its antiapoptotic activity (Deverman et al., 2002). In another study, insulin receptor substrate (IRS) protein binds to the Bcl-2 loop region, enhancing rather than inhibiting its antiapoptotic function (Ueno et al., 2000). It would be interesting therefore to study whether Nur77 and IRS compete for binding to Bcl-2, exhibiting opposing effects on apoptosis.

The Bcl-2 family members can be divided into two functional subgroups based on whether the BH3 domain is available (Gross et al., 1999). Members with buried BH3 domains are antiapoptotic, while members having an exposed BH3 domain are proapoptotic. Our analysis

Nur77/ΔDBD in HEK293T cells. Lysates were immunoprecipitated by anti-Bcl-2 antibody, and immunoprecipitates examined by immunoblotting using anti-Myc or anti-Bcl-2 antibody.

(F) Absence of Bax does not impair the apoptotic effect of Nur77/ΔDBD. Nur77/ΔDBD and Bcl-2 alone and together were transfected into HCT116 cells (+/−) and HCT116 cells lacking Bax (−/−). After 36 hr, apoptotic cells were determined as in Figure 5D.

(G) Expression of Bax and Bak in cancer cell lines. Cell extracts prepared from the indicated cancer cell lines were analyzed for Bax and Bak expression by immunoblotting.

(H) Inhibition of Bak expression by Bak siRNA in H460 lung cancer cells. H460 cells were transfected with Bak siRNA or control GFP siRNA. After 48 hr, cell lysates were assayed by immunoblotting using anti-Bak antibody.

(I and J) Inhibition of endogenous Bak expression suppresses 3-Cl-AHPC-induced apoptosis. H460 cells were transfected with Bak siRNA or control GFP siRNA. After 36 hr, cells were treated with 3-Cl-AHPC (10^{-6} M) for 24 hr. Apoptosis was determined by DAPI staining (I) and scored (J) as in Figures 5C and 5D.

using epitope-specific anti-Bcl-2 antibodies revealed that Bcl-2 undergoes a conformational change upon Nur77 binding. Given that Nur77/ΔDBD binding reduced epitope availability for an anti-Bcl-2 antibody to the BH3 binding pocket and enhanced the epitope availability for an antibody to the BH3-domain (Figures 7A–7C), it is likely that Nur77 binding induces a rearrangement of the Bcl-2 hydrophobic crevice, resulting in exposure of the otherwise hidden BH3 domain. Such a notion is supported by our findings that the Bcl-2/L137A mutant exhibited enhanced binding to Bak or Bcl-X_L upon Nur77/ΔDBD coexpression, while the Bcl-2 BH3 domain mutant (Bcl-2/Y108K) failed to show such a response (Figures 7D–7E). Based on the observation that Bcl-2 can associate with Bak in Nur77-overexpressing cells, we speculate that Nur77-converted Bcl-2 may similarly function as an agonist of Bak, in addition to an antagonist of Bcl-X_L. Future mutagenesis studies will help to determine whether this hypothesis is correct. However, it is noteworthy that of the 15 known BH3-only proteins in humans and mice, Bid and Bim are the only members that are capable of binding and activating proapoptotic Bcl-2-family proteins Bax and Bak (Korsmeyer et al., 2000; Marani et al., 2002), suggesting a possible role for Bcl-2 when converted to a BH3-displaying killer.

Caspase-mediated cleavage within the loop domain of Bcl-2 converts it into a proapoptotic molecule (Cheng et al., 1997; Grandgirard et al., 1998). However, we do not believe that the Nur77-mediated conversion of Bcl-2 from a protector to a killer involves cleavage of the protein, because we observed no hints of Bcl-2 cleavage in Nur77 overexpressing cells by immunoblotting, and because a mutant of Bcl-2, in which the caspase cleavage site has been mutated (Asp34), remains functional in collaborating with Nur77 to induce apoptosis although with reduced activity (Supplemental Figure S5 available on *Cell* website). Since caspase-mediated or experimental removal of the BH4 domain converts Bcl-2 into a killer, it is conceivable that the BH4 domain of Bcl-2 functions as an inhibitory domain to prevent the exposure of the BH3 domain. Three-dimensional structure of Bcl-2 reveals an extensive interaction between the BH4 domain and the hydrophobic groove (Petros et al., 2001). Therefore, it is tempting to speculate that Nur77, by binding to the loop region in Bcl-2, prevents the inhibitory effect of the BH4 domain, acting as an allosteric regulator to induce a reorganization of the hydrophobic cleft in Bcl-2, leading to exposure of its BH3 domain. This conformational change may be responsible for the conversion of Bcl-2 from an antiapoptotic to a proapoptotic molecule.

Our observations may help explain the paradoxical association of high levels of Bcl-2 protein expression with favorable clinical outcome for patients with several types of cancer, including breast, colon, and nonsmall cell lung cancer (reviewed in Reed, 1996). Possibly, in these tumors, elevated Bcl-2 is a liability, due to conversion of Bcl-2 from an antiapoptotic to a proapoptotic protein through interactions with Nur77 or other proteins. Also, elevated levels of a Nur77-family member are associated with favorable responses to chemotherapeutic agents in patients (Shipp et al., 2002). Interestingly, accumulation of somatic mutations in the region of the *BCL-2* gene encoding the loop domain has also been seen during clinical progression of lymphomas (Tanaka et al., 1992), suggesting the possibility of escape from the conversion mechanism in some types of cancer. Importantly, the discovery of a mechanism for converting Bcl-2 from a protector to a killer might be exploited eventually for developing anticancer drugs that turn overexpression of endogenous Bcl-2, which occurs in approximately half of all human malignancies, into an advantage that promotes tumor cell apoptosis.

Experimental Procedures

(See Supplemental Data available on *Cell* website for detailed procedures)

Bcl-2 siRNAs and Antisense Oligonucleotides

The target siRNA SMARTpools for Bcl-2 and Bak and the siRNA oligonucleotide for Nur77 (5′-CAG UCC AGC CAU GCU CCU dTdT) were purchased from Dharmacon Research Inc. They were transfected into cells according to the manufacturer's recommendations. Bcl-2 antisense oligonucleotide targeting Bcl-2 and negative control oligonucleotides were obtained from Calbiochem.

Nur77/Bcl-2 Interaction Assays

Reporter gene and GST pull-down assays were described previously (Li et al., 2000; Wu et al., 1997). For the mammalian two-hybrid assays, pcDNA-Gal4TAD-Nur77, pcDNA-Gal4TAD-Nur77/ΔDBD, pcDNA-Gal4DBD-Bcl-2/ΔTM, and pcDNA-Gal4DBD-RXRα were cloned and used. For Co-IP assays, HEK293T cells were transiently transfected with various expression plasmids in the presence of caspase inhibitors (zVAD-fmk) to prevent degradation of Nur77 protein due to apoptosis. Antibodies used are: monoclonal mouse anti-GFP (Medical and Biological Laboratories), monoclonal mouse anti-HA (Roche Molecular Biochemicals), monoclonal mouse anti-FLAG (Sigma), monoclonal mouse anti-Myc (Santa Cruz), polyclonal rabbit anti-Nur77 (Active Motif), or monoclonal mouse anti-Bcl-2 (Santa Cruz).

Isolation and Transfection of Human Peripheral Blood Lymphocytes (PBLs)

PBLs were isolated from leukocyte-enriched buffy coats from San Diego Blood Bank by centrifuging on Ficoll-paque Plus (Amersham Pharmacia Biotech). The mononuclear cells were cultured in RPMI containing 10% FBS and 20 mM HEPES. Freshly isolated cells (10^7 cells) were transfected using the human T Cell Nucleofector solution (Amaxa Biosystems) as per the procedure recommended by the manufacturer.

Acknowledgments

We thank L. Frazer for manuscript preparation; Lars Brive for helpful discussions; J. Kim, H. Li, A. Bhattacharya, Y. Altman, S. Williams, S. Kitada, H. Huynh, H. Zhang, X. Zhu, S. Krajewski, and J. Town for excellent technical assistance; and J. Stebbins for critical reading of the manuscript. HCT116 $Bax^{-/-}$ cells were a kind gift of B. Vogelstein. This work was in part supported by grants from the National Institutes of Health (CA87000, CA60988, and GM60554), U.S. Army Medical Research (USAMR) and Material Command, and California Tobacco-Related Diseases and the Breast Cancer Research Programs.

Received: July 30, 2003
Revised: December 22, 2003
Accepted: January 8, 2004
Published: February 19, 2004

References

Adams, J.M., and Cory, S. (1998). The Bcl-2 protein family: arbiters of cell survival. Science *281*, 1322–1326.

Chang, B.S., Minn, A.J., Muchmore, S.W., Fesik, S.W., and Thomp-

son, C.B. (1997). Identification of a novel regulatory domain in Bcl-X(L) and Bcl-2. EMBO J. *16*, 968–977.

Chen, J., Flannery, J.G., LaVail, M.M., Steinberg, R.H., Xu, J., and Simon, M.I. (1996). bcl-2 overexpression reduces apoptotic photoreceptor cell death in three different retinal degenerations. Proc. Natl. Acad. Sci. USA *93*, 7042–7047.

Cheng, E.H., Kirsch, D.G., Clem, R.J., Ravi, R., Kastan, M.B., Bedi, A., Ueno, K., and Hardwick, J.M. (1997). Conversion of Bcl-2 to a Bax-like death effector by caspases. Science *278*, 1966–1968.

Colussi, P.A., Quinn, L.M., Huang, D.C., Coombe, M., Read, S.H., Richardson, H., and Kumar, S. (2000). Debcl, a proapoptotic Bcl-2 homologue, is a component of the Drosophila melanogaster cell death machinery. J. Cell Biol. *148*, 703–714.

Deverman, B.E., Cook, B.L., Manson, S.R., Niederhoff, R.A., Langer, E.M., Rosova, I., Kulans, L.A., Fu, X., Weinberg, J.S., Heinecke, J.W., et al. (2002). Bcl-xL deamidation is a critical switch in the regulation of the response to DNA damage. Cell *111*, 51–62.

Fannjiang, Y., Kim, C.H., Huganir, R.L., Zou, S., Lindsten, T., Thompson, C.B., Mito, T., Traystman, R.J., Larsen, T., Griffin, D.E., et al. (2003). BAK alters neuronal excitability and can switch from anti- to pro-death function during postnatal development. Dev. Cell *4*, 575–585.

Grandgirard, D., Studer, E., Monney, L., Belser, T., Fellay, I., Borner, C., and Michel, M.R. (1998). Alphaviruses induce apoptosis in Bcl-2-overexpressing cells: evidence for a caspase-mediated, proteolytic inactivation of Bcl-2. EMBO J. *17*, 1268–1278.

Green, D.R., and Reed, J.C. (1998). Mitochondria and apoptosis. Science *281*, 1309–1312.

Griffiths, G.J., Dubrez, L., Morgan, C.P., Jones, N.A., Whitehouse, J., Corfe, B.M., Dive, C., and Hickman, J.A. (1999). Cell damage-induced conformational changes of the pro-apoptotic protein Bak in vivo precede the onset of apoptosis. J. Cell Biol. *144*, 903–914.

Gross, A., McDonnell, J.M., and Korsmeyer, S.J. (1999). BCL-2 family members and the mitochondria in apoptosis. Genes Dev. *13*, 1899–1911.

Guo, B., Godzik, A., and Reed, J.C. (2001). Bcl-G, a novel pro-apoptotic member of the Bcl-2 family. J. Biol. Chem. *276*, 2780–2785.

Holmes, W.F., Soprano, D.R., and Soprano, K.J. (2002). Elucidation of molecular events mediating induction of apoptosis by synthetic retinoids using a CD437-resistant ovarian carcinoma cell line. J. Biol. Chem. *277*, 45408–45419.

Holmes, W.F., Soprano, D.R., and Soprano, K.J. (2003). Comparison of the mechanism of induction of apoptosis in ovarian carcinoma cells by the conformationally restricted synthetic retinoids CD437 and 4-HPR. J. Cell. Biochem. *89*, 262–278.

Huang, D.C., and Strasser, A. (2000). BH3-Only proteins-essential initiators of apoptotic cell death. Cell *103*, 839–842.

Igaki, T., Kanuka, H., Inohara, N., Sawamoto, K., Nunez, G., Okano, H., and Miura, M. (2000). Drob-1, a Drosophila member of the Bcl-2/CED-9 family that promotes cell death. Proc. Natl. Acad. Sci. USA *97*, 662–667.

Kastner, P., Mark, M., and Chambon, P. (1995). Nonsteroid nuclear receptors: what are genetic studies telling us about their role in real life? Cell *83*, 859–869.

Kelekar, A., and Thompson, C.B. (1998). Bcl-2-family proteins: the role of the BH3 domain in apoptosis. Trends Cell Biol. *8*, 324–330.

Kolluri, S.K., Weiss, C., Koff, A., and Gottlicher, M. (1999). p27(Kip1) induction and inhibition of proliferation by the intracellular Ah receptor in developing thymus and hepatoma cells. Genes Dev. *13*, 1742–1753.

Kolluri, S.K., Bruey-Sedano, N., Cao, X., Lin, B., Lin, F., Han, Y.-H., Dawson, M.I., and Zhang, X.K. (2003). Mitogenic effect of orphan receptor TR3 and its regulation by MEKK1 in lung cancer cells. Mol. Cell. Biol. *23*, 8651–8667.

Korsmeyer, S.J., Wei, M.C., Saito, M., Weiler, S., Oh, K.J., and Schlesinger, P.H. (2000). Pro-apoptotic cascade activates BID, which oligomerizes BAK or BAX into pores that result in the release of cytochrome c. Cell Death Differ. *7*, 1166–1173.

Lee, J.M., Lee, K.H., Weidner, M., Osborne, B.A., and Hayward, S.D. (2002). Epstein-Barr virus EBNA2 blocks Nur77-mediated apoptosis. Proc. Natl. Acad. Sci. USA *99*, 11878–11883.

Lewis, J., Oyler, G.A., Ueno, K., Fannjiang, Y.R., Chau, B.N., Vornov, J., Korsmeyer, S.J., Zou, S., and Hardwick, J.M. (1999). Inhibition of virus-induced neuronal apoptosis by Bax. Nat. Med. *5*, 832–835.

Li, Y., Lin, B., Agadir, A., Liu, R., Dawson, M.I., Reed, J.C., Fontana, J.A., Bost, F., Hobbs, P.D., Zheng, Y., et al. (1998). Molecular determinants of AHPN (CD437)-induced growth arrest and apoptosis in human lung cancer cell lines. Mol. Cell. Biol. *18*, 4719–4731.

Li, H., Kolluri, S.K., Gu, J., Dawson, M.I., Cao, X., Hobbs, P.D., Lin, B., Chen, G., Lu, J., Lin, F., et al. (2000). Cytochrome c release and apoptosis induced by mitochondrial targeting of nuclear orphan receptor TR3. Science *289*, 1159–1164.

Liu, Z.G., Smith, S.W., McLaughlin, K.A., Schwartz, L.M., and Osborne, B.A. (1994). Apoptotic signals delivered through the T-cell receptor of a T-cell hybrid require the immediate-early gene nur77. Nature *367*, 281–284.

Liu, S., Wu, Q., Ye, X.F., Cai, J.H., Huang, Z.W., and Su, W.J. (2002). Induction of apoptosis by TPA and VP-16 is through translocation of TR3. World J. Gastroenterol. *8*, 446–450.

Mangelsdorf, D.J., and Evans, R.M. (1995). The RXR heterodimers and orphan receptors. Cell *83*, 841–850.

Marani, M., Tenev, T., Hancock, D., Downward, J., and Lemoine, N.R. (2002). Identification of novel isoforms of the BH3 domain protein Bim which directly activate Bax to trigger apoptosis. Mol. Cell. Biol. *22*, 3577–3589.

Nechushtan, A., Smith, C.L., Hsu, Y.T., and Youle, R.J. (1999). Conformation of the Bax C-terminus regulates subcellular location and cell death. EMBO J. *18*, 2330–2341.

Petros, A.M., Medek, A., Nettesheim, D.G., Kim, D.H., Yoon, H.S., Swift, K., Matayoshi, E.D., Oltersdorf, T., and Fesik, S.W. (2001). Solution structure of the antiapoptotic protein bcl-2. Proc. Natl. Acad. Sci. USA *98*, 3012–3017.

Reed, J.C. (1996). Mechanisms of Bcl-2 family protein function and dysfunction in health and disease. Behring Inst. Mitt. *97*, 72–100.

Reed, J.C. (1998). Bcl-2 family proteins. Oncogene *17*, 3225–3236.

Rodi, D.J., Janes, R.W., Sanganee, H.J., Holton, R.A., Wallace, B.A., and Makowski, L. (1999). Screening of a library of phage-displayed peptides identifies human bcl-2 as a taxol-binding protein. J. Mol. Biol. *285*, 197–203.

Sattler, M., Liang, H., Nettesheim, D., Meadows, R.P., Harlan, J.E., Eberstadt, M., Yoon, H.S., Shuker, S.B., Chang, B.S., Minn, A.J., et al. (1997). Structure of Bcl-xL-Bak peptide complex: recognition between regulators of apoptosis. Science *275*, 983–986.

Shipp, M.A., Ross, K.N., Tamayo, P., Weng, A.P., Kutok, J.L., Aguiar, R.C., Gaasenbeek, M., Angelo, M., Reich, M., Pinkus, G.S., et al. (2002). Diffuse large B-cell lymphoma outcome prediction by gene-expression profiling and supervised machine learning. Nat. Med. *8*, 68–74.

Srivastava, R.K., Mi, Q.S., Hardwick, J.M., and Longo, D.L. (1999). Deletion of the loop region of Bcl-2 completely blocks paclitaxel-induced apoptosis. Proc. Natl. Acad. Sci. USA *96*, 3775–3780.

Subramanian, T., and Chinnadurai, G. (2003). Pro-apoptotic activity of transiently expressed BCL-2 occurs independent of BAX and BAK. J. Cell. Biochem. *89*, 1102–1114.

Tanaka, S., Louie, D., Kant, J., and Reed, J.C. (1992). Application of a PCR-mismatch technique to the BCL-2 gene: detection of point mutations in BCL-2 genes of malignancies with A t(14,18). Leukemia *6* (*Suppl 3*), 15S–19S.

Uemura, H., and Chang, C. (1998). Antisense TR3 orphan receptor can increase prostate cancer cell viability with etoposide treatment. Endocrinology *139*, 2329–2334.

Ueno, H., Kondo, E., Yamamoto-Honda, R., Tobe, K., Nakamoto, T., Sasaki, K., Mitani, K., Furusaka, A., Tanaka, T., Tsujimoto, Y., et al. (2000). Association of insulin receptor substrate proteins with Bcl-2 and their effects on its phosphorylation and antiapoptotic function. Mol. Biol. Cell *11*, 735–746.

Uhlmann, E.J., Subramanian, T., Vater, C.A., Lutz, R., and Chinna-

durai, G. (1998). A potent cell death activity associated with transient high level expression of BCL-2. J. Biol. Chem. *273*, 17926–17932.

Vander Heiden, M.G., and Thompson, C.B. (1999). Bcl-2 proteins: regulators of apoptosis or of mitochondrial homeostasis? Nat. Cell Biol. *1*, E209–E216.

Wilson, A.J., Arango, D., Mariadason, J.M., Heerdt, B.G., and Augenlicht, L.H. (2003). TR3/Nur77 in colon cancer cell apoptosis. Cancer Res. *63*, 5401–5407.

Winoto, A., and Littman, D.R. (2002). Nuclear hormone receptors in T lymphocytes. Cell *109* (*Suppl*), S57–S66.

Woronicz, J.D., Calnan, B., Ngo, V., and Winoto, A. (1994). Requirement for the orphan steroid receptor Nur77 in apoptosis of T-cell hybridomas. Nature *367*, 277–281.

Wu, Q., Li, Y., Liu, R., Agadir, A., Lee, M.O., Liu, Y., and Zhang, X. (1997). Modulation of retinoic acid sensitivity in lung cancer cells through dynamic balance of orphan receptors nur77 and COUP-TF and their heterodimerization. EMBO J. *16*, 1656–1669.

Wu, Q., Liu, S., Ye, X.F., Huang, Z.W., and Su, W.J. (2002). Dual roles of Nur77 in selective regulation of apoptosis and cell cycle by TPA and ATRA in gastric cancer cells. Carcinogenesis *23*, 1583–1592.

Xue, D., and Horvitz, H.R. (1997). Caenorhabditis elegans CED-9 protein is a bifunctional cell-death inhibitor. Nature *390*, 305–308.

Zamzami, N., and Kroemer, G. (2001). The mitochondrion in apoptosis: how Pandora's box opens. Nat. Rev. Mol. Cell Biol. *2*, 67–71.

Zhang, X.K. (2002). Vitamin A and apoptosis in prostate cancer. Endocr. Relat. Cancer *9*, 87–102.

Nuclear Export and Mitochondrial Targeting of Nur77/TR3 Are Regulated by Retinoid X Receptor

Xihua Cao, Wen Liu, Feng Lin, Hui Li, Siva Kumar Kolluri, Bingzhen Lin, Young-hoon Han, Marcia I. Dawson, and Xiao-kun Zhang

The Burnham Institute Cancer Center
10901 N. Torrey Pines Road
La Jolla, CA 92037
U.S.A.

Running Title: Regulation of Nur77 apoptotic pathway by RXRα.

Key Words: Retinoid X Receptor; Nur77; Nuclear Export; Mitochondrial Targeting; Apoptosis.

Corresponding author:

Xiao-kun Zhang, Ph.D.
The Burnham Institute
Cancer Center
10901 N. Torrey Pines Road
La Jolla, CA 92037
USA
Phone: 858-646-3141
Fax: 858-646-3195
e-mail: xzhang@burnham-inst.org

ABSTRACT

Retinoid X receptor (RXR) plays a central role in the regulation of intracellular receptor signaling pathways by acting as a ubiquitous heterodimerization partner of many nuclear receptors, including the orphan receptor Nur77 (also known as TR3 or NGFI-B), which translocates from the nucleus to mitochondria, where it interacts with Bcl-2 to induce apoptosis. Here, we report that RXRα is required for nuclear export and mitochondrial targeting of Nur77 through their unique heterodimerization that is mediated by dimerization interfaces located in their DNA-binding domain. The effects of RXRα are attributed to a putative nuclear export sequence (NES) present in its carboxyl terminal region. RXRα ligands suppress NES activity by inducing RXRα homodimerization or altering RXRα/Nur77 heterodimerization. The RXRα NES is also silenced by RXRα heterodimerization with retinoic acid receptor (RAR) or vitamin D receptor (VDR). Consistently, we show that the mitochondrial targeting of the RXRα/Nur77 heterodimer and its induction of apoptosis are potently inhibited by RXR ligands. Together, our results reveal a novel nongenotropic function of RXRα and its involvement in the regulation of the Nur77-dependent apoptotic pathway.

INTRODUCTION

Retinoid X receptors (RXRs) belong to the nuclear receptor superfamily, consisting of a large number of ligand-regulated transcription factors that mediate the diverse physiological functions of their ligands, such as steroid hormones, retinoids, thyroid hormone, and vitamin D_3, in embryonic development, growth, differentiation, apoptosis, and homeostasis (29, 46). The superfamily also includes many orphan receptors whose ligands remain to be identified. All nuclear receptors consist of three major domains: the variable length N-terminal domain, the well-conserved DNA-binding domain (DBD) and the ligand-binding domain (LBD) (29, 46). The C-terminal LBD is multifunctional and, in addition to harboring a ligand binding site, contains regions for receptor dimerization and ligand-dependent transactivation function (AF-2). The DBD also contains a dimerization interface that determines target gene specificity (38, 55, 60, 85). RXRs mediate retinoid signaling through the RXR/retinoic acid receptor (RAR) heterodimer and the RXR/RXR homodimer (29, 46, 90). In addition, RXRs form heterodimers with many members of the subfamily 1 nuclear receptors, including vitamin D receptor (VDR), peroxisome proliferator-activated receptor (PPAR), and thyroid hormone receptor (TR), as well as several orphan receptors, such as liver X receptor (LXR), pregnane X receptor (PXR), constitutively activated receptor (CAR), and Nur77 (TR3 or NGFI-B) (29, 46). RXRs, therefore, play an essential role in the regulation of multiple nuclear hormone-signaling pathways through their unique and potent dimerization capacity. The vitamin A metabolite, 9-*cis*-retinoic acid (9-*cis*-RA), is a high-affinity ligand for RXRs (23, 39). It induces transactivation of the RXR homodimer (1, 29, 46, 89) and certain RXR heterodimers, such as the RXR/Nur77 heterodimer (17, 54).

Heterodimerization of RXR with its partners dramatically enhance their DNA binding and subsequently transcriptional regulation (29, 46, 90). On binding DNA, some nuclear receptors repress transcription of target genes through their interaction with transcriptional corepressors in the absence of ligands. Ligand binding by a transcriptional agonist causes a conformational change of receptors, allowing dissociation of transcriptional corepressors and association of transcriptional coactivators (80). In addition to DNA binding and interaction with receptor co-factors, recent studies suggest that subcellular distribution of RXR and its dimerization partners represents another mechanism that regulates their transcriptional activity. Despite being localized in the nucleus in many cell types, RXR (13, 27) and its partners, including RARs (13). TRs (3, 7, 93), VDR (57, 58) and NGFI-B/TR3/Nur77 (30, 40), were found in the cytoplasm in certain cell types and stages during development. Interestingly, RXR heterodimerization promotes nuclear localization of TR (3) and VDR (57).

Orphan receptor Nur77 (8, 21, 51) is an immediate-early response gene whose expression is rapidly induced by a variety of extracellular stimuli, including growth factors, the phorbol ester TPA and cAMP-dependent pathways. Nur77 and its closely related family members, Not-1 (also called Nurr1 and RNR-1) (36, 45) and NOR-1 (also called MINOR and TEC) (22, 52), constitute a distinct subfamily within the nuclear receptor superfamily (29, 46, 48). Nur77 was originally recognized for its role in cell proliferation and differentiation. Paradoxically, Nur77 was later found to be a potent pro-apoptotic molecule (47, 73, 84, 87). The expression of Nur77 was rapidly induced during the apoptosis of immature thymocytes and T-cell hybridomas as well as various types of cancer cells (25, 26, 28, 40, 41, 44, 62, 66, 74, 78). Overexpression of a dominant-negative Nur77 protein or inhibition of Nur77 expression by antisense Nur77 inhibited

apoptosis, whereas constitutive expression of Nur77 resulted in massive apoptosis (40, 41, 44, 66, 69, 74, 75).

Nur77 can function in the nucleus as a transcription factor to regulate the gene expression necessary to alter the cellular phenotype in response to various stimuli. Consistently, Nur77 response elements (NBRE or NurRE) have been identified (56, 72). In addition to its heterodimerization with RXR (17, 54), Nur77 can interact with the orphan receptor COUP-TF (77) that binds to the retinoic acid receptor β (RARβ) promoter and is required for efficient RARβ expression (42). Through its interaction with RXR and COUP-TF, Nur77 can modulate RARβ expression and the growth response of cells to retinoids (9, 77). Interestingly, the EWS/TEC (Nor-1) fusion protein generated by the t(9;22) chromosomal translocation in extraskeletal myxoid chondrosarcoma is about 270-fold more active than the native receptor in activating a reporter containing the NBRE (34, 35). This result suggests that the cancer-associated TEC (Nor-1) fusion receptor exerts its oncogenic activity by inducing the expression of target genes involved in cell proliferation. Thus, Nur77 may confer its growth-promoting activities through its action in the nucleus. This is supported by our recent observation that DNA binding and transactivation of Nur77 are required for its induction of cell proliferation (31).

Recent studies have demonstrated that Nur77 can also act outside the nucleus to mediate several important biological functions, including apoptosis and differentiation. Nur77, in response to apoptotic stimuli, translocates from the nucleus to the cytoplasm where it targets mitochondria to induce cytochrome *c* release and apoptosis (40). Our investigation of this phenomenon demonstrated that the pro-apoptotic effect of Nur77 does not require its transcriptional activity and DNA binding. Furthermore, Nur77 targets mitochondria through its interaction with Bcl-2, resulting in conversion of Bcl-2 from an anti-apoptotic to a pro-apoptotic molecule (43). Nur77 targets mitochondria in prostate cancer (40, 71), lung cancer (11, 31), colon cancer (71), ovarian cancer (25), and gastric cancer (28, 79) cells, and its mitochondrial localization is involved in Sindbis virus-induced apoptosis (37). The cytoplasmic action of Nur77 was also demonstrated by the translocation of NGFI-B from the nucleus to the cytoplasm in response to nerve growth factor (NGF) treatment in PC12 phaeochromocytoma cells, suggesting that the cytoplasmic action of NGFI-B is involved in NGF-induced PC12 cell differentiation (30). Thus, the diverse biological activities of Nur77 depend on its subcellular localization. The importance of TR3 pathways in regulating cancer cell growth is supported by the positive correlation between Nor-1 expression and survival in diffuse large B-cell lymphoma patients on chemotherapy (63)and a recent observation that TR3 is one of the 17-gene signature associated with metastasis of primary solid tumors (59).

Because Nur77 heterodimerizes with RXRα, we investigated the role of RXRα and its ligands in the regulation of the Nur77-dependent apoptotic pathway. Here, we report that RXRα migrates from the nucleus to mitochondria as a RXRα/Nur77 heterodimer in response to apoptotic stimuli. The migration is mediated by a putative nuclear export sequence (NES) present in the LBD of RXRα. The RXRα NES is active in the RXRα/Nur77 heterodimer formed through dimerization interfaces in their DBDs. Interestingly, in the presence of RXRα ligands, RXRα/Nur77 heterodimer is formed through dimerization interfaces in their LBD. Such a RXRα ligand-induced switch of RXRα/Nur77 heterodimerization interfaces silences the RXRα NES. Consistently, RXRα ligands effectively inhibit the mitochondrial targeting of the RXRα/Nur77 heterodimer and apoptosis. Together, our results demonstrate that RXRα and its

ligands plays a critical role in the regulation of the Nur77-dependent apoptotic pathway through their heterodimerization.

MATERIALS AND METHODS

Plasmid constructs. The construction of GFP-RXRα and Nur77 fusion as well as GFP-Nur77/ΔDBD and GFP-Nur77/Δ1 has been described (40). GFP-RXRα and GFP-Nur77 mutants were generated by cloning RXRα or Nur77 mutants into pGFP-N2 or pGFP-C2 vector (Clontech, USA). RXRα and Nur77 mutants, were generated by standard restriction enzyme digestion or amplified by polymerase chain reaction (PCR). The following oligonucleotides were used as primers: GAA GAT CTT CGA CAC CAA ACA TTT CCT GCC GCT C (upstream) and CGG AAT TCC GGC AGG CCT AAG TCA TTT GGT GCG G (downstream) for RXRα; CGG AAT TCC GTC GAG AGC CCC TTG GAG TCA GGG (downstream) for RXRα/385; CGG AAT TCC GCA AAG ATG GCG CCC ACC CCT GCG C (downstream) for RXRα/347; CCG GAA TTC CGG GAT GTG CTT GGT GAA GGA AGC (downstream) for RXRα/135; GAA GAT CTT CAC CAG CAG CGC CAA CGA GGA CAT G (upstream) and CGG AAT TCC GGC AGG CCT AAG TCA TTT GGT GCG G (downstream) for RXRα/C1; 5'-CGG GAT CCC GGT GCG CCA TCT GCG GGG ACC GC-3' (upstream) and 5'-CGG AAT TCG ACC CGC TTG TCA ATC AGG CAG TC-3' (downstream) for RXRα/182; 5'-CGG AAT TCG ACC ATG CCC ATG GCC ACG CAC TTC-3' (downstream) for RXRα/200; 5'-CGG AAT TCG ACG CCA CGC TGC CGC TCC TCC TG-3' (downstram) for RXRα/212; 5'-GAA GAT CTT CAT GCC CTG TAT CCA AGC CCA ATA TG-3' (upstream) and 5'-CGG AAT TCC GGC ACC AAG TCC TCC AGC TTG AGG TAG-3' (downstream) for Nur77; 5'-CGG AAT TCC GGT AGC ACC AGG CCT GAG CAG AAG ATG-3' (downstream) for Nur77/467; 5'-CGG AAT TCC GCG GAG AGC AGG TCG TAG AAC TGC TG (downstream) for Nur77/410; 5'-CGG AAT TCG CCC ACC GCC AGG CAC TTC TGG-3' (downstream) for Nur77/332; 5'-CGG AAT TCC GCT CCA CTG TGC GCT TGA AGA AGC CCT G-3' (downstream) for Nur77/296 ; 5'-CGG AAT TCC GGC AGG CCT TCG TAA GTC TGG CTG GGC (downstream) for Nur77/170. 5'-GAA GAT CTT CAT GGC CCT GTC CTC CAG TGG CTC TGA C-3' (upstream) for Nur77/Δ2. 5'-GAA GAT CTT CTC CGG TTC TCT GGA GGT CAT CCG C-3' (upstream) and 5'-CGG AAT TCC AGC ACC AGG CCT GAG CAG AAG ATG-3' (downstream) for Nur77/ΔC2, 5'-GAA GAT CTT CAT GGG CCT GGT GCT ACA CCG GCT G-3' (upstream) and 5'-CGG AAT TCC GGC ACC AAG TCC TCC AGC TTG AGG TAG-3' (downstream) for Nur77/ΔC3. BamH I and EcoRI fragment (324-462), BamH I and StuI fragment (324-402) and Bgl II and BamHI fragment (1-235) of RXRα were cloned into pGFP-C2 to generate GFP-RXRα/C2, GFP-RXRα/C3 and GFP-RXRα/235, respectively. Nur77 or RXRα mutants were also cloned into pcDNA3, pECE-Flag or pCMV-myc vector. For NES-RXRα, 5'-GAT CTT CAG GGT GCT GAC GGA GCT TGT GTC CAA GAT GCG GGA CAT GCA GAT GGA CAA GAC GGA GCT GGG CG-3' and AAT TCG CCC AGC TCC GTC TTG TCC ATC TGC ATG TCC CGC ATC TTG GAC ACA AGC TCC GTC AGC ACC CTG AA-3' were annealed and ligated into pGFP-C2. NESm-RXRα was generated with Quickchange site-directed mutagenesis kit (Stratagene) using primers 5'-AAG GCA CGG GAC GCA CAG ATG GAC AAG-3' and CTG TGC GTC CCG TGC CTT GGA CAC AAG-3'. RXRα/LLL was described previously (91). Bcl-2 expression vector and antibody were kindly provided by Dr. John C. Reed at our Institute.

RXRα siRNA. Small interfering RNAs (siRNAs) used in the experiments were obtained from Dharmacon Research Inc. The following siRNA sequence were used: RXRα siRNA, 5'

–AAG CAC UAU GGA GUG UAC AGC-3', 5'-GCU GUA CAC UCC AUA GUG CUU-3'. A 2.5 μl aliquot of 20 μmol/L siRNA/per well was transfected into cells grown in 12-well plates by using oligofectamine reagent (Invitrogen) according to manufacturer's recommendations. Two days after transfection the cells were harvested for Western blotting or performed for immunostaining.

Cell culture. LNCaP prostate cancer cells and H460 lung cancer cells were maintained in RPMI 1640 medium supplemented with 10% fetal bovine serum (FBS). CV-1 cells and HEK293T embryonic kidney cells were grown in DME medium supplemented with 10% FBS.

Protein-protein interaction assays. GST-pull-down and gel shift assays have been described previously (77, 88). For GST-pull-down assay, GST and GST-fusion proteins were expressed in *E. coli* BL21 and purified using glutathione-agarose affinity chromatography. The GST-fusion proteins were analyzed on 10% sodium dodecyl sulfate (SDS)-PAGE gels for integrity. ^{35}S-methionine labeled RXRα or Nur77 were produced by TNT-coupled transcription-translation system (Promega) and visualized by SDS-PAGE. *In vitro* binding assays were performed with glutathione-agarose beads (20 μl) coated with 10 μg of GST-fusion protein and 2-5 μl of ^{35}S-methionine-labelled protein in 200 of binding buffer (20 mM HEPES, pH 7.9, 100 mM KCI, 1 mM $MgC1_2$, 10 μM $ZnC1_2$ 2 mM DTT, 10% Glycerol, 0.05% Triton X-100 40 μg/ml Leupeptin). The reaction was allowed to proceed overnight at 4^{0}C with rocking. Beads were then collected by centrifugation and washed five times with 1 ml of NETN buffer (100 mM NaC1, 1 mM EDTA, 20 mM Tris-HCl, pH 8.0, 0.5% NP-40, 40 μg/ml Leupeptin). The beads were resuspended in 20 μl SDS PAGE sample buffer, boiled for 5 min. The eluted proteins were loaded in SDS-PAGE gel, dried and autoradiographed at –70^{0}C. For Co-immunoprecipitation assay, HEK 293T cells grown in 10-cm dish were transfected with 7.5 μg Flag-tagged TR3 and 7.5 μg GFP-tagged RXRα/385. Transfected HEK 293T cells were lysed in 300 μl of TAE buffer (10 mM Tris-HCI $_p$H 8.0, 10 mM NaC1, 10 mM EDTA, 1% NP-40, containing protease inhibitors (Sigma). Lysate (300 μl) was incubated with 2 μg of anti-Flag monocolonal antibody (M2, Sigma) at 4^{0}C for 2h. Immuno-complexes were then precipitated with 40 μl of protein A/G-sepharose (Santa Cruz). After extensive washing with TAE buffer, beads were boiled in 40 μl loading buffer and analyzed by Western blotting. Mouse IgG (Santa Cruz) was used as negative control.

Non-denaturing gel electrophoresis. Nuclear and cytoplasmic fractions of HEK293T cells expressing GFP-RXRα/C1 treated with or without 9-*cis*-RA were prepared and separated on a 8% non-denaturing Tris-Glycine Gel (Invitrogen) followed by immunoblotting.

Confocal microscopy. Cells were seeded on the chamber slides overnight and treated with apoptotic agents in medium containing 0.5% FBS. After treatments cells were fixed in 4% paraformaldehyde in PBS for 10 min and washed twice with PBS. Cells were then permeabilized with 1% triton X- 100 in PBS for 5 min. Fixed cells were pre-incubated for 30 min PBS containing 5% BSA at room temperature. Cells were stained with polyclonal anti-RXRα antibody (1:500 dilution) (D20, Santa Cruz) or monoclonal anti-Nur77 antibody (1:500 dilution)(Abgent) before detection of TITC-labeled anti-rabbit IgG (1:500 dilution)(Sigma). For mitochondrial staining, cells were incubated with anti-Hsp60 Goat IgG (1:500 dilution)(Santa Cruz), followed by anti-goat IgG conjugated with Cy3 (1:1000 dilution)(Sigma). For cytochrome *c* staining, cells were incubated with monoclonal anti-cytochrome *c* IgG (1:300 dilution)(Pharmingen), followed by anti-mouse IgG conjugated with Cy5 (1:500 dilution)(Amersham). For staining transfected protein, 1 μg of Myc-tagged TR3, Flag-tagged RXRα, or Bcl-2 was transfected into HEK293T cells grown in chamber slides in 6-well plates

overnight and treated with apoptotic agents. After treatment, cells were fixed and incubated with monoclonal anti-Myc IgG antibody (1:300 dilution)(9E10, Santa Cruz), followed by FITC-conjugated anti-mouse IgG (1:500 dilution)(Sigma) or Cy3 conjugated anti-mouse IgG (1:1000 dilution)(Sigma). For Bcl-2 staining, cells were incubated with polyclonal anti-Bcl-2 antibody (67), followed by Cy5-conjugated goat anti-rabbit antibody (1:500 dilution)(Sigma).

Cell fractionation. Subcellular fractionation was performed as described with minor modifications (40). Briefly, cells (1 x 10^7 cells) suspended in 0.5 ml hypotonic buffer (250 mM sucrose, 20 mM HEPES-KOH, pH 7.4, 10 mM KCl, 10 mM $MgCl_2$, 0.5 mM EGTA, 1.5 mM EDTA, pH 8.0, and 1 mM DTT) with proteinase inhibitors were homogenized, and cell extracts were centrifuged at 800 x g for 10 minutes. The pellet containing nuclei was resuspended in 200 µl 1.6 M sucrose in hypotonic buffer plus protease inhibitors and laid over 1 ml 2.0 M sucrose in the same buffer, then centrifuged at 150,000 x g for 90 minutes at 4°C to obtain the nuclear fraction. The supernatant was centrifuged at 10,000 x g for 30 minutes at 4°C to obtain the HM and cytosolic fractions. Nuclear and HM fractions were resuspended in 100 µl lysis buffer (10 mM Tris, pH 7.4, 150 mM NaCl, 1% Triton X-100, 5 mM EDTA, pH 8.0) with a cocktail of proteinase inhibitors for Western blotting analysis as described (40).

Transient transfection assays. Cells (1 x 10^5 cells/well) seeded in 24-well plates were transiently transfected using a modified calcium phosphate precipitation procedure, as described (42). For GFP studies, 1 µg of GFP or GFP constructs were transfected into cells seeded in 6-well plates by calcium phosphate precipitation.

Apoptosis assays. For TdT assay, cells were treated with or without indicated agents overnight after pretreatment of RXRα ligand 9-*cis*-RA or SR11237 for 12 hours, trypsinized washed with PBS and fixed in 1% formaldelyde and then resuspended in 70% ice-cold ethyl alcohol. Cells were then labeled with biotin-16-deocyuridine 5' triphosphate by terminal deoxynucleotidyltransferase and stained with avidinfluorescein isothiocyanante (Boehringer Mannheim). For nuclear morphological change analysis, LNCaP cells were trypsinized, washed with PBS, fixed with 3.7% paraformaldehyde, and stained with DAPI (4,6-diamidino-2-phenylindole) (50 µg/ml) to visualize nuclei by fluorescent microscopy.

Western blotting. Cell lysates were boiled in SDS sample buffer, resolved by SDS-polyacrylamide gel electrophoresis (12.5% polyacrylamide), and transferred to nitrocellulose. After transfer, the membranes were blocked in 5% milk in TBST (10 mM Tris-HCl, pH.8.0, 150 mM NaCl, 0.05% Tween 20) containing antibody. The membranes were then washed three times with TBST, then incubated for 1 h at room temperature in TBST containing horseradish peroxide-linked anti-immunoglobulin. After 3 washes in TBST, immunoreactive products were detected by chemiluminescence with an enhanced chemiluminescence system (ECL, Amersham). Anti-GFP antibody was purchased from Santa Cruz Bio.

RESULTS

RXRα targets mitochondria in response to apoptotic stimuli. Nur77 migrates from the nucleus to mitochondria to induce apoptosis in response to certain apoptotic stimuli (11, 25, 31, 37, 40, 71, 78). Since RXRα heterodimerizes with Nur77 (17, 54), we studied whether RXRα also targeted mitochondria. Subcellular localization of RXRα in LNCaP prostate cancer cells in the absence or presence of TPA, which potently induces LNCaP cell apoptosis (40), was

examined by confocal microscopy analysis. Immunostaining showed that RXRα predominantly localized in the nucleus in the absence of TPA treatment (Fig.1A). However, when cells were treated with TPA, RXRα was found in the cytoplasm. To study whether RXRα was associated with mitochondria, cells were stained for heat shock protein 60 (Hsp60), a mitochondria-specific protein (Fig. 1A). The extensive overlap in the distribution patterns of Hsp60 and RXRα suggested the association of RXRα with mitochondria. Similarly, treatment with TPA also resulted in mitochondrial localization of Nur77 (Fig. 1B), as previously reported (40). The enhanced staining of Nur77 in TPA-treated cells was due to induction of endogenous Nur77 expression by TPA. Thus, RXRα and Nur77 associate with mitochondria in LNCaP cells undergoing apoptosis.

RXRα and Nur77 mitochondrial targeting are mutually dependent. To study whether Nur77 and RXRα targeted mitochondria as a heterodimer, subcellular localization of Nur77 and RXRα was examined in LNCaP cells treated with or without TPA. In the absence of TPA, both Nur77 and RXRα resided mainly in the nucleus (Fig. 1C). However, when cells were treated with TPA, Nur77 and RXRα were colocalized in the cytoplasm and their distribution patterns overlaid extensively (Fig. 1C), suggesting their association in the cytoplasm. We also examined whether transfected RXRα and Nur77 targeted mitochondria in response to apoptosis induction. When expression vectors for RXRα and Nur77 were transfected into LNCaP cells, the expressed RXRα and Nur77 resided in the nucleus. However, when cells were treated with 3-Cl-AHPC, a apoptosis-inducing retinoid (92) both RXRα and Nur77 were found in the cytoplasm and their distributions overlaid (Fig. 1D). It is noteworthy that we have consistently observed that endogenous RXRα and Nur77 targeted mitochondria with much higher efficiency than the transfected receptors, suggesting the possible involvement of other protein factors in their targeting. We next determined whether RXRα cytoplasmic localization depended on Nur77 expression by examining its subcellular localization in LNCaP cells stably expressing Nur77 antisense RNA (40). Expression of Nur77 antisense RNA strongly inhibited TPA-induced Nur77 expression in LNCaP cells (40). In contrast to that observed in wild-type LNCaP cells (Fig. 1A), RXRα was found only in the nucleus in the Nur77 antisense stable clone, even though the cells were treated with TPA (Fig. 1E). To study whether Nur77 mitochondrial targeting required RXRα, we used the siRNA approach (15) to inhibit RXRα expression in LNCaP cells, then examined the subcellular localization of Nur77. Transfection of LNCaP cells with RXRα siRNA strongly reduced RXRα protein levels (Fig. 1F). In cells transfected with RXRα siRNA, Nur77 was mainly confined in the nucleus despite TPA treatment (Fig. 1F). Thus, cytoplasmic localization of Nur77 and RXRα is mutually dependent. We previously reported that Nur77 having its N-terminus deleted (Nur77/Δ1) acted as a dominant-negative mutant, which inhibited Nur77 mitochondrial targeting and apoptosis (40). Therefore, we examined whether Nur77/Δ1 also interfered with RXRα mitochondrial targeting. GFP-Nur77/Δ1 was transfected into LNCaP cells, which were then treated with TPA. RXRα immunostaining showed that RXRα was confined to the nucleus in cells transfected with GFP-Nur77/Δ1 in the absence or presence of TPA treatment (Fig. 1G). Thus, Nur77/Δ1 retained RXRα in the nucleus probably through their heterodimerization and the Nur77 N-terminal sequences are important for the TPA effect. It is noteworthy that the N-terminus of Nur77 is enriched with Serine, Threonine, and Tyrosine residues, suggesting the potential regulation of Nur77 activity by phosphorylation. To determine whether mitochondrial targeting of RXRα and Nur77 was specific to LNCaP cells and to the TPA treatment, we treated H460 lung cancer cells

with 3-Cl-AHPC that potently induced the apoptosis of lung cancer cells (data not shown). Similar to LNCaP cells, treatment of H460 cells with 3-Cl-AHPC resulted in extensive targeting of RXRα and Nur77 to mitochondria (Fig. 1H).

To further characterize the mitochondrial targeting of RXRα and Nur77, we conducted a time-course analysis of their targeting in LNCaP cells treated with TPA (Fig. 2A). Immunoblotting of mitochondria-enriched heavy membrane (HM) fractions showed that both RXRα and Nur77 began to be associated with mitochondria as early as 1 hour after cells were treated with the apoptotic stimulus. This result is consistent with our previous observation showing that Nur77 targeted mitochondria after LNCaP cells were treated with TPA for 1 hour (40). The simultaneous targeting of RXRα and Nur77 to mitochondria again suggested that they targeted mitochondria as a heterodimer. We previously reported that mitochondrial targeting of Nur77 initiated the release of cytochrome *c* from mitochondria (40). Consistently, we observed significant amounts of cytochrome *c* in the cytosolic fractions after LNCaP cells were treated with TPA for 1.5 hours. These results indicate that mitochondrial targeting of RXRα and Nur77 precedes the release of cytochrome *c*, further demonstrating the role of Nur77/RXRα mitochondrial targeting in triggering cytochrome *c* release. The requirement of RXRα in Nur77-dependent apoptosis is also illustrated by our observation that inhibition of RXRα expression by the expression of RXRα siRNA diminished the apoptotic effect of TPA in LNCaP cells (Fig. 2B). Similar results were also obtained in H460 lung cancer cells treated with 3-Cl-AHPC (Fig. 2C).

Subcellular localization of RXRα and Nur77 mutants. Previous studies showed that the cytoplasmic localization of NGFI-B and RXR was mediated through a CRM1-dependent nuclear export process (30). To study whether the translocation of the RXRα/Nur77 heterodimer from the nucleus to the cytoplasm is mediated through this process, we examined the effect of leptomycin B (LMB), an inhibitor of CRM1-dependent nuclear export (33). Treatment of LNCaP cells with LMB completely blocked TPA-induced cytoplasmic localization of both Nur77 and RXRα (Fig. 3A). This result suggests that the nuclear export of the RXRα/Nur77 heterodimer during apoptosis is mediated by a CRM1-dependent mechanism, similar to that observed for the RXR/NGFI-B heterodimer (30). To identify the putative nuclear export sequence (NES) responsible for the nuclear export of RXRα/Nur77 heterodimer, various Nur77 and RXRα mutants were constructed (Fig.3B) and fused to green fluorescent protein (GFP). The fusions were then transfected into HEK293T cells, and their cellular localization was examined by confocal microscopy (Fig. 3C). HEK293T cells were used for these studies because of their high transfection efficiency. GFP was equally distributed in both the nucleus and cytoplasm of HEK293T cells, indicating the absence of nuclear localization signal (NLS) and NES. GFP-Nur77 and GFP-RXRα, however, were found predominantly in the nucleus. The RXRα and Nur77 mutants with only the A/B domain, RXRα/135 and Nur77/170, were diffusely distributed in both the nucleus and cytoplasm. However, mutants that contain the A/B, C, and D domains and a portion of the E domain, RXRα/235, RXRα/347, Nur77/467 and Nur77/410, were confined to the nucleus, with the exception of RXRα/385 (see below). The nuclear localization of these mutants may reflect the presence of NLS in the DNA-binding domain (DBD) of the receptors (12). Indeed, a NLS was identified in the DBD of RXRα (57). Consistently, deletion of the DBD from Nur77 resulted in a mutant (Nur77/ΔDBD) that exclusively localized in the cytoplasm. Interestingly, C-terminus mutants of RXRα or Nur77, RXRα/C1, RXRα/C2, RXRα/C3, Nur77/ΔC2, and Nur77/ΔC3, were found predominantly in the cytoplasm.

Identification of a putative NES in RXRα. A previous study (30) demonstrated that the C-terminal half of Nur77 contains several NES sequences. To determine whether the cytoplasmic localization of the RXRα C-terminal-domain mutants was mediated by a CRM1-dependent mechanism, the effect of LMB on their cellular localization was examined (Fig. 4A). RXRα/C3 and RXRα/C2 accumulated exclusively in the cytoplasm of HEK293T cells. However, treatment with LMB resulted in their diffuse distribution (compare Fig. 3C and Fig. 4A). The inhibitory effect of LMB on the cytoplasmic localization of RXRα/C3 was further confirmed by immunoblotting of nuclear and cytoplasmic fractions prepared from HEK293T cells transfected with GFP-RXRα/C3. While GFP was equally distributed in both nuclear and cytoplasmic fractions (Fig. 4B), which is consistent with our confocal microscopy results (Fig. 3C), GFP-RXRα/C3 was only found in the cytoplasm (Fig. 4B). The exclusive cytoplasmic presence of GFP-RXRα/C3 was prevented when cells were treated with LMB (Fig. 4C). Our results are consistent with a previous observation that mutation of the RXRα NLS resulted in its predominant cytoplasmic localization (57) and suggest that RXRα/C3 contains an active NES.

The CRM1-dependent nuclear export is mediated by a Leu-rich NES (70). Inspection of RXR/C3 revealed the presence of a methionine-rich sequence, which had significant homology to previously identified NESs (Fig. 4D). To determine whether the RXRα sequence represented a putative NES, the DNA sequence representing the RXRα amino acids 348-368 was fused to GFP. The resulting GFP fusion, GFP-NES, was transfected into HEK293T cells. As shown in Fig. 4E, the GFP-NES protein was found exclusively in the cytoplasm, while the fusion was diffusely distributed in cells in the presence of LMB. Furthermore, replacing Met357 and Met360 in the NES with Ala (Fig. 4D) largely abolished its nuclear export activity (Fig. 4E). Thus, the RXRα amino acids 348-368 sequence represents a putative NES. This conclusion is also supported by our observation that GFP-RXRα/385 was exclusively localized in the cytoplasm, whereas removal of amino acid residues 348-385 from the mutant abolished its cytoplasmic localization, as indicated by the nuclear localization of GFP-RXRα/347 (Fig. 3C). To determine the role of the RXRα NES in mediating the nuclear export of Nur77 and RXRα, both Met357 and Met360 in full-length RXRα were replaced with Ala. The resulting mutant, RXRα/NESm, was cotransfected with Nur77 into LNCaP cells. Unlike RXRα and Nur77, which targeted mitochondria in response to 3-Cl-AHPC treatment (Fig. 1D), both RXRα/NESm and Nur77 remained in the nucleus despite 3-Cl-AHPC treatment (Fig. 4F). Thus, the RXRα NES is required for apoptosis-induced nuclear export of the RXRα/Nur77 heterodimer.

Our observation that RXRα/385 was exclusively confined to the cytoplasm even in the absence of an apoptotic stimulus (Fig. 3C) was intriguing since this mutant contains both the NLS and NES. This result suggests that removal of the C-terminal sequences (amino acid residues 386 to 462) strongly activates the RXRα NES and/or silences its NLS. To determine whether the superactivation of RXRα NES in RXRα/385 could confer cytoplasmic localization to Nur77, RXRα/385 was cotransfected into HEK293T cells with Nur77 or its mutant Nur77/Δ1 or Nur77/467, all of which alone resided in the nucleus (Fig. 3C). Our data showed that coexpression of RXRα/385 with Nur77 or either mutant resulted in their colocalization in the cytoplasm (Fig. 4G). The extensive colocalization of RXRα/385 with Nur77, Nur77/467, or Nur77/Δ1 suggests that they comigrated to the cytoplasm as a heterodimer. Thus, RXRα/385 was able to shuttle Nur77 to the cytoplasm. In contrast, Nur77/ΔC3 could not confer its cytoplasmic localization to RXRα when they were coexpressed (Fig. 4G). Thus, the RXRα NES plays a critical role in the nuclear export of the RXRα/Nur77 heterodimer.

Role of Bcl-2 in RXRα mitochondrial targeting. We recently reported that TR3 mitochondrial targeting requires its interaction with Bcl-2 (43). Therefore, we examined whether Bcl-2 expression modulated RXRα mitochondrial targeting. GFP-RXRα/385 was cotransfected with Bcl-2, and their distribution patterns were visualized by confocal microscopy. Fig. 5A shows that expression of Bcl-2 did not alter the diffuse distribution of GFP-RXRα/385. However, when Nur77 was cotransfected, GFP-RXRα/385 colocalized with both Nur77 and Bcl-2, as evidenced by punctate staining. This result indicated that Bcl-2 interacted with Nur77 but not RXRα. The requirement of Nur77 and Bcl-2 for RXR mitochondrial targeting was also illustrated by our cellular fractionation assay (Fig. 5B). GFP-RXRα/385 expressed in HEK293T cells did not show any accumulation in the mitochondria-enriched heavy membrane (HM) fraction in the absence or presence of Bcl-2 coexpression. However, when Nur77/Δ2, a Nur77 mutant lacking the N-terminal 122 amino acid residues, was coexpressed, significant amount of GFP-RXRα/385 was found in the HM fraction, while its cytosolic level decreased (Fig. 5B). Together, these results demonstrate that mitochondrial targeting of RXRα requires both Nur77 and Bcl-2 and that the RXRα/Nur77 heterodimer interacts with Bcl-2.

Mitochondrial targeting and apoptotic effect of RXRα and Nur77 mutants. To study the role of cytoplasmic mutants of Nur77 and RXRα in apoptosis, GFP-RXRα/C1, GFP-RXRα/385, GFP-Nur77/ΔC3, and GFP-Nur77/ΔDBD were transfected into LNCaP cells. Cells were then analyzed for nuclear morphological changes by DAPI staining (Fig. 6A). Interestingly, cells transfected with the Nur77 mutants exhibited extensive nuclear fragmentation and condensation, which are characteristics of apoptotic cells. In contrast, cells transfected with the RXRα mutants displayed normal nuclear morphology. Consistently, expression of Nur77/ΔDBD in LNCaP cells targeted mitochondria and triggered extensive cytochrome *c* release, while expression of RXR/C1 did not (Fig. 6B). The mitochondrial targeting of Nur77/ΔDBD in LNCaP cells but not in HEK293T cells likely reflects the expression of Bcl-2 in LNCaP cells but not in HEK293T cells (data not shown). Thus, the cytoplasmic Nur77 mutants are capable of targeting mitochondria and inducing cytochrome *c* release and apoptosis in LNCaP cells, whereas the RXRα mutants are not. These results suggest that RXRα may mainly act as a helper factor to facilitate the translocation of Nur77 from the nucleus to the cytoplasm.

Regulation of the RXRα NES activity by ligand binding and RXRα homodimerization. To determine whether RXRα ligands inhibited RXRα NES activity through their induction of RXRα dimerization (89, 91), we first examined their effects on the cytoplasmic accumulation of RXRα/C1 in HEK293T cells. Treatment of GFP-RXRα/C1-transfected cells with RXRα ligand 9-*cis*-RA or SR11237 resulted in the diffuse distribution of RXRα/C1 throughout the cells, whereas treatment with the RAR ligand *trans*-RA and RARα subtype-selective Am80 produced no such effect (Fig. 7A). The inhibitory effect of the RXR ligands on the cytoplasmic accumulation of RXRα/C1 was confirmed by immunoblotting analysis (Fig. 7B), which showed an equal distribution of GFP-RXRα/C1 in both cytoplasmic and nuclear fractions after cells were treated with 9-*cis*-RA or SR11237 but not with RARα ligand Am80. In contrast, GFP-RXRα/C1 was only found in the cytoplasm in nontreated cells.

We next examined the cellular distribution of GFP-RXRα/C1 expressed in HEK293T cells in the absence or presence of 9-*cis*-RA by nondenaturing polyacrylamide gel electrophoresis (PAGE). As is shown in Fig. 7C, GFP-RXRα/C1 was found only as a monomer in the cytoplasmic fraction. After cells were treated with 9-*cis*-RA, the monomeric form of GFP-RXRα/C1 in the cytoplasmic fraction disappeared, and only the homodimeric form was detected

only in the nuclear fraction. These studies demonstrate that monomeric RXRα exists in the cytoplasm, while liganded-homodimeric RXRα is in the nucleus. Thus, RXR ligands 9-*cis*-RA and SR11237 inhibit RXRα nuclear export probably by inducing RXRα homodimerization. We also analyzed the subcellular localization of two RXRα mutants, RXRα/385, which lacks the major homodimerization domain, and RXRα/LLL, which has Leu418, Leu420, and Leu430 in helix 10 replaced with Ala and fails to homodimerize in response to 9-*cis*-RA (91). Interestingly, both homodimerization-defective RXRα mutants were exclusively localized in the cytoplasm regardless of the presence of 9-*cis*-RA (Fig. 7D). We also used another RXRα mutant, RXRα/C1/C432A, to study the role of ligand in the regulation of RXRα subcellular localization. Cys432 is involved in the formation of RXRα ligand-binding pocket and primarily responsible for the shorter length of this L-shaped pocket compared to the linear RAR I-shaped pocket (14). Replacing Cys432 with Ala (RXRα/C1/C432A) impaired homodimerization in response to 9-*cis*-RA (data not shown). RXR/C1/C432A expressed in HEK293T cells was stained exclusively in the cytoplasm despite 9-*cis*-RA treatment (Fig. 7D). Together, these data demonstrate that subcellular localization of RXRα depends on its dimerization status and that homodimerization suppresses RXRα nuclear export.

Regulation of RXRα NES activity by heterodimerization. Heterodimerization of RXRα with other receptors, such as RAR and VDR, is required for their efficient DNA binding and transactivation (29, 46, 90). Therefore, we analyzed the subcellular localization of RXRα/VDR and RXRα/RAR heterodimers. GFP-RXRα was transfected alone or with either VDR (Fig. 8A) or RARα (Fig. 8B) into HEK293T cells. Without cotransfection, GFP-RXRα was distributed in both the cytoplasm and nucleus. However, on cotransfection of VDR or RARα, the cytoplasmic localization of GFP-RXRα was completely abolished and the levels of nuclear GFP-RXRα increased. Treatment of cells with the VDR ligand 1α,25-dihydroxyvitamin D_3 or the RAR ligand *trans*-RA did not further modulate the cellular distribution of cotransfected GFP-RXRα. The inhibitory effect of VDR was also examined by studying the subcellular localization of RXRα/C1 in the absence or presence of VDR coexpression. In the absence of VDR, RXRα/C1 exclusively localized in the cytoplasm of HEK293T cells. However, when VDR was cotransfected, RXRα/C1 was confined to the nucleus and its distribution pattern overlaid with that of VDR. Again, addition of 1α,25-dihydroxyvitamin D_3 had no effect on localization of both VDR and RXRα/C1 (Fig. 8C). Together, these results demonstrate that heterodimerization of RXRα with RAR and VDR suppresses RXRα NES activity in a ligand-independent manner.

Unique RXRα heterodimerization with Nur77. The above data demonstrate that RXRα NES activity was suppressed upon RXRα homodimerization and RXRα heterodimerization with VDR and RAR. Ironically, RXRα was required for the cytoplasmic localization of Nur77 through their heterodimerization. One possible explanation is that the RXRα/Nur77 heterodimer may be different from other RXRα heterodimers. Three types of RXR heterodimers have been described (29, 46). In some heterodimers, such as the RXR/VDR, RXR is a completely silent partner. In others, such as the RXR/RAR, RXR is a conditionally silent partner. In contrast, RXR acts as a fully active and competent partner of heterodimers with certain orphan receptors, such as Nur77 (17, 54). Heterodimerization of RXRα with RARα in solution largely depends on their dimerization interfaces localized in their LBD and has been mapped to a region in the carboxyl-terminus, corresponding to helices 9 and 10 in the canonical nuclear receptor LBD structure (6, 14, 18, 19). Results of studies on RXR/Nur77

heterodimerization that indicated different interaction modalities depending on systems and approaches (2, 61, 68) suggest that RXR and Nur77 may interact differently under different conditions. Our finding that RXRα/385 was able to shuttle Nur77/467 from the nucleus to the cytoplasm (Fig. 4G) suggests that RXRα may utilize regions other than the LBD C-terminus for binding Nur77. This possibility was studied by GST pull-down assays. Full-length RXRα was pulled-down by either GST-Nur77 or GST-RARα (Fig. 9A), whereas RXRα/385 was only pulled-down by GST-Nur77 but not by GST-RARα. Thus, in solution the RXRα C-terminus is required for its interaction with RARα but not with Nur77. Similarly, as Nur77/467 was effectively pulled-down by GST-RXRα (Fig. 9B), the Nur77 C-terminus was also dispensable for interaction with RXRα in solution. The interaction between RXRα/385 and Nur77 was also revealed by *in vivo* co-immunoprecipitation, which showed the efficient precipitation of GFP-RXRα/385 by anti-Flag antibody when Flag-Nur77 was coexpressed in HEK293T cells (Fig. 9C). In the reporter gene assays, both RXRα/385 and RXRα similarly inhibited the transactivation of Nur77 homodimer activity in the absence of 9-*cis*-RA (Fig. 9D). Addition of 9-*cis*-RA slightly enhanced the inhibitory effect of RXRα but not RXRα/385. The RXRα DBD also contains a dimerization interface (38, 55, 60, 85). To determine whether the dimerization interfaces in the DBDs of RXRα and Nur77 are involved in their heterodimerization in solution, several RXRα and Nur77 mutants were constructed (Fig. 9E), and analyzed for their interaction. The RXRα DBD alone (RXRα/135-200) was as efficient as the whole length RXRα in pulling down Nur77/467. Removal of the C-terminal portion from the RXRα DBD completely abolished its interaction with Nur77/467 (Fig. 9F). Similarly, Nur77 deleted with the D-E/F domains (Nur77/332) retained the ability to bind RXRα, while further deletion of the C-terminal portion from the Nur77 DBD completely abolished its ability to bind RXRα. Together, these results demonstrate that the dimerization interfaces in the DBDs of RXRα and Nur77 are mainly responsible for their interaction in solution.

Modulation of RXRα/Nur77 heterodimerization by RXR ligands. The RXR/Nur77 heterodimer binds and activates DNA sequences consisting of AGGTCA or like motifs arranged as a direct repeat with a 5-bp spacing (the DR-5 response element) (17, 54, 76). To characterize RXRα/Nur77 heterodimerization on DNA, gel-shift assays were conducted using the βRARE, a DR-5 element, as a probe (Fig. 10A). *In vitro* synthesized Nur77 and RXRα bound to the βRARE as a heterodimer (Fig. 10A), as reported previously (76, 77). However, when Nur77/467, which heterodimerizes with RXRα in solution (Fig. 9B), was incubated with RXRα, we did not detect any heterodimeric complex binding to the βRARE (Fig. 10A). Similarly, coincubation of RXRα/385 and Nur77 did not result in formation of a stable heterodimer on the βRARE (Fig. 10A). Thus, the C-termini of both Nur77 and RXRα are required for the formation of a stable RXRα/Nur77 heterodimer complex on the βRARE. This finding is also supported by our analysis of Nur77 mutants for their transactivation activity on the NurRE and βRARE (Fig. 10B). Removal of the Nur77 C-terminus did not affect its transactivation on NurRE as Nur77 and Nur77/467 similarly activated the NurRE (Fig. 10B). These results are consistent with recent reports that the major transactivation function of Nur77 is located in its N-terminus (68). In contrast, Nur77/467 failed to activate the βRARE on cotransfection with RXRα in either the absence or presence of RXR ligand SR11237, while cotransfection of full-length Nur77 and RXRα strongly activated the βRARE in response to SR11237 (Fig. 10B). The lack of transactivation activity displayed by Nur77/467 is likely a reflection of its inability to form βRARE bound heterodimers with RXRα (Fig. 10A).

To determine how RXR ligands influenced RXRα/Nur77 heterodimer binding to the βRARE, RXRα protein was exposed to its ligand SR11237 or 9-*cis*-RA prior to incubation with Nur77. Although the RXRα/Nur77 heterodimer bound to the βRARE in the absence of an RXR ligand, the addition of SR11237 or 9-*cis*-RA strongly enhanced binding by the heterodimer (Fig. 10C). These data suggest that RXRα/Nur77 heterodimers in solution may be incompetent for DNA binding and that RXR ligand binding may induce a C-terminal-stabilized heterodimer conformation that favors DNA binding. To address the possibility that an RXR ligand can modulate the RXRα/Nur77 heterodimerization interface, we used GST pull-down assays to study the effect of 9-*cis*-RA on the interaction between Nur77/467 and RXRα (Fig. 10D). Incubation of GST-RXRα with 9-*cis*-RA strongly reduced the ability of GST-RXRα to interact with Nur77/467, suggesting that 9-*cis*-RA binding may mask or alter a putative dimerization interface required for RXRα binding to Nur77 in solution. In comparison, the addition of 9-*cis*-RA did not affect the binding of RXRα/385 to GST-Nur77. Thus, the dimerization interface for the formation of the RXRα/Nur77 heterodimer in solution is different from that required for the formation of the DNA-bound heterodimer and is regulated by RXR ligand binding.

RXRα mitochondrial localization is inhibited by RXRα ligands. Inhibition of RXRα mitochondrial localization by its ligands was demonstrated by immunoblotting HM fractions from LNCaP cells. The accumulation of RXRα in the HM fraction after cells were treated with TPA or an analog of AHPN/CD437 (SR11453) (40) was inhibited by pretreatment with 9-*cis*-RA (Fig. 11A). Similar to its effect on RXRα, mitochondrial accumulation of Nur77 was also abolished by 9-*cis*-RA pretreatment (Fig. 11A). The observation that 9-*cis*-RA inhibited Nur77 mitochondrial targeting further suggests the role of RXRα in the regulation of Nur77 mitochondrial targeting.

Since RXRα comigrated with Nur77 from the nucleus to mitochondria in cells undergoing apoptosis, we investigated the effect of 9-*cis*-RA on cytochrome *c* release and apoptosis. Treatment of LNCaP cells with TPA induced the massive release of cytochrome *c* from mitochondria, as revealed by cytochrome *c* staining, which was diffusely distributed (Fig. 11B). However, on pretreatment with 9-*cis*-RA, cytochrome *c* staining was only detected in the mitochondria, as its distribution colocalized with that of Hsp60. LNCaP cells were also transfected with GFP-Nur77 to monitor the effect of 9-*cis*-RA on Nur77 mitochondrial targeting (Fig. 11B). TPA-induced cytochrome *c* release was accompanied with the mitochondrial localization of transfected GFP-Nur77. However, when cells were pretreated with 9-*cis*-RA, GFP-Nur77 was confined in the nucleus and cytochrome *c* release was inhibited (Fig. 11B). These data further demonstrate the role of Nur77 mitochondrial targeting in the induction of cytochrome *c* release and the inhibitory effect of RXR ligands on Nur77-dependent apoptosis. The inhibition of cytochrome *c* release by 9-*cis*-RA was further revealed by immunoblotting of cytosolic fractions prepared from LNCaP cells treated with TPA or the AHPN analog SR11453 (Fig. 11C). In the absence of 9-*cis*-RA, significant cytoplasmic cytochrome *c* was detected in treated cells, whereas pre-exposure of cells to 9-*cis*-RA prevented cytochrome *c* release (Fig. 11C). We also examined the effects of RAR and VDR ligands on mitochondrial localization of RXRα and Nur77 and cytochrome *c* release in LNCaP cells treated with 3-Cl-AHPC. Unlike the inhibitory effect of RXR ligand, treatment of LNCaP cells, which express RARs and VDR, with either RAR ligand Am80 or VDR ligand had no effect on 3-Cl-AHPC-induced mitochondrial localization of RXRα and Nur77 and cytochrome *c* release (Fig. 11D), in agreement with our co-transfection results (Fig. 8). Consistent with their effects on cytochrome *c* release, 9-*cis*-RA and SR11237 strongly antagonized the effect of SR11453 on mitochondrial membrane potential

change (Fig. 11E) and apoptosis of LNCaP cells revealed by DAPI staining (Fig. 11F) and the TdT assay (Fig. 11G). Thus, 9-*cis*-RA inhibits cytochrome *c* release and apoptosis in LNCaP cells by preventing nuclear export of the RXRα/Nur77 heterodimer.

DISCUSSION

We previously reported that Nur77 translocated from the nucleus to the cytoplasm where it targeted mitochondria to induce apoptosis (40). Our results presented here demonstrate that the translocation of Nur77 requires its heterodimerization with RXRα. This is illustrated by our observations that Nur77 and RXRα colocalized in the cytoplasm (Fig. 1C) and they targeted mitochondria simultaneously in LNCaP prostate cancer cells (Fig. 2). In addition, their mitochondrial targeting depended on their coexpression (Fig. 1). Moreover, expression of cytoplasmic RXRα mutant RXRα/385 conferred cytoplasmic localization to Nur77 (Fig. 4G), while overexpression of Nur77/Δ1 retained RXRα in the nucleus (Fig. 1G). These results are consistent with our observation that Nur77 mitochondrial targeting and its induction of cytochrome *c* release and apoptosis were suppressed by RXR ligands (Fig. 11). The translocation of the RXRα/Nur77 heterodimer from the nucleus to mitochondria is a rapid process, occurring one hour after cells are exposed to an apoptotic stimulus, and precedes the release of cytochrome *c* from mitochondria (Fig. 2). These results agree with our previous observation (40) and are consistent with the notion that the mitochondrial targeting of RXRα/Nur77 triggers apoptosis. Apoptosis induction by Nur77 mitochondrial targeting occurs in different types of cancer cells (11, 25, 28, 31, 37, 40, 43, 71, 79). Our results demonstrated that RXRα was also required for Nur77 translocation in H460 lung cancer cells (Fig. 1H, Fig. 2C). Thus, it is likely that RXRα and its ligands play a critical role in regulating Nur77-dependent apoptosis in various cancer cells.

We recently reported that Nur77 mitochondrial targeting is mediated through its interaction with Bcl-2, which mainly resides on the mitochondrial outer membrane (43). Consistently, Nur77 mutants, such as Nur77/ΔDBD, targeted mitochondria in LNCaP cells (Fig. 6B), which express Bcl-2, but not in HEK293T cells (Fig. 3C), which do not. Interestingly, mitochondrial targeting by RXRα occurred in HEK293T cells only when both Nur77 and Bcl-2 were coexpressed (Figs. 5A-B), while expression of Bcl-2 alone did not result in RXRα mitochondrial targeting. Transfection of Nur77 mutants, but not RXRα mutants, in LNCaP cells targeted mitochondria and induced apoptosis (Figs. 6A-B). These results suggest that RXRα does not interact with Bcl-2 rather functions as a shuttling protein in the Nur77-dependent apoptotic pathway.

The migration of RXRα/Nur77 heterodimers from the nucleus to the cytoplasm is CRM1-dependent. By extensive mutational analysis, we have identified a NES in the RXRα LBD that is required for the efficient nuclear export of RXRα and RXRα/Nur77 heterodimers (Fig. 7). A recent study suggested that NGFI-B has several NESs that are required for RXR/NGFI-B nuclear export in PC12 cells (30). The fact that RXRα also possesses a NES, which alone is capable of translocating GFP from the nucleus to the cytoplasm, offers an explanation for the efficient nuclear export of the RXRα/Nur77 heterodimer.

One unique property of the RXRα NES is that it lies in helix 7 of the RXR LBD, which undergoes an unusual conformational changes upon homodimerization, homotetramerization, and heterodimerization with RAR and PPAR (6, 18, 19). The RXRα helix 7 is an α-helix

structure in the RXRα monomer (5). However, in the context of RXRα dimer, tetramer, or heterodimer with PPARγ or RAR, a π–helix is formed due to the presence of a glutamic acid residue (E352) in the middle of the helix 7 (6, 18, 19). The transformation of helical geometry in the region, where the RXRα NES lies in, suggests that RXRα NES activity is subject to regulation by RXRα homodimerization and heterodimerization. Indeed, subcellular localization of RXRα is highly regulated by its dimerization. This finding is clearly illustrated by our analysis of RXRα distribution patterns using nondenaturing PAGE (Fig. 7C) that shows that RXRα/C1 existed as a monomer in the cytoplasm but in response to 9-*cis*-RA resided as a homodimer in the nucleus. RXRα mutants unable to homodimerize predominantly resided in the cytoplasm (Fig. 7D). Heterodimerization with certain nuclear receptors, including RARα and VDR, also suppressed RXR NES activity (Fig. 8). Thus, the RXRα NES is active in the RXRα monomer but is silenced by RXRα homodimerization and certain heterodimerizations. Such a conformational-change-mediated regulation of RXRα NES activity represents a unique regulatory mechanism that dictates subcellular localization of various RXRα homodimers and heterodimers, ultimately allowing efficient transcriptional regulation by RXRα homodimers and certain RXRα heterodimers. Our results are consistent with previous observations that RXRs play a critical role in determining nuclear localization of TR (3) and VDR (57, 58) through their heterodimerization.

Very intriguingly, heterodimers formed by RXRα and VDR or RAR reside in the nucleus, whereas RXRα/Nur77 is found in the cytoplasm when cells were treated with apoptotic stimuli (Fig. 1). Our results demonstrate that nuclear export of the RXRα/Nur77 heterodimer is due to its unique heterodimerization in solution (Figs. 9 and 10). RXR possesses two dimerization interfaces, which are located in the DBD and the LBD (55, 86). The strong dimerization interface in the LBD enables RXR homodimerization and heterodimerization with certain receptors, such as RAR and VDR in solution. In contrast, the weak dimerization interface in the DBD does not allow the formation of the RXR homodimer or heterodimer with RAR in the absence of a specific response element (60). Our data indicate that deletion of the major dimerization interface from the RXRα LBD (RXRα/385) did not impair the interaction of RXRα with Nur77 in solution, as revealed by an *in vitro* GST pull-down assay (Fig. 9A) and *in vivo* Co-IP assay (Fig. 9C), although the deletion completely abolished RXRα/385 interaction with RAR (Fig. 9A). Similarly, deletion of the C-terminal sequence from Nur77 had no effect on its interaction with RXRα (Fig. 9B). Our observation that the RXRα DBD alone was sufficient to interact with Nur77 (Fig. 9F) demonstrated that the formation of the RXRα/Nur77 heterodimer in solution is mediated by dimerization interfaces in their DBD. Given the fact that the RXRα NES is active in the RXRα monomer conformation, we envision that the unique RXRα/Nur77 heterodimer formed in solution through their DBD dimerization interfaces will ensure that the RXRα NES is situated is its active conformation, resulting in their nuclear export. This notion is consistent with our observation that RXRα/385 is able to shuttle Nur77 to the cytoplasm (Fig. 4G). Thus, the unique property of RXR dimerization interfaces allows cross-talk among RXR heterodimerization partners with respect to their subcellular localization and function (Fig. 8).

In contrast to their heterodimerization in solution, the C-terminal sequences of Nur77 and RXRα are required for the efficient binding of RXRα/Nur77 heterodimer to their specific response element βRARE (Fig. 10A) and transactivation (Fig. 10B), as is found for the RXR/RAR and RXR/TR heterodimers (88). Our observation that an RXR ligand can promote

RXRα/Nur77 heterodimer binding to the βRARE (Fig. 10C) is interesting since RXR ligands have not been previously shown to modulate DNA binding of other RXR heterodimers at least *in vitro* (88). This finding suggests that ligand binding can modulate RXRα/Nur77 interaction to favor DNA binding and transactivation. Such a modulation is reflected by the inhibition by 9-*cis*-RA of the heterodimerization of RXRα with Nur77/467 in solution (Fig. 10D). Thus, the induction of RXRα/Nur77 heterodimer DNA binding and transactivation by 9-*cis*-RA is associated with its inhibition of their DBD-mediated dimerization. It is tempting to speculate that ligand binding allows RXRα to interact with Nur77 through their LBD dimerization interfaces, which may silence the RXRα NES, as does RXR/VDR or RXR/RAR heterodimerization (Fig. 8). Thus, the nuclear export of the RXRα/Nur77 heterodimer may be suppressed by 9-*cis*-RA through its induction RXRα homodimerization or modulation of RXRα/Nur77 heterodimerization interfaces.

We found that RXR ligands 9-*cis*-RA and SR11237 effectively inhibited the release of cytochrome *c* induced by TPA or SR11453 in LNCaP cells (Fig. 11). As the inhibition was accompanied by the prevention of Nur77 and RXRα mitochondrial targeting (Fig. 11B), we suggest that RXR ligands suppress apoptosis by inhibiting mitochondrial targeting of RXRα/Nur77 heterodimer. The inhibitory effect of RXR ligands on apoptosis has been reported previously (4, 30, 65, 81-83). 9-*cis*-RA is known to potently inhibit the activation-induced apoptosis of T-cells and thymocytes (4, 30, 65, 81-83). The inhibitory effect of 9-*cis*-RA was enhanced in T-cell hybridomas overexpressing RXRβ, but attenuated in cells overexpressing dominant negative RXRβ (82). Our present study and the fact that Nur77 expression is necessary for activation-induced T-cell apoptosis suggest that inhibition of activation-induced apoptosis by RXR ligands may be mediated by their modulation of RXRα/Nur77 heterodimer activity.

RXRα/Nur77 nuclear export is also regulated by apoptotic stimuli. Endogenously expressed RXRα and Nur77 were found mainly in the nucleus (Fig. 1A), but resided at mitochondria after cells were treated with apoptotic stimuli (Fig. 1). How an apoptotic stimulus activates RXRα NES activity remains unknown. Our observations that RXRα and Nur77 nuclear export is highly regulated by their heterodimerization point to the possibility that the apoptotic stimulus may regulate an RXRα/Nur77 heterodimerization interface switch. This is consistent with observations that Nur77 activities are highly regulated by phosphorylation status (10, 16, 20, 24, 49, 53, 69) and many apoptotic stimuli act through various kinase pathways. Our premise is also consistent with the recent observation that Akt, a potent anti-apoptotic kinase, phosphorylates Nur77 (49, 53). Interestingly, the location of the Akt phosphorylation site in the Nur77 C-terminal extension points to the possibility that Akt phosphorylation may modulate the interaction of Nur77 with other proteins.

Different RXRα/Nur77 heterodimers may exist in a dynamic equilibrium depending on their cellular environment. Under normal conditions, both the DBD and LBD dimerization interfaces may participate in RXRα/Nur77 heterodimer formation, so that the dimers exist in both the nucleus and cytoplasm. In response to apoptotic stimuli, RXRα and Nur77 may preferentially heterodimerize through their DBD dimerization interfaces to activate the RXRα NES, resulting in their cytoplasmic localization. In contrast, binding by RXR ligands may induce a dimerization interface switch that silences the RXRα NES to ensure RXRα/Nur77 nuclear localization and efficient transcriptional regulation.

Evidence has been accumulating to demonstrate that many nuclear receptors act nongenotropically to regulate important biological processes. The estrogen receptor (ER) and androgen receptor modulate the Src/Shc/Erk-signaling pathway in a ligand-dependent manner to regulate cell proliferation. These effects can be dissociated from their transcriptional activity (32, 50). ER can also act outside the nucleus to activate phosphatidylinositol-3-OH kinase activity in a ligand-dependent and transcriptional regulation-independent manner (64). The results presented here demonstrate that RXRα also acts nongenotropically by migrating from the nucleus to mitochondria to trigger cytochrome *c* release and apoptosis in response to apoptotic stimuli. Thus, nongenotropic action appears to be an important mechanism by which nuclear receptors exert their biological effects. Our identification of a putative RXRα NES in helix 7 reveals an interesting regulatory mechanism that dictates subcellular localization of RXRα and its heterodimerization partners through ligands and dimerization. Our observation that RXR ligands regulate apoptosis by modulating RXRα/Nur77 heterodimer nuclear export provides a novel approach for developing RXR-based apoptosis regulators.

ACKNOWLEDGMENTS

We thank L. Frazer for preparation of the manuscript and members of Zhang's laboratory for discussions. This work is in part supported by grants to X-k. Zhang from the National Institute of Health, the US Army Medical Research and Material Command and the California Tobacco-Related Diseases Research Program and the California Breast Cancer Research Program.

REFERENCES

1. **A, I. J., N. S. Tan, L. Gelman, S. Kersten, J. Seydoux, J. Xu, D. Metzger, L. Canaple, P. Chambon, W. Wahli, and B. Desvergne.** 2004. In vivo activation of PPAR target genes by RXR homodimers. Embo J **23:**2083-91.
2. **Aarnisalo, P., C. H. Kim, J. W. Lee, and T. Perlmann.** 2002. Defining requirements for heterodimerization between the retinoid X receptor and the orphan nuclear receptor Nurr1. J Biol Chem **277:**35118-23.
3. **Baumann, C. T., P. Maruvada, G. L. Hager, and P. M. Yen.** 2001. Nuclear cytoplasmic shuttling by thyroid hormone receptors. multiple protein interactions are required for nuclear retention. J Biol Chem **276:**11237-45.
4. **Bissonnette, R. P., T. Brunner, S. B. Lazarchik, N. J. Yoo, M. F. Boehm, D. R. Green, and R. A. Heyman.** 1995. 9-cis retinoic acid inhibition of activation-induced apoptosis is mediated via regulation of fas ligand and requires retinoic acid receptor and retinoid X receptor activation. Mol Cell Biol **15:**5576-85.
5. **Bourguet, W., M. Ruff, P. Chambon, H. Gronemeyer, and D. Moras.** 1995. Crystal structure of the ligand-binding domain of the human nuclear receptor RXR-alpha. Nature **375:**377-82.
6. **Bourguet, W., V. Vivat, J. M. Wurtz, P. Chambon, H. Gronemeyer, and D. Moras.** 2000. Crystal structure of a heterodimeric complex of RAR and RXR ligand- binding domains. Mol Cell **5:**289-98.

7. **Bunn, C. F., J. A. Neidig, K. E. Freidinger, T. A. Stankiewicz, B. S. Weaver, J. McGrew, and L. A. Allison.** 2001. Nucleocytoplasmic shuttling of the thyroid hormone receptor alpha. Mol Endocrinol **15:**512-33.
8. **Chang, C., J. Kokontis, S. S. Liao, and Y. Chang.** 1989. Isolation and characterization of human TR3 receptor: a member of steroid receptor superfamily. J Steroid Biochem **34:**391-5.
9. **Chen, G. Q., B. Lin, M. I. Dawson, and X. K. Zhang.** 2002. Nicotine modulates the effects of retinoids on growth inhibition and RAR beta expression in lung cancer cells. Int J Cancer **99:**171-8.
10. **Davis, I. J., T. G. Hazel, R. H. Chen, J. Blenis, and L. F. Lau.** 1993. Functional domains and phosphorylation of the orphan receptor Nur77. Mol Endocrinol **7:**953-64.
11. **Dawson, M. I., P. D. Hobbs, V. J. Peterson, M. Leid, C. W. Lange, K. C. Feng, G. Chen, J. Gu, H. Li, S. K. Kolluri, X. Zhang, Y. Zhang, and J. A. Fontana.** 2001. Apoptosis induction in cancer cells by a novel analogue of 6-[3-(1- adamantyl)-4-hydroxyphenyl]-2-naphthalenecarboxylic acid lacking retinoid receptor transcriptional activation activity. Cancer Res **61:**4723-30.
12. **DeFranco, D. B.** 1999. Regulation of steroid receptor subcellular trafficking. Cell Biochem Biophys **30:**1-24.
13. **Dufour, J. M., and K. H. Kim.** 1999. Cellular and subcellular localization of six retinoid receptors in rat testis during postnatal development: identification of potential heterodimeric receptors. Biol Reprod **61:**1300-8.
14. **Egea, P. F., A. Mitschler, N. Rochel, M. Ruff, P. Chambon, and D. Moras.** 2000. Crystal structure of the human RXRalpha ligand-binding domain bound to its natural ligand: 9-cis retinoic acid. Embo J **19:**2592-601.
15. **Elbashir, S. M., J. Harborth, W. Lendeckel, A. Yalcin, K. Weber, and T. Tuschl.** 2001. Duplexes of 21-nucleotide RNAs mediate RNA interference in cultured mammalian cells. Nature **411:**494-8.
16. **Fahrner, T. J., S. L. Carroll, and J. Milbrandt.** 1990. The NGFI-B protein, an inducible member of the thyroid/steroid receptor family, is rapidly modified posttranslationally. Mol Cell Biol **10:**6454-9.
17. **Forman, B. M., K. Umesono, J. Chen, and R. M. Evans.** 1995. Unique response pathways are established by allosteric interactions among nuclear hormone receptors. Cell **81:**541-50.
18. **Gampe, R. T., Jr., V. G. Montana, M. H. Lambert, A. B. Miller, R. K. Bledsoe, M. V. Milburn, S. A. Kliewer, T. M. Willson, and H. E. Xu.** 2000. Asymmetry in the PPARgamma/RXRalpha crystal structure reveals the molecular basis of heterodimerization among nuclear receptors. Mol Cell **5:**545-55.
19. **Gampe, R. T., Jr., V. G. Montana, M. H. Lambert, G. B. Wisely, M. V. Milburn, and H. E. Xu.** 2000. Structural basis for autorepression of retinoid X receptor by tetramer formation and the AF-2 helix. Genes Dev **14:**2229-41.
20. **Hazel, T. G., R. Misra, I. J. Davis, M. E. Greenberg, and L. F. Lau.** 1991. Nur77 is differentially modified in PC12 cells upon membrane depolarization and growth factor treatment. Mol Cell Biol **11:**3239-46.
21. **Hazel, T. G., D. Nathans, and L. F. Lau.** 1988. A gene inducible by serum growth factors encodes a member of the steroid and thyroid hormone receptor superfamily. Proc Natl Acad Sci U S A **85:**8444-8.

22. **Hedvat, C. V., and S. G. Irving.** 1995. The isolation and characterization of MINOR, a novel mitogen-inducible nuclear orphan receptor. Mol Endocrinol **9:**1692-700.
23. **Heyman, R. A., D. J. Mangelsdorf, J. A. Dyck, R. B. Stein, G. Eichele, R. M. Evans, and C. Thaller.** 1992. 9-cis retinoic acid is a high affinity ligand for the retinoid X receptor. Cell **68:**397-406.
24. **Hirata, Y., K. Kiuchi, H. C. Chen, J. Milbrandt, and G. Guroff.** 1993. The phosphorylation and DNA binding of the DNA-binding domain of the orphan nuclear receptor NGFI-B. J Biol Chem **268:**24808-12.
25. **Holmes, W. F., D. R. Soprano, and K. J. Soprano.** 2003. Comparison of the mechanism of induction of apoptosis in ovarian carcinoma cells by the conformationally restricted synthetic retinoids CD437 and 4-HPR. J Cell Biochem **89:**262-78.
26. **Holmes, W. F., D. R. Soprano, and K. J. Soprano.** 2002. Elucidation of molecular events mediating induction of apoptosis by synthetic retinoids using a CD437-resistant ovarian carcinoma cell line. J Biol Chem **277:**45408-19.
27. **Janssen, J. J., E. D. Kuhlmann, A. H. van Vugt, H. J. Winkens, B. P. Janssen, A. F. Deutman, and C. A. Driessen.** 1999. Retinoic acid receptors and retinoid X receptors in the mature retina: subtype determination and cellular distribution. Curr Eye Res **19:**338-47.
28. **Jeong, J. H., J. S. Park, B. Moon, M. C. Kim, J. K. Kim, S. Lee, H. Suh, N. D. Kim, J. M. Kim, Y. C. Park, and Y. H. Yoo.** 2003. Orphan nuclear receptor Nur77 translocates to mitochondria in the early phase of apoptosis induced by synthetic chenodeoxycholic acid derivatives in human stomach cancer cell line SNU-1. Ann N Y Acad Sci **1010:**171-7.
29. **Kastner, P., M. Mark, and P. Chambon.** 1995. Nonsteroid nuclear receptors: what are genetic studies telling us about their role in real life? Cell **83:**859-69.
30. **Katagiri, Y., K. Takeda, Z. X. Yu, V. J. Ferrans, K. Ozato, and G. Guroff.** 2000. Modulation of retinoid signalling through NGF-induced nuclear export of NGFI-B. Nat Cell Biol **2:**435-40.
31. **Kolluri, S. K., X. Cao, N. Bruey-Sedano, B. Lin, F. Lin, Y. Han, M. I. Dawson, and X. Zhang.** 2003. Mitogenic effect of orphan receptor TR3 and its regulation by MEKK1 in lung cancer cells. Mol Cell Biol **23:**8651-8667.
32. **Kousteni, S., Bellido, T., Plotkin, L.I., O'Brien, C.A., Bodenner, D.L., Han, L., Han, K., DiGregorio, G.B., Katzenellenbogen, J.A., Katzenellenbogen, B.S., Roberson, P.K., Weinstein, R.S., Jilka, R.L., and Manolagas, S.C.** 2001. Nongenotropic, Sex-Nonspecific Signaling through the Estrogen or Androgen Receptors: Dissociation from Transcriptional Activity. Cell **104:**719-730.
33. **Kudo, N., N. Matsumori, H. Taoka, D. Fujiwara, E. P. Schreiner, B. Wolff, M. Yoshida, and S. Horinouchi.** 1999. Leptomycin B inactivates CRM1/exportin 1 by covalent modification at a cysteine residue in the central conserved region. Proc Natl Acad Sci U S A **96:**9112-7.
34. **Labelle, Y., J. Bussieres, F. Courjal, and M. B. Goldring.** 1999. The EWS/TEC fusion protein encoded by the t(9;22) chromosomal translocation in human chondrosarcomas is a highly potent transcriptional activator. Oncogene **18:**3303-8.
35. **Labelle, Y., J. Zucman, G. Stenman, L. G. Kindblom, J. Knight, C. Turc-Carel, B. Dockhorn-Dworniczak, N. Mandahl, C. Desmaze, M. Peter, and et al.** 1995.

Oncogenic conversion of a novel orphan nuclear receptor by chromosome translocation. Hum Mol Genet **4:**2219-26.

36. **Law, S. W., O. M. Conneely, F. J. DeMayo, and B. W. O'Malley.** 1992. Identification of a new brain-specific transcription factor, NURR1. Mol Endocrinol **6:**2129-35.
37. **Lee, J. M., K. H. Lee, M. Weidner, B. A. Osborne, and S. D. Hayward.** 2002. Epstein-Barr virus EBNA2 blocks Nur77- mediated apoptosis. Proc Natl Acad Sci U S A **99:**11878-83.
38. **Lee, M. S., S. A. Kliewer, J. Provencal, P. E. Wright, and R. M. Evans.** 1993. Structure of the retinoid X receptor alpha DNA binding domain: a helix required for homodimeric DNA binding. Science **260:**1117-21.
39. **Levin, A. A., L. J. Sturzenbecker, S. Kazmer, T. Bosakowski, C. Huselton, G. Allenby, J. Speck, C. Kratzeisen, M. Rosenberger, A. Lovey, and et al.** 1992. 9-cis retinoic acid stereoisomer binds and activates the nuclear receptor RXR alpha. Nature **355:**359-61.
40. **Li, H., S. K. Kolluri, J. Gu, M. I. Dawson, X. Cao, P. D. Hobbs, B. Lin, G. Chen, J. Lu, F. Lin, Z. Xie, J. A. Fontana, J. C. Reed, and X. Zhang.** 2000. Cytochrome c release and apoptosis induced by mitochondrial targeting of nuclear orphan receptor TR3 [see comments] [comment]. Science **289:**1159-64.
41. **Li, Y., B. Lin, A. Agadir, R. Liu, M. I. Dawson, J. C. Reed, J. A. Fontana, F. Bost, P. D. Hobbs, Y. Zheng, G. Q. Chen, B. Shroot, D. Mercola, and X. K. Zhang.** 1998. Molecular determinants of AHPN (CD437)-induced growth arrest and apoptosis in human lung cancer cell lines. Mol Cell Biol **18:**4719-31.
42. **Lin, B., G. Q. Chen, D. Xiao, S. K. Kolluri, X. Cao, H. Su, and X. K. Zhang.** 2000. Orphan receptor COUP-TF is required for induction of retinoic acid receptor beta, growth inhibition, and apoptosis by retinoic acid in cancer cells. Mol Cell Biol **20:**957-70.
43. **Lin, B., Kolluri, S., Lin, F., Liu, W., Han, Y.H., Cao, X., Dawson, M.I., Reed, J.C., and Zhang, X.K.** 2004. Conversion of Bcl-2 from Protector to Killer by Interaction with Nuclear Orphan Receptor Nur77/TR3. Cell **116:**527-540.
44. **Liu, Z. G., S. W. Smith, K. A. McLaughlin, L. M. Schwartz, and B. A. Osborne.** 1994. Apoptotic signals delivered through the T-cell receptor of a T-cell hybrid require the immediate-early gene nur77. Nature **367:**281-4.
45. **Mages, H. W., O. Rilke, R. Bravo, G. Senger, and R. A. Kroczek.** 1994. NOT, a human immediate-early response gene closely related to the steroid/thyroid hormone receptor NAK1/TR3. Mol Endocrinol **8:**1583-91.
46. **Mangelsdorf, D. J., and R. M. Evans.** 1995. The RXR heterodimers and orphan receptors. Cell **83:**841-50.
47. **Maruyama, K., T. Tsukada, S. Bandoh, K. Sasaki, N. Ohkura, and K. Yamaguchi.** 1995. Expression of NOR-1 and its closely related members of the steroid/thyroid hormone receptor superfamily in human neuroblastoma cell lines. Cancer Lett **96:**117-22.
48. **Maruyama, K., T. Tsukada, N. Ohkura, S. Bandoh, T. Hosono, and K. Yamaguchi.** 1998. The NGFI-B subfamily of the nuclear receptor superfamily (review). Int J Oncol **12:**1237-43.
49. **Masuyama, N., K. Oishi, Y. Mori, T. Ueno, Y. Takahama, and Y. Gotoh.** 2001. Akt inhibits the orphan nuclear receptor Nur77 and T-cell apoptosis. J Biol Chem **276:**32799-805.

50. **Migliaccio, A., G. Castoria, M. Di Domenico, A. de Falco, A. Bilancio, M. Lombardi, M. V. Barone, D. Ametrano, M. S. Zannini, C. Abbondanza, and F. Auricchio.** 2000. Steroid-induced androgen receptor-oestradiol receptor beta-Src complex triggers prostate cancer cell proliferation. Embo J **19:**5406-17.
51. **Milbrandt, J.** 1988. Nerve growth factor induces a gene homologous to the glucocorticoid receptor gene. Neuron **1:**183-8.
52. **Ohkura, N., M. Hijikuro, A. Yamamoto, and K. Miki.** 1994. Molecular cloning of a novel thyroid/steroid receptor superfamily gene from cultured rat neuronal cells. Biochem Biophys Res Commun **205:**1959-65.
53. **Pekarsky, Y., C. Hallas, A. Palamarchuk, A. Koval, F. Bullrich, Y. Hirata, R. Bichi, J. Letofsky, and C. M. Croce.** 2001. Akt phosphorylates and regulates the orphan nuclear receptor Nur77. Proc Natl Acad Sci U S A **98:**3690-4.
54. **Perlmann, T., and L. Jansson.** 1995. A novel pathway for vitamin A signaling mediated by RXR heterodimerization with NGFI-B and NURR1. Genes Dev **9:**769-82.
55. **Perlmann, T., K. Umesono, P. N. Rangarajan, B. M. Forman, and R. M. Evans.** 1996. Two distinct dimerization interfaces differentially modulate target gene specificity of nuclear hormone receptors. Mol Endocrinol **10:**958-66.
56. **Philips, A., S. Lesage, R. Gingras, M. H. Maira, Y. Gauthier, P. Hugo, and J. Drouin.** 1997. Novel dimeric Nur77 signaling mechanism in endocrine and lymphoid cells. Mol Cell Biol **17:**5946-51.
57. **Prufer, K., and J. Barsony.** 2002. Retinoid X receptor dominates the nuclear import and export of the unliganded vitamin D receptor. Mol Endocrinol **16:**1738-51.
58. **Prufer, K., A. Racz, G. C. Lin, and J. Barsony.** 2000. Dimerization with retinoid X receptors promotes nuclear localization and subnuclear targeting of vitamin D receptors. J Biol Chem **275:**41114-23.
59. **Ramaswamy, S., K. N. Ross, E. S. Lander, and T. R. Golub.** 2003. A molecular signature of metastasis in primary solid tumors. Nat Genet **33:**49-54.
60. **Rastinejad, F., T. Wagner, Q. Zhao, and S. Khorasanizadeh.** 2000. Structure of the RXR-RAR DNA-binding complex on the retinoic acid response element DR1. Embo J **19:**1045-54.
61. **Sacchetti, P., H. Dwornik, P. Formstecher, C. Rachez, and P. Lefebvre.** 2002. Requirements for Heterodimerization between the Orphan Nuclear Receptor Nurr1 and Retinoid X Receptors. J Biol Chem **277:**35088-96.
62. **Sakaue, M., H. Adachi, M. Dawson, and A. M. Jetten.** 2001. Induction of Egr-1 expression by the retinoid AHPN in human lung carcinoma cells is dependent on activated ERK1/2. Cell Death Differ **8:**411-24.
63. **Shipp, M. A., K. N. Ross, P. Tamayo, A. P. Weng, J. L. Kutok, R. C. Aguiar, M. Gaasenbeek, M. Angelo, M. Reich, G. S. Pinkus, T. S. Ray, M. A. Koval, K. W. Last, A. Norton, T. A. Lister, J. Mesirov, D. S. Neuberg, E. S. Lander, J. C. Aster, and T. R. Golub.** 2002. Diffuse large B-cell lymphoma outcome prediction by gene-expression profiling and supervised machine learning. Nat Med **8:**68-74.
64. **Simoncini, T., A. Hafezi-Moghadam, D. P. Brazil, K. Ley, W. W. Chin, and J. K. Liao.** 2000. Interaction of oestrogen receptor with the regulatory subunit of phosphatidylinositol-3-OH kinase. Nature **407:**538-41.

65. **Szondy, Z., U. Reichert, and L. Fesus.** 1998. Retinoic acids regulate apoptosis of T lymphocytes through an interplay between RAR and RXR receptors [see comments]. Cell Death Differ **5:**4-10.
66. **Uemura, H., and C. Chang.** 1998. Antisense TR3 orphan receptor can increase prostate cancer cell viability with etoposide treatment. Endocrinology **139:**2329-34.
67. **Wang, H. G., U. R. Rapp, and J. C. Reed.** 1996. Bcl-2 targets the protein kinase Raf-1 to mitochondria. Cell **87:**629-38.
68. **Wansa, K. D., J. M. Harris, and G. E. Muscat.** 2002. The activation function-1 domain of Nur77/NR4A1 mediates trans-activation, cell specificity, and coactivator recruitment. J Biol Chem **277:**33001-11.
69. **Weih, F., R. P. Ryseck, L. Chen, and R. Bravo.** 1996. Apoptosis of nur77/N10-transgenic thymocytes involves the Fas/Fas ligand pathway. Proc Natl Acad Sci U S A **93:**5533-8.
70. **Wen, W., J. L. Meinkoth, R. Y. Tsien, and S. S. Taylor.** 1995. Identification of a signal for rapid export of proteins from the nucleus. Cell **82:**463-73.
71. **Wilson, A. J., D. Arango, J. M. Mariadason, B. G. Heerdt, and L. H. Augenlicht.** 2003. TR3/Nur77 in colon cancer cell apoptosis. Cancer Res **63:**5401-7.
72. **Wilson, T. E., T. J. Fahrner, M. Johnston, and J. Milbrandt.** 1991. Identification of the DNA binding site for NGFI-B by genetic selection in yeast. Science **252:**1296-300.
73. **Winoto, A., and D. R. Littman.** 2002. Nuclear hormone receptors in T lymphocytes. Cell **109 Suppl:**S57-66.
74. **Woronicz, J. D., B. Calnan, V. Ngo, and A. Winoto.** 1994. Requirement for the orphan steroid receptor Nur77 in apoptosis of T- cell hybridomas. Nature **367:**277-81.
75. **Woronicz, J. D., A. Lina, B. J. Calnan, S. Szychowski, L. Cheng, and A. Winoto.** 1995. Regulation of the Nur77 orphan steroid receptor in activation-induced apoptosis. Mol Cell Biol **15:**6364-76.
76. **Wu, Q., M. I. Dawson, Y. Zheng, P. D. Hobbs, A. Agadir, L. Jong, Y. Li, R. Liu, B. Lin, and X. K. Zhang.** 1997. Inhibition of trans-retinoic acid-resistant human breast cancer cell growth by retinoid X receptor-selective retinoids. Mol Cell Biol **17:**6598-608.
77. **Wu, Q., Y. Li, R. Liu, A. Agadir, M. O. Lee, Y. Liu, and X. Zhang.** 1997. Modulation of retinoic acid sensitivity in lung cancer cells through dynamic balance of orphan receptors nur77 and COUP-TF and their heterodimerization. Embo J **16:**1656-69.
78. **Wu, Q., S. Liu, X. F. Ye, Z. W. Huang, and W. J. Su.** 2002. Dual roles of Nur77 in selective regulation of apoptosis and cell cycle by TPA and ATRA in gastric cancer cells. Carcinogenesis **23:**1583-92.
79. **Wu, W. S., Z. X. Xu, R. Ran, F. Meng, and K. S. Chang.** 2002. Promyelocytic leukemia protein PML inhibits Nur77-mediated transcription through specific functional interactions. Oncogene **21:**3925-33.
80. **Xu, L., C. K. Glass, and M. G. Rosenfeld.** 1999. Coactivator and corepressor complexes in nuclear receptor function. Curr Opin Genet Dev **9:**140-7.
81. **Yang, Y., J. Bailey, M. S. Vacchio, R. Yarchoan, and J. D. Ashwell.** 1995. Retinoic acid inhibition of ex vivo human immunodeficiency virus- associated apoptosis of peripheral blood cells. Proc Natl Acad Sci U S A **92:**3051-5.
82. **Yang, Y., S. Minucci, K. Ozato, R. A. Heyman, and J. D. Ashwell.** 1995. Efficient inhibition of activation-induced Fas ligand up-regulation and T cell apoptosis by retinoids

requires occupancy of both retinoid X receptors and retinoic acid receptors. J Biol Chem **270:**18672-7.

83. **Yang, Y., M. S. Vacchio, and J. D. Ashwell.** 1993. 9-cis-retinoic acid inhibits activation-driven T-cell apoptosis: implications for retinoid X receptor involvement in thymocyte development. Proc Natl Acad Sci U S A **90:**6170-4.
84. **Zamzami, N., and G. Kroemer.** 2001. The mitochondrion in apoptosis: how Pandora's box opens. Nat Rev Mol Cell Biol **2:**67-71.
85. **Zechel, C., X. Q. Shen, J. Y. Chen, Z. P. Chen, P. Chambon, and H. Gronemeyer.** 1994. The dimerization interfaces formed between the DNA binding domains of RXR, RAR and TR determine the binding specificity and polarity of the full-length receptors to direct repeats. Embo J **13:**1425-33.
86. **Zechel, C., X. Q. Shen, J. Y. Chen, Z. P. Chen, P. Chambon, and H. Gronemeyer.** 1994. The dimerization interfaces formed between the DNA binding domains of RXR, RAR and TR determine the binding specificity and polarity of the full-length receptors to direct repeats. Embo J **13:**1425-33.
87. **Zhang, X. K.** 2002. Vitamin A and apoptosis in prostate cancer. Endocr Relat Cancer **9:**87-102.
88. **Zhang, X. K., B. Hoffmann, P. B. Tran, G. Graupner, and M. Pfahl.** 1992. Retinoid X receptor is an auxiliary protein for thyroid hormone and retinoic acid receptors. Nature **355:**441-6.
89. **Zhang, X. K., J. Lehmann, B. Hoffmann, M. I. Dawson, J. Cameron, G. Graupner, T. Hermann, P. Tran, and M. Pfahl.** 1992. Homodimer formation of retinoid X receptor induced by 9-cis retinoic acid. Nature **358:**587-91.
90. **Zhang, X. K., and M. Pfahl.** 1993. Hetero- and homodimeric receptors in thyroid hormone and vitamin A action. Receptor **3:**183-91.
91. **Zhang, X. K., G. Salbert, M. O. Lee, and M. Pfahl.** 1994. Mutations that alter ligand-induced switches and dimerization activities in the retinoid X receptor. Mol Cell Biol **14:**4311-23.
92. **Zhang, Y., M. I. Dawson, R. Mohammad, A. K. Rishi, L. Farhana, K. C. Feng, M. Leid, V. Peterson, X. K. Zhang, M. Edelstein, D. Eilander, S. Biggar, N. Wall, U. Reichert, and J. A. Fontana.** 2002. Induction of apoptosis of human B-CLL and ALL cells by a novel retinoid and its nonretinoidal analog. Blood **100:**2917-25.
93. **Zhu, X. G., J. A. Hanover, G. L. Hager, and S. Y. Cheng.** 1998. Hormone-induced translocation of thyroid hormone receptors in living cells visualized using a receptor green fluorescent protein chimera. J Biol Chem **273:**27058-63.

FIGURE LEGENDS

FIG. 1. Nur77 and RXR comigrate from the nucleus to the cytoplasm. (A/B) RXRα (**A**) or Nur77 (**B**) targets mitochondria in response to apoptotic stimulus. LNCaP prostate cancer cells were treated with TPA (100 ng/ml) for 1 hr, then immunostained with either anti-RXRα (Santa Cruz Biotechnology, Inc) (A) or anti-Nur77 (Active Motif) (B) antibody followed by Cy3-conjugated secondary antibody (Sigma) to detect RXRα or Nur77 or with anti-Hsp60 (Santa Cruz Biotechnology, Inc) followed by FITC-conjugated secondary antibody (Sigma) to detect mitochondria. RXRα, Nur77 and mitochondria (Hsp60) were visualized using confocal microscopy, and the images of RXRα or Nur77 with those of mitochondria were overlaid (overlay). About 80% of cells displayed mitochondrial targeting of RXRα and Nur77 when cells were treated with TPA. One of three similar experiments is shown. **(C)** Nur77 and RXRα comigrate from the nucleus to the cytoplasm. LNCaP cells were treated with or without TPA for 1 hr, then immunostained with anti-RXRα antibody followed by FITC-conjugated secondary antibody, or with anti-Nur77 antibody (Abgent, San Diego) followed by Cy3-conjugated secondary antibody. RXRα and Nur77 were visualized using confocal microscopy and the images were overlaid (overlay). Approximately 80% of TPA-treated cells showed RXRα co-localization with Nur77. One of three similar experiments is shown. **(D)** 3-Cl-AHPC induces mitochondrial localization of transfected RXRα and Nur77. Expression vectors for myc-Nur77 and RXRα were transfected into LNCaP cells. Cells were then treated with 3-Cl-AHPC for 3 hr, then immunostained with anti-myc antibody (9E10, Santa Cruz Biotechnology, Inc) followed by FITC-conjugated secondary antibody, anti-RXRα antibody followed by Cy3-conjugated secondary antibody or anti-Hsp60 antibody followed by Cy5-conjugated secondary antibody (Tackson Immuno Res.). Myc-Nur77, RXRα, and Hsp60 were visualized and the images were overlaid. Overlay1 is the merge of myc-Nur77 and RXRα images, and Overlay 2 is the merge of myc-Nur77, RXRα, and Hsp60 images. About 30% of transfected cells exhibited colocalization presented. One of three similar experiments is shown. **(E)** Mitochondrial localization of RXRα is Nur77 dependent. LNCaP cells or LNCaP cells stably expressing Nur77 antisense RNA (Nur77/Antisense) (40) were treated with or without TPA for 1 hr, then immunostained with anti-RXRα antibody followed by Cy3-conjugated secondary antibody. Approximately 70% of cells displayed the effect presented. One of two similar experiments is shown. **(F)** Effect of RXR siRNA on RXRα levels and Nur77 localization. LNCaP cells were transfected with or without RXRα siRNA or control siRNA for 72 hr. Cell extracts were prepared and analyzed for RXRα expression by Western blotting. Cells were also analyzed for subcellular localization of RXRα and Nur77 by confocal microscopy. One of two similar experiments is shown. **(G)** Nur77/Δ1 prevents RXRα mitochondrial targeting. LNCaP cells were transfected with the GFP-Nur77/Δ1 expression vector, then treated with TPA for 1 hr, and immunostained with anti-RXRα antibody. RXRα and GFP-Nur77/Δ1 distributions were analyzed by confocal microscopy. About 80% of non-transfected cells showed cytoplasmic localization of RXRα after treatment with TPA, while more than 70% of cells transfected with GFP-Nur77/Δ1 showed RXRα nuclear localization with the same treatment. One of three similar experiments is shown. **(H)** 3-Cl-AHPC induces mitochondrial localization of RXRα and Nur77 in H460 lung cancer cells. H460 cells were treated with 3-Cl-AHPC (10^{-6} M) for 3 hr, then immunostained with anti-RXRα antibody followed by FITC-conjugated secondary antibody, anti-Nur77 followed by Cy3-conjugated secondary antibody, or anti-Hsp60 antibody followed by Cy5-conjugated secondary antibody

(Tackson Immuno Res.). RXRα, Nur77 and Hsp60 were visualized using confocal microscopy and the images were overlaid. Overlay1 represents the merge of RXRα and Nur77 images. Overlay2 indicates merged RXRα, Nur77 and Hsp60 images. Approximately 80% of 3-Cl-AHPC-treated cells showed the patterns presented. One of three similar experiments is shown.

FIG. 2. Time-course analysis of mitochondrial targeting of RXRα and Nur77 and the release of cytochrome *c* from mitochondria. **(A)** Time-course analysis of LNCaP cells in response to TPA. Cells were treated with TPA (100 ng/ml) for the indicated times. Mitochondria-enriched heavy-membrane (HM) and cytosolic fractions were prepared and analyzed for the presence of RXRα, Nur77, and cytochrome *c* as indicated. As a control, the whole cell extract was also analyzed. Expression of mitochondria-specific Hsp60 protein and nucleus-specific PARP protein was determined to control the purity of HM fractions. One of two similar experiments is shown. **(B)** Inhibition of RXRα expression suppresses the apoptotic effect of TPA. LNCaP cells were transfected with RXRα siRNA, followed by the treatment with TPA (100 ng/ml) for 3 hr. Cells were stained with DAPI and analyzed for nuclear morphologic changes. Apoptotic cells were scored by examining 300 cells for apoptotic morphology from three different experiments. **(C)** Time-course analysis of H460 cells in response to 3-Cl-AHPC. Cells were treated with 3-Cl-AHPC (10^{-6}M) and analyzed as described in (A). One of two similar experiments is shown.

FIG. 3. Mutagenic analysis of RXRα and Nur77. **(A)** Cytoplasmic localization of RXRα/Nur77 is mediated by CRM1-dependent nuclear export. LNCaP cells were treated with TPA (100 ng/ml) in the absence (control) or presence of leptomycin B (LMB, 2.5 ng/ml) (Sigma) and analyzed by confocal microscopy as described in Fig. 1C. About 80% cells showed the cytoplasmic localization of RXRα and Nur77 after treatment with TPA, while more than 50% of cells showed nuclear localization of RXRα and Nur77 when pre-treated with LMB. One of two similar experiments is shown. **(B)** Schematic representations of RXRα and Nur77 mutants. The DNA-binding domain (DBD), ligand-binding domain (LBD), and A-F domains are indicated. **(C)** Confocal microscopy analysis of Nur77 and RXRα mutants. The indicated plasmids were transfected into HEK293T cells and analyzed by confocal microscopy as described in Fig. 1A. More than 90% of transfected cells showed diffused distribution of GFP and GFP-RXRα/135. Nuclear localization of GFP-RXRα, RXRα/235, and RXRα/347 was found in 80%, 85%, and 60% of transfected cells, respectively. More than 90% of transfected cells showed exclusive cytoplasmic localization of RXRα/385, RXRα/C2 and RXRα/C3, while cytoplasmic localization of RXRα/C1 was found in 70% of transfected cells. Nuclear localization of GFP-Nur77 and its mutants, GFP-Nur77/Δ2, GFP-Nur77/Δ1, GFP-Nur77/467, and GFP-Nur77/410 was found in more than 90% of transfected cells, while cytoplasmic localization of GFP-Nur77/ΔDBD, cytoplasmic localization of GFP-Nur77/ΔDBD, GFP-Nur77/ΔC2, and GFP-Nur77/ΔC3 was observed in 80%, 60% and 70% of transfected cells, respectively. One of four similar experiments is shown.

FIG. 4. Identification of a nuclear export sequence in RXRα. **(A)** Effect of LMB on subcellular localization of RXRα mutants. The indicated expression vector for GFP fusion proteins was transfected into HEK293T cells and analyzed by confocal microscopy. Approximately 70% of transfected cells displayed diffused distribution of RXRα/C2 and

RXRα/C3 after treatment with LMB. One of four similar experiments is shown. **(B)** RXRα/C3 exclusively resides in the cytoplasm. GFP-RXRα/C3 was transfected into HEK293T cells, and its localization was analyzed by cellular fractionation followed by western blotting using anti-GFP antibody (Santa Cruz Bio. Inc.). One of three similar experiments is shown. **(C)** The effect of LMB on subcellular localization of RXRα/C3. RXRα/C3 was transfected into HEK293T cells, which were then treated with or without LMB (2.5 ng/ml) for 6 hr. Localization of RXRα/C3 was analyzed as described in B. One of three similar experiments is shown. **(D)** Schematic representation of the RXRα NES. The identified RXRα NES is compared with known NESs identified in the indicated genes. The bold letters indicate conserved amino acid residues. **(E)** The RXRα NES is capable of directing GFP to the cytoplasm. The putative RXRα NES (RVLTELVSKMRDMQMDKTELG) or its mutant (RVLTELVSKARDAQMDKTELG) (NESm) was fused to GFP, and the expression vectors were transfected into HEK293T cells. Cells were treated with or without LMB for 6 hr, then stained for Hsp60 and analyzed by confocal microscopy. Approximately 90% of GFP-NES transfected cells exhibited cytoplasmic localization, while less than 20% of GFP-NESm-transfected cells displayed the same cytoplasmic localization. One of three similar experiments is shown. **(F)** Mutation of the RXRα NES impairs the 3-Cl-AHPC-induced mitochondrial localization of RXRα/Nur77 heterodimer. Myc-Nur77 was cotransfected with GFP-RXRα/NESm into LNCaP cells, which were then treated with 3-Cl-AHPC (10^{-6} M) for 3 hr. Cells were stained for Nur77 by anti-myc antibody and analyzed by the confocal microscopy. About 90% of transfected cells showed nuclear localization of Myc-Nur77 and RXRα/NESm, even after treatment of 3-Cl-AHPC. **(G)** RXRα NES is required for cytoplasmic localization of Nur77. The indicated expression vectors were cotransfected into HEK293T cells. Their subcellular localization was analyzed by confocal microscopy as described in Fig. 1A. Less than 10% of transfected cells showed cytoplasmic localization of GFP-Nur77, Nur77/467 and Nur77/Δ1, which was increased to 30%, 40% and 40% upon cotransfection with Flag-RXRα/385, respectively. About 80% of transfected cells showed nuclear localization of Flag-RXRα, with or without Nur77/ΔC3 cotransfection. One of three similar experiments is shown.

FIG. 5. Mitochondrial targeting and apoptotic effects of cytoplasmic RXRα and Nur77 mutants. **(A)** Mitochondrial targeting of RXRα/385 in HEK293T cells requires Nur77 and Bcl-2. Expression vectors of GFP-RXRα/385 and Bcl-2 were transfected together with or without myc-Nur77 vector into HEK293T cells. Cells were then immunostained with anti-myc antibody (9E10, Santa Cruz Biotechnology Inc) followed by Cy3-conjugated secondary antibody, or with anti-Bcl-2 antibody followed by Cy5-conjugated secondary antibody. GFP-RXRα/385, myc-Nur77 and Bcl-2 were visualized by confocal microscopy. Overlay1 represents the merger of the GFP-RXRα/385 and myc-Nur77 images, and Overlay2 is the merger of GFP-RXRα/385, myc-Nur77 and Bcl-2 images. Approximately 70% of cells transfected with GFP-RXRα/385 and myc-Nur77 exhibited co-localization with Bcl-2, while less than 5% of cells transfected with GFP-RXRα/385 alone showed co-localization with Bcl-2. **(B)** Accumulation of RXRα/385 at mitochondria in HEK293T cells requires both Nur77 and Bcl-2. Flag-RXRα/385, GFP-Nur77/Δ2, and Bcl-2 were transfected into HEK293T cells as indicated. Heavy membrane (HM) and cytosolic fractions were prepared and levels of Flag-RXRα/385, GFP-Nur77/Δ2, and Bcl-2 were determined by immunoblotting using anti-Flag (Sigma), anti-GFP, and anti-Bcl-2 antibody,

respectively. For control, levels of Hsp60 and PARP were also determined. One of two similar experiments is shown.

FIG. 6. Mitochondrial targeting and apoptosis effects of cytoplasmic RXRα and Nur77 mutants. (**A**). Cytoplasmic Nur77 mutants but not RXRα mutants induce apoptosis. The indicated GFP-RXRα or GFP-Nur77 mutant was transfected into LNCaP cells. After 48 hr, cells were stained by DAPI and analyzed for nuclear morphologic change by microscopy. Arrows indicate cells with extensive nuclear condensation or fragmentation. Percentages of apoptotic cells were determined by examining 200 GFP-positive cells for nuclear fragmentation and/or chromatin condensation. Bars represent average ± means from 3 experiments. (**B**) Cytoplasmic Nur77 mutant but not RXRα mutant induces cyt *c* release. GFP-Nur77/ΔDBD or GFP-RXRα/C1 expression vector was transfected into LNCaP cells. Cells were then stained for mitochondria (Hsp60) and cyt *c*, and analyzed by confocal microscopy. Cyt *c* release was observed in 80% of cells showing Nur77/ΔDBD mitochondrial targeting, while it was not found in cell transfected with RXRα/C1. One of two similar experiments is shown.

FIG 7. Regulation of RXRα nuclear export by its ligands and homodimerization. (A/B) Analysis of subcellular localization of RXRα/C1 in the absence or presence of retinoids. GFP-RXRα/C1 was transfected into HEK293T cells, which were then treated with the indicated retinoid, stained with Hsp60, and analyzed by confocal microscopy (**A**). The inhibitory effect of RXR ligands on the cytoplasmic localization of RXRα/C1 was observed in 80% of transfected cells, while more than 90% of transfected cells failed to respond to RAR ligands. Nuclear and cytoplasmic extracts were also prepared and analyzed for expression of GFP-RXRα/C1 by Western blotting using anti-GFP antibody (**B**). One of three similar experiments is shown. **(C)** RXRα/C1 dimerization status determines its subcellular localization. GFP-RXRα/C1 was transfected into HEK293T cells, which were not treated or treated with 9-*cis*-RA (10^{-7} M). Nuclear and cytoplasmic extracts were prepared and analyzed by non-denaturing PAGE and anti-GFP antibody. The same extracts were analyzed by denaturing PAGE for expression of PARP and Hsp60 to ensure fraction purity. One of two similar experiments is shown. **(D)** Confocal microscopy analysis of RXR homodimerization-defective mutants. GFP-RXRα/385, GFP-RXRα/LLL or GFP-RXRα/C1/C432A was transfected into HEK293T cells. Cells were treated with or without 9-*cis*-RA (10^{-7} M) and analyzed by confocal microscopy. Approximately 80% of transfected cells showed nuclear localization of GFP-RXRα, which was slightly increased to 85% after treatment of 9-*cis*-RA. Cytoplasmic localization of GFP-RXRα/385 (90%), GFP-RXRα/LLL (65%), GFP-RXRα/C1/C432 (85%) was not affected by 9-*cis*-RA treatment. One of three similar experiments is shown.

FIG 8. Regulation of RXRα nuclear export by heterodimerization. (A) Regulation of RXR nuclear export by VDR (**A**) and RARα (**B**). Expression vector for VDR (**A**) or RARα (**B**) was transfected into HEK293T cells together with GFP-RXRα expression vector. Cells were then treated with the indicated ligand, Vit D_3 (10^{-7} M) or Am80 (10^{-6} M). Nuclear and cytoplasmic extracts were prepared and analyzed for expression of transfected GFP-RXRα by anti-GFP antibody. Expression of transfected VDR or RARα was also determined. One of two similar experiments is shown. **(C)** Confocal analysis of the effect of VDR expression on RXR localization. The GFP-RXRα/C1 expression vector was transfected into HEK293T cells

together with or without the VDR expression vector. Cells were then treated with VD_3 (10^{-7} M), stained with anti-VDR antibody (Santa Cruz Biotechnology) followed by cy3–conjugated secondary antibody (Sigma) and analyzed by confocal microscopy. About 70% of transfected cells showed cytoplasmic localization of RXRα/C1, while more than 80% of co-transfected cells showed nuclear localization of RXRα/C1 and VDR, which was not clearly enhanced by VD_3 treatment. One of three similar experiments is shown.

FIG. 9. C-termini of RXRα and Nur77 are not required for RXRα/Nur77 interaction in solution. **(A/B)** GST-pull-down assays for determination of RXRα/Nur77 heterodimerization. GST-Nur77, GST-RXRα or GST control protein immobilized on glutathione-Sepharose (20 μl) was incubated with *in vitro* synthesized ^{35}S-labeled Nur77 or RXRα (5 μl) as indicated. Bound proteins were analyzed by SDS-PAGE/autoradiography. One of three similar experiments is shown. **(C)** Co-IP assay for Nur77 and RXRα/385 interaction. Expression vectors for Flag epitope tagged-Nur77 (Flag-Nur77) and GFP-RXRα/385 were cotransfected into HEK293T cells. The expressed Flag-Nur77 and GFP-RXRα/385 were then immunoprecipitated by using either anti-Flag antibody or control IgG, and immunoprecipitates were examined by western blotting using anti-GFP antibody. The same membranes were also blotted with anti-Flag antibody to determine precipitation specificity and efficiency. Input represents 5% of total cell extract used in the precipitation assays. One of two similar experiments is shown. **(D)** Reporter gene assay. $(NurRE)_2$-*tk*-CAT (100 ng), β-galactosidase (100 ng) and Nur77 (25 ng) expression vectors were transiently transfected into HEK293T cells together with or without RXRα or RXRα/385. Cells were treated with or without 9-*cis*-RA (10^{-7} M) as indicated. CAT activity was determined and normalized relative to βgalactosidase (β-gal) activity. Bars represent averages ± means from two different experiments. **(E)** Schematic representations of RXRα and Nur77 mutants. The DNA-binding domain (DBD), ligand-binding domain (LBD), and A-F domains are indicated. **(F)** GST-pull-down assays for determination of RXRα/Nur77 heterodimerization. The indicated GST-RXRα, its mutants or GST control protein was immobilized on glutathione-Sepharose (20 μl) and incubated with *in vitro* synthesized ^{35}S-labeled Nur77 or its mutants (5 μl) as indicated. Bound proteins were analyzed by SDS-PAGE/autoradiography. One of three similar experiments is shown.

FIG 10. 9-*cis*-RA modulates RXRα/Nur77 heterodimerization and promotes DNA binding. **(A)** The C-terminal domains of Nur77 and RXRα are required for the formation of RXRα/Nur77 heterodimer on DNA. The indicated Nur77, RXRα or their mutants were synthesized *in vitro* and analyzed for binding to the βRARE by gel-shift assays. One of three similar experiments is shown. **(B)** Differential requirement of the Nur77 C-terminus for transactivation of the Nur77 response element NurRE and the βRARE. $(NurRE)_2$-*tk*-CAT (100 ng) or βRARE-*tk*-CAT(100 ng), β-gal expression vector (100 ng) and the expression vector for Nur77 or a Nur77 mutant (20 ng) were transiently transfected into HEK293T cells with or without the RXRα expression vector. CAT activity was determined and normalized relative to β-gal activity. One of three similar experiments is shown. **(C)** Effect of RXR ligands on binding of RXRα-Nur77 heterodimers to the βRARE. Equivalent amounts of *in vitro* synthesized Nur77 and RXRα were incubated alone or together with or without RXR ligand SR11237 and analyzed by gel-retardation assays using the βRARE as a probe. One of two similar experiments is shown. **(D)** RXR ligand modulates RXRα/Nur77 heterodimerization in

solution. GST-pull-down assays for determination of RXRα/Nur77 heterodimerization. The indicated GST fusions immobilized on glutathione-Sepharose (20 μl) was incubated with *in vitro* synthesized ^{35}S-labeled receptor protein (5 μl) as indicated. Bound proteins were analyzed by SDS-PAGE/autoradiography. One of two similar experiments is shown.

FIG 11. Effect of RXR ligands on RXR mitochondrial targeting and apoptosis. **(A)** Effect of 9-*cis*-RA on mitochondrial localization of RXRα and Nur77. HM fractions were prepared from LNCaP cells treated with or without TPA or SR11453 (10^{-6} M) for 3 hr with or without a 9-*cis*-RA pretreatment for 12 hr, and analyzed for expression of Nur77 or RXRα by immunoblotting. One of two similar experiments is shown. **(B)** 9-*cis*-RA inhibits Nur77-dependent release of cytochrome *c* from mitochondria. GFP-Nur77 expression vector was transfected into LNCaP cells, treated with or without 9-*cis*-RA for 12 hr before TPA treatment (1 hr). Cells were stained for mitochondria (Hsp60) and cytochrome *c* (Cyt *c*), and analyzed by confocal microscopy. 100% of cells displayed diffused Cyt *c* staining treated with TPA, while 60% of cells showed punctate Cyt *c* staining when cells were co-treated with TPA and 9-*cis*-RA. **(C)** Inhibition of Cyt *c* release by 9-*cis*-RA. LNCaP cells were treated with or without 9-*cis*-RA (10^{-7} M) for 12 hr before treatment with TPA (100 ng/ml) or SR11453 for 1 hr. Cytosolic fractions were analyzed for Cyt *c* by immunoblotting. A nonspecific band at ~ 70 kd served as a control for equal loading of proteins. One of three similar experiments is shown. **(D)** RAR and VDR ligands fail to inhibit mitochondrial localization of RXRα and Nur77 and cyt *c* release. LNCaP cells were treated with 3-Cl-AHPC (10^{-6} M) for 3 hr after pretreatment of SR11237 (10^{-6} M), RAR ligand Am80 (10^{-6} M), or VDR ligand Vit D_3 (10^{-7} M). HM and cytosolic fractions were prepared and analyzed for mitochondrial localization of RXRα and Nur77 as well as cyt c release described above. **(E)** RXR ligands prevent SR11453 induced mitochondrial membrane potential change ($\Delta\psi m$). LNCaP cells were pretreated with 9-cis-RA or SR11237 for 12 hr before treatment with SR11453 (10^{-6} M) for 18 hr. Cells were then incubated with Rh123 for 30 min and analyzed by FACScalibur cytometry. One of three similar experiments is shown. **(F)** Inhibition of apoptosis by RXR ligands. LNCaP cells were pretreated with 9-*cis*-RA or SR11237 for 12 hr before treatment with SR11453 for 48 hr. Apoptosis was determined by nuclear staining with DAPI. The percent of cells fluorescencing within the range of Rh123 were considered as depolarized (i.e., $\Delta\psi m$ disrupted). Bars represent average ± means from two experiments. **(G)** LNCaP cells were pretreated 9-*cis*-RA or SR11237 for 12 hr before treatment with SR11453 or TPA for 24 hr. Apoptosis was determined by the terminal deoxynucleotidyl transferase (TdT) assay. One of two similar experiments is shown.

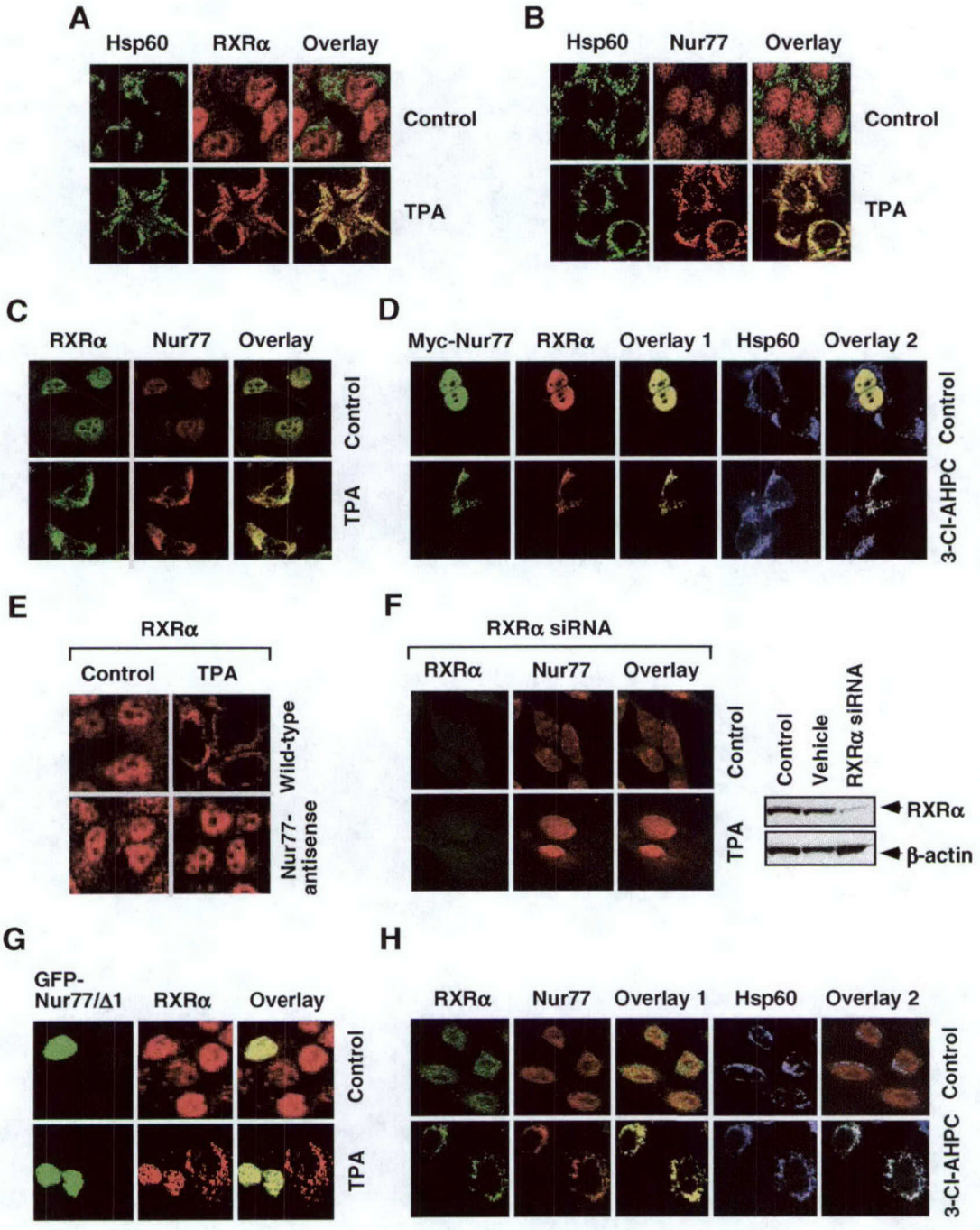
A
Hsp60
RXRα
Overlay
Control
TPA
B
Hsp60
Nur77
Overlay
Control
TPA
C
RXRα
Nur77
Overlay
Control
TPA
D
Myc-Nur77
RXRα
Overlay 1
Hsp60
Overlay 2
Control
3-Cl-AHPC
E
RXRα
Control
TPA
Wild-type
Nur77-antisense
F
RXRα siRNA
RXRα
Nur77
Overlay
Control
TPA
Control
Vehicle
RXRα siRNA
RXRα
β-actin
G
GFP-Nur77/Δ1
RXRα
Overlay
Control
TPA
H
RXRα
Nur77
Overlay 1
Hsp60
Overlay 2
Control
3-Cl-AHPC

FIGURE 1

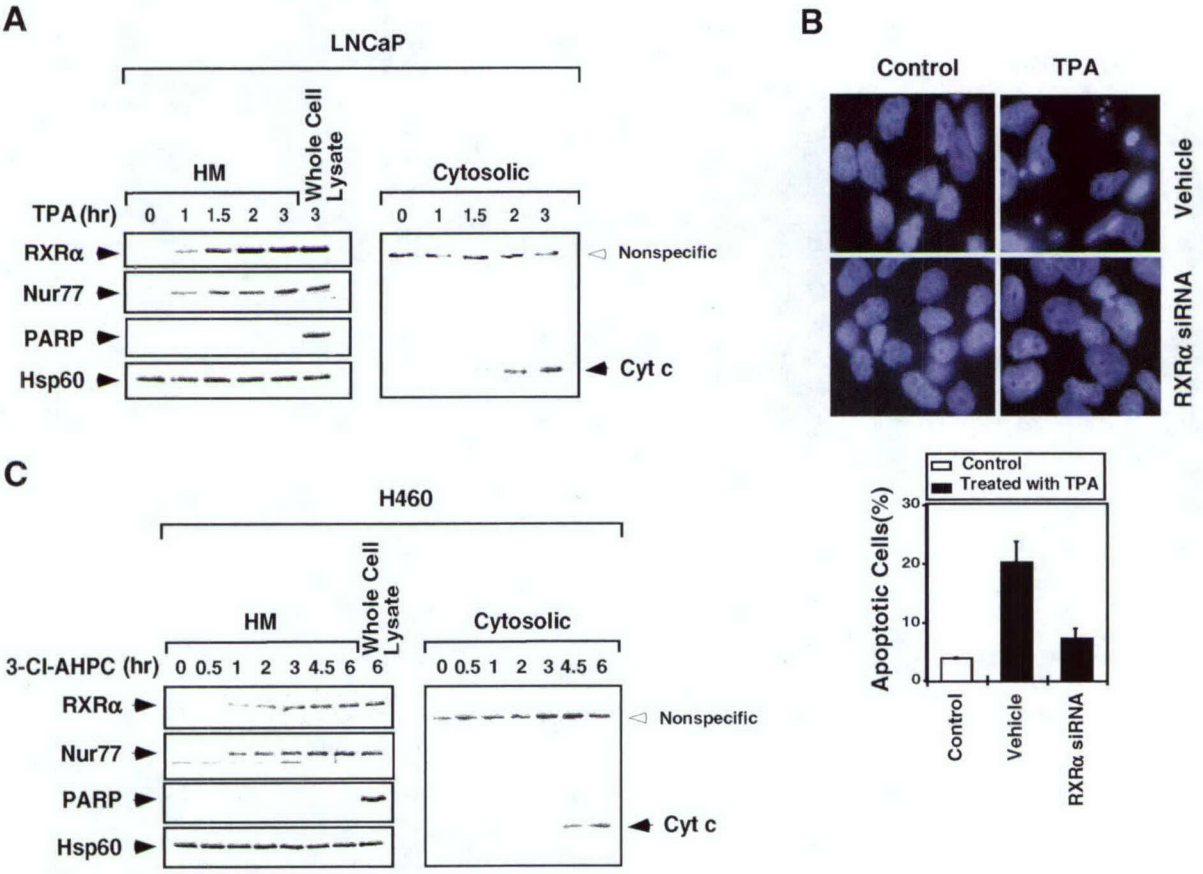
A
LNCaP
HM
Whole Cell Lysate
Cytosolic
TPA (hr)
0 1 1.5 2 3 3
0 1 1.5 2 3
RXRα
Nur77
PARP
Hsp60
Nonspecific
Cyt c
B
Control
TPA
Vehicle
RXRα siRNA
C
H460
HM
Whole Cell Lysate
Cytosolic
3-Cl-AHPC (hr)
0 0.5 1 2 3 4.5 6 6
0 0.5 1 2 3 4.5 6
RXRα
Nur77
PARP
Hsp60
Nonspecific
Cyt c
Control
Treated with TPA
Apoptotic Cells(%)
30
20
10
0
Control
Vehicle
RXRα siRNA

FIGURE 2

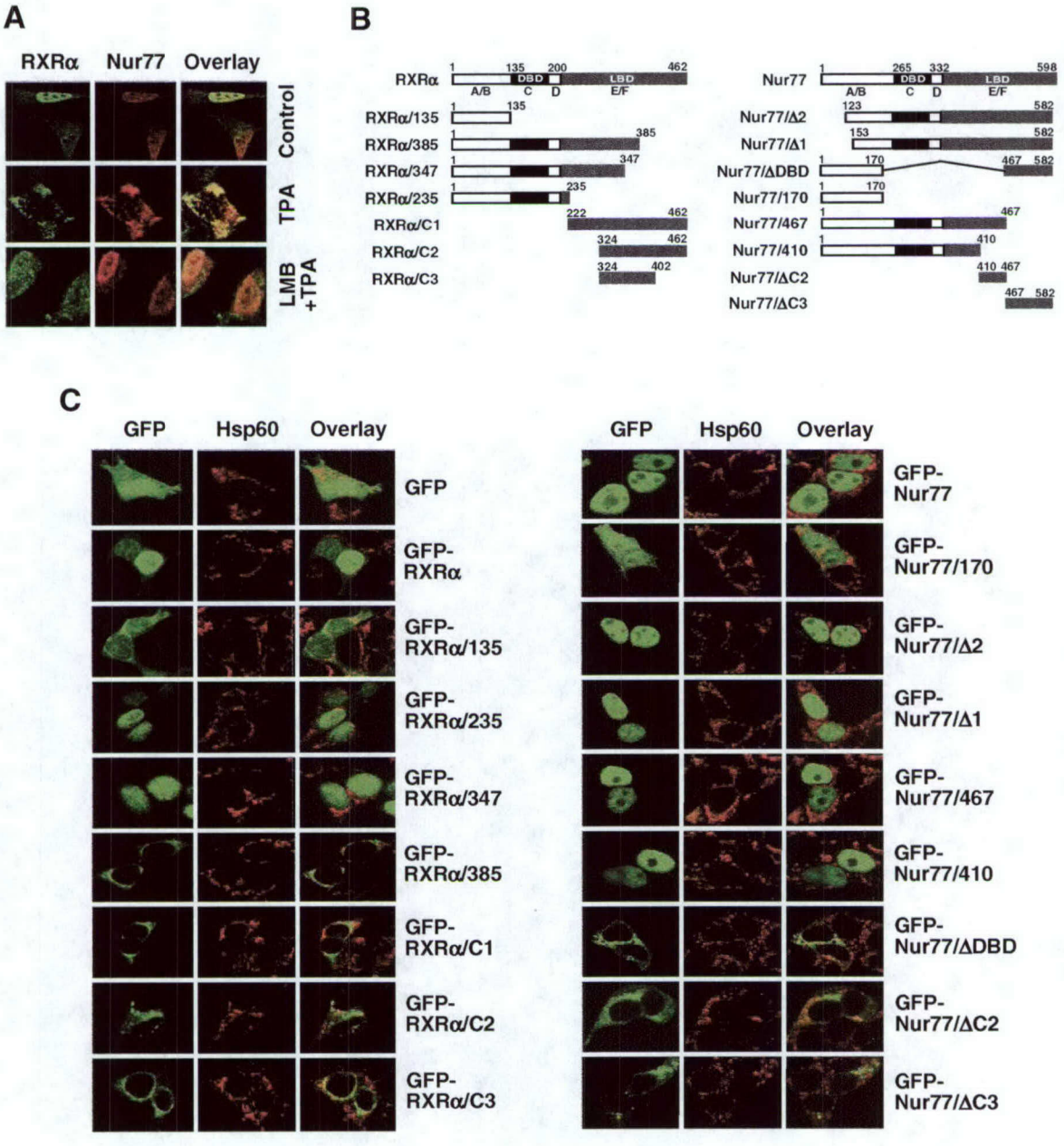
A
RXRα
Nur77
Overlay
Control
TPA
LMB +TPA
B
RXRα
RXRα/135
RXRα/385
RXRα/347
RXRα/235
RXRα/C1
RXRα/C2
RXRα/C3
DBD
LBD
A/B
C
D
E/F
Nur77
Nur77/Δ2
Nur77/Δ1
Nur77/ΔDBD
Nur77/170
Nur77/467
Nur77/410
Nur77/ΔC2
Nur77/ΔC3
C
GFP
Hsp60
Overlay
GFP
GFP-RXRα
GFP-RXRα/135
GFP-RXRα/235
GFP-RXRα/347
GFP-RXRα/385
GFP-RXRα/C1
GFP-RXRα/C2
GFP-RXRα/C3
GFP-Nur77
GFP-Nur77/170
GFP-Nur77/Δ2
GFP-Nur77/Δ1
GFP-Nur77/467
GFP-Nur77/410
GFP-Nur77/ΔDBD
GFP-Nur77/ΔC2
GFP-Nur77/ΔC3

FIGURE 3

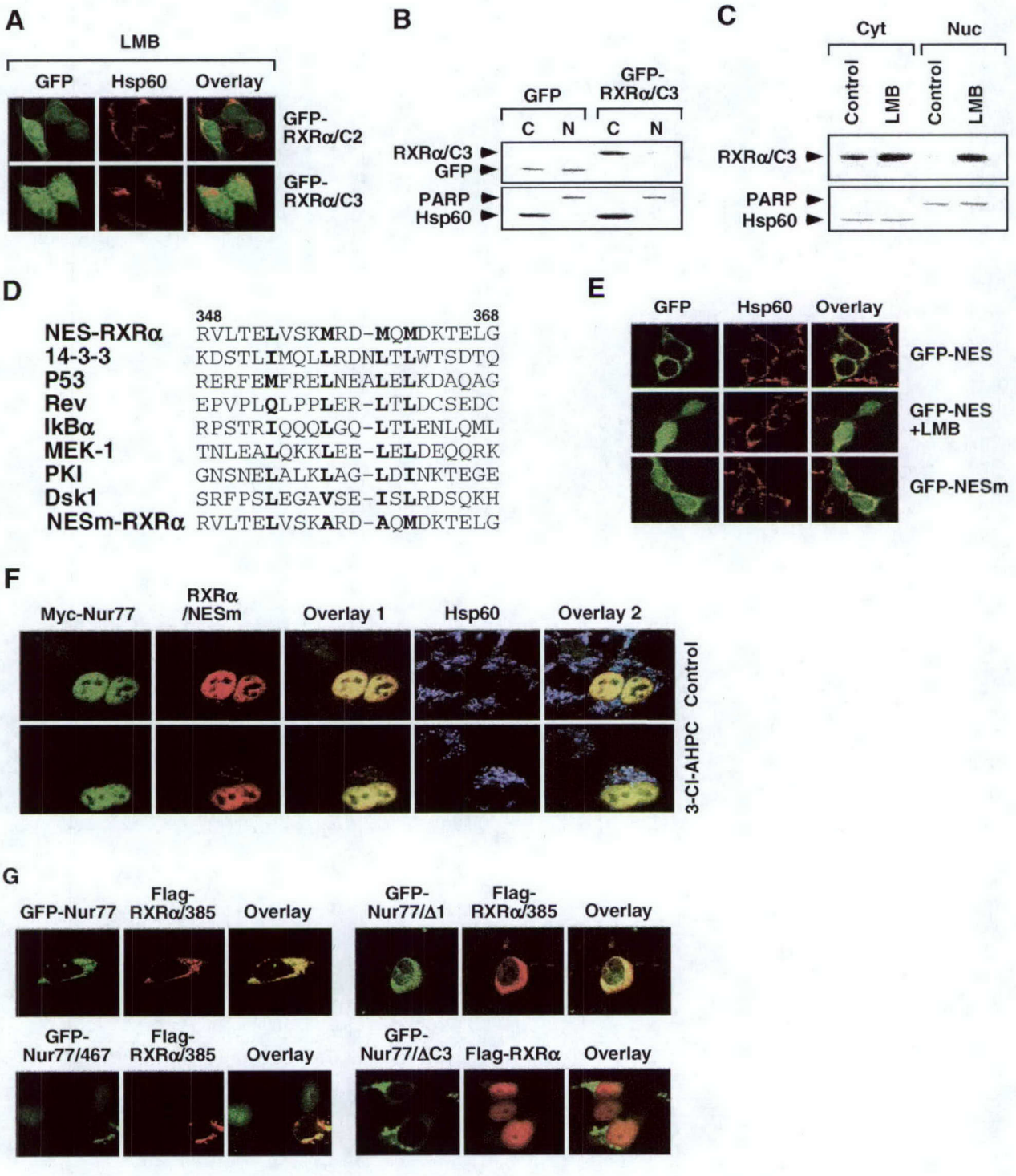
A
LMB
GFP
Hsp60
Overlay
GFP-RXRα/C2
GFP-RXRα/C3
B
GFP
GFP-RXRα/C3
C
N
C
N
RXRα/C3
GFP
PARP
Hsp60
C
Cyt
Nuc
Control
LMB
Control
LMB
RXRα/C3
PARP
Hsp60
D
348
368
NES-RXRα RVLTELVSKMRD-MQMDKTELG
14-3-3 KDSTLIMQLLRDNLTLWTSDTQ
P53 RERFEMFRELNEALELKDAQAG
Rev EPVPLQLPPLER-LTLDCSEDC
IkBα RPSTRIQQQLGQ-LTLENLQML
MEK-1 TNLEALQKKLEE-LELDEQQRK
PKI GNSNELALKLAG-LDINKTEGE
Dsk1 SRFPSLEGAVSE-ISLRDSQKH
NESm-RXRα RVLTELVSKARD-AQMDKTELG
E
GFP
Hsp60
Overlay
GFP-NES
GFP-NES +LMB
GFP-NESm
F
Myc-Nur77
RXRα /NESm
Overlay 1
Hsp60
Overlay 2
Control
3-Cl-AHPC
G
GFP-Nur77
Flag-RXRα/385
Overlay
GFP-Nur77/Δ1
Flag-RXRα/385
Overlay
GFP-Nur77/467
Flag-RXRα/385
Overlay
GFP-Nur77/ΔC3
Flag-RXRα
Overlay

FIGURE 4

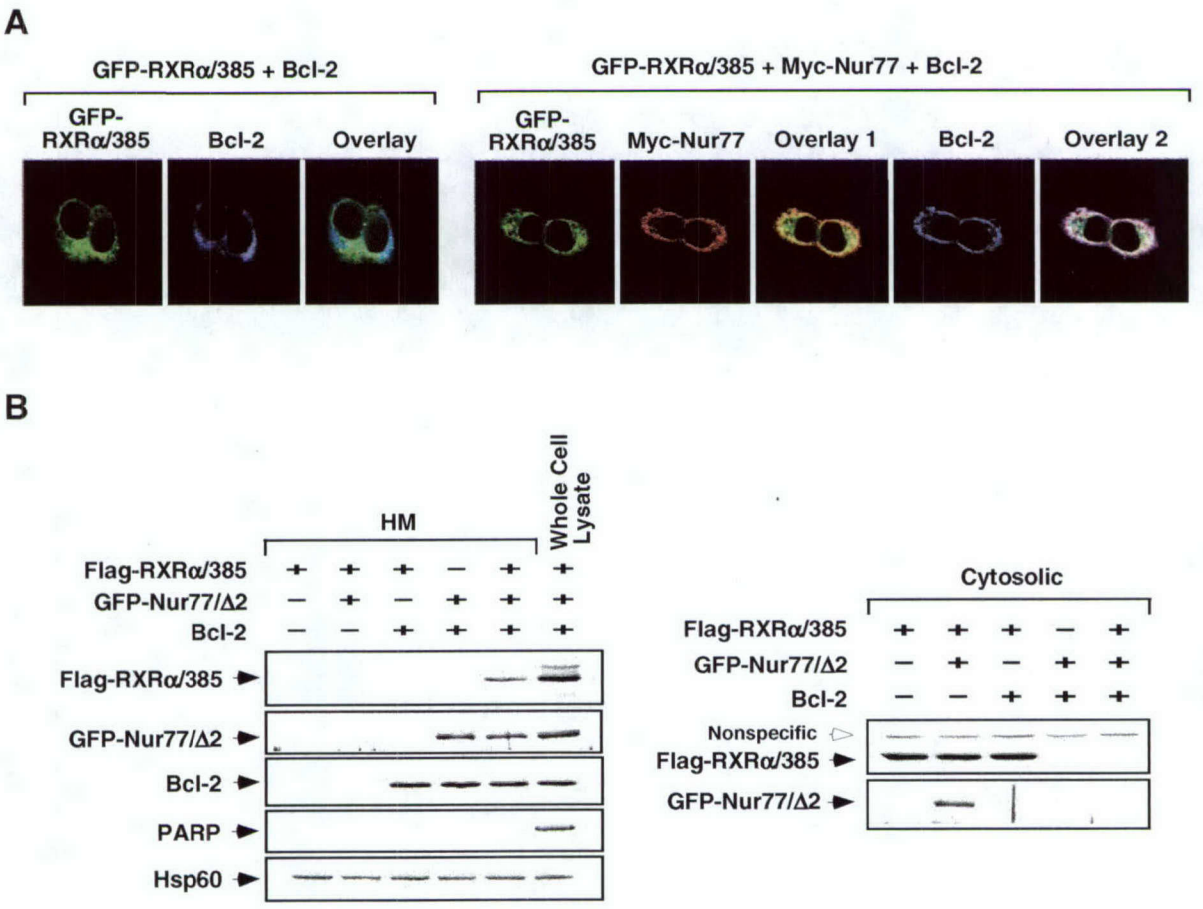
A
GFP-RXRα/385 + Bcl-2
GFP-RXRα/385 + Myc-Nur77 + Bcl-2
GFP-RXRα/385
Bcl-2
Overlay
GFP-RXRα/385
Myc-Nur77
Overlay 1
Bcl-2
Overlay 2
B
HM
Whole Cell Lysate
Flag-RXRα/385 + + + − + +
GFP-Nur77/Δ2 − + − + + +
Bcl-2 − − + + + +
Flag-RXRα/385
GFP-Nur77/Δ2
Bcl-2
PARP
Hsp60
Cytosolic
Flag-RXRα/385 + + + − +
GFP-Nur77/Δ2 − + − + +
Bcl-2 − − + + +
Nonspecific
Flag-RXRα/385
GFP-Nur77/Δ2

FIGURE 5

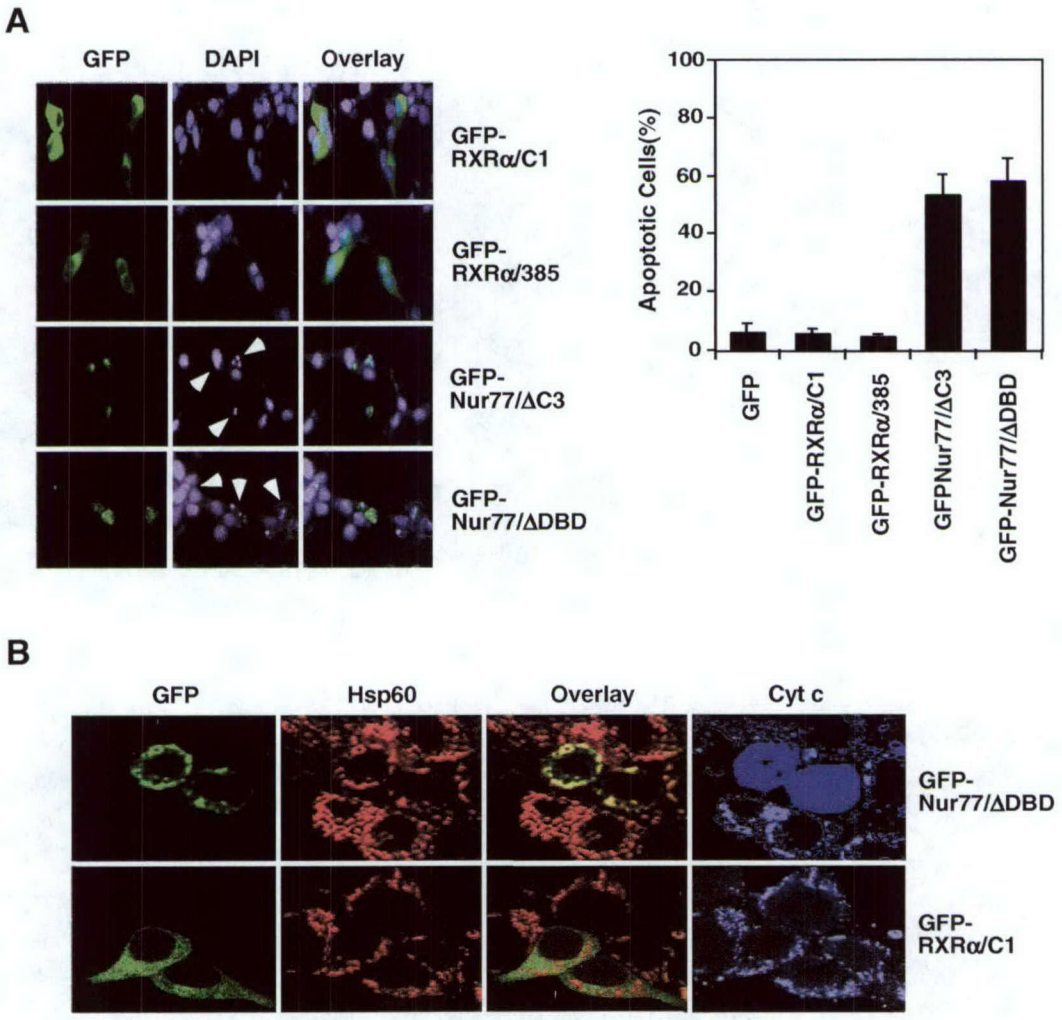
A
GFP
DAPI
Overlay
GFP-
RXRα/C1
GFP-
RXRα/385
GFP-
Nur77/ΔC3
GFP-
Nur77/ΔDBD
Apoptotic Cells(%)
100
80
60
40
20
0
GFP
GFP-RXRα/C1
GFP-RXRα/385
GFPNur77/ΔC3
GFP-Nur77/ΔDBD
B
GFP
Hsp60
Overlay
Cyt c
GFP-
Nur77/ΔDBD
GFP-
RXRα/C1

FIGURE 6

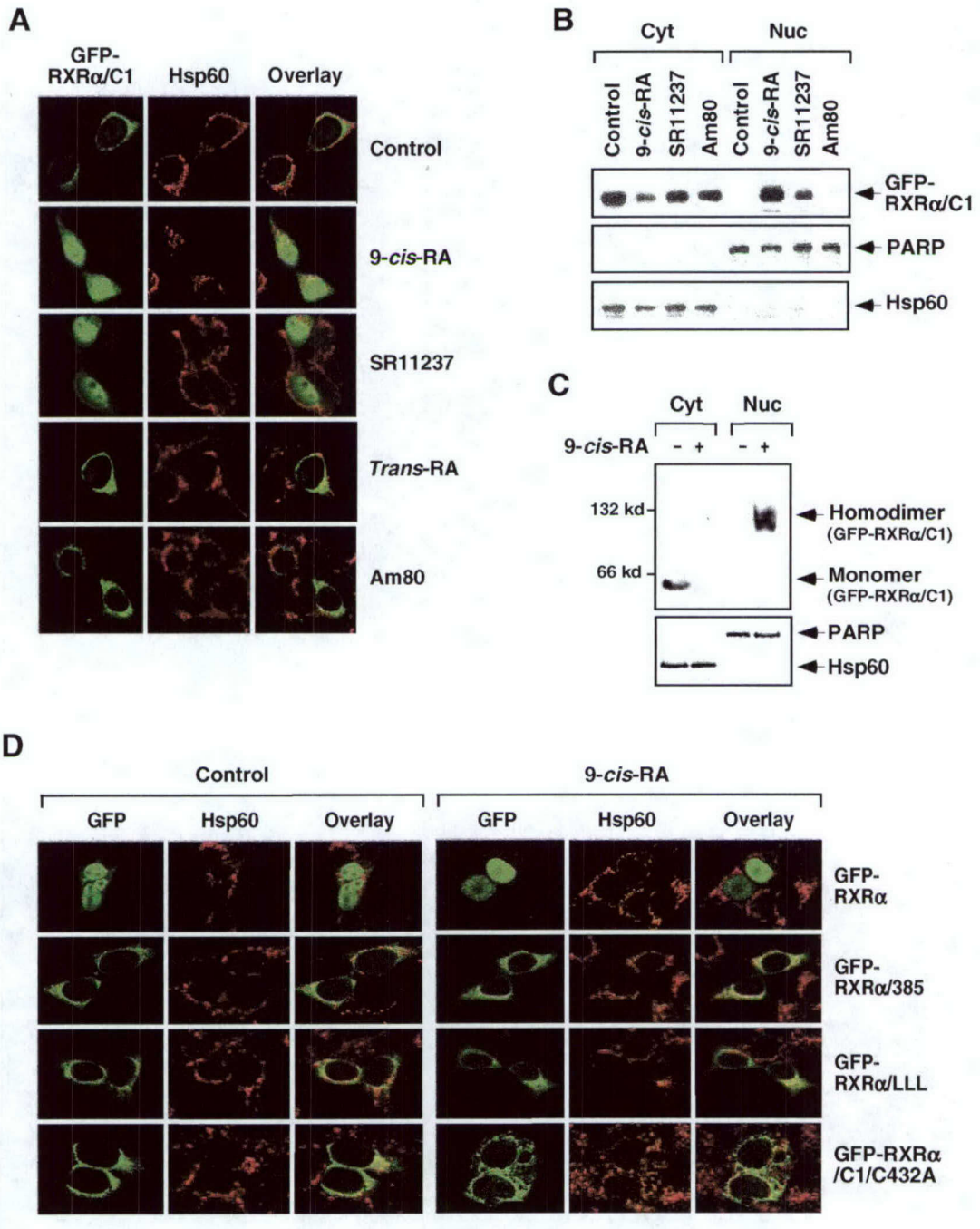
A
GFP-RXRα/C1
Hsp60
Overlay
Control
9-cis-RA
SR11237
Trans-RA
Am80
B
Cyt
Nuc
Control
9-cis-RA
SR11237
Am80
Control
9-cis-RA
SR11237
Am80
GFP-RXRα/C1
PARP
Hsp60
C
Cyt
Nuc
9-cis-RA
- + - +
132 kd
66 kd
Homodimer (GFP-RXRα/C1)
Monomer (GFP-RXRα/C1)
PARP
Hsp60
D
Control
9-cis-RA
GFP
Hsp60
Overlay
GFP
Hsp60
Overlay
GFP-RXRα
GFP-RXRα/385
GFP-RXRα/LLL
GFP-RXRα/C1/C432A

FIGURE 7

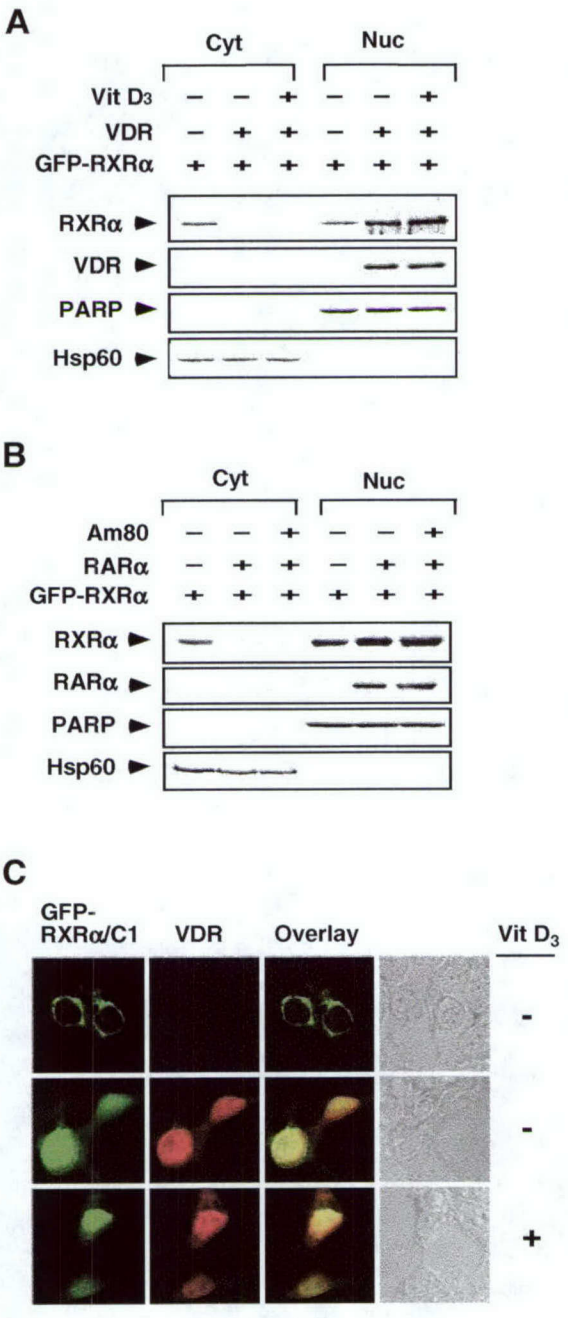
A
Cyt
Nuc
Vit D3 – – + – – +
VDR – + + – + +
GFP-RXRα + + + + + +
RXRα
VDR
PARP
Hsp60
B
Cyt
Nuc
Am80 – – + – – +
RARα – + + – + +
GFP-RXRα + + + + + +
RXRα
RARα
PARP
Hsp60
C
GFP-RXRα/C1
VDR
Overlay
Vit D3
-
-
+

FIGURE 8

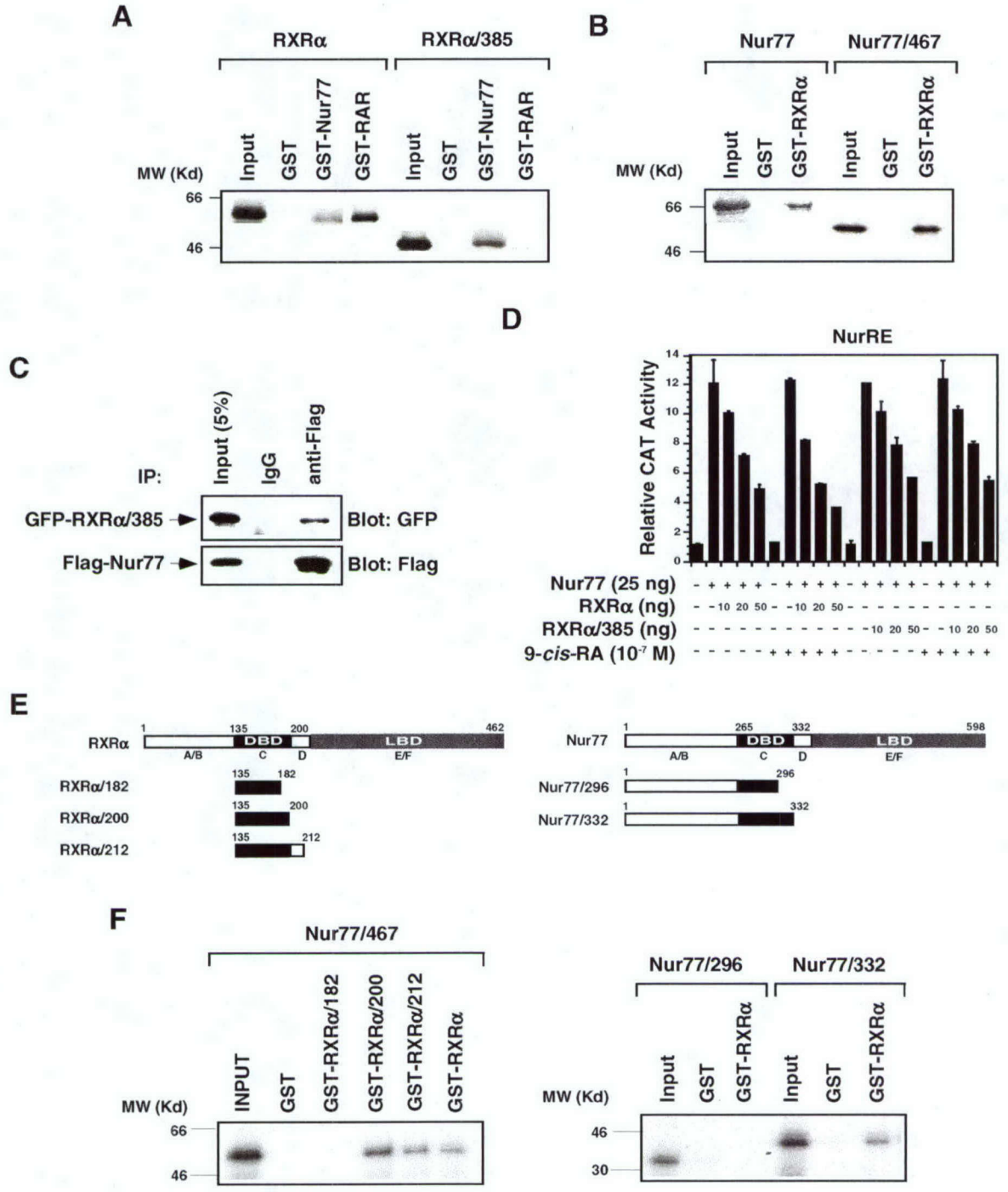
A
RXRα
RXRα/385
Input
GST
GST-Nur77
GST-RAR
MW (Kd)
66
46
B
Nur77
Nur77/467
GST-RXRα
C
IP:
Input (5%)
IgG
anti-Flag
GFP-RXRα/385
Blot: GFP
Flag-Nur77
Blot: Flag
D
NurRE
Relative CAT Activity
Nur77 (25 ng)
RXRα (ng)
RXRα/385 (ng)
9-cis-RA (10-7 M)
E
RXRα
A/B
DBD
C
D
LBD
E/F
RXRα/182
RXRα/200
RXRα/212
Nur77
Nur77/296
Nur77/332
F
INPUT
GST-RXRα/182
GST-RXRα/200
GST-RXRα/212
GST-RXRα

FIGURE 9

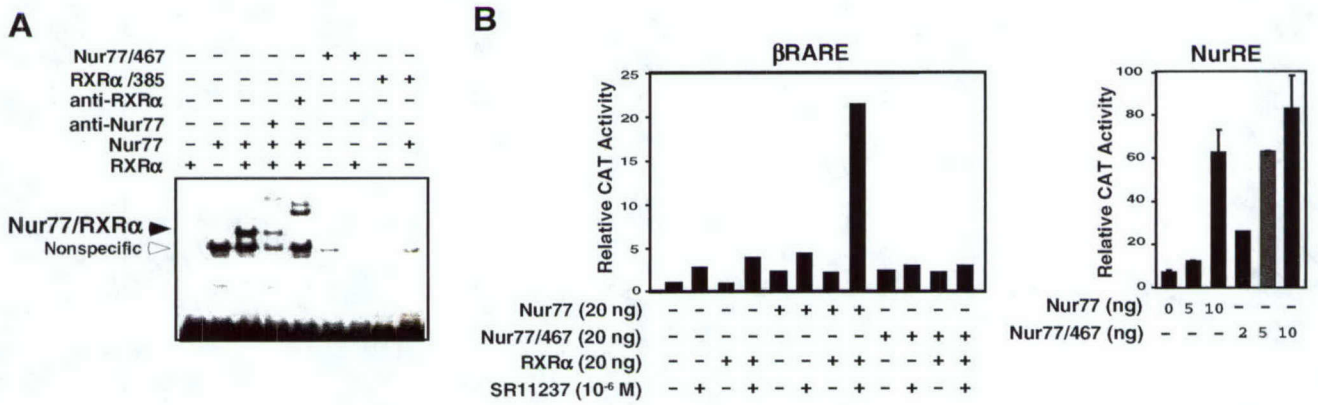
A
Nur77/467
RXRα /385
anti-RXRα
anti-Nur77
Nur77
RXRα
Nur77/RXRα
Nonspecific
B
βRARE
NurRE
Relative CAT Activity
Nur77 (20 ng)
Nur77/467 (20 ng)
RXRα (20 ng)
SR11237 (10⁻⁶ M)
Nur77 (ng)
Nur77/467 (ng)
C
SR11237
anti-RXRα
anti-Nur77
Nur77
RXRα
RXRα/Nur77
Nonspecific
9-cis-RA
D
RXRα/385
Nur77/467
Input
GST
GST-Nur77
GST-RXRα
9-cis-RA

FIGURE 10

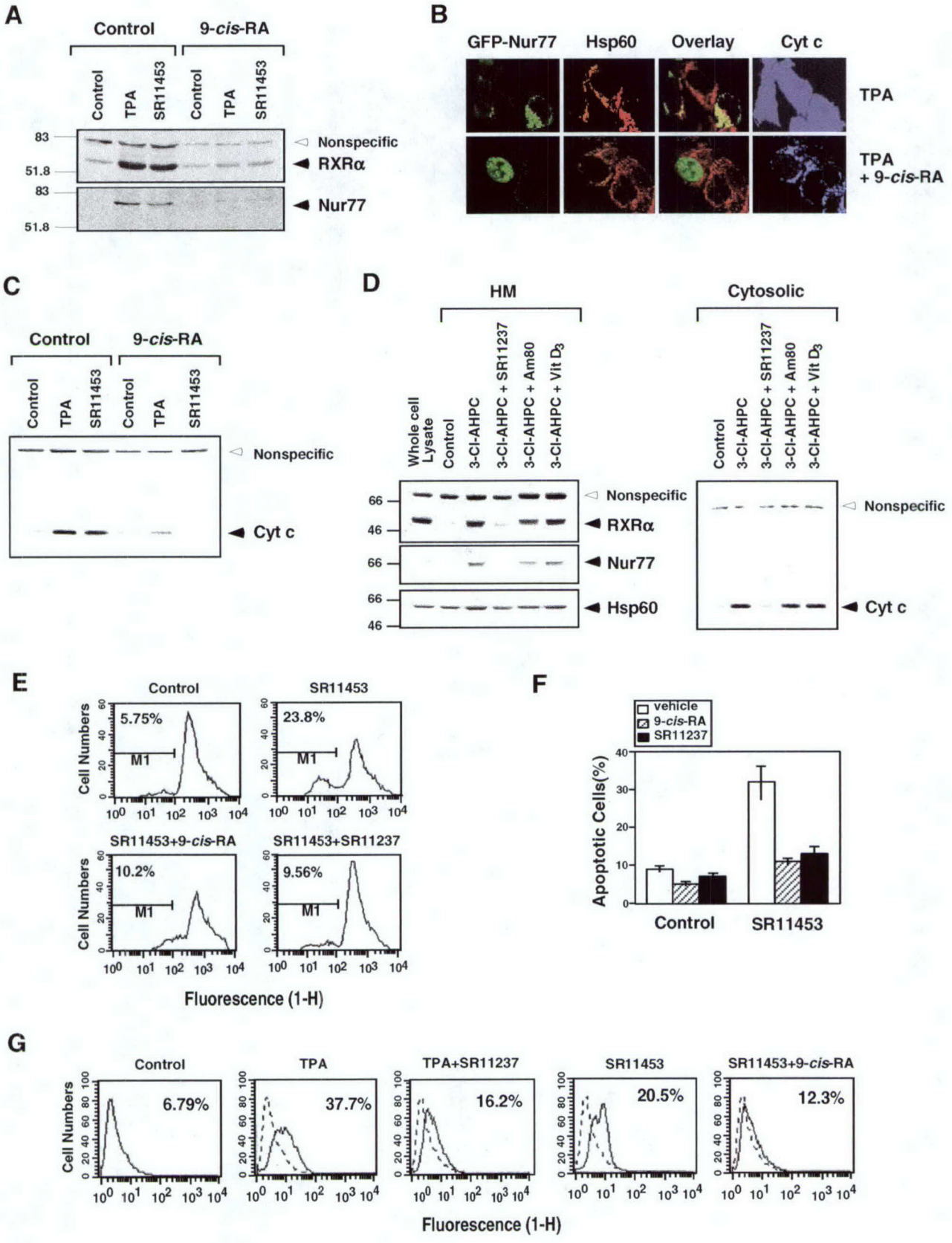
A
Control
9-cis-RA
Control
TPA
SR11453
Control
TPA
SR11453
83
51.8
83
51.8
Nonspecific
RXRα
Nur77
B
GFP-Nur77
Hsp60
Overlay
Cyt c
TPA
TPA
+ 9-cis-RA
C
Control
9-cis-RA
Control
TPA
SR11453
Control
TPA
SR11453
Nonspecific
Cyt c
D
HM
Cytosolic
Whole cell Lysate
Control
3-Cl-AHPC
3-Cl-AHPC + SR11237
3-Cl-AHPC + Am80
3-Cl-AHPC + Vit D3
Control
3-Cl-AHPC
3-Cl-AHPC + SR11237
3-Cl-AHPC + Am80
3-Cl-AHPC + Vit D3
66
46
66
66
46
Nonspecific
RXRα
Nur77
Hsp60
Nonspecific
Cyt c
E
Control
SR11453
5.75%
23.8%
M1
M1
SR11453+9-cis-RA
SR11453+SR11237
10.2%
9.56%
M1
M1
Cell Numbers
Cell Numbers
Fluorescence (1-H)
F
vehicle
9-cis-RA
SR11237
Apoptotic Cells(%)
Control
SR11453
G
Control
TPA
TPA+SR11237
SR11453
SR11453+9-cis-RA
6.79%
37.7%
16.2%
20.5%
12.3%
Cell Numbers
Fluorescence (1-H)

FIGURE 11

[CANCER RESEARCH 63, 3531–3538, July 1, 2003]

Appendix 3

Regulation of Retinoic Acid Receptor β Expression by Peroxisome Proliferator-activated Receptor γ Ligands in Cancer Cells[1]

Sharon Y. James, Feng Lin, Siva Kumar Kolluri, Marcia I. Dawson, and Xiao-kun Zhang[2]

Cancer Center, The Burnham Institute, La Jolla, California 92037

ABSTRACT

The peroxisome proliferator-activated receptor γ (PPARγ) is a nuclear receptor family member that can form a heterodimeric complex with retinoid X receptor (RXR) and initiate transcription of target genes. In this study, we have examined the effects of the PPARγ ligand ciglitazone and the RXR ligand SR11237 on growth and induction of retinoic acid receptor (RAR) β expression in breast and lung cancer cells. Our results demonstrated that ciglitazone and SR11237 cooperatively inhibited the growth of ZR-75-1 and T-47D breast cancer and Calu-6 lung cancer cells. Gel shift analysis indicated that PPARγ, in the presence of RXR, formed a strong complex with a retinoic acid response element (β retinoic acid response element) in the RARβ promoter. In reporter gene assays, RXR ligands and ciglitazone, but not the PPARγ ligand 15d-PGJ_2, cooperatively promoted the transcriptional activity of the β retinoic acid response element. Ciglitazone, but not 15d-PGJ_2, strongly induced RARβ expression in human breast and lung cancer cell lines when used together with SR11237. The induction of RARβ expression by the ciglitazone and SR11237 combination was diminished by a PPARγ-selective antagonist, bisphenol A diglycidyl ether. All-*trans*-retinoic acid or the combination of ciglitazone and SR11237 was able to induce RARβ in all-*trans*-retinoic acid-resistant MDA-MB-231 breast cancer cells only when the orphan receptor chick ovalbumin upstream promoter transcription factor was expressed, or in the presence of the histone deacetylase inhibitor trichostatin A. These studies indicate the existence of a novel RARβ-mediated signaling pathway of PPARγ action, which may provide a molecular basis for developing novel therapies involving RXR and PPARγ ligands in potentiating antitumor responses.

INTRODUCTION

PPARγ[3] is a ligand-activated transcription factor belonging to the steroid/thyroid receptor superfamily, which plays a critical role in the control of adipogenesis (1–4). Specific ligands of PPARγ, including the thiazolidinedione class of antidiabetic agents, the prostanoid 15d-PGJ_2, and certain polyunsaturated fatty acids, have been identified (5, 6). PPARγ expression is not limited to adipocytes because activation of PPARγ by its ligands has been shown to promote growth inhibition, differentiation, and/or apoptosis of various cancer cells (5, 7–9), including breast (10–18) and non-small cell lung carcinoma tissues (19–22).

Retinoids, comprising the native and synthetic derivatives of vitamin A, are promising agents for the prevention and treatment of human cancers, including those of breast and lung (23, 24). The biological effects of retinoids are mainly mediated by their nuclear receptors, RAR and RXR, which each exist as α, β, and γ isoforms (1, 25, 26). PPARγ heterodimerizes with RXR, and the resulting heterodimer binds strongly to its DNA-specific sequence, the PPRE (3, 4). Recent studies have shown that PPARγ/RXR also binds to the estrogen response element (27). PPARγ and RXR ligands have been found to cooperatively induce differentiation and apoptosis of breast and colon cancer cells through interaction with PPARγ/RXR (17, 18, 23, 28).

RARβ plays a critical role in mediating the growth-inhibitory effects of retinoids in various cancer cells (29, 30). The aberrant expression or loss of RARβ in a variety of cancer cell lines suggests that decreased RARβ expression may contribute to retinoid resistance (31–38), implying that RARβ may act as a tumor suppressor. Regulation of RARβ gene expression is principally mediated by the retinoic acid response element (βRARE) in its promoter, to which RAR/RXR heterodimers bind strongly. Activation of RAR/RXR heterodimers is principally mediated via RAR, whereas RXR serves as a silent partner (25). The TR3/RXR heterodimer also binds to the βRARE, which is activated by RXR ligands (39). Thus, the βRARE can be transcriptionally controlled by various heterodimers and their ligands. Other factors also influence RARβ gene expression. The COUP-TF, which is not expressed in many cancer cells, is required for induction of RARβ by ATRA (40). Lack of RARβ expression in cancer cells has also been attributed to abnormal regulation of histone acetylation/deacetylation, which modulates chromatin structure and gene transcription, or hypermethylation of the RARβ promoter (41–45).

In the present study, we evaluated the growth-inhibitory effect of the PPARγ ligand ciglitazone alone and in combination with the RXR ligand (rexinoid) SR11237. Our results showed that ciglitazone and SR11237 cooperatively inhibited the growth and induced apoptosis of breast and lung cancer cell lines. In studying the possible underlying molecular mechanisms, we observed that PPARγ could bind strongly to the βRARE as a PPARγ/RXR heterodimer. The combination of RXR ligands with ciglitazone, but not 15d-PGJ_2, strongly activated the βRARE and induced RARβ expression in breast and lung cancer cells. The induction of RARβ expression by rexinoids and ciglitazone was reduced by a PPARγ antagonist, BADGE (46), indicating the involvement of PPARγ/RXR heterodimers. Together, our results demonstrate that PPARγ can bind to the βRARE as a PPARγ/RXR heterodimer and that induction of RARβ may contribute to the anticancer effect of certain PPARγ ligands.

MATERIALS AND METHODS

Reagents and Cell Lines. The RXR-selective retinoids SR11237, SR11246, and SR11345 were prepared as reported previously (47–49). ATRA and TSA were obtained from Sigma Chemicals (St. Louis, MO). The PPARγ ligands 15d-PGJ_2, ciglitazone, and BADGE were obtained from Cayman Chemicals (Ann Arbor, MI). All reagents were dissolved in a 1:1 ratio of ethanol and DMSO and stored in amber containers at −20°C. Other analytical-grade reagents were obtained from Sigma Chemicals unless otherwise stated.

Received 10/28/02; accepted 4/24/03.

The costs of publication of this article were defrayed in part by the payment of page charges. This article must therefore be hereby marked *advertisement* in accordance with 18 U.S.C. Section 1734 solely to indicate this fact.

[1] S. J. and S. K. K. are supported by Postdoctoral Research Fellowships from the California Breast Cancer Research Program (BCRP 7FB-0062) and the United States Army Medical Research Program (DAMD17-00-1-0173), respectively. M. I. D. and X-k. Z. are supported by National Cancer Institute Grant PO1 CA51993. X-k. Z. is also supported by grants from the NIH (5RO1 CA 60988-09 and 7PO1 CA 87000-01A1) and the United States Army Medical Research Program (DAMD17-00-1-0172).

[2] To whom requests for reprints should be addressed, at Cancer Center, The Burnham Institute, 10901 North Torrey Pines Road, La Jolla, CA 92037. Phone: (858) 646-3141; Fax: (858) 646-3195; E-mail: xzhang@burnham-inst.org.

[3] The abbreviations used are: PPARγ, peroxisome proliferator-activated receptor γ; 15d-PGJ_2, 15-deoxy-$\Delta^{12,14}$ prostaglandin J_2; ATRA, all-*trans*-retinoic acid; βRARE, β retinoic acid response element; BADGE, bisphenol A diglycidyl ether; COUP-TF, chick ovalbumin upstream promoter transcription factor; DR, direct repeat; HDAC, histone deacetylase; PPRE, peroxisome proliferator response element; RAR, retinoic acid receptor; RXR, retinoid X receptor; TSA, trichostatin A; CAT, chloramphenicol transferase; β-gal, β-galactosidase; MTS, 3-(4,5-dimethylthiazol-2yl)-5-(3-carboxymethoxyphenyl)-2-(4-sulfophenyl)-2*H*-tetrazolium; BrdUrd, 5-bromo-2′-deoxyuridine; tk, thymidine kinase.

MDA-MB-231, T-47D, and ZR-75-1 cell lines were routinely maintained in DMEM (MDA-MB-231) or RPMI 1640 (T-47D and ZR-75-1), supplemented with 10% FCS, 100 units/ml penicillin, and 100 μg/ml streptomycin (Irvine Scientific, Santa Ana, CA). Calu-6 were maintained in MEM Earle's Salt Medium (Irvine Scientific) supplemented with 10% FCS and antibiotics. For for Western analysis studies, cells were cultured in their respective medium supplemented with 5% charcoal-treated FCS and antibiotics.

Plasmids. The PPARγ expression vector was kindly provided by Dr. Mark Leid (Oregon State University, Corvallis, OR). Expression vectors for RXRα and reporter gene βRARE-tk-CAT have been described previously (26, 50).

Transfection Assays. MDA-MB-231 and ZR-75-1 cells were seeded at 2×10^5 cells/ml in 6-well plates for 16–24 h before transfection. Cells were transfected with βRARE-tk-CAT plasmid (200 ng), β-gal (200 ng) expression vector (pCH 110; Amersham Biosciences), and carrier DNA (pBluescript; Stratagene, La Jolla, CA) to a final concentration of 2000 ng total DNA/well using LipofectAMINE Plus reagent (Invitrogen, Carlsbad, CA). Cells were treated for 20 h with RXR and PPARγ ligands. CAT activity was normalized with β-gal activity for transfection efficiency.

Western Blot Analysis. Treated cell cultures were subjected to Western blot analysis as described previously (51). Preblocked nitrocellulose membranes were incubated with 1 μg/ml equivalent of anti-RARβ rabbit polyclonal antibody (Santa Cruz Biotechnology, Santa Cruz, CA). RARβ protein was detected by horseradish peroxidase-conjugated antirabbit secondary antibody (Amersham Biosciences), and specific bands were visualized by enhanced chemiluminescence (ECL; Amersham Biosciences). Equivalent loading of samples was determined by reprobing the nitrocellulose membrane with a mouse monoclonal antibody recognizing β-actin (Sigma Chemicals).

Gel Shift Analysis. *In vitro*-synthesized RXR and PPARγ receptor proteins (Promega, Madison, WI) were incubated with RXR and PPARγ ligands alone or in combination and treated with a rabbit polyclonal anti-PPARγ antibody (Santa Cruz Biotechnology) for 20 min before the addition of ^{32}P-labeled βRARE oligonucleotide. Gel shift analysis was performed as described previously (35).

Cell Proliferation and Apoptosis Studies. Treated cells were trypsinized, pelleted by centrifugation at 2000 rpm for 5 min, resuspended in 1 ml of PBS, and fixed in 70% ice-cold ethanol. After two additional PBS washes, the cells were resuspended in PBS containing 50 μg/ml propidium iodide (Sigma Chemicals) and 100 μg/ml DNase-free RNase A (Roche Diagnostics, Indianapolis, IN). Cell suspensions were incubated for 30 min at 37°C with protection from light and analyzed using a FACScatter-Plus flow cytometer (Becton Dickinson, San Jose, CA).

To assess cell viability, cells were seeded at 1×10^3 cells/well in 96-well microtiter plates and treated with varying concentrations of SR11237 and ciglitazone, with medium and ligands replaced every 48 h. After treatment, 20 μl of MTS/phenozine methosulfate solution (Promega) were added to each well, and incubation was continued for 2–4 h at 37°C in the dark. Absorbance (490 nm) was measured on a Bio-Rad 550 microplate reader.

BrdUrd Analysis. Treated cells were incubated with BrdUrd (20 μM; Sigma Chemicals) for 2 h before harvesting of cells. After trypsinization and two PBS washes, cells were pelleted by centrifugation and permeabilized with 4% paraformaldehyde. After a 20-min incubation at room temperature, 0.1% saponin (Sigma Chemicals) was added to the cell suspension, and the incubation was continued for 10 min. The cells were then centrifuged, washed twice with PBS containing 0.1% saponin, and resuspended in PBS containing 30 μg of DNase I (Roche Diagnostics). After a 1-h incubation with either an anti-BrdUrd fluorescent antibody or an isotope control antibody (Becton Dickinson), cells were given a final PBS wash before being analyzed using the FACScatter-Plus flow cytometer (Becton Dickinson).

Statistical Analysis. One-way ANOVA with the Dunnett's post test (GraphPad Prism software) was used to assess significance of treatments at the 5% level for growth inhibition studies.

RESULTS

Ciglitazone and SR11237 Cooperatively Inhibit the Growth of Cancer Cell Lines. Both retinoids and PPARγ ligands are potent regulators of cancer cell growth. Because PPARγ heterodimerizes with RXR (5, 52), we investigated the inhibitory effect of their ligands, alone or in combination, on the growth of breast and lung cancer cells. Fig. 1*A* illustrates the effects of the rexinoid SR11237 and the PPARγ ligand ciglitazone on the growth of the hormone-dependent breast cancer cell lines ZR-75-1 and T-47D and the lung cancer cell line Calu-6. Cell proliferation was assessed by MTS assay after 8 (ZR-75-1 and Calu-6) or 10 (T-47D) days of treatment. All three cell lines have been reported to be sensitive to growth inhibition by ATRA (35, 53). Treatment of these cell lines with ATRA strongly inhibited their growth in a dose-dependent manner (Fig. 1*A*). SR11237 did not exhibit a significant effect on T-47D cell growth, whereas in ZR-75-1 and Calu-6 cells, the rexinoid modestly inhibited cell growth when used at 1 μM (10% and 22% for ZR-75-1 and Calu-6 cells, respectively; Fig. 1*A*). Ciglitazone (1 μM) did not have any marked antiproliferative effects in these cancer cell lines. However, when SR11237 and ciglitazone were used in combination, cooperative effects on cell growth were observed in the three cell lines. In ZR-75-1 cells, a 2-fold growth-inhibitory effect was observed when using 1 μM SR11237 and 1 μM ciglitazone (10% with SR11237 *versus* 23% with the combination). In addition, cotreatment of ZR-75-1 cells with 1 μM SR11237 and 10 μM ciglitazone further enhanced growth inhibition by 47% (Fig. 1*A, middle graph*). Cotreatment of T-47D cells with SR11237 and ciglitazone resulted in 51% growth inhibition, compared with the antiproliferative effects of each ligand used alone, whereas an additive effect was observed in Calu-6 cells.

We also evaluated the antiproliferative effects of SR11237 and ciglitazone by BrdUrd incorporation. ZR-75-1 cells were treated for 72 h with SR11237 alone or in combination with ciglitazone. As shown in Fig. 1*B*, SR11237 or ciglitazone alone did not inhibit BrdUrd incorporation relative to control. In contrast, the combination decreased BrdUrd incorporation by 46%. Additional studies were performed to determine whether the combination induced apoptosis (Fig. 1*C*). ZR-75-1 cells were treated for 5 days with SR11237 alone or in the presence of ciglitazone. After treatment, cells were harvested and stained with propidium iodide for flow cytometry. Apoptotic cells were determined by measuring sub-G_1-phase cells. When the cells were treated with the combination of SR11237 and ciglitazone, 7.6% of the cells were apoptotic compared with control (Fig. 1*C*). Taken together, these results demonstrate that ciglitazone and a RXR ligand can cooperatively inhibit growth and induce apoptosis in cancer cells.

Induction of RARβ by a PPARγ Ligand in Cancer Cell Lines. Induction of RARβ has been correlated with the growth-inhibitory and apoptosis-inducing effects of retinoids in breast and lung cancer cells (30, 35, 36). We then determined whether the antiproliferative effects observed using rexinoids and PPARγ ligands could be attributed to their ability to induce RARβ. Western analysis was used to investigate whether RXR and PPARγ ligands were capable of regulating RARβ protein expression. ZR-75-1, T-47D, and Calu-6 cells were treated for 24 h with SR11237, in the absence or presence of ciglitazone. In these cell lines, ATRA readily induced RARβ, as reported previously (35), whereas ciglitazone did not show any effect (Fig. 2). SR11237 only weakly induced RARβ in all of the cell lines. However, cotreatment with SR11237 and ciglitazone resulted in a marked expression of RARβ protein. Together, these data demonstrate that ciglitazone strongly induces RARβ expression in combination with a RXR ligand.

Differential Effects of PPARγ Ligands on RARβ Expression. Next, we examined whether other known PPARγ ligands were able to induce RARβ. We evaluated the prostanoid 15d-PGJ_2 and rosiglitazone, two well-characterized PPARγ ligands (5, 6). T-47D, ZR-75-1, and Calu-6 cells were first treated with 15d-PGJ_2 alone or with SR11237. Unlike SR11237 and ciglitazone cotreatment (Fig. 2), SR11237 and 15d-PGJ_2 did not induce RARβ (Fig. 3), thus highlight-

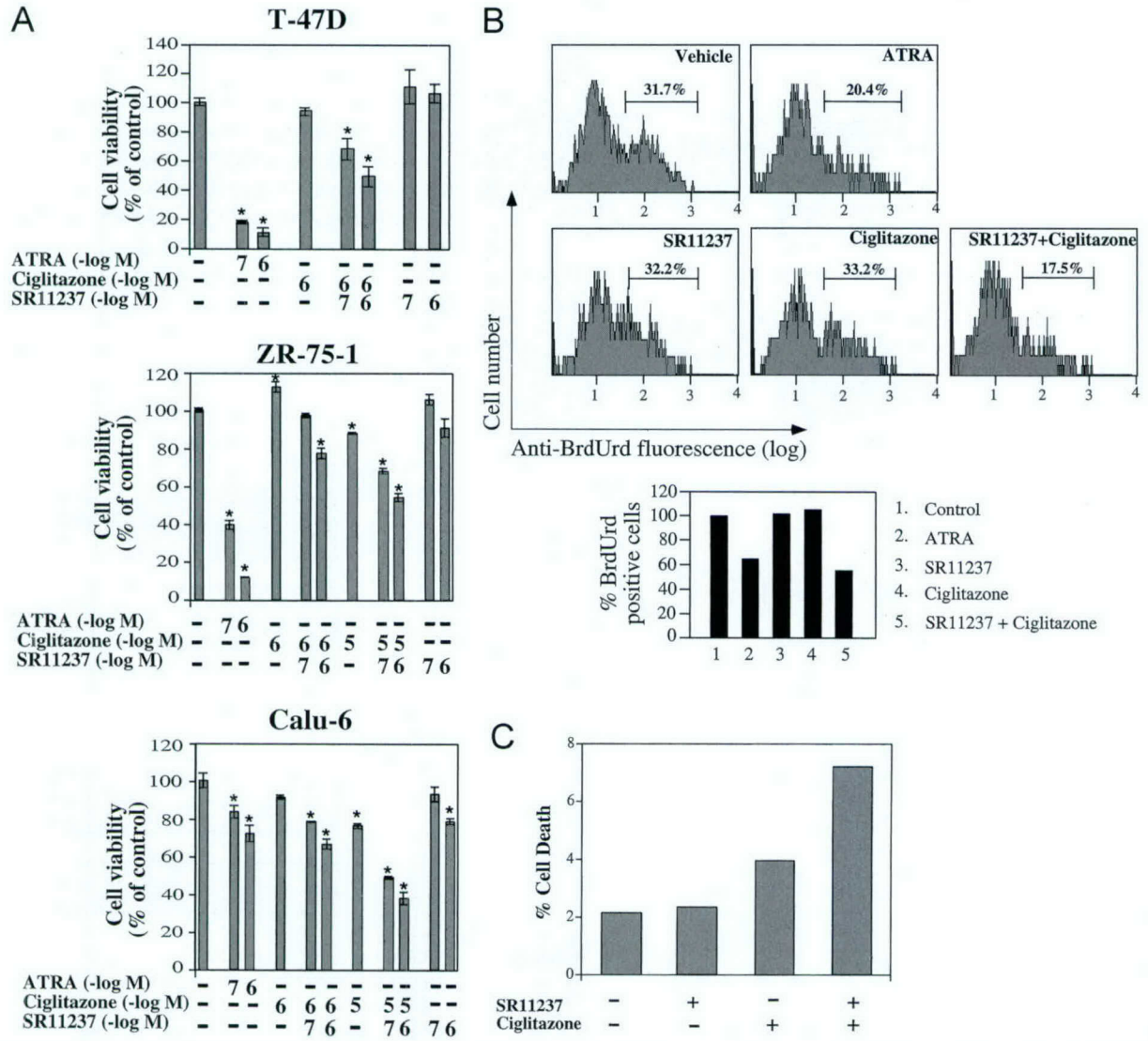

Fig. 1. PPARγ ligand ciglitazone and RXR ligand SR11237 cooperatively inhibit growth and induce apoptosis of cancer cells. *A*, inhibition of cell proliferation by RXR and PPARγ ligands. T-47D, ZR-75-1, and Calu-6 cells were treated for 10 (T-47D) or 8 (ZR-75-1 and Calu-6) days with the indicated concentrations of ATRA, SR11237, or ciglitazone. After treatment, inhibition of cell proliferation was assessed by MTS assay. Cell viability is expressed as a percentage of the control ± SE ($n = 4$). *, $P < 0.05$. *B*, rexinoid and ciglitazone cooperatively inhibit breast cancer cell proliferation. ZR-75-1 cells were treated for 72 h with ATRA alone (1 μM, as positive control) or with SR11237 (1 μM) or ciglitazone (10 μM), either alone or in combination. Cell proliferation was assessed by BrdUrd incorporation (*top graphs*). The data are presented as a histogram (*bottom graph*). *C*, induction of apoptosis by RXR and PPARγ ligands. ZR-75-1 cells were treated for 5 days with SR11237 (1 μM) or ciglitazone (10 μM), either alone or in combination. Apoptotic cells were determined by measuring the sub-G_1 peak of cells using propidium iodide staining and flow cytometry. Results are representative of three separate experiments.

ing the differential effects of the PPARγ ligands on modulating RARβ expression in combination with a RXR-selective retinoid. We also found that rosiglitazone alone or with SR11237 did not induce RARβ (Fig. 3). Thus, not all PPARγ ligands are capable of inducing RARβ expression in cancer cells.

PPARγ Mediates the Effects of Ciglitazone in Inducing RARβ. To determine whether the induction of RARβ by ciglitazone (in combination with SR11237) was mediated by PPARγ, we examined the effect of BADGE a PPARγ antagonist. BADGE was shown to block the ability of PPARγ ligands to activate the transcriptional and adipogenic function of PPARγ (46). Fig. 4 illustrates that BADGE alone did not affect basal RARβ expression in T-47D cells. However, BADGE significantly attenuated ciglitazone/SR11237-induced RARβ. The effect of BADGE was specific because it did not inhibit ATRA-induced RARβ expression. Similar attenuation of ciglitazone/SR11237-induced RARβ by BADGE was observed in ZR-75-1 cells (data not shown). These data strongly suggest that induction of RARβ expression by ciglitazone (in combination with SR11237) is mediated via activation of PPARγ.

PPARγ Binds to the βRARE as a PPARγ/RXR Heterodimer. The βRARE present in the RARβ promoter mediates transcriptional regulation of RARβ expression by RAR and RXR heterodimers (50, 54). To determine whether induction of RARβ by ciglitazone and SR11237 was also mediated via βRARE, we studied the possibility that PPARγ was capable of interacting with the βRARE. *In vitro*-translated PPARγ protein was analyzed for binding to the βRARE by the gel shift assay (Fig. 5*A*). PPARγ alone did not exhibit clear binding to the βRARE. However, PPARγ in combination with *in vitro*-synthesized RXRα protein produced a prominent complex. Binding was not affected when PPARγ/RXR was preincubated with SR11237 or ciglitazone. However, when *in vitro*-translated RXR and PPARγ were incubated with an anti-PPARγ antibody, binding of the RXR/PPARγ heterodimer to βRARE was attenuated, indicating that the PPARγ antibody blocked the ability of PPARγ to bind to βRARE

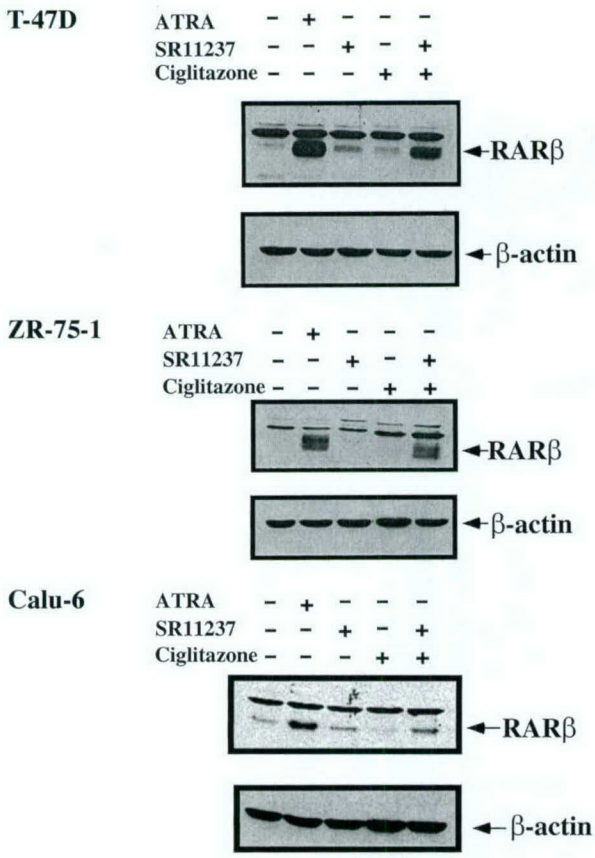

Fig. 2. Regulation of RARβ protein expression by RXR and PPARγ ligands. T-47D, ZR-75-1, and Calu-6 cells were treated for 24 h with SR11237 (1 μM) or ciglitazone (10 μM), either alone or in combination. Cells were also treated with ATRA (1 μM) as a positive control. Cell lysates were prepared, and RARβ protein expression was assessed by Western analysis (51).

(Fig. 5*B*). These data demonstrate that PPARγ can bind to the βRARE as a PPARγ/RXR heterodimer.

Differential Regulation of βRARE Transcriptional Activity by PPARγ Ligands. The observation that PPARγ/RXR binds to the βRARE suggested that it represented another RXR-containing heterodimeric complex that activates the βRARE. Therefore, we studied whether RXR and PPARγ ligands could activate the βRARE. A reporter containing the CAT gene fused to the βRARE (50) was transiently transfected into MDA-MB-231 cells, which were treated with SR11237 alone or in combination with ciglitazone. As revealed in Fig. 6*A*, SR11237, but not ciglitazone, slightly induced βRARE transcriptional activity. Moreover, induction of βRARE was synergized by cotreatment with ciglitazone. We also examined whether the synergistic effect on activating βRARE could be extended to other PPARγ and RXR ligands. Ciglitazone, but not 15d-PGJ_2 or rosiglitazone, strongly induced βRARE activity together with SR11237 (Fig. 6*A*). This correlated with the effects of these PPARγ ligands on induction of RARβ protein expression (Figs. 2 and 3). Similar results were obtained using ZR-75-1 breast cancer cells (Fig. 6*B, top graph*). Thus, not all PPARγ ligands that activate the PPRE similarly activate βRARE together with SR11237. We also examined the effect of the RXR ligands SR11246 and SR11345 on βRARE activity in ZR-75-1 cells (48, 49). Again, ciglitazone strikingly enhanced transcriptional activity of the βRARE induced by SR11246 and SR11345 (Fig. 6*B*).

Antagonistic Effects of Other PPARγ Ligands on RARβ Expression. The differential effect of PPARγ ligands on SR11237-induced RARβ expression (Figs. 2 and 3) prompted us to investigate whether PPARγ ligands antagonized one another's activity. The observation that ciglitazone synergized with SR11237 in inducing RARβ expression suggested that binding of ciglitazone to PPARγ and binding of SR11237 to RXR resulted in transactivation of the βRARE by PPARγ/RXR heterodimers. In contrast, binding of PPARγ with 15d-PGJ_2 may either not activate or suppress the transcriptional activity of PPARγ/RXR on the βRARE. Therefore, we determined whether 15d-PGJ_2 interfered with PPARγ activation by ciglitazone. Fig. 7 shows that in ZR-75-1 cells, 15d-PGJ_2 inhibited RARβ expression induced by the combination of SR11237 and ciglitazone. Thus, 15d-PGJ_2 acts as an antagonist of PPARγ with respect to the induction of RARβ by ciglitazone.

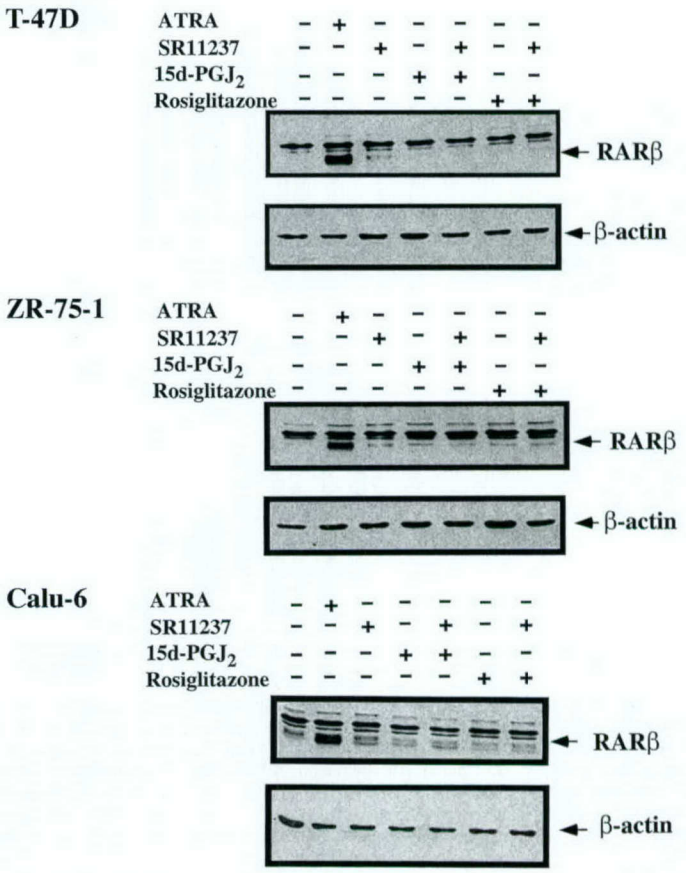

Fig. 3. Differential effects of PPARγ ligands in inducing RARβ expression. T47D, ZR-75-1 and Calu-6 cells were treated for 24 h with SR11237 (1 μM), 15d-PGJ_2 (5 μM), or rosiglitazone (10 μM), alone or with SR11237 + 15d-PGJ_2 or SR11237 + rosiglitazone in combination. Cells were also treated with ATRA (1 μM), as a positive control. RARβ protein expression was assessed by Western analysis.

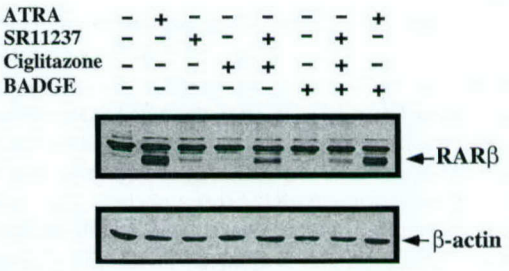

Fig. 4. A PPARγ antagonist blocks induction of RARβ protein expression. T-47D cells were pretreated for 3 h with the PPARγ antagonist BADGE (20 μM), after which the cells were treated with SR11237 (1 μM) or ciglitazone (10 μM), alone or in combination. RARβ protein expression was determined by Western analysis.

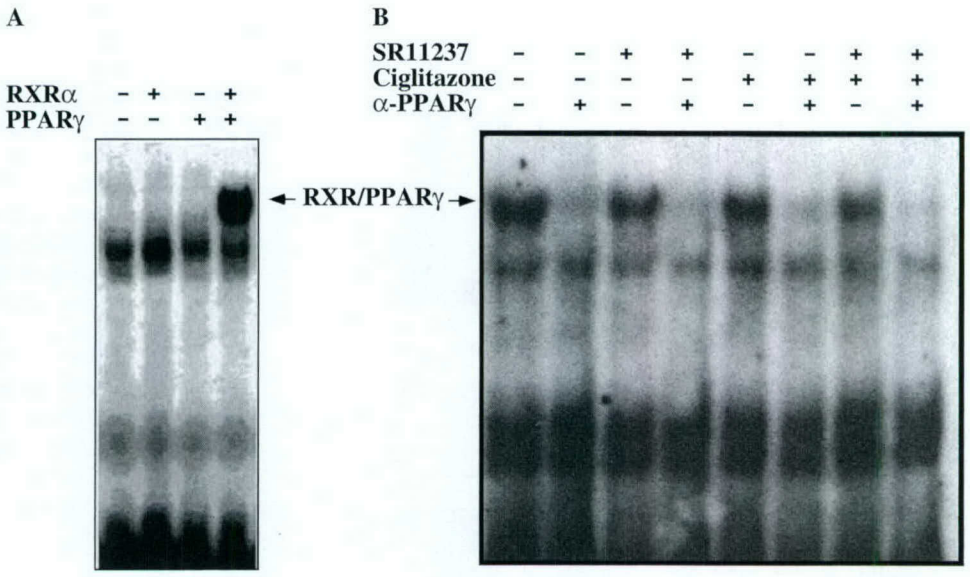

Fig. 5. RXR and PPARγ bind to βRARE as a heterodimeric complex. *A, in vitro*-translated RXR and PPARγ were incubated with ^{32}P-radiolabeled βRARE, either alone or in combination. The resulting reactions were then analyzed by gel shift analysis. *B, in vitro*-translated RXRα and PPARγ were incubated with SR11237 (1 μM) and/or ciglitazone (10 μM), in the absence or presence of anti-PPARγ rabbit polyclonal antibody (α-PPARγ). After a further incubation with ^{32}P-radiolabeled βRARE, the reactions were analyzed by gel shift analysis.

Mechanisms of RARβ Induction in MDA-MB-231 Cells: Role of HDACs and the Orphan Receptor COUP-TF. ATRA does not induce RARβ expression in the estrogen-independent breast cancer cell line MDA-MB-231 (35, 41–43, 55, 56). Therefore, we examined whether SR11237 and ciglitazone could induce RARβ in these cells. In agreement with previous observations (35), treatment of MDA-MB-231 cells with ATRA did not induce RARβ expression (Fig. 8*A*). SR11237 and ciglitazone, either alone or in combination, did not induce RARβ expression, despite the expression of RXRα and PPARγ (data not shown). Histone acetylation and DNA methylation have been reported to contribute to silencing RARβ gene expression in the MDA-MB-231 cell line (41, 44). HDAC inhibitors, such as TSA, have been shown to suppress the effects of corepressors (41). Therefore, to determine whether inhibitors of histone deacetylation played a role in augmenting induction of RARβ by RXR and PPARγ ligands, MDA-MB-231 cells were treated with SR11237, alone or in combination with ciglitazone and TSA. Cotreatment of cells with ATRA and TSA readily induced RARβ protein expression (Fig. 8*A*). Cells cotreated with SR11237, ciglitazone, and TSA also induced RARβ. These results suggest that histone deacetylation may represent a mechanism through which RARβ expression is suppressed in MDA-MB-231 cancer cells.

We reported previously that the orphan receptor COUP-TF is required for RARβ expression by ATRA and is not expressed in MDA-MB-231 cells (40). COUP-TF enhances RARβ expression by increasing the recruitment of receptor coactivators to the RARβ promoter. Stable expression of COUP-TF in MDA-MB-231 cells restored the ability of ATRA to induce RARβ expression (40). Therefore, we examined whether COUP-TF expression was also involved in the induction of RARβ by SR11237 and ciglitazone. Treatment of MDA-MB-231 COUP-TF stable clone cells with ATRA resulted in strong expression of RARβ, as reported previously (40). SR11237 or ciglitazone alone slightly induced RARβ expression in this COUP-TF stable clone (Fig. 8*B*). As observed previously with the T-47D, ZR-75-1, and Calu-6 cells (Fig. 3), 15d-PGJ$_2$, either alone or in combination with SR11237, did not induce RARβ expression in the MDA-MB-231 COUP-TF stable cells. In contrast, SR11237 and ciglitazone markedly induced RARβ expression (Fig. 8*B*). Thus, the expression of COUP-TF modulates the induction of RARβ by PPARγ/RXR heterodimers, as well as the RAR/RXR heterodimers.

DISCUSSION

Retinoids are effective in suppressing tumor development in many animal carcinogenesis models and are being evaluated in clinical trials for prevention and treatment of cancers (23, 24). As an illustration, the rexinoid LGD1069 suppresses mammary tumor development and inhibits the growth of established tumors *in vivo* (57, 58). This retinoid was recently approved for treatment of cutaneous T-cell lymphoma on the basis of clinical trial results and highlights the potential for rexinoids as effective cancer therapeutic agents. Unfortunately, a major limitation in retinoid therapy is that the concentrations needed for anticancer activity also produce adverse effects. Among recent anticancer approaches, combination therapy may lead to synergistic growth-inhibitory effects on cancer cells, thereby allowing the use of lower concentrations to reduce toxicity associated with retinoid treatment (23, 24). In this study, we demonstrate that the PPARγ ligand ciglitazone and the RXR ligand SR11237 cooperatively inhibited the growth of breast and lung cancer cells, whereas either one alone did not markedly inhibit growth (Fig. 1*A*). The combination resulted in an enhanced inhibition of cell growth, BrdUrd incorporation, and induction of apoptosis (Fig. 1). Previous studies showed that the rexinoids enhanced the antidiabetic activity of PPARγ ligands (59). Our present results indicate that the combination of rexinoids and PPARγ ligands may represent a new approach to effectively inhibit the growth of cancer cells.

The cooperative effect of rexinoids and PPARγ ligands is likely mediated by their receptors RXR and PPARγ and their heterodimerization. In elucidation of the downstream pathways mediating the RXR and PPARγ heterodimers, we observed that induction of RARβ, a potent growth inhibitor (29, 30), is involved in the cooperative growth inhibition of PPARγ and RXR ligands. Rexinoids and ciglitazone alone did not show an appreciable effect on RARβ expression. However, their combination strongly induced RARβ expression in breast cancer and lung cancer cells to a degree that was comparable with that of ATRA (Fig. 2). Thus, our results suggest that induction of RARβ expression accounts for the cooperative growth-inhibitory effect of rexinoids and ciglitazone.

The effect of ciglitazone in inducing RARβ is mediated by PPARγ. This was demonstrated by our observation that RARβ induction was attenuated by the PPARγ antagonist BADGE (Fig. 4). Induction of RARβ by ATRA is mainly mediated by RAR/RXR heterodimers that

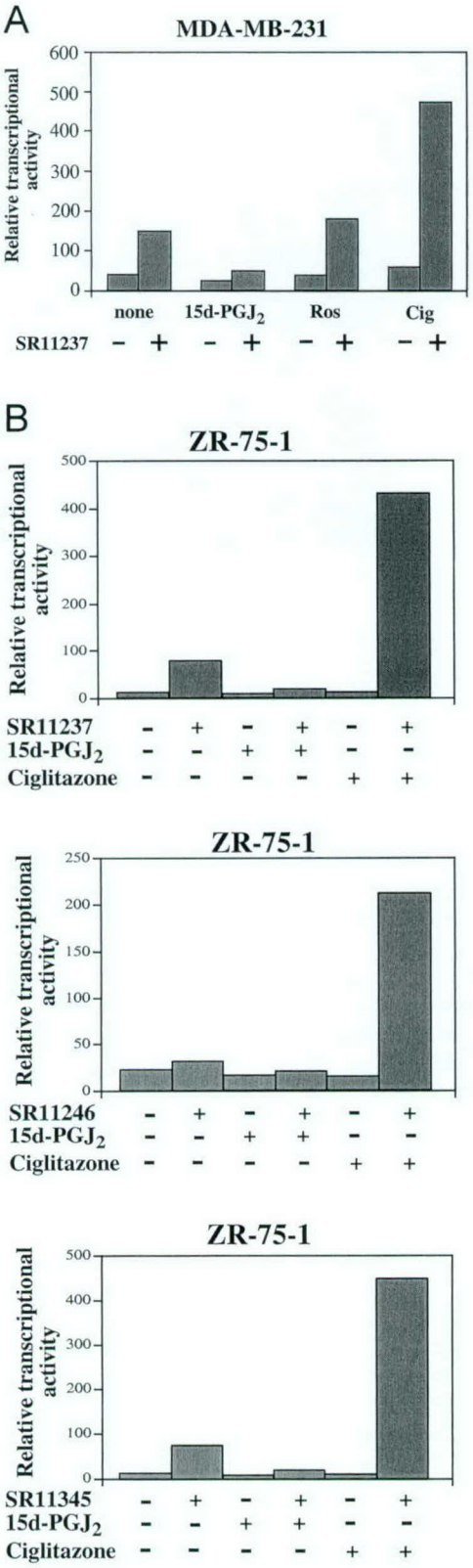

Fig. 6. PPARγ ligands differentially promote βRARE transcriptional activity. The MDA-MB-231 and ZR-75-1 breast cancer cell lines were transiently transfected with 200 ng of βRARE-tk-CAT (50) and 200 ng of β-gal expression vector. Transfected cells were treated for 20 h with the indicated RXR-selective ligands (1 μM) or PPARγ ligands (5 μM 15d-PGJ_2, 10 μM ciglitazone, or rosiglitazone), either alone or in combination. Transcriptional activity of βRARE was assessed by CAT assay, using β-gal as an internal standard to evaluate transfection efficiency. Results are representative of three separate experiments, and values are expressed as relative transcriptional activity. *A*, effect of RXR and PPARγ ligands on inducing βRARE in MDA-MB-231 cells. *B*, effect of RXR and PPARγ ligands on inducing βRARE transcriptional activity in ZR-75-1 cells.

bind to the βRARE in the RARβ promoter (50, 54). In studying how PPARγ and RXR mediated the RARβ induction by rexinoids and ciglitazone, we demonstrated that the PPARγ/RXR heterodimeric complex bound to the βRARE (Fig. 5) and induced its transcriptional activation in the presence of rexinoids and ciglitazone (Fig. 6). We demonstrated previously (39, 60) that rexinoids could induce RARβ expression through TR3/RXR heterodimers via βRARE. The results from the present study demonstrate that the PPARγ/RXR heterodimer represents another RXR-containing heterodimer that mediates the effect of RXR ligands on RARβ induction and growth inhibition.

Classical retinoids fail to induce RARβ expression in certain lung cancer cell lines and in the estrogen-independent MDA-MB-231 breast cancer cells (35, 41–44, 61–64). Lack of RARβ induction has contributed to the retinoid resistance of cancer cells (29, 30). We reported previously (40) that the inability of RAR/RXR heterodimers to activate the RARβ promoter in ATRA-resistant MDA-MB-231 cells was due to lack of the orphan receptor COUP-TF. Our present data indicate that the SR11237 and ciglitazone combination failed to induce RARβ expression in wild-type MDA-MB-231 cells (Fig. 8*A*)

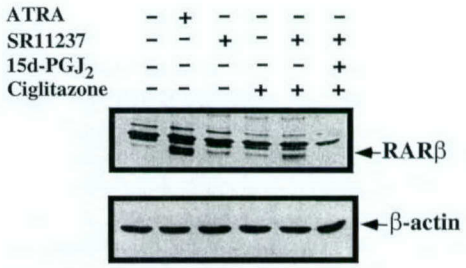

Fig. 7. 15d-PGJ_2 antagonizes RARβ expression induced by rexinoid and ciglitazone. ZR-75-1 cells were treated for 24 h with ATRA alone (1 μM) or with SR11237 (1 μM), ciglitazone (10 μM), or 15d-PGJ_2 (5 μM), either alone or in combination. RARβ protein expression was determined by Western analysis.

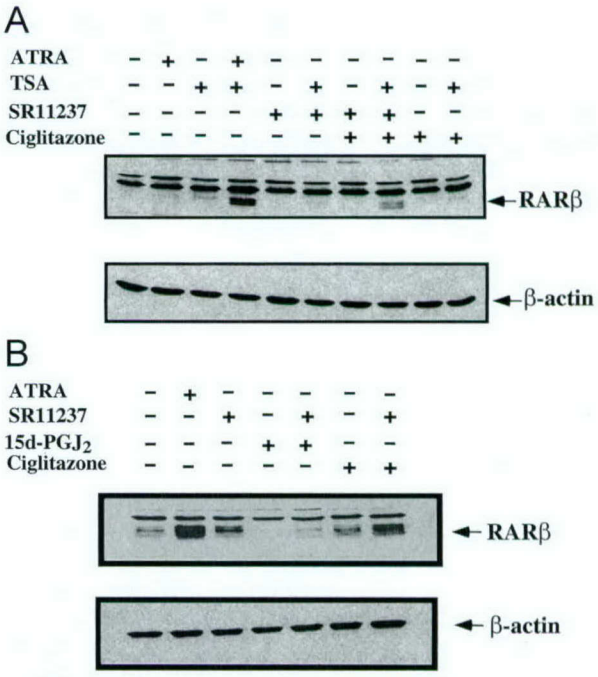

Fig. 8. RXR and PPARγ ligands differentially regulate RARβ expression in wild-type MDA-MB-231 and MDA-MB-231 COUP-TF stable cells. *A*, MDA-MB-231 cells were treated for 48 h with SR11237 (1 μM) ciglitazone (10 μM), or TSA (100 ng/ml), alone or in combination. RARβ protein expression was determined by Western analysis. *B*, MDA-MB-231 COUP-TF stable cells were treated for 24 h with SR11237 (1 μM), 15d-PGJ_2 (5 μM), or ciglitazone (10 μM), alone or in combination, and analyzed for RARβ expression by Western analysis.

but strongly induced RARβ in MDA-MB-231 cells stably expressing COUP-TF (Fig. 8*B*). These results indicate a requirement for COUP-TF in activating RARβ promoter by the PPARγ/RXR heterodimer. Similar to ATRA, we observed that the combination of ciglitazone and SR11237 strongly induced RARβ in wild-type MDA-MB-231 cells when the HDAC inhibitor TSA was present (Fig. 8*A*). These results suggest that histone deacetylation is another mechanism responsible for silencing RARβ expression.

One interesting observation in the present study is that PPARγ ligands differentially regulate βRARE activity and induction of RARβ expression. Ciglitazone, troglitazone, rosiglitazone, and 15d-PGJ_2 act as potent agonists of the PPARγ/RXR heterodimer on the PPRE (3–8). However, only ciglitazone activated βRARE when used with rexinoids (Fig. 6). Combination of rosiglitazone or 15d-PGJ_2 with a rexinoid failed to induce RARβ in these cancer cell lines (Fig. 3). Thus, different PPARγ ligands exhibit opposing effects on transactivation of the PPARγ/RXR heterodimer. Why there is such disparity among the PPARγ compounds and their ability to cooperate with RXR ligands to induce RARβ is presently unclear. One obvious explanation would be the differences in ligand structure, which may bind in an alternate conformation when bound to PPARγ/RXR heterodimers complexed with the βRARE. This difference in binding may then impair or fail to initiate efficient transcription, perhaps through inappropriate recruitment of corepressors or coactivators. Regulation of retinoid signaling by receptor polarity and allosteric control of ligand binding has been well demonstrated for RAR/RXR heterodimers. Binding of RAR/RXR heterodimers with RAR ligand strongly activates the DR5 element, whereas the binding suppresses RXR agonist activity on the DR1 element (65, 66). The differential effects of ligands to activate RAR on response elements was shown to result from opposite polarities of the RXR/RAR heterodimer to asymmetrically oriented half-sites (65). Previous studies demonstrated that PPARγ binds to the 5′-half-site position of the PPRE, whereas RXR occupies the 3′-half site (67, 68). It is likely that similar receptor polarity and allosteric control of transcription of RXR ligand activity by PPARγ ligand binding exists with respect to the PPRE, which is a DR1 response element, and βRARE, a DR5 element. Whether such an allosteric mechanism exists for the PPARγ/RXR heterodimer requires further investigation. Regardless of the underlying molecular mechanisms, our observation provides an opportunity to identify specific PPARγ ligands for inhibiting cancer cell growth through inducing RARβ expression in combination with rexinoids.

In summary, we have demonstrated that rexinoids and ciglitazone can synergistically inhibit the growth of breast and lung cancer cells through their induction of RARβ. Our results demonstrate that PPARγ/RXR heterodimers can bind to the βRARE and promote its transcriptional activity in response to rexinoids and certain PPARγ ligands. Further characterization of the effect of PPARγ ligands on the transactivation of βRARE by PPARγ/RXR heterodimers and the underlying molecular mechanisms may lead to the identification of potent and specific PPARγ ligands that inhibit cancer cell growth through this novel signaling pathway.

ACKNOWLEDGMENTS

We thank Laura Frazer for preparation of the manuscript and John Kim for proofreading of the manuscript.

REFERENCES

1. Mangelsdorf, D. J., Thummel, C., Beato, M., Herrlich, P., Schutz, G., Umesono, K., Blumberg, B., Kastner, P., Mark, M., Chambon, P., *et al.* The nuclear receptor superfamily: the second decade. Cell, *83:* 835–839, 1995.
2. Moller, D. E., and Berger, J. The mechanisms of action of PPARs. Annu. Rev. Med., *53:* 409–435, 2002.
3. Rosen, E. D., Walkey, C. J., Puigserver, P., and Spiegelman, B. M. Transcriptional regulation of adipogenesis. Genes Dev., *14:* 1293–1307, 2000.
4. Rangwala, S. M., and Lazar, M. A. Transcriptional control of adipogenesis. Annu. Rev. Nutr., *20:* 535–559, 2000.
5. Rosen, E. D., and Spiegelman, B. M. PPARγ: a nuclear regulator of metabolism, differentiation, and cell growth. J. Biol. Chem., *276:* 37731–37734, 2001.
6. Hihi, A. K., Michalik, L., and Wahli, W. PPARs: transcriptional effectors of fatty acids and their derivatives. Cell. Mol. Life Sci., *59:* 790–798, 2002.
7. Sporn, M. B., Suh, N., and Mangelsdorf, D. J. Prospects for prevention and treatment of cancer with selective PPARγ modulators (SPARMs). Trends Mol. Med., *7:* 395–400, 2001.
8. Kersten, S., Desvergne, B., and Wahli, W. Roles of PPARs in health and disease. Nature (Lond.), *405:* 421–424, 2000.
9. Murphy, G. J., and Holder, J. C. PPARγ agonists: therapeutic role in diabetes, inflammation and cancer. Trends Pharmacol. Sci., *21:* 469–474, 2000.
10. Clay, C. E., Atsumi, G. I., High, K. P., and Chilton, F. H. Early *de novo* gene expression is required for 15-deoxy-$\Delta^{12,14}$-prostaglandin J_2-induced apoptosis in breast cancer cells. J. Biol. Chem., *276:* 47131–47135, 2001.
11. Kilgore, M. W., Tate, P. L., Rai, S., Sengoku, E., and Price, T. M. MCF-7 and T47D human breast cancer cells contain a functional peroxisomal response. Mol. Cell. Endocrinol., *129:* 229–235, 1997.
12. Mueller, E., Sarraf, P., Tontonoz, P., Evans, R. M., Martin, K. J., Zhang, M., Fletcher, C., Singer, S., and Spiegelman, B. M. Terminal differentiation of human breast cancer through PPARγ. Mol. Cell, *1:* 465–470, 1998.
13. Suh, N., Wang, Y., Williams, C. R., Risingsong, R., Gilmer, T., Willson, T. M., and Sporn, M. B. A new ligand for the peroxisome proliferator-activated receptor γ (PPARγ), GW7845, inhibits rat mammary carcinogenesis. Cancer Res., *59:* 5671–5673, 1999.
14. Pignatelli, M., Cortes-Canteli, M., Lai, C., Santos, A., and Perez-Castillo, A. The peroxisome proliferator-activated receptor γ is an inhibitor of ErbBs activity in human breast cancer cells. J. Cell Sci., *114:* 4117–4126, 2001.
15. Thoennes, S. R., Tate, P. L., Price, T. M., and Kilgore, M. W. Differential transcriptional activation of peroxisome proliferator-activated receptor γ by ω-3 and ω-6 fatty acids in MCF-7 cells. Mol. Cell. Endocrinol., *160:* 67–73, 2000.
16. Yin, F., Wakino, S., Liu, Z., Kim, S., Hsueh, W. A., Collins, A. R., Van Herle, A. J., and Law, R. E. Troglitazone inhibits growth of MCF-7 breast carcinoma cells by targeting G_1 cell cycle regulators. Biochem. Biophys. Res. Commun., *286:* 916–922, 2001.
17. Elstner, E., Muller, C., Koshizuka, K., Williamson, E. A., Park, D., Asou, H., Shintaku, P., Said, J. W., Heber, D., and Koeffler, H. P. Ligands for peroxisome proliferator-activated receptor γ and retinoic acid receptor inhibit growth and induce apoptosis of human breast cancer cells *in vitro* and in BNX mice. Proc. Natl. Acad. Sci. USA, *95:* 8806–8811, 1998.
18. Mehta, R. G., Williamson, E., Patel, M. K., and Koeffler, H. P. A ligand of peroxisome proliferator-activated receptor γ, retinoids, and prevention of preneoplastic mammary lesions. J. Natl. Cancer Inst. (Bethesda), *92:* 418–423, 2000.
19. Theocharis, S., Kanelli, H., Politi, E., Margeli, A., Karkandaris, C., Philippides, T., and Koutselinis, A. Expression of peroxisome proliferator activated receptor γ in non-small cell lung carcinoma: correlation with histological type and grade. Lung Cancer, *36:* 249–255, 2002.
20. Satoh, T., Toyoda, M., Hoshino, H., Monden, T., Yamada, M., Shimizu, H., Miyamoto, K., and Mori, M. Activation of peroxisome proliferator-activated receptor γ stimulates the growth arrest and DNA-damage inducible 153 gene in non-small cell lung carcinoma cells. Oncogene, *21:* 2171–2180, 2002.
21. Tsubouchi, Y., Sano, H., Kawahito, Y., Mukai, S., Yamada, R., Kohno, M., Inoue, K., Hla, T., and Kondo, M. Inhibition of human lung cancer cell growth by the peroxisome proliferator-activated receptor γ agonists through induction of apoptosis. Biochem. Biophys. Res. Commun., *270:* 400–405, 2000.
22. Chang, T. H., and Szabo, E. Induction of differentiation and apoptosis by ligands of peroxisome proliferator-activated receptor γ in non-small cell lung cancer. Cancer Res., *60:* 1129–1138, 2000.
23. Lippman, S. M., and Lotan, R. Advances in the development of retinoids as chemopreventive agents. J. Nutr., *130:* 479S–482S, 2000.
24. Altucci, L., and Gronemeyer, H. The promise of retinoids to fight against cancer. Nat. Rev. Cancer, *1:* 181–193, 2001.
25. Chambon, P. A decade of molecular biology of retinoic acid receptors. FASEB J., *10:* 940–954, 1996.
26. Zhang, X. K., Hoffmann, B., Tran, P. B., Graupner, G., and Pfahl, M. Retinoid X receptor is an auxiliary protein for thyroid hormone and retinoic acid receptors. Nature (Lond.), *355:* 441–446, 1992.
27. Nunez, S. B., Medin, J. A., Braissant, O., Kemp, L., Wahli, W., Ozato, K., and Segars, J. H. Retinoid X receptor and peroxisome proliferator-activated receptor activate an estrogen responsive gene independent of the estrogen receptor. Mol. Cell. Endocrinol., *127:* 27–40, 1997.
28. Stoll, B. A. Linkage between retinoid and fatty acid receptors: implications for breast cancer prevention. Eur. J. Cancer Prev., *11:* 319–325, 2002.
29. Zhang, X. K. Vitamin A and apoptosis in prostate cancer. Endocr. Relat. Cancer, *9:* 87–102, 2002.
30. Zhang, X. K., Liu, Y., and Lee, M. O. Retinoid receptors in human lung cancer and breast cancer. Mutat. Res., *350:* 267–277, 1996.
31. Gebert, J. F., Moghal, N., Frangioni, J. V., Sugarbaker, D. J., and Neel, B. G. High frequency of retinoic acid receptor β abnormalities in human lung cancer. Oncogene, *6:* 1859–1868, 1991.

32. Houle, B., Leduc, F., and Bradley, W. E. Implication of RARβ in epidermoid (squamous) lung cancer. Genes Chromosomes Cancer, *3:* 358–366, 1991.
33. Hu, L., Crowe, D. L., Rheinwald, J. G., Chambon, P., and Gudas, L. J. Abnormal expression of retinoic acid receptors and keratin 19 by human oral and epidermal squamous cell carcinoma cell lines. Cancer Res., *51:* 3972–3981, 1991.
34. Nervi, C., Vollberg, T. M., George, M. D., Zelent, A., Chambon, P., and Jetten, A. M. Expression of nuclear retinoic acid receptors in normal tracheobronchial cells and in lung carcinoma cells. Exp. Cell Res., *195:* 163–170, 1991.
35. Liu, Y., Lee, M. O., Wang, H. G., Li, Y., Hashimoto, Y., Klaus, M., Reed, J. C., and Zhang, X. Retinoic acid receptor β mediates the growth-inhibitory effect of retinoic acid by promoting apoptosis in human breast cancer cells. Mol. Cell. Biol., *16:* 1138–1149, 1996.
36. Swisshelm, K., Ryan, K., Lee, X., Tsou, H. C., Peacocke, M., and Sager, R. Down-regulation of retinoic acid receptor β in mammary carcinoma cell lines and its up-regulation in senescing normal mammary epithelial cells. Cell Growth Differ., *5:* 133–141, 1994.
37. Berard, J., Laboune, F., Mukuna, M., Masse, S., Kothary, R., and Bradley, W. E. Lung tumors in mice expressing an antisense RARβ2 transgene. FASEB J., *10:* 1091–1097, 1996.
38. Lotan, R., Xu, X. C., Lippman, S. M., Ro, J. Y., Lee, J. S., Lee, J. J., and Hong, W. K. Suppression of retinoic acid receptor β in premalignant oral lesions and its up-regulation by isotretinoin. N. Engl. J. Med., *332:* 1405–1410, 1995.
39. Wu, Q., Dawson, M. I., Zheng, Y., Hobbs, P. D., Agadir, A., Jong, L., Li, Y., Liu, R., Lin, B., and Zhang, X. K. Inhibition of *trans*-retinoic acid-resistant human breast cancer cell growth by retinoid X receptor-selective retinoids. Mol. Cell. Biol., *17:* 6598–6608, 1997.
40. Lin, B., Chen, G. Q., Xiao, D., Kolluri, S. K., Cao, X., Su, H., and Zhang, X. K. Orphan receptor COUP-TF is required for induction of retinoic acid receptor β, growth inhibition, and apoptosis by retinoic acid in cancer cells. Mol. Cell. Biol., *20:* 957–970, 2000.
41. Bovenzi, V., and Momparler, R. L. Antineoplastic action of 5-aza-2′-deoxycytidine and histone deacetylase inhibitor and their effect on the expression of retinoic acid receptor β and estrogen receptor α genes in breast carcinoma cells. Cancer Chemother. Pharmacol., *48:* 71–76, 2001.
42. Sirchia, S. M., Ferguson, A. T., Sironi, E., Subramanyan, S., Orlandi, R., Sukumar, S., and Sacchi, N. Evidence of epigenetic changes affecting the chromatin state of the retinoic acid receptor β2 promoter in breast cancer cells. Oncogene, *19:* 1556–1563, 2000.
43. Widschwendter, M., Berger, J., Hermann, M., Muller, H. M., Amberger, A., Zeschnigk, M., Widschwendter, A., Abendstein, B., Zeimet, A. G., Daxenbichler, G., and Marth, C. Methylation and silencing of the retinoic acid receptor β2 gene in breast cancer. J. Natl. Cancer Inst. (Bethesda), *92:* 826–832, 2000.
44. Sirchia, S. M., Ren, M., Pili, R., Sironi, E., Somenzi, G., Ghidoni, R., Toma, S., Nicolo, G., and Sacchi, N. Endogenous reactivation of the RARβ2 tumor suppressor gene epigenetically silenced in breast cancer. Cancer Res., *62:* 2455–2461, 2002.
45. Momparler, R. L., and Bovenzi, V. DNA methylation and cancer. J. Cell Physiol., *183:* 145–154, 2000.
46. Wright, H. M., Clish, C. B., Mikami, T., Hauser, S., Yanagi, K., Hiramatsu, R., Serhan, C. N., and Spiegelman, B. M. A synthetic antagonist for the peroxisome proliferator-activated receptor γ inhibits adipocyte differentiation. J. Biol. Chem., *275:* 1873–1877, 2000.
47. Lehmann, J. M., Jong, L., Fanjul, A., Cameron, J. F., Lu, X. P., Haefner, P., Dawson, M. I., and Pfahl, M. Retinoids selective for retinoid X receptor response pathways. Science (Wash. DC), *258:* 1944–1946, 1992.
48. Dawson, M. I., Jong, L., Hobbs, P. D., Cameron, J. F., Chao, W. R., Pfahl, M., Lee, M. O., Shroot, B., and Pfahl, M. Conformational effects of retinoid receptor selectivity. 2. Effects of retinoid bridging group on retinoid X receptor activity and selectivity. J. Med. Chem., *38:* 3368–3383, 1995.
49. Dawson, M. I., Hobbs, P. D., Jong, L., Xiao, D., Chao, W. R., Pan, C., and Zhang, X. K. sp2-bridged diaryl retinoids: effects of bridge-region substitution on retinoid X receptor selectivity. Bioorg. Med. Chem. Lett., *10:* 1307–1310, 2000.
50. Hoffmann, B., Lehmann, J. M., Zhang, X. K., Hermann, T., Husmann, M., Graupner, G., and Pfahl, M. A retinoic acid receptor-specific element controls the retinoic acid receptor-β promoter. Mol. Endocrinol., *4:* 1727–1736, 1990.
51. James, S. Y., Mercer, E., Brady, M., Binderup, L., and Colston, K. W. EB1089, a synthetic analogue of vitamin D, induces apoptosis in breast cancer cells *in vivo* and *in vitro.* Br. J. Pharmacol., *125:* 953–962, 1998.
52. Mangelsdorf, D. J., and Evans, R. M. The RXR heterodimers and orphan receptors. Cell, *83:* 841–850, 1995.
53. Li, Y., Dawson, M. I., Agadir, A., Lee, M. O., Jong, L., Hobbs, P. D., and Zhang, X. K. Regulation of RARβ expression by RAR- and RXR-selective retinoids in human lung cancer cell lines: effect on growth inhibition and apoptosis induction. Int. J. Cancer, *75:* 88–95, 1998.
54. Sucov, H. M., Murakami, K. K., and Evans, R. M. Characterization of an autoregulated response element in the mouse retinoic acid receptor type β gene. Proc. Natl. Acad. Sci. USA, *87:* 5392–5396, 1990.
55. Fontana, J. A., Hobbs, P. D., and Dawson, M. I. Inhibition of mammary carcinoma growth by retinoidal benzoic acid derivatives. Exp. Cell Biol., *56:* 254–263, 1988.
56. van der Burg, B., van der Leede, B. M., Kwakkenbos-Isbrucker, L., Salverda, S., de Laat, S. W., and van der Saag, P. T. Retinoic acid resistance of estradiol-independent breast cancer cells coincides with diminished retinoic acid receptor function. Mol. Cell. Endocrinol., *91:* 149–157, 1993.
57. Gottardis, M. M., Bischoff, E. D., Shirley, M. A., Wagoner, M. A., Lamph, W. W., and Heyman, R. A. Chemoprevention of mammary carcinoma by LGD1069 (Targretin): an RXR-selective ligand. Cancer Res., *56:* 5566–5570, 1996.
58. Bischoff, E. D., Gottardis, M. M., Moon, T. E., Heyman, R. A., and Lamph, W. W. Beyond tamoxifen: the retinoid X receptor-selective ligand LGD1069 (TARGRETIN) causes complete regression of mammary carcinoma. Cancer Res., *58:* 479–484, 1998.
59. Mukherjee, R., Davies, P. J., Crombie, D. L., Bischoff, E. D., Cesario, R. M., Jow, L., Hamann, L. G., Boehm, M. F., Mondon, C. E., Nadzan, A. M., Paterniti, J. R., Jr., and Heyman, R. A. Sensitization of diabetic and obese mice to insulin by retinoid X receptor agonists. Nature (Lond.), *386:* 407–410, 1997.
60. Chen, G. Q., Lin, B., Dawson, M. I., and Zhang, X. K. Nicotine modulates the effects of retinoids on growth inhibition and RARβ expression in lung cancer cells. Int. J. Cancer, *99:* 171–178, 2002.
61. Kim, Y. H., Dohi, D. F., Han, G. R., Zou, C. P., Oridate, N., Walsh, G. L., Nesbitt, J. C., Xu, X. C., Hong, W. K., Lotan, R., *et al.* Retinoid refractoriness occurs during lung carcinogenesis despite functional retinoid receptors. Cancer Res., *55:* 5603–5610, 1995.
62. Zhang, X. K., Liu, Y., Lee, M. O., and Pfahl, M. A specific defect in the retinoic acid response associated with human lung cancer cell lines. Cancer Res., *54:* 5663–5669, 1994.
63. van der Leede, B. M., van den Brink, C. E., and van der Saag, P. T. Retinoic acid receptor and retinoid X receptor expression in retinoic acid-resistant human tumor cell lines. Mol. Carcinog., *8:* 112–122, 1993.
64. Moghal, N., and Neel, B. G. Evidence for impaired retinoic acid receptor-thyroid hormone receptor AF-2 cofactor activity in human lung cancer. Mol. Cell. Biol., *15:* 3945–3959, 1995.
65. Kurokawa, R., DiRenzo, J., Boehm, M., Sugarman, J., Gloss, B., Rosenfeld, M. G., Heyman, R. A., and Glass, C. K. Regulation of retinoid signalling by receptor polarity and allosteric control of ligand binding. Nature (Lond.), *371:* 528–531, 1994.
66. Zechel, C., Shen, X. Q., Chen, J. Y., Chen, Z. P., Chambon, P., and Gronemeyer, H. The dimerization interfaces formed between the DNA binding domains of RXR, RAR and TR determine the binding specificity and polarity of the full-length receptors to direct repeats. EMBO J., *13:* 1425–1433, 1994.
67. IJpenberg, A., Jeannin, E., Wahli, W., and Desvergne, B. Polarity and specific sequence requirements of peroxisome proliferator- activated receptor (PPAR)/retinoid X receptor heterodimer binding to DNA. A functional analysis of the malic enzyme gene PPAR response element. J. Biol. Chem., *272:* 20108–20117, 1997.
68. Hsu, M. H., Palmer, C. N., Song, W., Griffin, K. J., and Johnson, E. F. A carboxyl-terminal extension of the zinc finger domain contributes to the specificity and polarity of peroxisome proliferator-activated receptor DNA binding. J. Biol. Chem., *273:* 27988–27997, 1998.

THE JOURNAL OF BIOLOGICAL CHEMISTRY
Vol. 277, No. 24, Issue of June 14, pp. 21414–21422, 2002
Printed in U.S.A.

Appendix 4

Regulation of Retinoic Acid-induced Inhibition of AP-1 Activity by Orphan Receptor Chicken Ovalbumin Upstream Promoter-Transcription Factor*

Received for publication, February 25, 2002, and in revised form, April 2, 2002
Published, JBC Papers in Press, April 4, 2002, DOI 10.1074/jbc.M201885200

Feng Lin, Siva Kumar Kolluri, Guo-quan Chen, and Xiao-kun Zhang‡

From the Burnham Institute, Cancer Center, La Jolla, California 92037

Retinoids are therapeutically effective in the treatment of various cancers, and some of the therapeutic action of retinoids can be ascribed to their potent inhibition of AP-1 activity that regulates transcription of genes associated with cell growth. We recently reported that the expression of orphan receptor chicken ovalbumin upstream promoter-transcription factor (COUP-TF) plays a role in mediating the growth inhibitory effect of *trans*-retinoic acid (*trans*-RA) in cancer cells. To gain insight into the molecular mechanism by which COUP-TF regulates *trans*-RA activity, we evaluated the effect of COUP-TF on antagonism of AP-1 activity by *trans*-RA. Our results demonstrated a positive correlation between COUP-TF expression and the ability of *trans*-RA to inhibit AP-1 activity in various cancer cell lines. In transient transfection assay, expression of COUP-TF strongly inhibited tumor promoter 12-*O*-tetradecanoylphorbol-13-acetate-induced AP-1 transactivation activity and transactivation of c-Jun/c-Fos in both a *trans*-RA-dependent and –independent manner. *In vitro* studies demonstrated that the addition of COUP-TF inhibited c-Jun DNA binding through a direct protein-protein interaction that is mediated by the DNA binding domain of COUP-TF and the leucine zipper of c-Jun. Stable expression of COUP-TF in COUP-TF-negative MDA-MB231 breast cancer cells restored the ability of *trans*-RA to inhibit 12-*O*-tetradecanoylphorbol-13-acetate-induced c-Jun expression. The effect of COUP-TF in enhancing the *trans*-RA-induced antagonism of AP-1 activity required expression of retinoic acid receptors (RARs), since stable expression of COUP-TF in COUP-TF-negative HT-1376 bladder cancer cells, which do not express RARα and RARβ, failed to restore *trans*-RA-induced AP-1 repression. Thus, COUP-TF, through its physical interaction with AP-1, promotes anticancer effects of retinoids by potentiating their anti-AP-1 activity.

Retinoids, the natural and synthetic vitamin A analogs, exert profound effects on many biological processes, including cell proliferation and differentiation (1, 2), and are recognized as promising agents for the prevention and treatment of various cancers. The effects of retinoids are mainly mediated by two nuclear receptor classes, the retinoic acid receptor (RAR)[1] and retinoid X receptor (RXR) (3–5). Both are encoded by three different genes (α, β, and γ) and function as ligand-inducible transcription factors *in vivo* mainly as RXR/RAR heterodimers. *trans*-Retinoic acid (*trans*-RA) binds RARs, whereas 9-*cis*-RA binds both RARs and RXRs. Binding of retinoids to their receptors induces receptor conformational changes that switch on transcription of genes containing RA response elements (RAREs) (3–5). In addition to their positive regulation of RARE-containing genes, retinoid receptors, in response to their ligands, can inhibit effects induced by the tumor promoter 12-*O*-tetradecanoylphorbol-13-acetate (TPA) and the transcriptional activity of the proto-oncogenes c-Jun and c-Fos (6), which are components of the AP-1 complex, which often has a role in cancer cell proliferation (7). The activation of AP-1-responsive genes by TPA or c-Jun/c-Fos through TPA response elements (TREs) is repressed by retinoid receptors in a ligand-dependent manner (8–10). Conversely, AP-1 represses transactivation of retinoid receptors (8, 9). This mutual antagonism appears to play a critical role in regulating cell growth and differentiation (6). For example, overexpression of c-Jun conferred retinoid resistance to breast cancer cells (11), while overexpression of retinoid receptors enabled *trans*-RA to inhibit AP-1 activity in ovarian cancer cells and their growth (12). The functional interaction between AP-1 and retinoid receptors is also observed for other nuclear receptors, including glucocorticoid receptor (13–16), thyroid hormone receptor (17), vitamin D receptor, estrogen receptor (18, 19), and androgen receptor (AR) (18).

The anti-AP-1 activities shown by liganded retinoid receptors appear to contribute significantly to the therapeutic efficacy of retinoids against hyperproliferative diseases (6). Transcription of various AP-1-responsive genes, such as collagenase and stromelysin, which have roles in tumor progression and invasiveness (20), is inhibited by retinoids (8–10) and has been reported to contribute to their reversal of human bronchial epithelial squamous differentiation (21). Retinyl methyl ether, which effectively prevents mammary cancer in animals, strongly suppressed AP-1 activity in breast cancer cell (22). Interestingly, RARβ, a negative regulator of cancer cell growth (23), potently inhibits AP-1 activity and collagenase expression in both breast and lung cancer cells (24). Recent studies demonstrate that retinoids that specifically inhibit AP-1 activity but antagonize RAR transactivation on RAREs inhibited the growth of many different types of cancer cells (25–27). Anti-AP-1 retinoids inhibited squamous differentiation of human

* This work is supported in part by grants from the National Institutes of Health and the United States Army Medical Research and Material Command (to X. Z.). The costs of publication of this article were defrayed in part by the payment of page charges. This article must therefore be hereby marked "*advertisement*" in accordance with 18 U.S.C. Section 1734 solely to indicate this fact.

‡ To whom correspondence should be addressed: Burnham Institute, Cancer Center, 10901 North Torrey Pines Rd., La Jolla, CA 92037. Tel.: 858-646-3141; Fax: 858-646-3195; E-mail: xzhang@burnham.org.

[1] The abbreviations used are: RAR, retinoic acid receptor; RXR, retinoid X receptor; RA, retinoic acid; RARE, RA response element; TPA, 12-*O*-tetradecanoylphorbol-13-acetate; TRE, TPA response element; CBP, cAMP-response element-binding protein; DMEM, Dulbecco's modified Eagle's medium; FCS, fetal calf serum; GST, glutathione *S*-transferase.

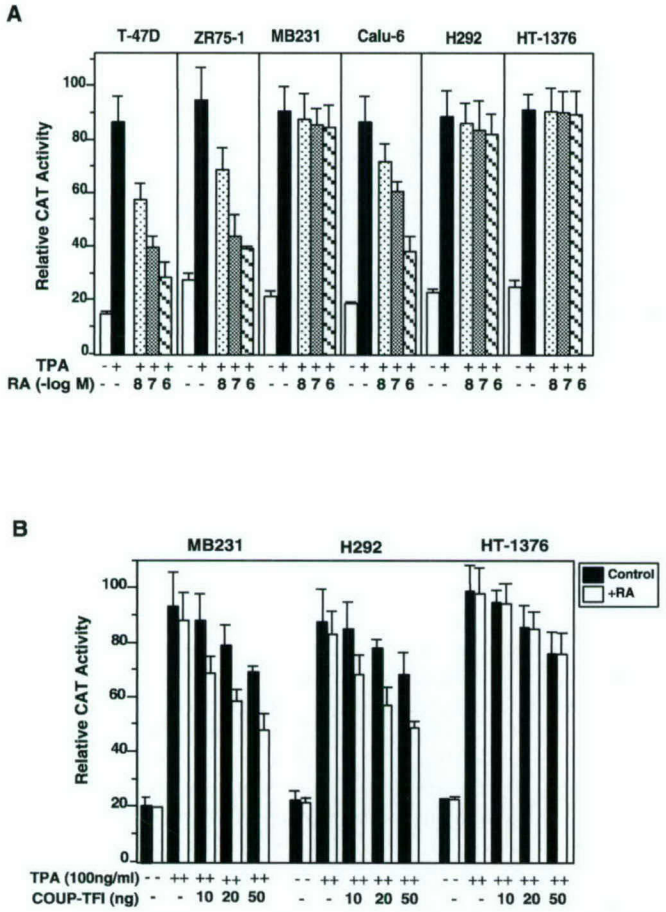

FIG. 1. **COUP-TF expression and *trans*-RA-induced anti-AP-1 activity correlate in cancer cell lines.** *A*, inhibition of TPA-induced collagenase promoter activity by *trans*-RA. The −73Col-CAT reporter was transfected into the indicated cancer cell lines. After transfection, the cells were incubated in DMEM medium containing 0.5% FCS for 24 h and treated with either TPA (100 ng/ml) alone or with the indicated concentrations of *trans*-RA. After 12 h, the cells were harvested, and CAT activity was determined. The activities of cotransfected β-galactosidase were used as controls for transfection efficiency. *B*, effect of COUP-TF expression in COUP-TF-negative cancer cell lines on inhibition of AP-1 activity by *trans*-RA. The −73Col-CAT reporter was transfected with or without COUP-TF into COUP-TF-negative cancer cell lines (MDA-MB231, H292, and HT-1376). Cells were incubated in medium (see "Experimental Procedures") containing 0.5% FCS for 24 h and then treated with either TPA (100 ng/ml) alone or with 10^{-6} M *trans*-RA. After 12 h, cells were harvested, and CAT activity was determined. The activities of cotransfected β-galactosidase were used as reference values.

bronchial epithelial cells (21), TPA-induced transformation and the clonal growth of the promotion-sensitive JB6 mouse epidermal cell line (28), and papilloma formation in animals (29). Thus, anti-AP-1 activity of retinoids contributes to their chemopreventive and chemotherapeutic effects, presumably by blocking the processes of tumor promotion and cell transformation.

The mechanism by which retinoids inhibit AP-1 activity remains largely unclear. Unlike the effect of retinoid receptors on RAREs, inhibition of AP-1 activity by retinoid receptors is independent of retinoid receptor-RARE interaction (8–10). Previous studies suggested several possible mechanisms for AP-1 inhibition by retinoid receptors. First, retinoid receptors are reported to physically interact with c-Jun and/or c-Fos (8, 9). This interaction results in the mutual inhibition of their DNA binding and transactivation functions and could explain the cross-talk occurring between AP-1 and retinoid signaling. However, a large excess of either retinoid receptor protein or c-Jun and c-Fos proteins was required to inhibit *in vitro* binding to the TRE or RARE, respectively (8, 9). Because the *in vivo* footprint assay for glucocorticoid receptor and AP-1 interaction did not reveal any effect on DNA binding (30), whether RAR and AP-1 directly interact *in vivo* remains to be established. Subsequently, it was suggested that blocking activation of the Jun N-terminal kinase signaling pathway that activates AP-1 might be responsible for AP-1 inhibition by retinoid and other nuclear receptors (31). Although this mechanism may explain how retinoids inhibit AP-1 activity under some conditions, it does not address how mutual inhibition occurs. Recent results suggest that the molecular basis of receptor-mediated inhibition of AP-1 transcriptional activation might be due to competition for a common coactivator, such as the cAMP-response element-binding protein (CBP), which is required for transcriptional activation by both the AP-1 complex and RARs (32). However, a domain of RAR capable of inhibiting AP-1 activity, such as the DNA-binding domain (33), does not interact with CBP (32). The development of retinoids that specifically inhibit AP-1 activity without transactivating RARs (25, 26) also argues against the involvement of RAR coactivators in RARs-AP-1 cross-talk. Thus, the availability of CBP is unlikely to be the sole modulator of RAR and AP-1-signaling pathways, and other adapter proteins may be involved in the antagonism of AP-1 activity by RARs.

Recent studies demonstrate that orphan receptor COUP-TF is involved in regulation retinoid responses (34, 35). COUP-TF is encoded by two distinct genes, COUP-TFI (EAR-3) (36, 37) and COUP-TFII (ARP-1) (38). Both show exceptional homology and overlapping expression patterns, suggesting their redundant functions (39). COUP-TF can modulate retinoid responses through either its high affinity binding to various RAREs or its heterodimerization with RXR (40–43). We previously reported that COUP-TF expression was required for cancer cell growth inhibition by *trans*-RA (35). We further demonstrated that the effect of COUP-TF is partly due to its induction of RARβ that mediates growth inhibition by retinoids in various cancer cells (35).

To further understand how COUP-TF is involved in the regulation of *trans*-RA activity in cancer cells, we investigated the effect of COUP-TF on antagonism of AP-1 activity by *trans*-RA. Our data demonstrate that COUP-TF expression in various cancer cell lines correlated with the ability of *trans*-RA to suppress AP-1 transcriptional activity. In addition, we found that COUP-TF effectively suppressed AP-1 transcriptional activity by interacting with c-Jun to cause loss of c-Jun DNA binding. This interaction required COUP-TF DNA-binding domain and the c-Jun leucine-zipper domain. Although AP-1 inhibition by COUP-TF did not require *trans*-RA, COUP-TF strongly potentiated the AP-1 antagonism by *trans*-RA when RARs were expressed. Our results demonstrate that interaction between COUP-TF and AP-1 is involved in regulating anti-AP-1 activity of retinoids in cancer cells and suggest that COUP-TF plays a role in the cross-talk between retinoid and AP-1 signalings.

EXPERIMENTAL PROCEDURES

Cell Culture—HeLa ovarian and MDA-MB231 breast cancer cells were grown in Dulbecco's modified Eagle's medium (DMEM) supplemented with 10% fetal calf serum (FCS); Calu-6 lung cancer and HT-1376 bladder cancer cells were grown in MEM containing 10% FCS; and T-47D and ZR-75-1 breast cancer and H292 lung cancer cells were grown in RPMI-1460 medium with 10% FCS.

Plasmid Construction—CAT reporter constructs TRE-tk-CAT and −73Col-CAT have been described (8, 17, 22, 24), as have expression vectors for RARα, COUP-TF, c-Jun, and c-Fos (8, 17, 22, 24, 44). pcDNA3-COUP-TFII C-terminal deletion mutants pcDNA3-COUP-TFIIΔ7, pcDNA3-COUP-TFIIΔ30, and pcDNA3-COUP-TFIIΔ108 were generated as described (35). pcDNA3-COUP-TFII N-terminal deletion mutants were

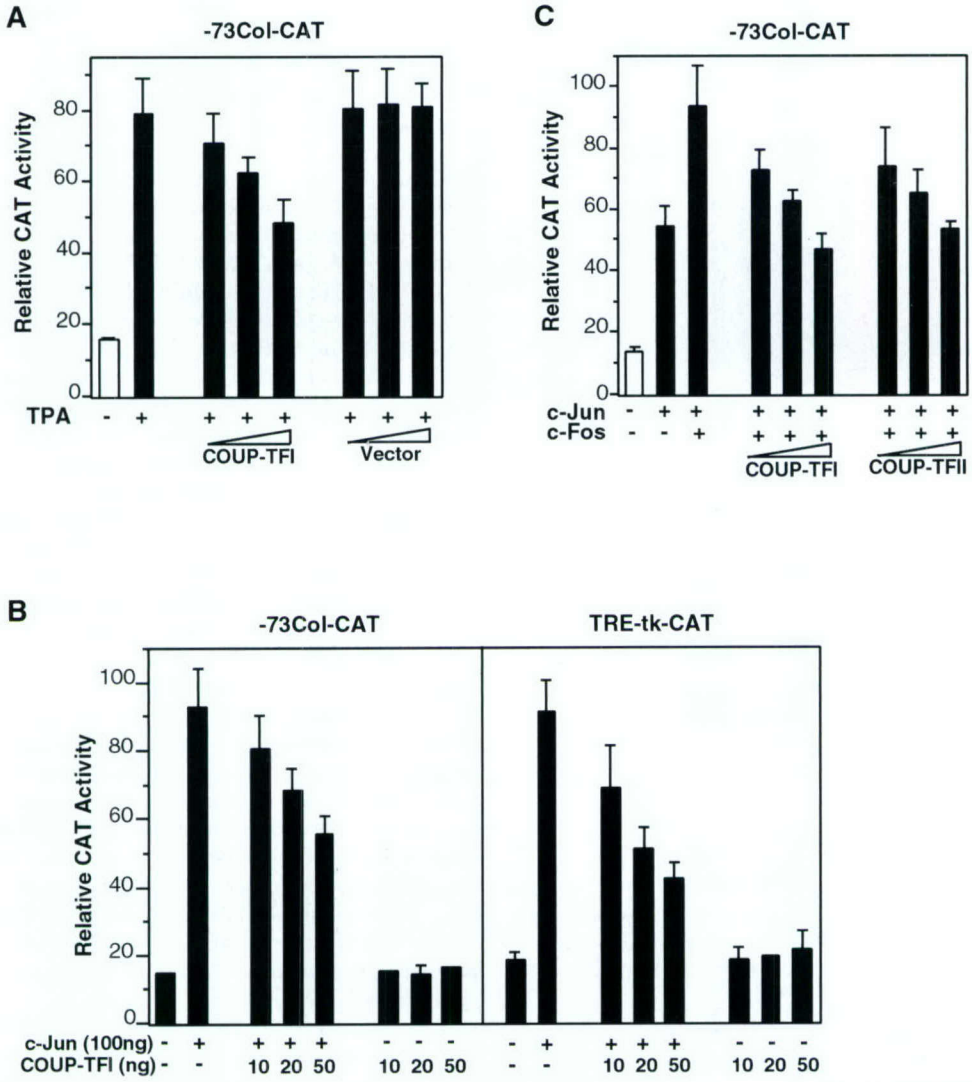

FIG. 2. **Inhibition of AP-1 activity by COUP-TF.** *A*, inhibition of TPA-induced collagenase promoter activity by COUP-TF in HeLa cells. The −73Col-CAT reporter was cotransfected without or with COUP-TFI expression vector (10, 20, or 50 ng) or the control pcDNA3 vector into cells. After transfection, cells were incubated in DMEM medium containing 0.5% FCS for 24 h and then treated with or without TPA (100 ng/ml). After 12 h, the cells were harvested, and CAT activity was determined. *B*, inhibition of c-Jun-induced −73Col-CAT and TRE-tk-CAT activity by COUP-TF in HeLa cells. The −73Col-CAT or TRE-tk-CAT reporter was cotransfected with/without c-Jun in the presence or absence of COUP-TFI expression vector (10, 20, and 50 ng) into cells. After transfection, cells were incubated in DMEM medium containing 0.5% FCS for 24 h, and CAT activity was determined. *C*, inhibition of c-Jun and c-Fos activities by COUP-TF in HeLa cells. The −73Col-CAT reporter was cotransfected with/without c-Jun (50 ng) and/or c-Fos (50 ng) expression vectors either in the presence or absence of COUP-TFI or COUP-TFII expression vector (10, 20, and 50 ng) into HeLa cells. The cells were then harvested, and CAT activity was determined.

constructed by cloning PCR products from COUP-TFII into pcDNA3 (Stratagene) using the following forward primers: TATAGGTACCATGGCGCCGCCCGTGCCC for pcDNA3-COUP-TFIIΔN25; ATATGGTACCATGACGCCAGCCCAGACG for pcDNA3-COUP-TFIIΔN50; AATTGGTACCATGCACATCGAGTGCGTG for pcDNA3-COUP-TFIIΔN75; and ATTAGGTACCATGCACCATCGCAACCAG for pcDNA3COUP-TFIIΔN125. The oligonucleotide GTGGCAGTTGAGGGGATCC was used as the reverse primer for these mutants.

Transient and Stable Transfection Assays—HeLa cells (1×10^5 cells/well) were plated in 24-well plates for 16–24 h before transfection as described (34, 35, 45), and other cancer cells (5×10^5 cell/well) were seeded in six-well plates. A modified calcium phosphate precipitation procedure was used for transient transfections (34, 35, 45). Briefly, 200 ng of reporter plasmid, 100 ng of β-galactosidase of expression vector (pCH 110; Amersham Biosciences), and various amounts of each expression vector were mixed with carrier DNA (pBluescript) to give 1000 ng of total DNA/well. CAT activity was normalized for transfection efficiency to the responding β-Gal activity. For stable transfections, the pRC/CMV-COUP-TF recombinant was transfected into MDA-MB231 and HT-1376 cells by the calcium phosphate precipitation method, and the stable clones were screened with G418 (Invitrogen) as described (35). Integration and expression of transfected cDNA were determined by Southern blotting and Northern blotting, respectively.

Preparation of Receptor Proteins—Receptor proteins for RARα, TR3, COUP-TF, and its mutants were synthesized by *in vitro* transcription-translation using rabbit reticulocyte lysates (Promega) as described previously (34). Amounts of translated proteins were determined by [^{35}S]methionine incorporation and SDS-PAGE with quantitation by incorporated radioactivity after normalization relative to methionine content.

Gel Retardation Assay—A fragment of the collagenase promoter region −73 to +63 containing one AP-1-binding site (TRE) was excised from a collagenase-CAT construct (8). In addition, the AP-1 binding sequence 5′-GATCCGGATGAGTCACCA-3′ was synthesized. Two fragments were labeled with [^{32}P]dCTP for use as probes for protein-DNA interaction. *In vitro* translated protein was incubated with the probe in a 20-μl reaction mixture containing 10 mM HEPES, pH 7.9, 50 mM KCl, 1 mM dithiothreitol, 2.5 mM $MgCl_2$, 10% glycerol, and 1 μg of poly(dI-dC) at 25 °C for 15 min. DNA-protein complexes were resolved on 5% nondenaturing polyacrylamide gels, and then gels were dried and analyzed by autoradiography.

GST Pull-down Assay—To prepare glutathione *S*-transferase (GST)–c-Jun or GST-c-Jun mutant fusion proteins, each c-Jun DNA or c-Jun mutant fragment was cloned in frame into the expression vector

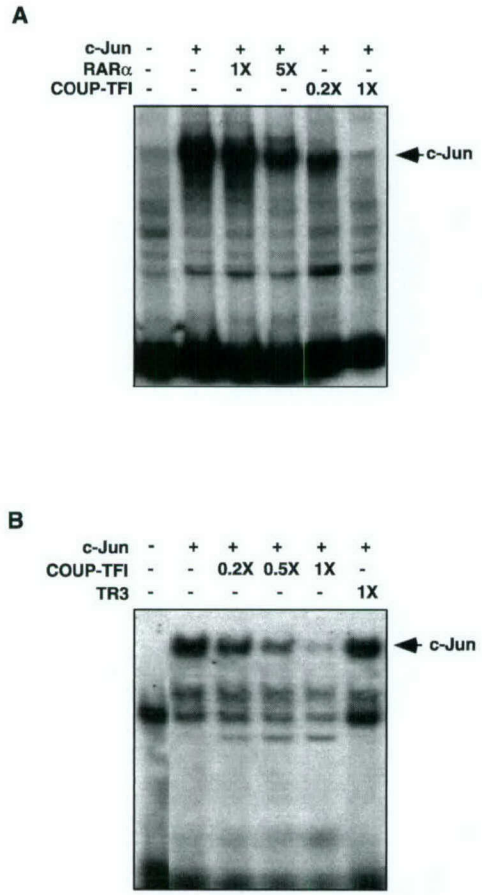

FIG. 3. **Inhibition of c-Jun binding to DNA by COUP-TF.** *In vitro* synthesized c-Jun was preincubated with the indicated molar excess of COUP-TF, RARα, or *TR3*. Unprogrammed reticulocyte lysate was added to maintain an equal protein concentration in each reaction. Following preincubation, the reaction mixtures were incubated with ^{32}P-labeled collagenase promoter (*A*) or the TRE (*B*) and analyzed by gel retardation. The *arrowhead* indicates the c-Jun-binding complex.

pGEX-3X (Amersham Biosciences). Fusion proteins were expressed in bacteria using the manufacturer's procedure and analyzed by gel retardation assays and Western blotting (data not shown). To determine the interaction between COUP-TF and c-Jun, the fusion proteins were immobilized on glutathione-Sepharose beads. The vector protein (GST), prepared under the same conditions as a control, was also immobilized. Beads were preincubated with bovine serum albumin (1 mg/ml) at room temperature for 5 min. ^{35}S-labeled *in vitro* translated COUP-TF proteins (2–5 μl, depending on translation efficiency) were then added to the beads. The beads in 200 μl in EBC buffer (140 mM NaCl, 0.5% Nonidet P-40, 100 mM NaF, 200 mM sodium orthovanadate, and 50 mM Tris, pH 8.0) were rocked continuously for 1 h at 4 °C. After washing 5 times with NETN buffer (100 mM NaCl, 1 mM EDTA, 20 mM Tris, pH 8.0, 0.5% Nonidet P-40), bound proteins were analyzed by SDS-PAGE and autoradiography.

Northern Blotting—For Northern analysis, total RNAs were prepared using an RNeasy Mini Kit (Qiagen, Hilden, Germany). Total RNA (30 μg) from different cell lines treated with or without *trans*-RA (10^{-6} M) in the presence or absence of TPA (100 ng/ml) was analyzed by Northern blotting as described (46).

RESULTS

Correlation between COUP-TF Expression and Inhibition of AP-1 Activity by trans-RA—We recently reported that expression of COUP-TF is required for growth inhibition and apoptosis induction by *trans*-RA in various cancer cells (35). Since inhibition of AP-1 activity by retinoids is known to contribute to their anticancer effects, we studied whether COUP-TF expression was involved in the process. The effect of *trans*-RA on inhibiting AP-1 activity (Fig. 1*A*) was evaluated in COUP-TF–positive T-47D and ZR-75–1 breast cancer and Calu-6 lung cancer cell lines and in COUP-TF–negative MDA-MB231 breast cancer, H292 lung cancer, and HT-1376 bladder cancer cell lines (35). AP-1 activity induced by TPA was determined by transient transfection using the reporter −73Col-CAT, which contains a TRE that binds AP-1 (8). TPA-induced reporter activity was strongly inhibited in a *trans*-RA-dependent manner in the COUP-TF–positive ZR-75-1, T-47D, and Calu–6 cell lines. In contrast, *trans*-RA showed very little effect on TPA–induced −73Col-CAT activity in the COUP-TF–negative MDA-MB231, H292, and HT-1376 cell lines. Thus, COUP-TF expression correlates positively with the ability of *trans*-RA to inhibit AP-1 transcriptional activity.

Trans-RA-dependent and –independent Antagonism of AP-1 Activity by COUP-TF—The positive association between COUP-TF expression and *trans*-RA-induced anti-AP-1 activity suggested that COUP-TF was required for *trans*-RA to inhibit AP-1 activity and that the absence of COUP-TF expression in MDA-MB231, H292, and HT-1376 cells might be responsible for the lack of *trans*-RA activity. Therefore, we transiently transfected the COUP-TF expression vector and the −73Col-CAT reporter into the COUP-TF-negative cell lines, in which *trans*-RA did not inhibit AP-1 transcriptional activity (Fig. 1*B*). Upon COUP-TF transfection, *trans*-RA inhibited TPA-induced reporter activity in both MDA-MB231 and H292 cells in a COUP-TF concentration-dependent manner. Interestingly, COUP-TF transfection alone produced some inhibition of AP-1 activity. This observation suggested that COUP-TF inhibited AP-1 activity in both *trans*-RA–dependent and -independent manners in MDA-MB231 and H292 cells. When evaluated in HT-1376 cells, COUP-TF expression was able to inhibit AP-1 activity independently of *trans*-RA (Fig. 1*B*). However, it failed to confer the ability of *trans*-RA to inhibit TPA-induced reporter activity, even at high transfection levels, suggesting that *trans*-RA-dependent inhibition of AP-1 activity by COUP-TF is impaired in this cell line.

The above results suggested that COUP-TF alone inhibited AP-1 activity. We then examined the anti-AP-1 activity of COUP-TF in HeLa cells, in which TPA strongly induced the transcription of the transfected −73Col-CAT reporter. Similar to that observed in other cancer cell lines (Fig. 1*B*), COUP-TFI cotransfection inhibited TPA-induced reporter activity in a COUP-TFI concentration-dependent manner (Fig. 2*A*). Cotransfection of COUP-TFII produced almost identical results (data not shown). Activation of collagenase promoter by TPA occurs mainly through induction of AP-1 activity that activates the TRE in the promoter (7). We therefore examined whether COUP-TF expression also interfered with transactivation activity of c-Jun homodimer and c-Jun/c-Fos heterodimer. Cotransfection of −73Col-CAT with the c-Jun expression vector into HeLa cells led to about 5-fold induction of reporter expression (Fig. 2*B*), presumably due to activation of the collagenase promoter by the c-Jun homodimer. The c-Jun–induced −73Col-CAT reporter activity was repressed when COUP-TFI expression vector was cotransfected. Similarly, −73Col-CAT reporter activity induced by c-Jun/c-Fos heterodimers was inhibited by COUP-TFI and COUP-TFII (Fig. 2*C*). To determine that inhibition of collagenase promoter activity by COUP-TF was mediated by the TRE, we evaluated how COUP-TFI affected the TRE-tk-CAT reporter, which has a TRE sequence fused to the thymidine kinase promoter (Fig. 2*B*). Our result showed that cotransfection of COUP-TFI significantly inhibited c-Jun-induced TRE-tk-CAT activity (Fig. 2*B*). These results clearly demonstrate that COUP-TF inhibits transcriptional activity of c-Jun homodimer and c-Jun/c-Fos heterodimer and that the inhibition of AP-1 activity by COUP-TF on the TRE is respon-

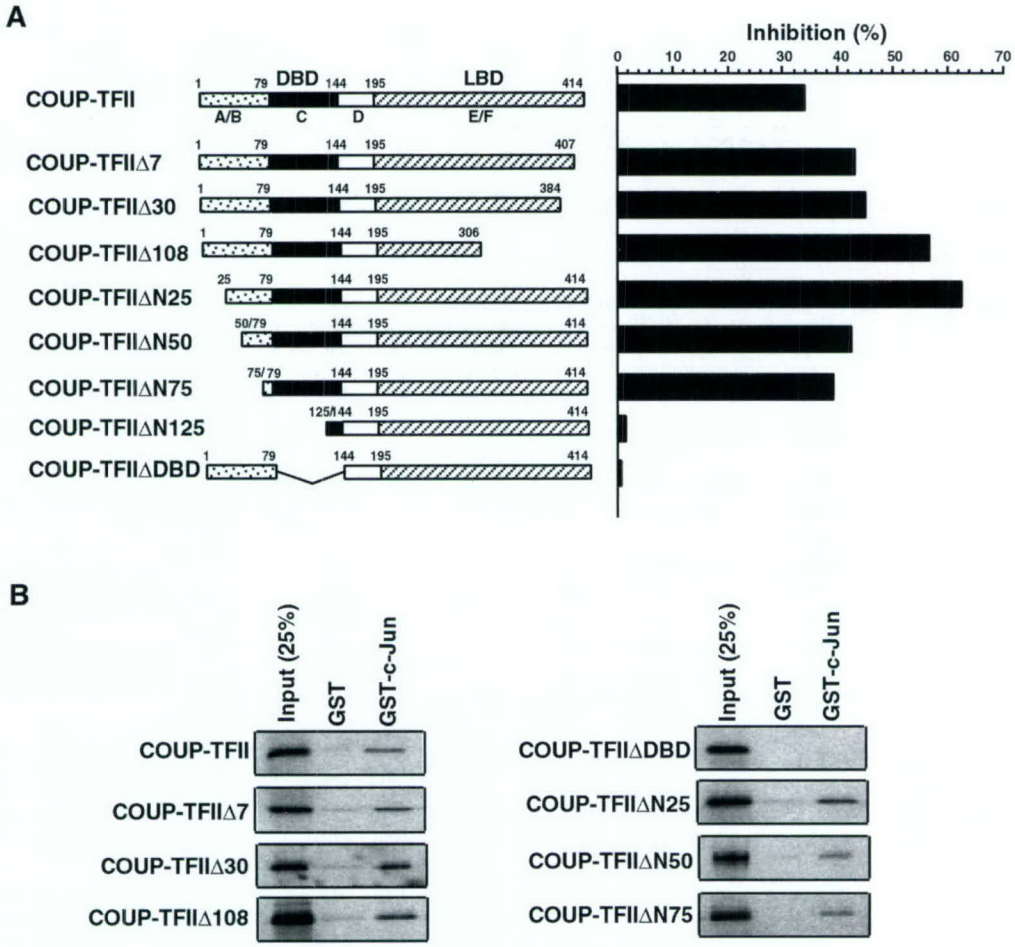

FIG. 4. **Interaction of c-Jun and COUP-TF and their domain requirements.** *A*, inhibition of transcriptional activity of AP-1 by COUP-TF mutants in HeLa cells. *Left*, schematic representation of COUP-TFII and its mutants. The DNA binding domain (*DBD*) and ligand-binding domain (*LBD*) of COUP-TFII are indicated. *Right*, effect of COUP-TFII mutants on AP-1 activity. The −73Col-CAT reporter was cotransfected without or with c-Jun (100 ng) alone or together with the indicated COUP-TFII mutants (50 ng). After transfection, cells were incubated in DMEM containing 0.5% FCS for 24 h. After 12 h, the cells were harvested, and CAT activity was determined. Reporter activity is shown as percentage of inhibition. *B*, interaction between c-Jun and COUP-TFs. c-Jun was synthesized in bacteria using pGEX-3X expression vector. GST-c-Jun fusion protein was immobilized on the glutathione-Sepharose beads. As a control, the same amount of glutathione *S*-transferase was also immobilized on the beads. *In vitro* translated ^{35}S-labeled COUP-TF and its mutant proteins were then mixed with the beads. After extensive washing, the bound proteins were analyzed by SDS-PAGE. The input proteins are shown for comparison.

sible for its antagonism of TPA activity.

Inhibition of c-Jun Binding to DNA by COUP-TF—Inhibition of AP-1 activity by several nuclear receptors has been shown to be due to their inhibition of AP-1 binding to DNA (8, 9, 13–15, 17, 22, 47). To study whether inhibition of AP-1 DNA binding by COUP-TF was involved in its inhibition of AP-1 activity, the purified collagenase promoter fragment was used as a probe in gel shift assays for binding of *in vitro* synthesized c-Jun protein in the absence or presence of COUP-TF protein (Fig. 3*A*). c-Jun alone formed a strong complex with the promoter. However, upon preincubation with COUP-TF protein, c-Jun binding was significantly inhibited. The addition of COUP-TF protein did not show any new complex formed with the collagenase promoter, indicating that the inhibitory effect of COUP-TF is not due to its direct binding to the collagenase promoter. We also studied the effect of COUP-TF on binding of c-Jun to the TRE. Preincubation with COUP-TF protein similarly inhibited c-Jun binding to the TRE derived from the collagenase promoter (Fig. 3*B*). As a comparison, preincubation of c-Jun with TR3 orphan receptor (34) that could not antagonize c-Jun transactivation (data not shown) did not inhibit c-Jun binding to the TRE. This result demonstrated that the inhibitory effect of COUP-TF on c-Jun binding to the collagenase promoter is not due to regions other than the TRE in the promoter. Next, we compared the inhibitory effect of COUP-TF with that of RARα that is known to repress AP-1 activity and inhibit c-Jun binding to TRE (8). Whereas an equal amount of COUP-TF significantly inhibited c-Jun binding to the collagenase promoter, an equal amount of RARα did not show any detectable inhibition (Fig. 3*A*). Inhibition of c-Jun binding required a 5-fold excess of RARα, similar to that observed before (8). The addition of *trans*-RA did not enhance the inhibitory effect of RARα (Ref. 8 and data not shown). Together, these results demonstrate that the inhibition of c-Jun binding to the TRE contributes to its suppression of AP-1 transcriptional activity by COUP-TF and that COUP-TF is a more effective inhibitor than RARα.

Interaction of c-Jun and COUP-TF—Our observation that COUP-TF inhibits transactivation and DNA binding by c-Jun prompted us to examine whether COUP-TF and c-Jun interact directly using GST pull-down assay (Fig. 4). *In vitro* synthesized radiolabeled COUP-TFII was specifically pulled down by bacterially expressed GST-c-Jun hybrid protein but not by GST protein (Fig. 4*B*), demonstrating that COUP-TF and c-Jun interact in solution. To identify the domain of COUP-TFII responsible for interacting with c-Jun, COUP-TFII deletion mutants (Fig. 4*A*) were constructed and analyzed on the −73Col-CAT reporter for antagonism of AP-1 activity in HeLa cells (Fig. 4*A*) and for their interaction with c-Jun using the

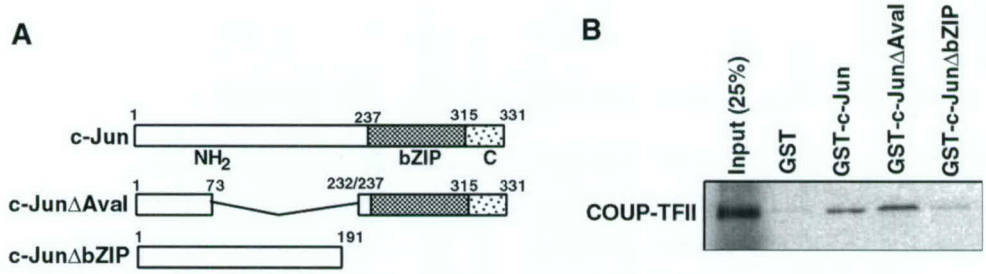

FIG. 5. **The domain of c-Jun required for interaction with COUP-TF.** *A*, schematic representation of c-Jun and its mutants. The amino terminus (NH_2), the basic region, the leucine zipper (*bZIP*), and the carboxyl terminus (*C*) are indicated. *B*, interaction between COUP-TF and c-Jun mutants. c-Jun and its mutant proteins were synthesized in bacteria using the pGEX-3X expression vector (Amersham Biosciences). GST-c-Jun and the mutant fusion proteins (GST-c-JunΔ*Ava*I and GST-c-JunΔbZIP) were immobilized on the glutathione-Sepharose beads. As a control, the same amount of glutathione transferase was immobilized on the beads. *In vitro* translated ^{35}S-labeled COUP-TFII was then mixed with the beads. After extensive washing, bound proteins were analyzed by SDS-PAGE. Input proteins are shown for comparison.

GST pull-down assay (Fig. 4*B*). Cotransfection of the c-Jun expression vector alone induced reporter transcription (Fig. 4*A*), whereas cotransfection with one of the C-terminal deletion mutants COUP-TFIIΔ7, COUP-TFIIΔ30, or COUP-TFIIΔ108 strongly inhibited c-Jun-induced reporter activity, as was observed using the wild-type COUP-TFII. N-terminal domain deletion mutants, such as COUP-TFIIΔN25, COUP-TFIIΔN50, and COUP-TFIIΔN75, also retained the inhibitory effect on AP-1 activity by COUP-TFII. In contrast, partial (COUP-TFIIΔN125) or complete deletion of the DNA-binding domain (COUP-TFIIΔDBD) abrogated anti-c-Jun activity completely. In the GST pull-down assay, COUP-TFII mutants that effectively suppressed AP-1 activity, such as COUP-TFIIΔ7, COUP-TFIIΔ30, COUP-TFIIΔ108, COUP-TFIIΔN25, COUP-TFIIΔN50, and COUP-TFIIΔN75, were pulled down by GST-c-Jun protein, whereas COUP-TFIIΔDBD, which failed to suppress AP-1 activity, was not (Fig. 4*B*). Thus, inhibition of AP-1 transcriptional activity by the COUP-TFII mutants correlated with their ability to interact with c-Jun. These observations further suggest that a direct c-Jun/COUP-TF interaction accounts for the inhibition of AP-1 activity by COUP-TF and that the DBD of COUP-TF is essential.

We also identified the region of c-Jun required for COUP-TF interaction (Fig. 5). Deletion of amino acids 73–232 from c-Jun (c-JunΔ*Ava*I) did not affect its ability to pull down COUP-TFII. In contrast, deletion of the C-terminal domain of c-Jun from amino acid 191 to 331 (c-JunΔbZIP), which encompasses the leucine-zipper region and basic region, completely abolished its ability to pull down COUP-TFII. Thus, the C-terminal domain, but not the N-terminal domain, of c-Jun is responsible for COUP-TF interaction.

Stable Expression of COUP-TF in COUP-TF-negative MDA-MB231 Cells Restores the Ability of trans-RA to Inhibit AP-1 Activity—To further examine the role of COUP-TF in *trans*-RA-induced inhibition of AP-1 activity, we analyzed the effect of *trans*-RA on TPA–induced c-Jun expression in MDA-MB231 breast cancer cells and MDA-MB231 cells stably transfected with COUP-TF (MB231/COUP#16) (35). Treatment of both cell lines with TPA strongly induced c-Jun expression as determined by Northern blotting (Fig. 6). Induction of c-Jun expression by TPA was probably due to an AP-1-binding site in the c-Jun promoter (7). Treatment with *trans*-RA did not affect basal c-Jun expression in both lines and did not inhibit TPA-induced c-Jun expression in MDA-MB231 cells. However, pretreatment of MB231/COUP#16 cells with *trans*-RA completely abolished TPA-induced c-Jun expression. These results demonstrate that COUP-TF expression is required for inhibition of AP-1 activity in MDA-MB231 cells by *trans*-RA.

Stable Expression of COUP-TF Does Not Lead to trans-RA-dependent Inhibition of AP-1 Activity in HT-1376 Cells Lacking RARα/β Expression—We also evaluated whether stable expression of COUP-TF affected TPA–induced c-Jun expression in HT-1376 bladder cancer cells (Fig. 7). The stable clone, HT-1376/COUP#7, which expresses high levels of COUP-TF, was analyzed for the effect of *trans*-RA on TPA activity (Fig. 7). About a 4-fold induction of c-Jun expression by TPA was observed in HT-1376 cells. However, the induction of c-Jun expression was largely reduced in HT-1376/COUP#7 cells, with only about a 2-fold induction. Interestingly, the basal level of c-Jun expression was also slightly reduced in HT-1376/COUP#7 cells. Despite the reduction of c-Jun expression in the absence or presence of TPA, *trans*-RA failed to inhibit basal and TPA-induced c-Jun expression in both wild-type and

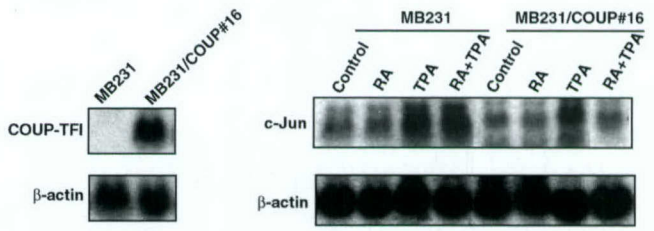

FIG. 6. **Stable expression of COUP-TF in COUP-TF-negative, RAR-positive MDA-MB231 cells restores the ability of *trans*-RA to inhibit AP-1 activity.** Total RNAs prepared from MDA-MB-231 or MDA-MB231 cells stably expressing COUP-TF (MB231/COUP#16) (35) treated with or without the indicated agents were analyzed for the expression of c-Jun. The expression of β-actin is shown to confirm the similar loading of RNA in each lane.

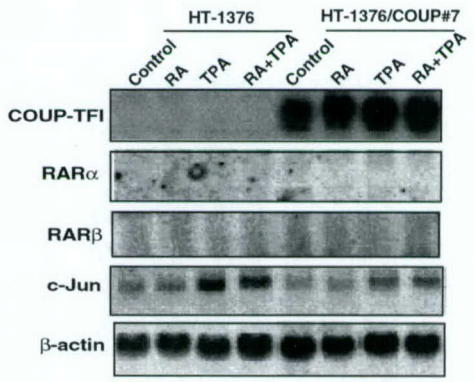

FIG. 7. **Stable expression of COUP-TF in COUP-TF and RAR-negative HT-1376 cells does not lead to *trans*-RA-dependent inhibition of AP-1 activity.** Total RNAs prepared from HT-1376 or HT-1376 cells stably expressing COUP-TF (HT-1376/COUP 7) treated with or without the indicated agents were analyzed for the expression of c-Jun, RARα, and RARβ. The expression of β-actin is shown to confirm similar loading of RNA in each lane.

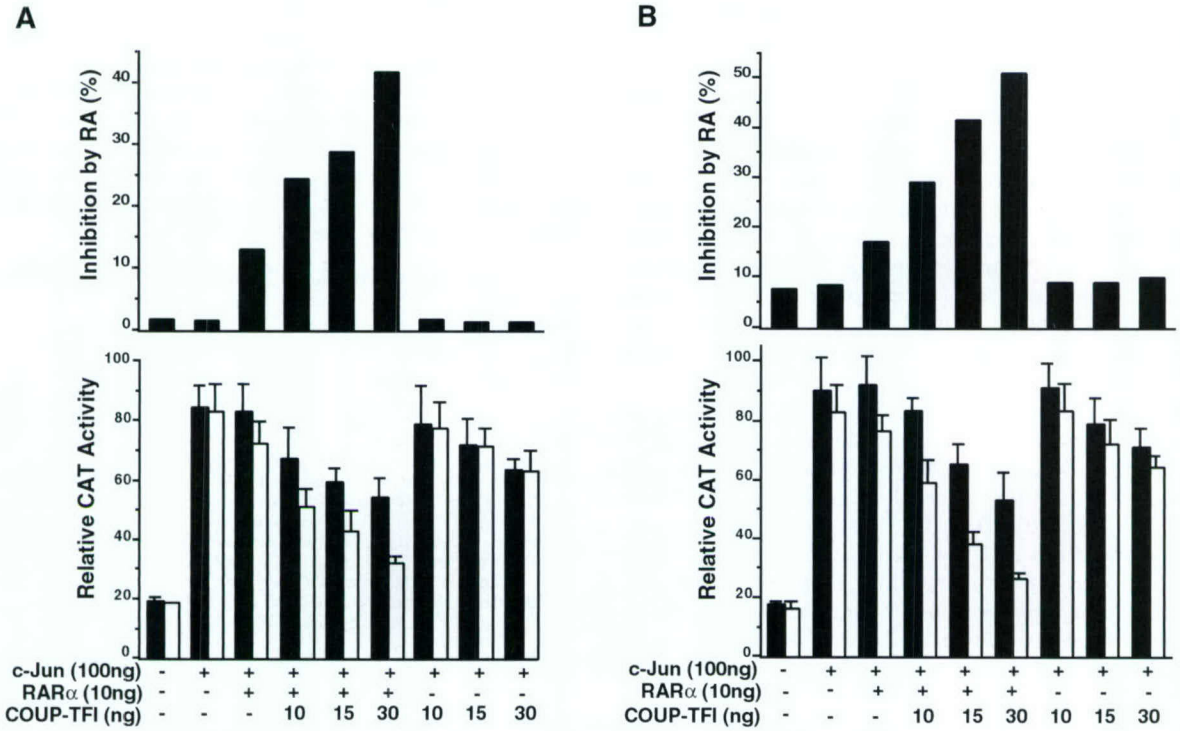

FIG. 8. **Effect of COUP-TF and RARα coexpression on antagonism of AP-1 activity by *trans*-RA.** The −73Col-CAT reporter was transfected together with c-Jun alone or together with COUP-TF and/or RARα expression vectors into HT-1376 (*A*) or HeLa (*B*) cells. After transfection, the cells were incubated in medium containing 0.5% FCS for 24 h and then treated with or without *trans*-RA. After 12 h, the cells were harvested, and CAT activity was determined. The *top panels* show the percentage of inhibition of c-Jun activity by *trans*-RA based on data shown in the *bottom panels*, in which *filled bars* represent control and *open bars* represent *trans*-RA treatment.

COUP-TF-expressing cells. Thus, COUP-TF expression is not sufficient to confer *trans*-RA-induced anti-AP-1 activity in HT-1376 cells.

RAR Expression Is Required for COUP-TF to Facilitate Antagonism of AP-1 Activity by trans-RA—Our observations that transient (Fig. 1*B*) or stable (Fig. 7) expression of COUP-TF in HT-1376 cells failed to modulate antagonism of AP-1 activity by *trans*-RA led us to investigate RAR expression. Unlike MDA-MB231 cells that express RARα (48) and RARβ when COUP-TF is expressed (35), HT-1376 cells did not express detectable RARα or RARβ (Fig. 7), although RARγ was expressed (data not shown). This result suggested that modulation of *trans*-RA-induced anti-AP-1 activity by COUP-TF might require RARα or RARβ. The effect of RARα expression on the ability of COUP-TF to regulate *trans*-RA activity was then examined using transient transfection in HT-1376 cells. The −73Col-CAT reporter was transfected into HT-1376 cells with or without c-Jun and COUP-TF and/or RARα vector. Transfected cells were treated with or without *trans*-RA. As shown in Fig. 8*A*, transfected COUP-TF repressed AP-1 activity in the absence of *trans*-RA. In contrast, transfected RARα (10 ng) led to inhibition of AP-1 activity in a *trans*-RA dependent manner. The addition of COUP-TF significantly enhanced the *trans*-RA-induced inhibition of AP-1 activity by RARα (Fig. 8*A*). Similar results were observed using HeLa cells (Fig. 8*B*). Thus, efficient inhibition of AP-1 activity by *trans*-RA activity by COUP-TF requires both COUP-TF and RARα.

DISCUSSION

Retinoids are effective growth inhibitors of cancer cells. Inhibition of AP-1 activity has been proposed as one mechanism by which retinoids exert their anticancer effects (6). Despite extensive studies in the last few years, how retinoids specifically antagonize AP-1 activity remains largely unknown. Here, we provide evidence that COUP-TF is involved in regulating the antagonism of AP-1 transactivational activity by *trans*-RA. COUP-TF, by physically interacting with c-Jun, inhibits AP-1 DNA binding and transactivation and is required for efficient inhibition of AP-1 activity by liganded RARs. Our results suggest that COUP-TF plays a role in the cross-talk between retinoid and AP-1 signaling pathways.

We recently reported that the expression of COUP-TF positively correlates with the inhibition of the growth of various cancer cell lines by *trans*-RA and that COUP-TF is underexpressed in many *trans*-RA-resistant cancer cell lines (35). Stable expression of COUP-TF in COUP-TF-negative cancer cells restores their sensitivity to *trans*-RA, demonstrating that COUP-TF can mediate anticancer effects of *trans*-RA (35). By studying anti-AP-1 activity of *trans*-RA in various cancer cell lines, we found a close correlation between COUP-TF expression and the anti-AP-1 activity of *trans*-RA (Fig. 1). In COUP-TF-positive ZR-75–1, T-47D, and Calu-6 cancer cell lines (35), *trans*-RA strongly inhibited the ability of TPA to activate transcription of the collagenase promoter, whereas in COUP-TF-negative MDA-MB231, H292, and HT-1376 cell lines, *trans*-RA failed to suppress TPA activity (Fig. 1). This finding is consistent with a previous study showing that *trans*-RA effectively inhibited AP-1 activity in ZR-75–1 and T-47D cells but not in MDA-MB231 cells (49). The requirement of COUP-TF in *trans*-RA-mediated AP-1 inhibition was further demonstrated by our findings that transient expression of COUP-TF in COUP-TF-negative cells (Fig. 1*B*) restored the ability of *trans*-RA to inhibit TPA-induced AP-1 transactivation and that stable expression of COUP-TF in MBA-MB231 cells enabled *trans*-RA to inhibit TPA-induced c-Jun expression (Fig. 6).

We have reported that COUP-TF expression contributes to growth inhibition by *trans*-RA in cancer cells because COUP-TF on binding to the RARβ promoter induces RARβ expression (35). RARβ is reported to be a potent AP-1 inhibitor

(24), suggesting that COUP-TF-induced RARβ probably contributes to the inhibition of AP-1 activity (Fig. 6). Our observations that COUP-TF can effectively interact with c-Jun *in vitro* (Figs. 3 and 4) and inhibit AP-1 transcriptional activity on transient transfection (Fig. 2) also suggest that COUP-TF is directly involved in antagonizing AP-1 activity.

Inhibition of AP-1 activity appears to be a common characteristic of nuclear receptors, as has been demonstrated for the progesterone, estrogen, androgen, thyroid hormone, glucocorticoid, and retinoid receptors, which can functionally interact with the AP-1 complex. This study reveals that the orphan receptor COUP-TF behaves similarly. The molecular basis of the interaction between nuclear receptors and AP-1 pathways remains largely unknown. Models proposed include direct protein-protein interaction (8, 9, 13–15), inhibition of Jun N-terminal kinase activity (31), and competition for CBP (32). Our results of GST pull-down assays (Figs. 4*B* and 5) and mutation analysis (Figs. 4 and 5) support the first model. The requirement for the COUP-TF DBD for c-Jun binding is similar to observations that the DBDs of glucocorticoid receptor (14, 15) and RAR (47) are essential for their interaction with AP-1. Interestingly, the *in vitro* DNA-binding study showed that COUP-TF is a more effective inhibitor of AP-1 binding than RARα (Fig. 3) on the basis of the levels of each receptor to exert this effect.

In contrast to inhibition of AP-1 activity by other receptors that require their respective ligands, COUP-TF effectively inhibited AP-1 transactivation in the absence of any ligand (Fig. 2). Such a ligand-independent inhibition of AP-1 activity may restrict expression levels of AP-1-responsive genes in cancer cells (Figs. 6 and 7). Interestingly, we observed that COUP-TF expression potentiates antagonism of AP-1 activity by *trans*-RA. However, regulation of *trans*-RA activity by COUP-TF appears to require RARα or RARβ, because transiently transfected COUP-TF was unable to confer anti-AP-1 activity to *trans*-RA in HT-1376 cells lacking RARα or -β (Fig. 8*A*) or HeLa cells (Fig. 8*B*) unless RARα was cotransfected. In addition, stable expression of COUP-TF restored *trans*-RA-induced anti-AP-1 activity in MDA-MB231 cells (Fig. 6) having RARs (48) but not in HT-1376 cells lacking RARα and -β (Fig. 7). Thus, expression of both RARα/β and COUP-TF is required for optimal inhibition of AP-1 activity by *trans*-RA.

Although we do not fully understand how COUP-TF and RARα coexpression maximizes inhibition of AP-1 activity by *trans*-RA, our finding of physical interaction between COUP-TF and RARα (35, 50) suggests its involvement in this process. Based on our observation that COUP-TF more effectively inhibits c-Jun binding to DNA than RARα (Fig. 3), it is tempting to speculate that COUP-TF, with its ability to interact with both RAR (35, 50) and c-Jun (Fig. 3), may function as a bridging factor to mediate RAR/AP-1 interaction. In this model, the COUP-TF/RAR heterodimer would strongly interact with AP-1 in the presence of *trans*-RA to inhibit the DNA binding of AP-1 and its transactivation. Similarly, COUP-TF, by interacting with c-Jun, might also potentiate the inhibition of RARα/β transactivation by AP-1. Unfortunately, perhaps due to rapid formation of the COUP-TF homodimer after COUP-TF expression *in vitro* (40, 51), we were unsuccessful in demonstrating the interaction between RAR/COUP-TF heterodimer and c-Jun in gel shift or GST pull-down assays (data not shown). Another possible mechanism for inhibiting AP-1 transactivation by COUP-TF may involve its recruiting of a transcriptional corepressor. COUP-TF has been widely considered as a potent negative transcriptional regulator (40–43) due to its effective interaction with corepressors, such as N-CoR and SMRT (52). The interaction between COUP-TF and both RAR and AP-1 may recruit transcriptional corepressors to the complex, thereby enhancing the mutual repression of AP-1 and RAR transcriptional activity. Interestingly, COUP-TF interacts with a variety of nuclear receptors, including RXR (41), TR (40, 50), estrogen receptor (53, 54), and peroxisome proliferator-activated receptor (55). It remains to be determined whether and how COUP-TF is involved in modulating the anti-AP-1 activity by their ligands.

Acknowledgment—We thank Dr. Marcia I. Dawson for reviewing the manuscript.

REFERENCES

1. Lotan, R. (1980) *Biochim. Biophys. Acta* **605,** 33–91
2. Gudas, L. J., Sporn, M. B., and Roberts, A. B. (1994) in *The Retinoids*, 2nd Ed. (Sporn, M. B., Roberts, A. B., and Goodman, D. S., eds) pp. 443–520, Raven Press, New York
3. Mangelsdorf, D. J., and Evans, R. M. (1995) *Cell* **83,** 841–850
4. Kastner, P., Mark, M., and Chambon, P. (1995) *Cell* **83,** 859–869
5. Zhang, X. K., and Pfahl, M. (1993) *Receptor* **3,** 183–191
6. Pfahl, M. (1993) *Endocr. Rev.* **14,** 651–658
7. Angel, P., and Karin, M. (1991) *Biochim. Biophys. Acta* **1072,** 129–157
8. Yang-Yen, H. F., Zhang, X. K., Graupner, G., Tzukerman, M., Sakamoto, B., Karin, M., and Pfahl, M. (1991) *New. Biol.* **3,** 1206–1219
9. Schule, R., Rangarajan, P., Yang, N., Kliewer, S., Ransone, L. J., Bolado, J., Verma, I. M., and Evans, R. M. (1991) *Proc. Natl. Acad. Sci. U. S. A.* **88,** 6092–6096
10. Nicholson, R. C., Mader, S., Nagpal, S., Leid, M., Rochette-Egly, C., and Chambon, P. (1990) *EMBO J.* **9,** 4443–4454
11. Yang, L., Kim, H. T., Munoz-Medellin, D., Reddy, P., and Brown, P. H. (1997) *Cancer Res.* **57,** 4652–4661
12. Soprano, D. R., Chen, L. X., Wu, S., Donigan, A. M., Borghaei, R. C., and Soprano, K. J. (1996) *Oncogene* **12,** 577–584
13. Jonat, C., Rahmsdorf, H. J., Park, K. K., Cato, A. C., Gebel, S., Ponta, H., and Herrlich, P. (1990) *Cell* **62,** 1189–1204
14. Yang-Yen, H. F., Chambard, J. C., Sun, Y. L., Smeal, T., Schmidt, T. J., Drouin, J., and Karin, M. (1990) *Cell* **62,** 1205–1215
15. Schule, R., Rangarajan, P., Kliewer, S., Ransone, L. J., Bolado, J., Yang, N., Verma, I. M., and Evans, R. M. (1990) *Cell* **62,** 1217–1226
16. Zhang, X. K., Dong, J. M., and Chiu, J. F. (1991) *J. Biol. Chem.* **266,** 8248–8254
17. Zhang, X. K., Wills, K. N., Husmann, M., Hermann, T., and Pfahl, M. (1991) *Mol. Cell. Biol.* **11,** 6016–6025
18. Shemshedini, L., Knauthe, R., Sassone-Corsi, P., Pornon, A., and Gronemeyer, H. (1991) *EMBO J.* **10,** 3839–3849
19. Teyssier, C., Belguise, K., Galtier, F., and Chalbos, D. (2001) *J. Biol. Chem.* **276,** 36361–36369
20. Crawford, H. C., and Matrisian, L. M. (1996) *Enzyme Protein* **49,** 20–37
21. Lee, H. Y., Dawson, M. I., Walsh, G. L., Nesbitt, J. C., Eckert, R. L., Fuchs, E., Hong, W. K., Lotan, R., and Kurie, J. M. (1996) *Cell Growth Differ.* **7,** 997–1004
22. Agadir, A., Shealy, Y. F., Hill, D. L., and Zhang, X. (1997) *Cancer Res.* **57,** 3444–3450
23. Zhang, X. K., Liu, Y., and Lee, M. O. (1996) *Mutat. Res.* **350,** 267–277
24. Lin, F., Xiao, D., Kolluri, S. K., and Zhang, X. (2000) *Cancer Res.* **60,** 3271–3280
25. Fanjul, A., Dawson, M. I., Hobbs, P. D., Jong, L., Cameron, J. F., Harlev, E., Graupner, G., Lu, X. P., and Pfahl, M. (1994) *Nature* **372,** 107–111
26. Chen, J. Y., Penco, S., Ostrowski, J., Balaguer, P., Pons, M., Starrett, J. E., Reczek, P., Chambon, P., and Gronemeyer, H. (1995) *EMBO J.* **14,** 1187–1197
27. Yang, L., Munoz-Medellin, D., Kim, H. T., Ostrowski, J., Reczek, P., and Brown, P. H. (1999) *Breast Cancer Res. Treat.* **56,** 277–291
28. Li, J. J., Dong, Z., Dawson, M. I., and Colburn, N. H. (1996) *Cancer Res.* **56,** 483–489
29. Huang, C., Ma, W. Y., Dawson, M. I., Rincon, M., Flavell, R. A., and Dong, Z. (1997) *Proc. Natl. Acad. Sci. U. S. A.* **94,** 5826–5830
30. Konig, H., Ponta, H., Rahmsdorf, H. J., and Herrlich, P. (1992) *EMBO J.* **11,** 2241–2246
31. Caelles, C., Gonzalez-Sancho, J. M., and Munoz, A. (1997) *Genes Dev.* **11,** 3351–3364
32. Kamei, Y., Xu, L., Heinzel, T., Torchia, J., Kurokawa, R., Gloss, B., Lin, S. C., Heyman, R. A., Rose, D. W., Glass, C. K., and Rosenfeld, M. G. (1996) *Cell* **85,** 403–414
33. DiSepio, D., Sutter, M., Johnson, A. T., Chandraratna, R. A., and Nagpal, S. (1999) *Mol. Cell. Biol. Res. Commun.* **1,** 7–13
34. Wu, Q., Li, Y., Liu, R., Agadir, A., Lee, M. O., Liu, Y., and Zhang, X. (1997) *EMBO J.* **16,** 1656–1669
35. Lin, B., Chen, G. Q., Xiao, D., Kolluri, S. K., Cao, X., Su, H., and Zhang, X. K. (2000) *Mol. Cell. Biol.* **20,** 957–970
36. Miyajima, N., Kadowaki, Y., Fukushige, S., Shimizu, S., Semba, K., Yamanashi, Y., Matsubara, K., Toyoshima, K., and Yamamoto, T. (1988) *Nucleic Acids Res.* **16,** 11057–11074
37. Wang, L. H., Tsai, S. Y., Cook, R. G., Beattie, W. G., Tsai, M. J., and O'Malley, B. W. (1989) *Nature* **340,** 163–166
38. Ladias, J. A., and Karathanasis, S. K. (1991) *Science* **251,** 561–565
39. Qiu, Y., Krishnan, V., Pereira, F. A., Tsai, S. Y., and Tsai, M. J. (1996) *J.*

Steroid Biochem. Mol. Biol. **56,** 81–85
40. Tran, P., Zhang, X. K., Salbert, G., Hermann, T., Lehmann, J. M., and Pfahl, M. (1992) *Mol. Cell. Biol.* **12,** 4666–4676
41. Kliewer, S. A., Umesono, K., Heyman, R. A., Mangelsdorf, D. J., Dyck, J. A., and Evans, R. M. (1992) *Proc. Natl. Acad. Sci. U. S. A.* **89,** 1448–1452
42. Cooney, A. J., Tsai, S. Y., O'Malley, B. W., and Tsai, M. J. (1992) *Mol. Cell. Biol.* **12,** 4153–4163
43. Widom, R. L., Rhee, M., and Karathanasis, S. K. (1992) *Mol. Cell. Biol.* **12,** 3380–3389
44. Zhang, X. K., Hoffmann, B., Tran, P. B., Graupner, G., and Pfahl, M. (1992) *Nature* **355,** 441–446
45. Wu, Q., Dawson, M. I., Zheng, Y., Hobbs, P. D., Agadir, A., Jong, L., Li, Y., Liu, R., Lin, B., and Zhang, X. K. (1997) *Mol. Cell. Biol.* **17,** 6598–6608
46. Li, Y., Lin, B., Agadir, A., Liu, R., Dawson, M. I., Reed, J. C., Fontana, J. A., Bost, F., Hobbs, P. D., Zheng, Y., Chen, G. Q., Shroot, B., Mercola, D., and Zhang, X. K. (1998) *Mol. Cell. Biol.* **18,** 4719–4731
47. Zhou, X. F., Shen, X. Q., and Shemshedini, L. (1999) *Mol. Endocrinol.* **13,** 276–285
48. Liu, Y., Lee, M. O., Wang, H. G., Li, Y., Hashimoto, Y., Klaus, M., Reed, J. C., and Zhang, X. (1996) *Mol. Cell. Biol.* **16,** 1138–1149
49. van der Burg, B., Slager-Davidov, R., van der Leede, B. M., de Laat, S. W., and van der Saag, P. T. (1995) *Mol. Cell. Endocrinol.* **112,** 143–152
50. Berrodin, T. J., Marks, M. S., Ozato, K., Linney, E., and Lazar, M. A. (1992) *Mol. Endocrinol.* **6,** 1468–1478
51. Butler, A. J., and Parker, M. G. (1995) *Nucleic Acids Res.* **23,** 4143–4150
52. Shibata, H., Nawaz, Z., Tsai, S. Y., O'Malley, B. W., and Tsai, M. J. (1997) *Mol. Endocrinol.* **11,** 714–724
53. Klinge, C. M., Silver, B. F., Driscoll, M. D., Sathya, G., Bambara, R. A., and Hilf, R. (1997) *J. Biol. Chem.* **272,** 31465–31474
54. Klinge, C. M. (1999) *J. Steroid Biochem. Mol. Biol.* **71,** 1–19
55. Robinson, C. E., Wu, X., Nawaz, Z., Onate, S. A., and Gimble, J. M. (1999) *Endocrinology* **140,** 1586–1593

Antagonist Analogue of 6-[3′-(1-Adamantyl)-4′-hydroxyphenyl]-2-naphthalenecarboxylic Acid (AHPN) Family of Apoptosis Inducers That Effectively Blocks AHPN-Induced Apoptosis but Not Cell-Cycle Arrest

Marcia I. Dawson, Danni L. Harris, Gang Liu, Peter D. Hobbs, Christopher W. Lange, Ling Jong, Nathalie Bruey-Sedano, Sharon Y. James, Xiao-kun Zhang, Valerie J. Peterson, Mark Leid, Lulu Farhana, Arun K. Rishi, and Joseph A. Fontana

The Burnham Institute, Cancer Center, 10901 North Torrey Pines Road, La Jolla, California 92037; Molecular Research Institute, 2495 Old Middlefield Road, Mountain View, California 94043; SRI International, Retinoid Program, 333 Ravenswood Avenue, Menlo Park, California 94025; Oregon State University, College of Pharmacy, Corvallis, Oregon 97331; and Wayne State University and John D. Dingell Medical Center, Department of Veterans Affairs, 4646 John R Street, Detroit, Michigan 48201

JOURNAL OF
MEDICINAL CHEMISTRY®

Reprinted from
Volume 47, Number 14, Pages 3518–3536

Antagonist Analogue of 6-[3′-(1-Adamantyl)-4′-hydroxyphenyl]-2-naphthalenecarboxylic Acid (AHPN) Family of Apoptosis Inducers That Effectively Blocks AHPN-Induced Apoptosis but Not Cell-Cycle Arrest

Marcia I. Dawson,*,† Danni L. Harris,§ Gang Liu,† Peter D. Hobbs,‡ Christopher W. Lange,⊗ Ling Jong,‡ Nathalie Bruey-Sedano,† Sharon Y. James,† Xiao-kun Zhang,† Valerie J. Peterson,# Mark Leid,# Lulu Farhana,⊥,▽ Arun K. Rishi,⊥ and Joseph A. Fontana⊥,▽

The Burnham Institute, Cancer Center, 10901 North Torrey Pines Road, La Jolla, California 92037; Molecular Research Institute, 2495 Old Middlefield Road, Mountain View, California 94043; SRI International, Retinoid Program, 333 Ravenswood Avenue, Menlo Park, California 94025; Oregon State University, College of Pharmacy, Corvallis, Oregon 97331; and Wayne State University and John D. Dingell Medical Center, Department of Veterans Affairs, 4646 John R Street, Detroit, Michigan 48201

Received October 15, 2003

The retinoid 6-[3′-(1-adamantyl)-4′-hydroxyphenyl]-2-naphthalenecarboxylic acid (AHPN) and its active analogues induce cell-cycle arrest and programmed cell death (apoptosis) in cancer cells independently of retinoic acid receptor (RAR) interaction. Its analogue, (*E*)-4-[3′-(1-adamantyl)-4′-hydroxyphenyl]-3-(3′-acetamidopropyloxy)cinnamic acid (3-A-AHPC) selectively antagonized cell apoptotic events (TR3/nur77/NGFI-B expression and nuclear-to-mitochondrial translocation) but not the proliferative events (cell-cycle arrest and $p21^{WAF1/CIP1}$ expression) induced by proapoptotic AHPN and its analogues. The syntheses of 3-A-AHPC and proapoptotic (*E*)-6-[3′-(1-adamantyl)-4′-hydroxyphenyl]-5-chloronaphthalenecarboxylic acid (5-Cl-AHPN) are described. Computational studies on AHPN, AHPC, and three substituted analogues (5-Cl-AHPN, 3-Cl-AHPC, and 3-A-AHPC) suggested reasons for their diametric effects on RAR activation. Density functional theory studies indicated that the 1-adamantyl (1-Ad) groups of the AHPN and AHPC configurations assumed positions that were nearly planar with the aromatic rings of their polar termini. In contrast, in the configurations of the substituted analogues having chloro and 3-acetamidopropyloxy groups, rather than a hydrogen, ortho to the diaryl bonds, the diaryl bond torsion angles increased so that the 1-Ad groups were oriented out of this plane. Docking and molecular dynamics of AHPN, AHPC, and these substituted analogues in the RARγ ligand-binding domain illustrated how specific substituents on the AHPN and AHPC scaffolds modulated the positions and dynamics of the 1-Ad groups. As a result, the position of RARγ helix H12 in forming the coactivator-binding site was impacted in a manner consistent with the experimental effect of each analogue on RARγ transcriptional activation.

Introduction

Previously, we established that the retinoid 6-[3′-(1-adamantyl)-4′-hydroxyphenyl]-2-naphthalenecarboxylic acid (CD437[1]/AHPN, **1** in Figure 1) inhibited cancer cell growth and induced cancer cell apoptosis (programmed cell death) by signaling pathways that did not involve the direct interaction of AHPN with the retinoic acid receptor subtypes (RARs) α, β, and γ,[2−5] which function as nuclear transcription factors.[6] AHPN was first reported as an RARγ-selective retinoid.[1] Earlier, Dawson and co-workers had observed that the levels of MCF-7 anchorage-dependent cell growth inhibition by retinoids positively correlated with their abilities to interact with RARα, whereas their inhibition of anchorage-independent (clonal) growth only correlated with their transcriptional activation of RARα.[7] Fitzgerald and co-workers extended these observations of the correlation between growth inhibition by retinoids and RARα activation to other breast cancer cell lines.[8] Our inability to observe a correlation between the inhibition of ovarian cancer cell growth and RAR subtype activation by AHPN and its analogues (AHPNs)[9] underscored our hypothesis that AHPN signaling in cancer cells occurred through a pathway that did not involve the activation of RARs by this new class of apoptosis-inducing agents. Although the signaling pathway by which AHPN and its analogues initiate apoptosis remains to be fully elucidated, we found[10] that it involved the intrinsic apoptotic pathway of mitochondrial membrane potential change, mitochondrial cytochrome *c* release into the cytosol, followed by the binding of cytochrome *c* to the apaf-12 complex that, in turn, activated procaspase-9. The activated enzyme initiated a caspase cascade of cell degradation that included irreversible morphological

* To whom correspondence should be addressed. Phone: 858-646-3165. Fax: 858-646-3197. E-mail: mdawson@burnham.org.
† The Burnham Institute.
§ Molecular Research Institute.
‡ SRI International.
⊥ Wayne State University.
▽ Department of Veterans Affairs.
Oregon State University.
⊗ Current address: Discovery Partners International, Chem. RX Division, 385 Oyster Point Blvd., South San Francisco, CA 94080.

10.1021/jm030524k CCC: $27.50
Published on Web 06/05/2004

changes, DNA cleavage, nuclear fragmentation, and other processes indicative of apoptosis.

Our efforts to define this pathway led to the further discovery of a novel paradigm[10] for the extranuclear behavior of the nuclear receptor TR3/nur77/NGFI-B (human/mouse/rat TR3)[11-13] and retinoid X receptor (RXR)[14] that, like the RARs, functions in the nucleus as a transcription factor. We established that AHPN and its analogues induced the expression of TR3 and its migration from the nucleus to mitochondria,[10] where TR3 modulated the function of the anti-apoptotic protein Bcl-2, which typically protects mitochondria from apoptotic insults.[15] On interacting with TR3, Bcl-2 was no longer able to protect the cell from apoptosis but underwent a conformational change that promoted apoptosis.[16] We also discovered that chemotherapeutic drugs, such as etoposide, were able to induce prostate cancer cell apoptosis through this pathway.[10]

An apoptotic signaling pathway for the AHPNs that does not involve typical RAR signaling is actually advantageous. The retinoids currently approved for the treatment of cancer and other proliferative diseases—*all-trans*-retinoic acid (*trans*-RA, **4**), 9-*cis*-RA (**5**), 13-*cis*-RA, and Targretin/bexarotene (**6**)—have adverse effects.[17-29] In retinoid-treated patients, these effects have included hypertriglyceridemia leading to pancreatitis, pseudotumor cerebri, RA syndrome (respiratory failure), hypothyroidism, and teratogenesis, all of which limit effective dosage and discourage compliance. Transcriptional activation of RARγ by retinoids has been reported to correlate with retinoid toxicity.[30-33] In addition, transformed cells often lose sensitivity to growth inhibition by retinoids through the loss of functional RARs, particularly RARβ, which has been thought to function as a tumor suppressor.[34-38]

Recently, we identified two new apoptotic AHPNs: 6-[3′-(1-adamantyl)-4′-hydroxyphenyl]-5-chloro-2-naphthalenecarboxylic acid (5-Cl-AHPN, **2**)[39] and (*E*)-4-[3′-(1-adamantyl)-4′-hydroxyphenyl]-3-chlorocinnamic acid (3-Cl-AHPC, **9**).[40] Herein, by using diverse computational chemistry approaches in combination with bioassay results, we present a rationale for the lack of retinoid transcriptional activity displayed by these substituted AHPN analogues. We also report the synthesis of the related antagonist, 3-(3′-acetamidopropyloxy)-AHPC (3-A-AHPC, **10**) in addition to that of the apoptosis inducer 5-Cl-AHPN. Our studies showed that 3-A-AHPN blocked the apoptotic signaling pathway induced by AHPN (**1**), 5-Cl-AHPN, and 3-Cl-AHPC in cancer cells and the binding of labeled AHPN to its putative nuclear receptor[4] without impacting the ability of AHPN and its proapoptotic analogues to induce cell-cycle arrest[2] and the expression of the cyclin-dependent kinase inhibitor p21$^{WAF1/CIP1}$.[3]

Design/Synthesis

Shortly after our observation of the apoptotic activity of AHPN (**1**),[2] we undertook the synthesis of analogues, including 5-Cl-AHPN (**2**), 3-Cl-AHPC (**9**), and AHPC (**11**), with the goal of removing retinoid activity to reduce any adverse effects that would be associated with transcriptional activation of the RARs. We elected to focus on the *E*-cinnamic acid scaffold of AHPC for two reasons. First, synthetic precursors to substituted cinnamic acids were far more readily available than those for similarly substituted naphthalenecarboxylic acids. Second, we hypothesized that by replacing the naphthalenecarboxylic acid moiety of AHPN with a cinnamic acid group we would reduce retinoid activity. Prior to 1990, we had synthesized the cinnamic acid **15**[41] as an analogue of the retinoid TTNN (**16**).[42] This strategy was not particularly useful for retinoid design as evidenced by the two-log higher EC_{50} value determined for **15** in reversing the keratinization of vitamin A-deficient tracheal epithelium in organ culture (TOC assay) compared to that of TTNN.[41] We subsequently found that the activity of retinoids in the TOC assay[41,43] correlated with their ability to transcriptionally activate the RARs bound to their RA-responsive elements (RAREs) in the promoter regions of retinoid-responsive genes. There-

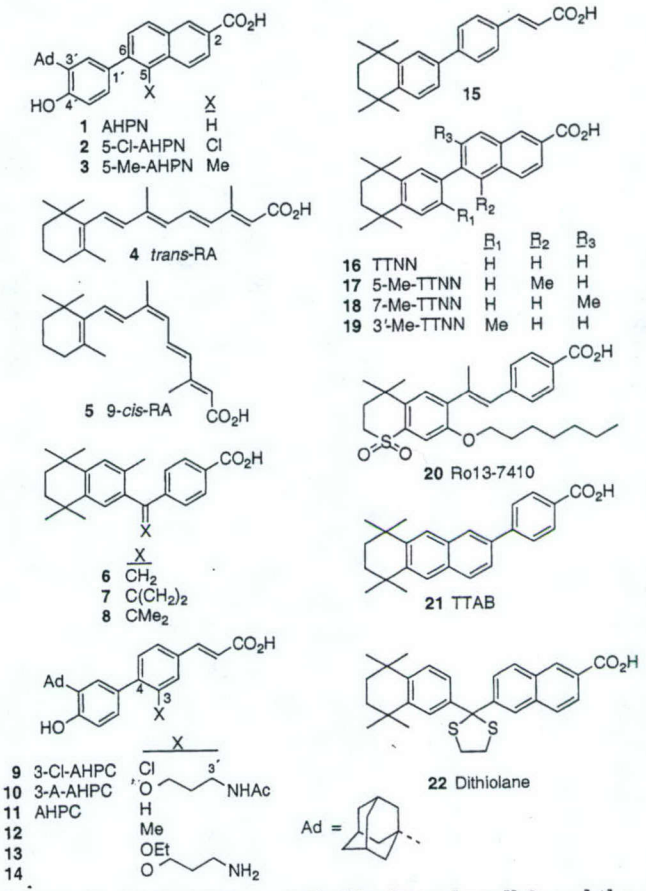

Figure 1. 6-[3′-(1-Adamantyl)-4′-hydroxyphenyl]-2-naphthalenecarboxylic acid (AHPN, **1**); AHPN analogues 5-chloro-AHPN (5-Cl-AHPN, **2**) and 5-methyl-AHPN (5-Me-AHPN, **3**); retinoic acid receptor (RAR)-selective agonist *trans*-retinoic acid (*trans*-RA, **4**); RAR and retinoid X receptor (RXR) panagonist 9-*cis*-retinoic acid (9-*cis*-RA, **5**); RXR-selective retinoids Targretin (11247, **6**), 11173 (**7**), and 11345 (**8**); (*E*)-4-[3′-(1-adamantyl)-4′-hydroxyphenyl]cinnamic acid (AHPC, **11**); AHPC analogues 3-chloro-AHPC (3-Cl-AHPC, **9**), 3-(3′-acetamidopropyloxy)-AHPC (3-A-AHPC, **10**), 3-Me-AHPC (**12**), 3-EtO-AHPC (**13**), and 3-(3′-aminopropyloxy)-AHPC (**14**); RARβ,γ-selective (*E*)-4-(5′,6′,7′,8′-tetrahydro-5′,5′,8′,8′-tetramethyl-2′-naphthalenyl)cinnamic acid (**15**), 6-(5′,6′,7′,8′-tetrahydro-5′,5′,8′,8′-tetramethyl-2′-naphthalenyl)-2-naphthalenecarboxylic acid (TTNN, **16**), 5-Me-TTNN (**17**), 7-Me-TTNN (**18**), 3′-Me-TTNN (**19**); RARα-selective antagonist Ro41-5253 (**20**); RAR-selective agonist 4-(5′,6′,7′,8′-tetrahydro-5′,5′,8′,8′-tetramethyl-2′-anthracenyl)benzoic acid (TTAB, **21**); and RARγ-selective antagonist 2-(5′,6′,7′,8′-tetrahydro-5′,5′,8′,8′-tetramethyl-2′-naphthalenyl)-2-(6′-carboxynaphthalene)-1,3-dithiolane (11253, **22**).

Table 1. Cancer Cell Apoptosis and Growth Inhibition Activities Induced by AHPN, AHPC, and Analogues Compared to Their Calculated Inter-Ring Dihedral Angles

	apoptosis (%)[a]				growth inhibition (%)[b]		
	HL-60R (24 h)		MDA-MB-231 (96 h)		H460 (144 h)		
analogue	0.1×10^{-6} M	1.0×10^{-6} M	0.5×10^{-6} M	1.0×10^{-6} M	0.1×10^{-6} M	1.0×10^{-6} M	angle[c] (deg)
AHPN (**1**)	78	98	26	46	20	80	31
5-Me-AHPN (**3**)	29	70	14	–	–	–	29
AHPC (**11**)	90	98	53	58	–	–	21
3-Me-AHPC (**12**)	10	95	5	30	–	–	–
3-EtO-AHPC (**13**)	0	29	–[d]	–	14	52	–
5-Cl-AHPN (**2**)	62	94	21	41	56	71	61
3-Cl-AHPC (**9**)	51	94	31	43	–	–	51
3-A-AHPC (**10**)	0	0	0	1	–	–	70

[a] Average of triplicates ± ≤ 10% for HL-60R leukemia and MDA-MB-231 breast cancer apoptosis as determined by acridine orange staining. [b] Average of triplicates ± ≤10% for H460 lung cancer apoptosis as determined by DAPI staining. [c] AHPN scaffold 5−6−1′−2′ or AHPC scaffold 3−4−1′−2′ dihedral angle determined by AM1. [d] Not determined.

fore, we rationalized that AHPC, the cinnamic acid analogue of AHPN, would have comparably reduced retinoid agonist activity. This hypothesis only held for the activation of RARα by AHPC. Transcriptional activations of RAR subtypes α, β, and γ on the $(TREpal)_2$-*tk*-CAT reporter induced by 1.0×10^{-6} M AHPC were 8%, 85%, and 103%, respectively, whereas those induced by 1.0×10^{-6} M AHPN were 21%, 78%, and 88%. Fortunately, because apoptosis-inducing activity was retained by AHPC, we pursued further modifications of the AHPC scaffold. The synthesis and apoptotic activity of AHPC were recently reported by Cincinelli et al.[44]

Introducing a methyl group at the 5- or 7-naphthalene ring position of TTNN (**16**), which was ortho to the central diaryl bond, also decreased retinoid agonist activity, as was evidenced by the higher EC_{50} values for 5-Me-TTNN (**17**) and 7-Me-TTNN (**18**) in the TOC assay compared to that of TTNN.[41] The ED_{50} values for both analogues in inhibiting the induction of mouse epidermal ornithine decarboxylase (ODC) by the tumor promoter 12-*O*-tetradecanoylphorbol-13-acetate were also higher than that for TTNN.[45] As in the TOC assay, the inhibitory activities of retinoids in the ODC assay[45] correlated with their abilities to function as RAR transcriptional agonists on an RARE such as the TREpal,[46] a synthetic RE[6] used to evaluate the transcriptional activation of both RAR and retinoid X receptor (RXR) subtypes by retinoids.[47−52] The 3′-methyl analogue (**19**) of TTNN also had lower activity in the ODC assay.[45] Moreover, by introducing a 3′-methyl group onto the tetrahydrotetramethylnaphthalene (TTN) ring of a retinoid that bound RXRs to inhibit its interaction with the homologous RARs, we successfully obtained highly RXR-selective retinoids such as **6**−**8**.[51−54] The use of this strategy was also reported by other groups.[55,56] On the basis of these findings, we elected to introduce methyl groups ortho to the diaryl bridges of AHPN (**1**) and AHPC (**11**). Replacing the TTN ring of TTNN (**16**) by a 3′-(1-adamantyl)-4′-hydroxyphenyl group was also found to reduce retinoid agonist activity.[1] We combined these features in 5-Me-AHPN (**3**), which at 1.0×10^{-7} M had growth inhibitory activity approaching that of AHPN on MCF-7 and BT-20 breast cancer cells and was also not able to activate RARα. However, its activations of RARβ and RARγ were enhanced.[57] Thus, this strategy for designing AHPNs lacking RAR transcriptional activation activity required modification.

Fortunately, further work indicated that introducing an electronegative chloro group at a position ortho to the diaryl bond on the AHPN and AHPC scaffolds satisfactorily reduced RAR activation activity. Both 5-Cl-AHPN (**2**)[39] and 3-Cl-AHPC (**9**)[40] were efficient inducers of apoptosis but had minimal ability to activate the RARs.[39,40] Therefore, a means of blocking the ability of an ANPN analogue to activate the RARs was available. Moreover, while neither *trans*-RA (**4**) nor 9-*cis*-RA (**5**) was able to displace labeled AHPN[4] from the putative AHPN receptor in HL-60R cell extracts, nonlabeled AHPN (**1**) and 5-Cl-AHPN (**2**) were effective competitive inhibitors.[4] These results provided additional evidence that AHPN and analogues such as 5-Cl-AHPN and 3-Cl-AHPC induced cancer cell apoptosis through a pathway that did not involve RAR signaling.

Because access to an antagonist would facilitate probing AHPN-signaling pathways, we also accomplished the design and synthesis of 3-A-AHPC (**10**). Its design was based on our observation that the apoptotic activities of AHPN analogues decreased as the length of their substituents at the 3-cinnamyl ring and 5-naphthyl ring positions increased without comparable decreases in their abilities to compete with tritiated AHPN for binding to the putative AHPN receptor in HL-60R leukemia and MDA-MB-468 breast cancer cell nuclear extracts.[4] HL-60R cell apoptosis induced by 24-h treatments with 1.0×10^{-6} M AHPC (**11**), 3-Me-AHPC (**12**), and 3-EtO-AHPC (**13**) was 98%, 95%, and 29% respectively, of the vehicle-alone treated control (Table 1). The Fontana group has found that this leukemia cell line was particularly convenient for assessing apoptosis induced by AHPN analogues without the interference of possible interactions with RARs. Standard retinoids such as *trans*-RA (**4**) and 9-*cis*-RA (**5**) were unable to induce apoptosis at similar concentrations because the RARβ and RARγ proteins were absent and the RARα mutant present was dysfunctional in competently binding standard retinoids due to the deletion of its carboxyl terminus.[58] In MDA-MB-231 breast cancer cells, which were also resistant to growth inhibition by RAR-selective retinoids[2] (data not shown), 96-h treatments with 1.0×10^{-6} M AHPC and 3-Me-AHPC produced 58% and 30% apoptosis, respectively. These results also support a retinoid-independent signaling pathway for the AHPNs, as well as our findings about the impact of the substitutents ortho to their diaryl bonds on apoptosis.

Scheme 1[a]

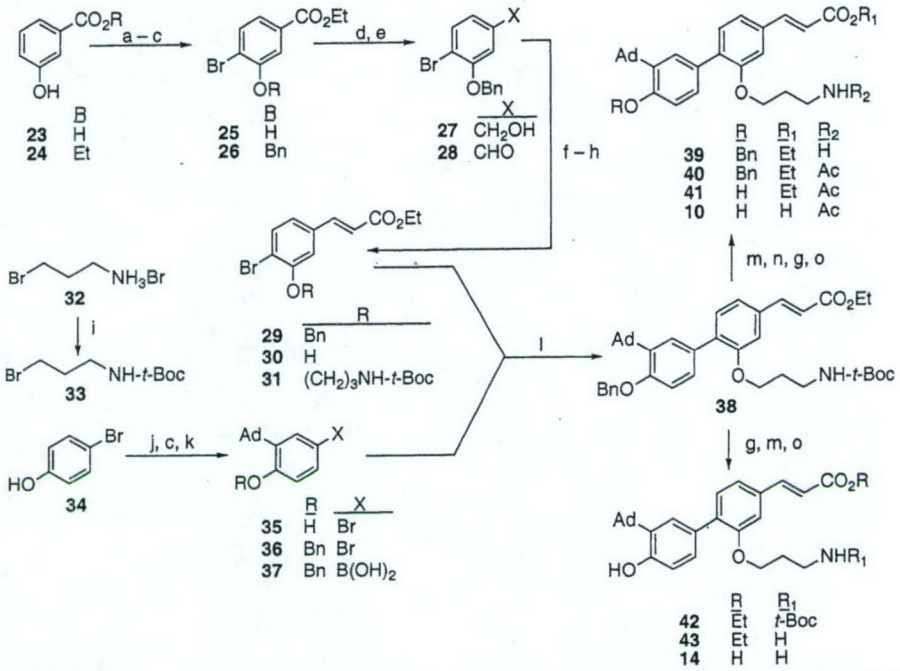

[a] (a) EtOH, $MeSO_3H$, PhH, reflux. (b) Br_2, HOAc. (c) BnBr, Na_2CO_3, Me_2CO, Et_2O/THF, −78 °C, reflux. (d) DIBAL, THF, −78 °C; H_3O^+. (e) PCC, CH_2Cl_2. (f) $[(EtO)_2P(O)CH_2CO_2Et$, $KN(SiMe_3)_2]$, −78° to 20 °C. (g) BBr_3, CH_2Cl_2, −78 °C; H_2O. (h) **33**, K_2CO_3, Me_2CO, reflux. (i) $(t\text{-Boc})_2O$, Et_3N, CH_2Cl_2, 0−20 °C. (j) 1-AdOH, H_2SO_4, CH_2Cl_2. (k) [*n*-BuLi, THF]; $B(Oi\text{-Pr})_3$; H_3O^+. (l) $Pd(PPh_3)_4$, aq Na_2CO_3, reflux. (m) H_3O^+, EtOH, reflux. (n) Ac_2O, py, CH_2Cl_2. (o) NaOH, MeOH, reflux; H_3O^+.

The synthesis of 3-Cl-AHPC (**9**) was previously reported by our group.[40] Antagonist 3-A-AHPC (**10**) was synthesized by a similar route, which is shown in Scheme 1. The challenge in the syntheses of 3-A-AHPC and its free amine (**14**) was the presence of three reactive groups (phenolic hydroxyl, carboxylic acid, and amide) that required selective protection and deprotection so that both compounds would be accessible from intermediate **38**. For this reason, the *tert*-butylcarbonyl group was used to protect the amine so that its removal could be achieved in the presence of both benzyl and ester protecting groups, but the amine group would remain protected during the removal of the benzyl group using boron tribromide at −78 °C. Briefly, the diaryl bond of 3-A-AHPC was introduced using a palladium(0)-catalyzed diaryl coupling of the aryl boronic acid **37**[39] with the protected (*E*)-4-bromocinnamate **31**. A three-step sequence allowed the selective removal of the protecting groups from **38**, which was immediately transformed to **10** and its related amine (**14**). The latter will be tethered to a support for use in the affinity purification of the AHPN receptor protein from HL-60R nuclear extracts.[4] The *E*-cinnamyl double bond of intermediate **29**, from which **31** was derived, was introduced by the Horner−Emmons−Wadsworth olefination of aldehyde **28** using the anion of triethyl phosphonoacetate. Isomer **29** was readily separated from a small amount (<5%) of the related *Z*-isomer by chromatography. The overall yield of the 11-step convergent sequence from **23** to **10** was 12%.

The synthesis of 5-Cl-AHPN (**2**) is outlined in Scheme 2 and resembles that reported for 3-Cl-AHPC (**9**).[40] The 5-chloro group of **46** was introduced specifically by α-chlorination of ,ethyl 6-hydroxy-2-naphthalenecarboxylate (**45**) using sulfuryl chloride, as had been expected because the chlorination of β-naphthol was

Scheme 2[a]

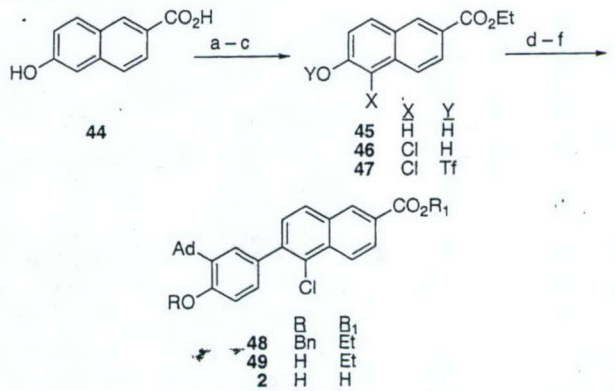

[a] (a) EtOH, H_2SO_4, reflux. (b) SO_2Cl_2, HOAc, 70 °C; H_2O. (c) $(CF_3SO_2)_2O$, pyridine, CH_2Cl_2, 0−20 °C. (d) **37**, $Pd(PPh_3)_4$, LiCl, aq Na_2CO_3, DME. (e) BBr_3, CH_2Cl_2, −78 °C; H_2O. (f) aq NaOH, EtOH, reflux; H_3O^+.

reported to occur at the α-position.[59] Palladium-catalyzed diaryl coupling of triflate **47**, which was derived from **46**, with arylboronic acid **37** and deprotection provided 5-Cl-AHPN in 22% overall yield for the six steps beginning with **44**.

Computational Studies

Ligand Determinants of Transcriptional Activation. Often, molecular determinants that affect nuclear receptor transcriptional activation can be due to subtle effects of the ligand on receptor conformation.[60−63] Small changes in the properties of a ligand group may significantly alter either the binding mode of the ligand to the receptor or the magnitude of the interaction of the ligand with receptor binding-site residues so as to profoundly affect conformation. Our docking and molecular dynamics studies suggested that its large 3-(3′-

acetamidopropoxy) group rendered 3-A-AHPC (**10**) incapable of transcriptionally activating RARγ by preventing helix H12 from forming the coactivator-binding site. Therefore, with the binding of the coactivator protein blocked,[64] the recruitment of the multiprotein complex responsible for gene transcription could not occur.[65] The negative effect of the 3-(3′-acetamidopropoxy) group of 3-A-AHPC on RAR activation activity was not surprising because a methyl group at the 3′-position of the TTN ring enhanced the RXR selectivity of retinoids, and longer 3′-alkyl groups decreased RAR transcriptional activation in analogues of TTNN (**16**) and other retinoids.[66,67] For example, Ro-41-5253 (**20**) having a 3′-heptyloxy substituent was a potent RARα antagonist,[66] and the 3′-butyl analogue of 11173 (**7**) antagonized RXRα activation by 9-*cis*-RA (**5**).[60] Further computational probing of AHPN and AHPC analogues having similarly situated substitutents suggested that some ortho groups prevented RAR agonism by a more subtle means than by causing large changes in the LBD conformation that were distinct from those caused by AHPN (**1**). Our experimental results supported this conclusion. The ortho Cl group prevented RARβ and RARγ transcriptional activation by both 5-Cl-AHPN (**2**) and 3-Cl-AHPC (**9**). In contrast, the similarly sized 5- and 3-methyl groups of 5-Me-AHPN (**3**)[57] and 3-Me-AHPC (**12**), respectively, did not produce similar effects on RARs β and γ.

To understand why chloro group substitution ortho to the diaryl bond in AHPN analogues negatively impacted RAR activation, whereas a methyl group did not, computational studies were conducted using both the structure reported for the crystalline RARγ LBD–*trans*-RA (**4**) complex (Protein Data Bank (PDB) entry 3LBD) and small-molecule ab initio computational methods. In these studies, electron-correlation effects were included to accurately determine the torsional potential surface of each compound, which depicted how conformational energy varied as a function of torsion angle size. Because the results of density functional theory (DFT) calculations on the torsional energy barriers of substituted biphenyls[68] were in good agreement with experimental values,[69] nonlocal DFT low-energy conformations and torsional potential surfaces were determined for AHPN (**1**), 5-Cl-AHPN (**2**), 3-Cl-AHPC (**9**), 3-A-AHPC (**11**), and AHPC (**12**). The torsional potential surfaces were computed by parametrically varying the diaryl bond torsion angles while fully optimizing all other atomic positions for each step. CPK models of the optimized lowest-energy configurations of these AHPNs are illustrated in Figure 2A. The torsional potential surface for each analogue was mapped as a function of the change in the diaryl bond torsion angle 5–6–1′–2′ for AHPN and 5-Cl-AHPN and 3–4–1′–2′ for AHPC, 3-Cl-AHPC, and 3-A-AHPC, and is depicted graphically in Figure 2B. The relaxed potential surface scans indicated that the torsional potential surfaces of AHPN and AHPC were significantly different from those of the three substituted analogues. The geometry optimization and the potential surface results implied that the preferred shapes for low-energy conformations of AHPN and AHPC were more planar. Therefore, we hypothesized that if binding by a compact linear ligand was required to induce the RARγ conformation necessary for coactivator binding and transcriptional activation, the diaryl torsion angles of 5-Cl-AHPN and 3-Cl-AHPC would have been compressed to such an extent

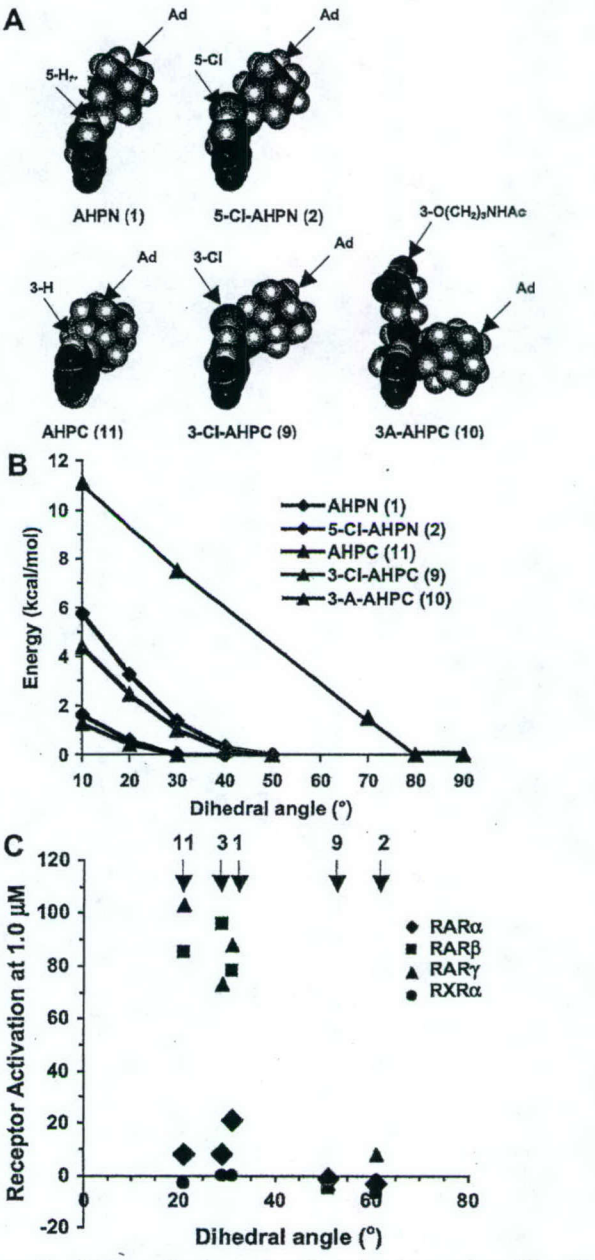

Figure 2. Ortho substituents affect the inter-ring (diaryl) bond twist in AHPN (**1**) and its analogues. A. Comparison of DFT geometry-optimized structures of AHPN and 5-Cl-AHPN (**2**) (top row), and AHPC (**11**), 3-Cl-AHPC (**9**), and 3-A-AHPC (**10**) (bottom row). Differences in inter-ring twist angles and, consequently, structure widths are depicted. Compounds are shown in space-filling format with C and Cl colored in green, O in red, N in blue, and H in white. B. Low-energy inter-ring dihedral angles reflect differences in the torsional potential surfaces of AHPN, AHPC, and their analogues that are modulated by substitutents ortho to the diaryl bond. Total energy calculated for each complex as a variable of the 5–6–1′–2′ AHPN or 5-Cl-AHPN or the 3–4–1′–2′ 3-Cl-AHPC or 3-A-AHPC torsion angle was plotted. C. Impact of substituents ortho to the diaryl bond on torsion angles of AHPN, AHPC, and their analogues and on their RARs α, β, and γ and RXRα transcriptional activation activities. Notice that on the AHPN and AHPC scaffolds that are selective for transcriptional activation of RARβ and RARγ, the chloro group had a far greater negative impact on receptor activation than a methyl group.

that the potential energies of their complexes with the RARγ LBD would have had to rise to energetically disfavored levels. Consequently, any binding by 5-Cl-AHPN and 3-Cl-AHPC to the RARγ LBD would favor 'inactive' or antagonist-like holo-receptor configurations. In Figure 2C, the negative correlation between torsional angle size and RARβ and RARγ transactivation is presented graphically for six of the analogues listed in Table 1. As shown, RXRα was not activated by these analogues, and RARα activation was very low or not existent.

We used molecular dynamics to explicitly test the hypothesis that binding of 5-Cl-AHPN (**2**) or 3-Cl-AHPC (**9**) would induce an RARγ antagonist conformation. Our results are presented in Figures 2 and 3. Docking of 5-Cl-AHPN into the RARγ ligand-binding pocket (LBP), which was obtained from the X-ray crystallographic structure of the human RARγ LBD−9-*cis*-RA (**5**) complex,[65] using the energy-based Larmarkian Genetic Algorithm (LGA) produced lowest-energy configurations in which the 5-Cl-AHPN carboxylate group interacted with the LBD helix H5 arginine-278 (Figure 3A), as had the 9-*cis*-RA carboxylate,[65] and with the hydroxyl side-chain of serine-289, which was located between the two β-sheet regions adjacent to the LBP (data not shown). The 3′-(1-adamantyl) (1-Ad) group of docked 5-Cl-AHPN nestled against the LBP hydrophobic groups of tryptophan-227 on helix H3 and those of isoleucine-412 and methionine-415 on helix H12 (Figure 3A). The 9-*cis*-RA β-cyclogeranylidene ring made similar contacts.[65] In the 5-Cl-AHPN-docking simulation, LBD helices H11 and H12 formed portions of "the roof" of the LBP, as was reported for the RARγ LBD−9-*cis*-RA complex.[65] Docking of AHPN (**1**) into the LBP yielded a low-energy binding configuration comparable to that observed for 5-Cl-AHPN (Figure 3A). These results suggested to us that the effects of the substituent ortho to the diaryl bond could not be explained by the initial configuration of the ligand docked in the holo-RARγ LBD complex but resulted from time-dependent receptor−ligand complex conformational effects.

The superposition of the 300-ps molecular dynamics configurations resulting from the simulations of the RARγ LBD complexes with AHPN (**1**) and 5-Cl-AHPN (**2**) is shown in Figure 3B. Because the docked configurations of AHPN and 5-Cl-AHPN overlapped significantly at their carboxylate termini, only 5-Cl-AHPN and the nearby LBD helical backbones in both conformations have been displayed so that backbone differences near the docked compounds were visible. While the position of the helix H10 backbone of the RARγ LBD was almost invariant in the two conformations, portions of the backbones of helices H11 (residues 393−403) and H12 (residues 410−415) adjacent to the docked compounds differed appreciably. These differences were also evident on comparing the distance-time series that tracked the AHPN and 5-Cl-AHPN−helix contact distances (Figure 3 panels C and D, respectively). Compared to the 5-hydrogen, the 5-chloro group significantly impacted the compound shape (Figure 2A) and the torsional potential surface (Figure 2B), both of which, in turn, impacted the forces on helix H12 (Figure 3A) and its conformation (Figure 3B). As a result, the time-dependent conformations of their complexes with the RARγ LBD, as reflected in the relative calculated distances between their 1-Ad carbons and the RARγ H12 isoleucine-412 backbone Cα (Figure 3C) and side-chain CD1 (Figure 3D) carbons during the periods of close contacts of each ligand with helix H12, were quite different. The time-dependence plots for the AHPN−helix H12 contact distances showed only the small fluctuations characteristic of tight or compact contacts, whereas those for the 5-Cl-AHPN−helix H12 contact distances showed the significant structural fluctuations indicative of a larger range of contact distances. These results suggested that the time-dependent dynamics of the conformations of helix H12 in the RARγ LBD when bound by AHPN or an analogue were significantly affected by the identity of the substituent ortho to the diaryl bond in AHPN and its analogues.

Initial docking of 3-A-AHPC (**10**) to the RARγ LBD produced low-energy configurations similar to those observed for 3-Cl-AHPC (**9**) for the interactions between the 3-A-AHPC carboxylate and the RARγ LBD arginine-278 and serine-289. In fact, one such docked configuration showed that the 3′-acetamidopropoxy group (3-A) of 3-A-AHPC contacted the same helix H12 residues and that the 3-A acetamido group was oriented toward the helix H11 arginine-396 (see Figure 3B). In addition to producing the same contacts as those of AHPN (shown in Figure 3A), the greatly accentuated twist in the diaryl bond of 3-A-AHPC produced nonplanar configurations in which the orientations of its 1-Ad group permitted close contacts with residues near and on helix H12, including leucine-416 (Figure 3E).

In Figure 3F are shown portions of the dynamics trajectory analyses of solvated RARγ LBD complexes with AHPC (**11**) and 3-A-AHPC (**10**), in which periodic boundary conditions and particle-mesh Ewald summations of electrostatic interactions were employed to provide realistic boundary forces, the damping of surface fluctuations, and the elimination of electrostatic potential truncation artifacts. These simulations having a realistic boundary force, which provided fluctuation damping at the surface of the protein, revealed that the 3-A group of 3-A-AHPC caused larger local fluctuations in residues proximate to helix H12 than the 3-chloro group of 3-Cl-AHPC did on the basis the 1-Ad C−leucine-416(CD2) C distances over time (Figure 3, panels E and F). These results were clearly analogous to those shown for AHPN (**1**) and 5-Cl-AHPN (**2**) in Figure 3C. While the compact shape of AHPC allowed intimate contacts between AHPC and residues 411−416 on helix H12, the twisted shape of 3-A-AHPC produced perturbations in local dynamics on short subnanosecond time scales that were significant enough to cause the transient opening of the LBP to the LBD surface to allow the entry of "bulk" water. The greater fluctuations evident in the distance plot for 3-A-AHPC shown in Figure 3F and the finding that LBP opening to the surface enabled bulk water entry suggested that the 3-A group had perturbed local dynamics.

Biological Results

The binding of 3-Cl-AHPC (**9**) to the RAR subtypes and RXRα was determined in competition radioligand-binding experiments using the recombinant receptor subtype LBDs and their panagonist ligand [^{3}H]9-*cis*-RA.

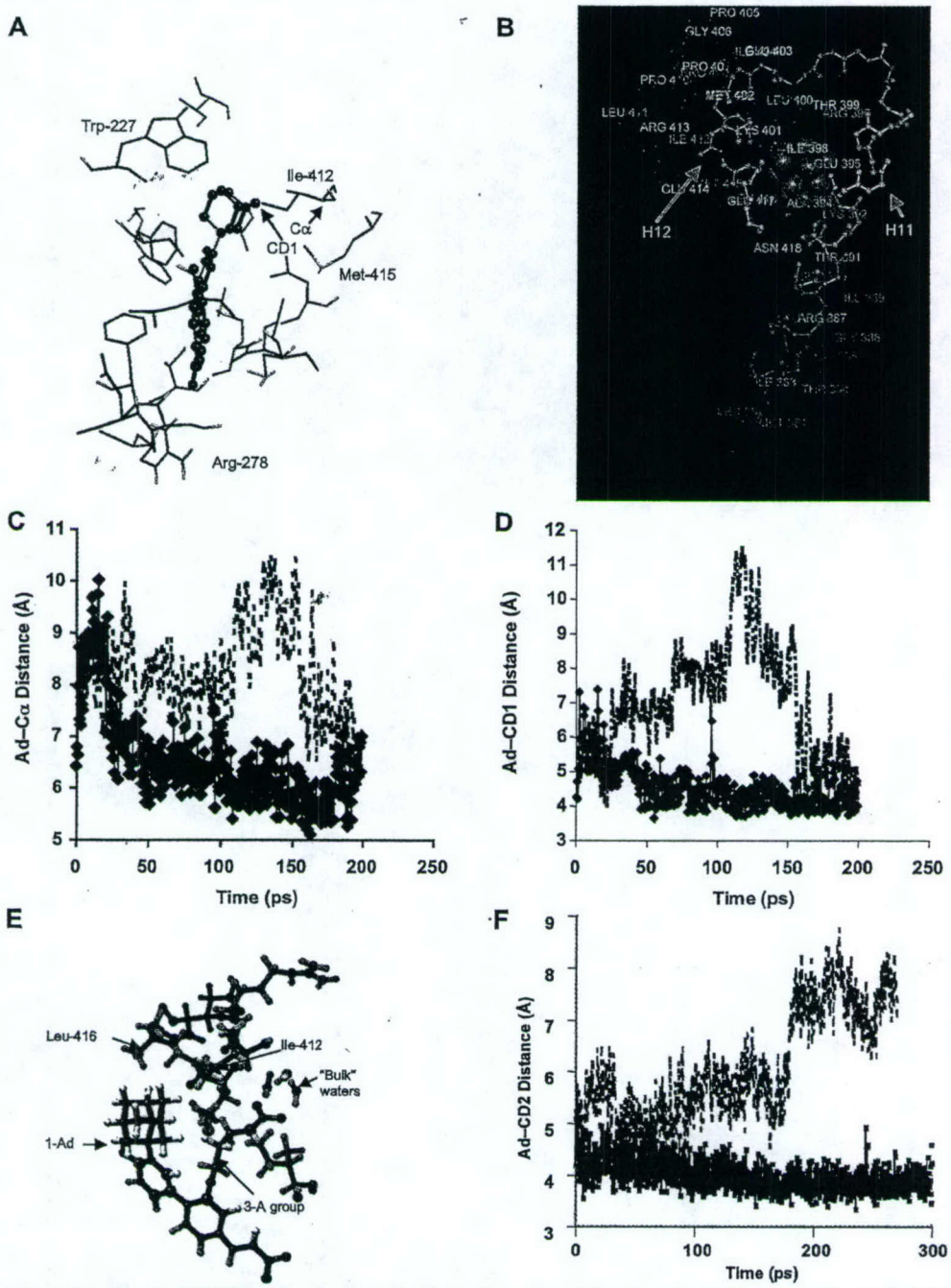

Figure 3. A substituent ortho to AHPN inter-ring bond affects time-dependent contacts between the 3′-(1-Ad) group and RARγ LBD helix H12. A. Energy-based docking of 5-Cl-AHPN (**2**) in the RARγ LBD. The lowest energy-based docked 5-Cl-AHPN orientation (shown in ball-and-stick format without Hs) and residue contacts in the RARγ LBP pocket are shown. The RARγ LBD−9-*cis*-RA (**5**) 3LBD crystal structure[65] was used for docking. The contacts of the 1-Ad group, including those with the isoleucine (Ile)-412 CD1 carbon of helix H12, are shown. Atom colorations are as in Figure 2A and S is in yellow; only Hs on side-chain heteroatoms are depicted. B. AHPN (**1**) and 5-Cl-AHPN have differential effects on the local RARγ LBD backbone conformation. The 300-ps time-points of MD simulations of AHPN (white) and 5-Cl-AHPN (magenta) in the RARγ LBD were superposed. To highlight differences, only the backbone atoms of RARγ LBD residues 371−418 and 5-Cl-AHPN are shown. The 3′-(1-Ad) and 4′-OH groups of 5-Cl-AHPN are viewed head-on. AHPN with the exception of the 3′-(1-Ad)-4′-OH-phenyl group had the same configuration as 5-Cl-AHPN in the LBP. The conformations of helix H10 (375−392) are similar, whereas those for helices H11 (393−403) and H12 (410−415) that are proximate to the 1-adamantyl (1-Ad) contacts are perturbed in the RARγ LBP−5-Cl-AHPN complex (magenta arrows) compared to the AHPN-bound conformation (gray arrows). C and D. Time dependence of the distance between the helix H12 isoleucine (Ile)-412 backbone Cα (C) or the side-chain CD1 (D) carbon (labeled in panel A) and the 1-Ad carbons of AHPN (solid line) and 5-Cl-AHPN (dashed line) in simulations of AHPN and 5-Cl-AHPN bound to the RARγ LBD are depicted graphically. E. Docking demonstrates 3-A-AHPC (**10**)−RARγ LBD helix H12 contacts. As a result of the larger diaryl bond dihedral angle, the 3-A side-chain and the 1-Ad group of 3-A-AHPC contact Ile-412 and leucine (Leu)-416, respectively. Both amino acid residues and 3-A-AHPC are represented in matchstick format with hydrogens shown in gray and other atom colorations as in Figure 2A. F. Results of molecular dynamics on AHPC (**11**) and 3-A-AHPC bound to the RARγ LBD. Time dependence of the distance between the helix H12 Leu-416 side-chain CD2 carbon and the 1-Ad carbons of AHPC (solid line) and 3-A-AHPC (dashed line). In contrast to the small fluctuations caused by close contacts between the AHPC 1-Ad and the Leu-316 CD2 carbons, large structural fluctuations resulted from the contacts between the 3-A-AHPC 1-Ad and Leu-316 CD2 carbon atoms.

Compared to nonlabeled 9-*cis*-RA (**5**), 3-Cl-AHPC (both at 1.0×10^{-6} M) only marginally displaced [^{3}H]9-*cis*-RA bound to RARα, RARβ, and RXRα (31%, 17%, and 16% displacement, respectively; Figure 4A), but quite effectively displaced [^{3}H]9-*cis*-RA bound to RARγ (83% displacement; Figure 4A). These results suggested that 3-Cl-AHPC efficiently and selectively competed with [^{3}H]9-*cis*-RA for binding to RARγ.

The binding of a coactivator protein to its site on the surface of a nuclear receptor permits the recruitment of the multiprotein complex that initiates gene transcription. X-ray crystallographic studies demonstrated that on binding a ligand capable of inducing transcriptional activation, the RARγ LBD underwent an appreciable conformational change so that its helix H12 moved from an extended conformation to one that formed the coactivator binding site with helices H3 and H4 on the LBD surface.[65] Thus, an RARγ agonist induced a change in the apo-RARγ LBD conformation to one that was more compact and protease-resistant, which was detectable by using the differential protease sensitivity assay (DPSA) coupled with mass spectral identification of the peptide fragments resulting from limited proteolysis.[70] The ability of 3-Cl-AHPC (**9**) to induce a conformational change in the [^{35}S]methionine-labeled RARγ ([^{35}S]RARγ) LBD that was indicative of agonist activity was evaluated by DPSA to determine if the peptide fragments produced would be the same as those from the LBD bound by the agonist 9-*cis*-RA (**5**). Incubation of the LBD with 9-*cis*-RA (1.0×10^{-6} M) followed by partial tryptic digestion produced two protease-resistant fragments, PF30 and PF31 (compare Figure 4B lanes 2−6 showing the proteolysis profile of the apo-RARγ LBD with lanes 12−16 showing that of the holo-LBD−9-*cis*-RA complex). PF30 and PF31 corresponded to the RARγ LBD Glu^{173}−Lys^{451} and Glu^{170}−Lys^{451} sequences, respectively.[70] 3-Cl-AHPC (5.0×10^{-6} M) also induced the formation of PF30 and PF31 (compare Figure 4B lanes 2−6 with lanes 7−11 showing the proteolytic profile of the holo-LBD−3-Cl-AHPC complex). Interestingly, the fragments induced by 3-Cl-AHPC binding appeared to be somewhat less stable to proteolytic digestion than the fragments induced by the binding of 9-*cis*-RA (compare lanes 10 and 11 with lanes 15 and 16). Nonetheless, the 3-Cl-AHPC-bound [^{35}S]RARγ LBD was clearly more resistant to tryptic digestion than the apo-[^{35}S]RARγ. Thus, the results of the DPSA studies suggested that binding by 3-Cl-AHPC and 9-*cis*-RA induced grossly similar conformational changes within the LDB of RARγ.

The RARγ comformational change that occurred on binding by a retinoid agonist was found to lead to the dissociation of an apo-receptor-associated corepressor protein such as NCoR, followed by the recruitment of a transcriptional coactivator protein such as p300.[70] Therefore, corepressor dissociation and coactivator recruitment studies were conducted to determine whether binding by 3-Cl-AHPC (**9**) promoted and/or stabilized a RARγ conformation that disfavored corepressor binding but favored coactivator binding in a manner similar to that of the classical RAR transcriptional agonists such as TTAB (**21**).[71] Both corepressor (NCoR 2110−2453) and coactivator (p300 1−450) proteins were expressed as glutathione *S*-transferase (GST) fusions in bacteria,

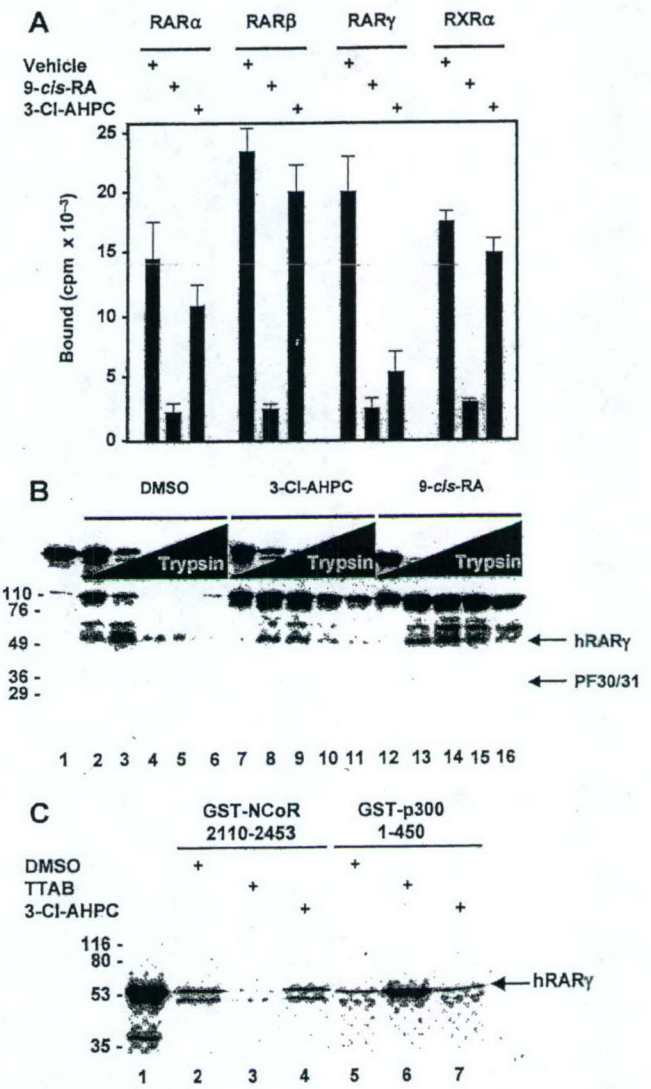

Figure 4. 3-Cl-AHPC (**9**) lacks RARγ agonist activity in vitro. A. Competition radioligand-binding experiments. Recombinant, bacterially expressed RAR subtype and RXRα LBDs (approximately 1.0×10^{-8} M) were incubated with 1.0×10^{-9} M [11,12-^{3}H$_2$]9-*cis*-RA (43 Ci/mmol) with or without 1.0×10^{-9} M nonlabeled 9-*cis*-RA (**5**) or 3-Cl-AHPC as indicated. Bound and free radioligand were separated by gel filtration using Sephadex G-50. B. 3-Cl-AHPC-bound [^{35}S]RARγ LBD is less susceptible to protolytic degradation than the *apo*-LBD. DPSAs were conducted using [^{35}S]RARγ LBD preincubated with either vehicle (DMSO, 0.1% v/v), 9-*cis*-RA (1.0×10^{-6} M), or 3-Cl-AHPC (5.0×10^{-6} M) as indicated. The receptor was then digested with increasing concentrations of trypsin-TPCK (10, 100, 250, 500, and 1000 μg/mL) for 15 min at 22 °C. Trypsin was inactivated, and the digest was subjected to electrophoresis on a denaturing gel and autoradiography. C. 3-Cl-AHPC-induced conformational change is not sufficient to induce either the dissociation of corepressor from or the recruitment of coactivator to the [^{35}S]RARγ LBD. GST-pulldown experiments were conducted using [^{35}S]RARγ LBD and either GST-NCoR 2110−2453 or GST-p300 1−450 as indicated in the presence of Me_2SO (0.1% v/v), TTAB (**21**) (1.0×10^{-6} M), or 3-Cl-AHPC (5.0×10^{-6} M) as indicated. [^{35}S]RARγ bound to GST-fusion proteins was visualized by gel electrophoresis and autoradiography. The radioligand binding data shown in A represents the mean ± SEM of three independent experiments. The autoradiographs shown in B and C are representative of three and four independent experiments, respectively.

purified, and used as affinity matrixes for the binding of the [^{35}S]RARγ LBD in standard GST-pulldown experiments, as we previously described.[70] TTAB strongly

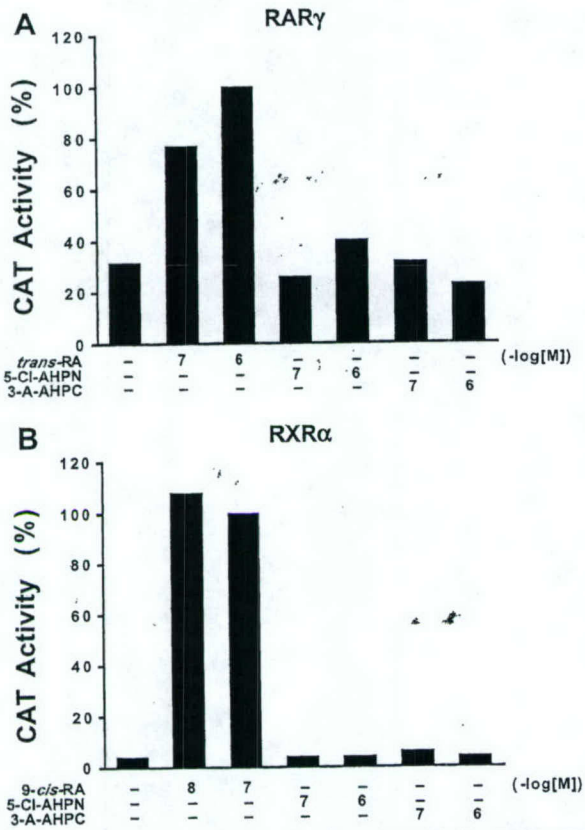

Figure 5. Transcriptional activation of RARγ by 5-Cl-AHPN (**2**) and 3-A-AHPC (**10**) compared to *trans*-RA (**4**) and that of RXRα compared to 9-*cis*-RA (**5**) on the $(TREpal)_2$-*tk*-CAT reporter in transfected CV-1 cells. Cells were treated with 1.0×10^{-7} M or 1.0×10^{-6} M 5-Cl-AHPC, 3-A-AHPC or *trans*-RA; or 1.0×10^{-8} M or 1.0×10^{-7} M 9-*cis*-RA. Reporter gene activity was normalized to that of cotransfected β-galactosidase gene activity and expressed relative to that of 1.0×10^{-6} M *trans*-RA on RARγ or 1.0×10^{-7} M 9-*cis*-RA on RXRα as 100% as described in Methods. See Experimental Section for methodology.

induced both the dissociation of GST-NCoR from [^{35}S]RARγ (compare lanes 1 and 2 in Figure 4C) and the binding of GST-p300 to [^{35}S]RARγ (compare lanes 5 and 6). In sharp contrast, 3-Cl-AHPC neither induced the dissociation of GST-NCoR from the [^{35}S]RARγ LBD (compare lanes 1 and 3) nor the binding of GST-p300 to [^{35}S]RARγ (compare lanes 5 and 7). These findings indicate that, although 3-Cl-AHPC bound to RARγ and enhanced its proteolytic stability, the type of RARγ LBD conformational change caused by 3-Cl-AHPC was not sufficient to induce either NCoR dissociation or p300 recruitment. In this respect, the behavioral profile of 3-Cl-AHPC resembled that observed for 2-(5′,6′,7′,8′-tetrahydro-5′,5′,8′,8′-tetramethyl-2′-naphthalenyl)-2-(6′-carboxy-2′-naphthalenyl)-1,3-dithiolane (**22**), which we previously characterized as an RARγ-selective retinoid that effectively antagonized the transactivation of RARγ by such agonists as *trans*-RA (**4**).[70] Subsequently, we found that the lack of RAR transcriptional agonist activity in 3-Cl-AHPC was supported by the results of reporter assays in CV-1 cells transfected with the $(TREpal)_2$-*tk*-CAT construct and a vector for RARα, β, or γ or RXRα. 3-Cl-APHC at 1.0×10^{-7} M and 1.0×10^{-6} M was transcriptionally inactive (data not shown). Similarly, both 5-Cl-AHPN (**2**) and 3-A-AHPC (**10**) at the same concentrations were unable to effectively

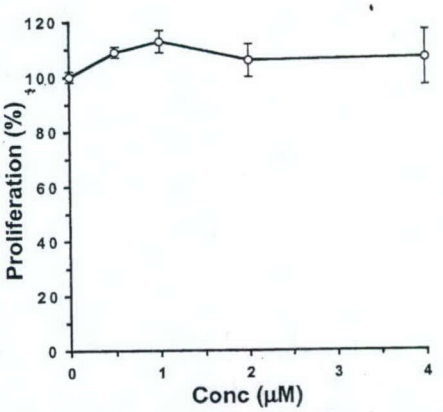

Figure 6. 3-A-AHPC (**10**) does not block 3-Cl-AHPC (**9**)-mediated inhibition of MDA-MB-468 breast cancer cell proliferation. Cells (1.0×10^6) were incubated for 24 h before the indicated concentrations of 3-A-AHPC were added. After 2 h, 0.5×10^{-6} M 3-Cl-AHPC was added, and incubation was continued for 72 h. Cells were then harvested, and proliferation in the presence of 3-A-AHPC and 3-Cl-AHPC was assessed using a colorimetric assay (see Experimental Section) and expressed relative to that of the 3-Cl-AHPC alone-treated control.

activate RARγ and RXRα (Figure 5 panels A and B, respectively).

As cancers progress to more aggressive phenotypes, the regulatory controls that hormones and retinoids exert on their proliferation can be lost. For example, unlike the MCF-7 breast cancer cell line, the growth of MDA-MB-231 and MDA-MB-468 breast cancer cell lines is neither regulated by estrogen[72] nor inhibited by standard retinoids.[2,34] Thus, the latter two cancer cell lines represent more aggressive tumors and have been used to evaluate compounds for apoptotic activity that would not be mediated by retinoid-signaling pathways. In addition, both cell lines lack functional p53,[2,72] a tumor suppressor protein involved in regulating the G_1-checkpoint of the cell cycle. p53 has been found to induce cell-cycle arrest in part through its induction of the expression of cell-cycle inhibitor $p21^{WAF1/CIP1}$, thereby permitting a cell to undergo repair in response to a stress event or to commit apoptosis. The induction of $p21^{WAF1/CIP1}$ that is independent of p53 status[73] is therapeutically advantageous because in approximately 50% of tumor samples, including those from breast cancer patients, p53 is absent or present as a nonfunctional mutant.[72,74,75] In the MDA-MB-231 and MDA-MB-468 breast cancer cell lines, AHPN (**1**)[2] and 3-Cl-AHPC (**9**) were found to induce cell-cycle arrest in G_0/G_1 through their posttranscriptional stabilization of $p21^{WAF1/CIP1}$ message and protein,[3] followed by apoptosis.[2,3]

In both breast cancer cell lines, the antagonist 3-A-AHPC (**10**) alone had no effects on cell-cycle arrest and apoptosis induction, whereas both processes were readily induced by AHPN (**1**) and its apoptotic analogues such as 5-Cl-AHPN (**2**) and 3-Cl-AHPC (**9**). Even at a concentration as high as 4.0×10^{-6} M, 3-A-AHPC after 48 or 72 h had only a minimal effect on the MDA-MB-468 cell cycle as determined by counting cell numbers (data not shown). Moreover, 3-A-AHPC at an 8-fold higher concentration was not able to block the ability of 0.5×10^{-6} M 3-Cl-AHPC to inhibit MDA-MB-468 cell proliferation (Figure 6), as evidenced by its inability to

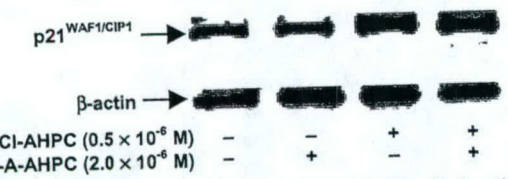

igure 7. 3-A-AHPC (**10**) does not block the induction of $21^{WAF1/CIP1}$ by 3-Cl-AHPC (**9**) in MDA-MB-468 breast cancer ells. Cells were grown in the presence or absence of 0.5×0^{-6} M 3-Cl-AHPC or 2.0×10^{-6} M 3-A-AHPC for 72 h, then arvested. Western blots using anti-$p21^{WAF1/CIP1}$ antibody were erformed[3] (see experimental methods). β-Actin was used as he loading control.

ıalt cell-cycle arrest. Next, we examined the effect of -A-AHPC on the abilities of AHPN and 3-Cl-AHPC to nduce the expression of $p21^{WAF1/CIP1}$ protein in MDA-ΛB-468 cells (Figure 7). Alone, 3-A-AHPC had no letectable effect on $p21^{WAF1/CIP1}$ protein levels and did ıot block the induction of $p21^{WAF1/CIP1}$ by 3-Cl-AHPC Figure 7). However, 3-A-AHPC markedly inhibited ΛDA-MB-468 cell apoptosis induced by 3-Cl-AHPC or AHPN (Figure 8A). Antagonist 3-A-AHPC also inhibited ıpoptosis induced by AHPN in retinoid-resistant HL-30R leukemia cells (Figure 8B) and MDA-MB-231 breast cancer cells (Figure 8C). Even after 72 h, 3-A-AHPC alone had no apoptotic activity in HL-60R cells and had only about 6% of the apoptotic activity of AHPN against MDA-MB-231 cells, a level which we have found was within background limits in these cells. These results substantiate our earlier findings that AHPN and its analogues function through two signaling pathways in cancer cells—cell-cycle arrest and apoptosis,[2,10,73,76,77] of which only apoptosis is inhibited by the antagonist 3-A-AHPC.

We also evaluated the effects of 5-Cl-AHPN (**2**), 3-Cl-AHPC (**9**), and 3-A-AHPC (**10**) on H460 lung cancer and LNCaP prostate cancer cell lines, both of which are retinoid-sensitive and express wild-type p53 (Figure 9). 5-Cl-AHPN at 1.0×10^{-6} M induced their apoptosis at 36 h, which was partially suppressed (34% to 9%, and 31% to 15%, respectively) by an equal concentration of antagonist 3-A-AHPC, as is indicated by staining for nuclear fragmentation (Figure 9A). A 5-fold excess of 3-A-AHPC was able to decrease 1.0×10^{-6} M 3-Cl-AHPC-induced apoptosis in H460 cells from 77% to 5% (Figure 9B). AHPN (**1**), 5-Cl-AHPN, and 3-Cl-AHPC at 1.0×10^{-6} M were comparably effective at inducing

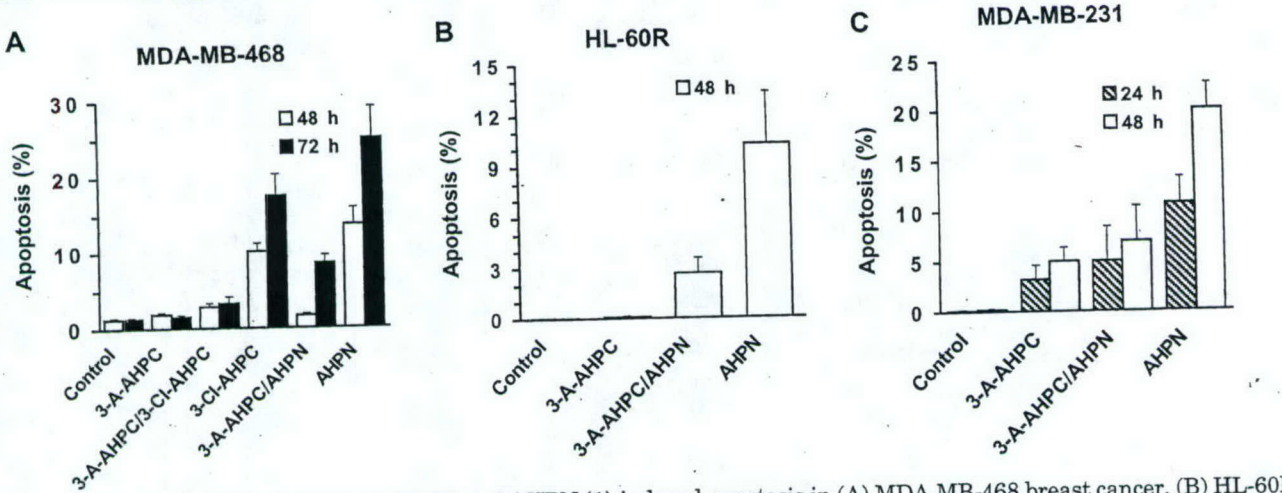

Figure 8. 3-A-AHPC (**10**) blocks 3-Cl-AHPC (**9**) and AHPN (**1**)-induced apoptosis in (A) MDA-MB-468 breast cancer, (B) HL-60R leukemia, and (C) MDA-MB-231 breast cancer cell lines. Cells were grown in the presence or absence of 0.5×10^{-6} M 3-Cl-AHPC or 0.5×10^{-6} M AHPN alone, with or without added 2.0×10^{-6} M 3-A-AHPC. Cells were harvested at 24, 48, or 72 h and acridine orange-stained.[3] Apoptotic cell numbers were determined (see methods).

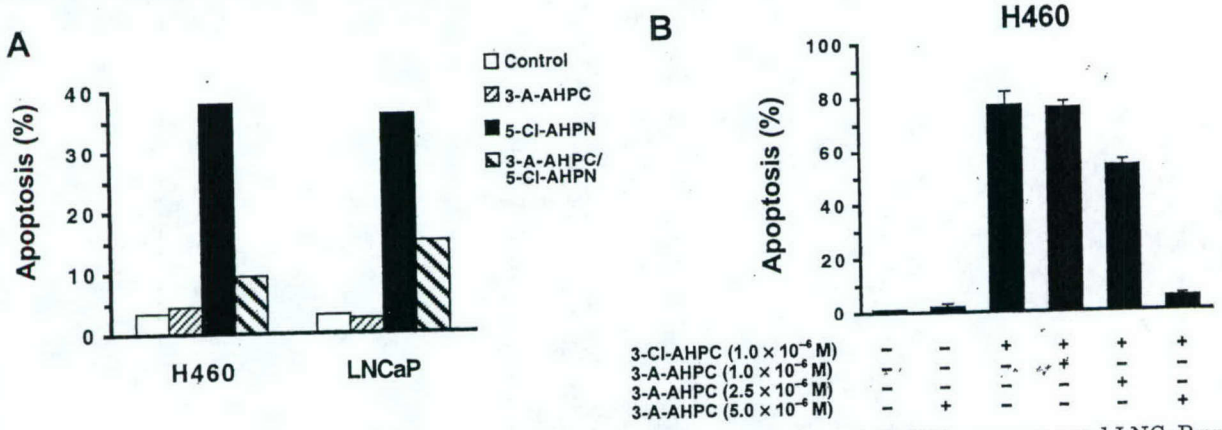

Figure 9. 3-A-AHPC (**10**) inhibits cancer cell apoptosis induced by AHPN analogues. A. H460 lung cancer and LNCaP prostate cancer cells were treated for 36 h with 1.0×10^{-6} 5-Cl-AHPN (**2**) or 1.0×10^{-6} M 3-A-AHPC alone or combined, then DAPI-stained (see methods) for visualization of nuclear morphology by fluorescence microscopy. Apoptosis levels were determined in 200-cell samples in three different fields. B. H460 cells were treated with 3-Cl-AHPC (**9**) (1.0×10^{-6} M) alone or combined with 3-A-AHPC (1.0×10^{-6} M, 2.5×10^{-6} M, or 5.0×10^{-6} M) or 3-A-AHPC (5.0×10^{-6}) alone or vehicle alone for 36 h, then DAPI-stained (see methods) and examined as in A to determine apoptosis.

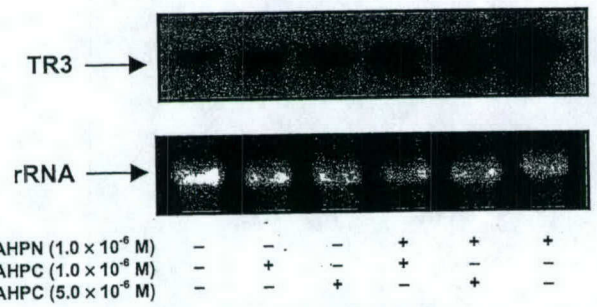

Figure 10. 3-A-AHPC (**10**) inhibits TR3 mRNA expression induced by 5-Cl-AHPN (**2**) in H460 lung cancer cells. Cells were treated for 4 h with 5-Cl-AHPN (1.0×10^{-6} M) or 3-A-AHPC (1.0×10^{-6} or 5.0×10^{-6} M) alone or combined. Total mRNAs were prepared and analyzed for TR3 expression by Northern blotting (see methods). Ethidium bromide-stained ribosomal RNA was used as the loading control.

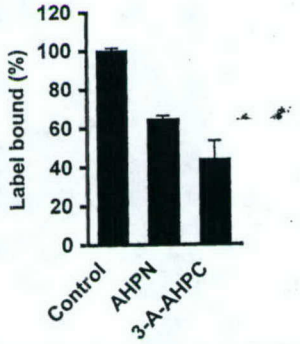

Figure 11. 3-A-AHPC (**10**) inhibits [5,5′-$^3H_2$]AHPN binding to the AHPN receptor. Nuclear extracts were prepared from HL-60R cells as we described.[4] [$^3H_2$]AHPN (1.0×10^{-8} M, 150 000 dpm) was added to the nuclear extracts in the presence or absence of nonlabeled AHPN (**1**) or 3-A-AHPC (2.0×10^{-5} M) or vehicle alone. Binding was assessed as described in the methods.

apoptosis in retinoid-resistant, p53-deficient H292 human lung cancer cells after a 40-h treatment (data not shown). Thus, the apoptotic activity found for these compounds in retinoid-refractory, p53-nonfunctional breast cancer cells extended to similarly deficient lung cancer cells, in addition to retinoid-sensitive breast, lung, and prostate cancer cells.

Earlier, we established[10] a novel pathway by which prostate and lung cancer cells underwent apoptosis induced by AHPN (**1**) and its apoptotic analogues, namely induction of the expression of the nuclear transcription factor TR3 followed by its translocation from the nucleus to the mitochondrial membrane. The association between TR3 and mitochondria was followed by mitochondrial outer membrane permeabilization and the release of mitochondrial cytochrome *c* into the cytosol,[15,78] leading to caspase activation and apoptosis.[79] As indicated in Figure 10, antagonist 3-A-AHPC (**10**) alone had no effect on the expression of TR3 mRNA in H460 cells but was able to inhibit the induction of TR3 expression by 5-Cl-AHPN (**2**).

By using binding assays and Scatchard analysis, we previously demonstrated that [5,5′-$^3H_2$]AHPN, which we had synthesized,[4] bound to a novel protein(s) contained in both HL-60R and MDA-MB-231 cell nuclear extracts.[4] Our results strongly suggested that this protein was not an RAR or RXR subtype because the RAR/RXR panagonist [10,11-$^3H_2$]9-*cis*-RA was not able to effectively compete with AHPN (**1**) for binding, and 9-*cis*-RA (**5**) did not effectively displace bound [5,5′-$^3H_2$]AHPN.[4] We next examined whether 3-A-AHPC (**10**) could inhibit the binding of [5,5′-$^3H_2$]AHPN to HL-60R nuclear extracts. As shown in Figure 11, 3-A-AHPC had efficacy similar to that shown by AHPN in displacing the tritiated label. Similar results were observed using 3-Cl-AHPC (**9**) (data not shown). Thus, 3-A-AHPC is capable of interacting with the same protein as apoptotic AHPN and 3-Cl-AHPC.

Discussion

While the configurations derived from dynamics in model simulations of AHPN (**1**) and 5-Cl-AHPN (**2**) docked in the RARγ LBP[65] could not be characterized as "holo" (bound) or "apo" (nonbound) in character, they did suggest to us that dramatic differences in local dynamics affected the recognition of a coactivator or corepressor protein by the receptor−ligand complex. Our computational results also suggested that small changes in the nature of substituents ortho to the diaryl bond in AHPN and its analogues impacted the positions of their 1-Ad groups relative to their polar termini (Figure 2A). Thus, in contrast to hydrogen and methyl groups, chloro groups significantly affected the inter-aromatic ring torsional potential surfaces so that they, in turn, altered the positions and dynamics of the 3′-(1-Ad) groups. In contrast, the carboxylate groups in these compounds remained anchored to the RARγ LBD helix H5 arginine-278.

DFT energy-minimized configurations of AHPN (**1**), 5-Cl-AHPN (**2**), 3-Cl-AHPC (**9**), 3-A-AHPC (**10**), and AHPC (**11**) are shown in Figure 2A. Our docking studies suggested that (i) 5-Cl-AHPN as initially docked was tightly packed into the LBP with close contacts to RARγ helix H12 residues; (ii) a chloro group ortho to the diaryl bond in an AHPN analogue produced a larger twist angle between the aryl rings than did an ortho hydrogen or methyl group; and (iii) the larger angle caused the 3′-(1-Ad) group to more frequently occupy positions that resulted in unfavorable interactions with the RARγ LBD helix H12. These in silico results suggested that both the position of the 3′-(1-Ad) group and the effective compound width were significantly affected by the identity of the substituent ortho to the diaryl bond on an AHPN or AHPC scaffold, which, in turn, influenced the dynamics of regions in the RAR LBD that were responsible for transcriptional response recognition.

Our experimental results supported the molecular dynamics results. Earlier, we observed that transcriptional agonist binding to the RARγ LBD produced a more compact tertiary structure that was more resistant to limited proteolytic digestion than that of the apo-receptor,[5] whereas binding by an antagonist produced a more open configuration that was more sensitive to proteolysis. The chloro group ortho to the AHPN diaryl bond reduced the ability of the AHPN analogue 3-Cl-AHPC (**9**) to interact with the RARγ LBD in terms of both its binding affinity to RARγ and the proteolytic stability of the resulting complex (Figure 4) compared to that formed by a standard retinoid agonist such as 9-*cis*-RA (**5**). Although the same peptide fragments were produced from both complexes, those from the 3-Cl-AHPC-containing complex were found to be less stable.

This result suggested that the peptides had different tertiary structures despite their originating from the cleavage of the same lysine-451 amide bond in the C-terminus of RARγ (domain F). Evidently, the subtle differences in the positions of the RARγ domain E helix H12 that occurred on binding these ligands, which were suggested by our molecular dynamics studies, did not sufficiently impact the tertiary structure of domain F so as to affect the enzymatic cleavage point but apparently made a less dramatic impact. The affinity of 3-Cl-AHPC (**9**) for the RARγ LBD was apparently lower than that of 9-*cis*-RA because a higher concentration of 3-Cl-AHPC was required to produce the same level of proteolysis obtained using 9-*cis*-RA. Moreover, 3-Cl-AHPC was not able to induce the dissociation of co-repressor NCoR from the RARγ LBD or the recruitment of coactivator p300. Thus, subtle differences in the ortho substituent were able to control the degree of retinoid agonist character of the AHPNs bound in the RAR LBP, as was also evidenced by the contrasting impacts of the ortho methyl and chloro groups on RARγ transcriptional activation as reported by Dawson et al.[57] and shown in Figure 4, respectively, despite their similar sizes. Short time-scale dynamics studies (Figure 3, panels C and D) suggested that the configuration of helix H12 in RARγ bound to 5-Cl-AHPN (**2**) was less compact and produced the larger fluctuations more characteristic of those found in the apo-RARγ LBD than that of H12 in the RARγ LBD−AHPN (**1**) complex. The effect of the 3-(3′-acetamidopropoxy) group of 3-A-AHPC on the inter-ring torsion angle was even more pronounced (Figure 2, panels A and B), as was its impact on the local fluctuations of residues near and on helix H12 (Figure 3, panels E and F). Thus, these computational results provide a distinct structure−activity linkage for our substituted AHPN/AHPC analogues that may be harnessed to hamper the formation of the binding site for RAR transcriptional coactivators and minimize RAR-related toxic adverse effects while retaining apoptotic activity.

In addition to their apoptotic activity in breast cancer,[2,3,80−82] lung cancer,[5,77,83−86] and leukemia cell lines,[4,5,39,40,87−89] AHPN (**1**) and its analogues inhibited the growth and/or induced the apoptosis of other cancer cell lines, including those derived from cervical,[90] esophageal,[91] lymphoma,[92] melanoma,[93,94] neuroblastoma,[95] ovarian,[9,96−98] and prostate cancers.[10,99−101] AHPN-induced apoptosis in breast cancer cells was preceded by the expression of the cyclin kinase inhibitor $p21^{WAF1/CIP1}$ and G_0/G_1 cell-cycle arrest and was independent of the functional status of p53,[2,3] which has been found to be mutated or lost in approximately half of all tumors.[74,75] Thus, AHPN represents an important progenitor for identifying more effective agents that induce cancer cell apoptosis. This therapeutic strategy is supported by a recent finding by the Lotan group that lung cancer cells were far more sensitive to AHPN than the normal cells from which they originated[86] and our own promising in vivo findings using 3-Cl-AHPC (**9**) in a murine acute myelogenous leukemia model.[39,40]

We found that 3-A-AHPC (**10**) inhibited the induction of apoptosis by AHPN (**1**) and 3-Cl-AHPC (**9**) and the binding of both to the putative AHPN receptor in HL-60R and MDA-MB-231 nuclear extracts. The expression of TR3,[10,16,77,98] which has an essential role in the apoptosis-signaling pathway induced by AHPN analogues, was also inhibited by 3-A-AHPC. However, 3-A-AHPC did not suppress AHPN or 3-Cl-AHPC-induced $p21^{WAF1/CIP1}$ protein expression and cell-cycle arrest. These results suggest to us that the inhibition of cell proliferation, as measured by the blockade of cell-cycle progression, and the induction of apoptosis, as measured by cell morphological changes, that are induced by active members of the AHPN family represent two separate events or perhaps even separate signaling pathways. Other evidence supporting our premise of dual pathways exists in reports of cancer cell line mutants in which only one of these AHPN-sensitive pathways operates.[98,102]

The identification of an antagonist of AHPN-induced apoptosis, 3-A-AHPC (**10**), that is structurally and configurationally similar to the apoptotic analogues 5-Cl-AHPN (**2**) and 3-Cl-AHPC (**9**) strongly suggests that several earlier hypotheses on the mechanism by which AHPN initiates apoptosis may not be valid. First, because both the inducers and the inhibitor of apoptosis have similarly situated phenolic hydroxyl groups, the premise that AHPN-induced apoptosis occurs solely as the result of nonspecific free-radical generation[103,104] appears unlikely. Nonspecific mitochondrial membrane permeabilization has also been postulated as an AHPN signaling pathway.[105,106] Our findings that 3-A-AHPC blocks both 5-Cl-AHPN-induced apoptosis and TR3 expression are strong evidence that the apoptosis-initiating event probably occurs upstream of any direct effects on the mitochondrial membrane. With 3-A-AHPC available, we now have an excellent opportunity to dissect these separate AHPN-signaling pathways: (i) the 3-A-AHPC-independent suppression of cell proliferation by the induction of cell-cycle arrest; and (ii) the induction of TR3-mediated apoptosis, which is blocked by 3-A-AHPC.

Experimental Section

Chemistry. General. Starting materials were obtained from commercial sources. Unless otherwise mentioned, during workup procedures organic layers were washed with water and sat. brine, dried (anhydrous Na_2SO_4), filtered, and concentrated at reduced pressure. Standard column chromatography employed silica gel (Merck 60) as did flash chromatography (Merck, grade 9385, 230−400 mesh). Experimental procedures were not optimized and were typically conducted only twice. Melting point temperatures were determined in capillary tubes using a Mel-Temp II apparatus and are uncorrected. Fourier transform IR spectra were obtained on powdered samples, unless otherwise specified, using an FT-IR Mason satellite infrared spectrophotometer. ^{1}H NMR spectra were recorded on a 300-MHz Varian Unity Inova spectrometer unless otherwise indicated, whereas 400 MHz spectra were recorded on a Bruker instrument. Shift values are expressed in ppm (δ) relative to Me_4Si as the internal standard. Unless otherwise mentioned, spectra were run on compounds dissolved in $^2HCCl_3$. MALDI−FAB mass spectra were obtained by using an Applied Biosystems Voyager De-Pro MALDI-TOF instrument at the Institute, and MALDI−FTMS high-resolution mass spectra on an IonSpec Ultima instrument at The Scripps Research Institute (La Jolla, CA).

Ethyl 4-Bromo-3-hydroxybenzoate (25). According to a reported procedure,[107] $MeSO_3H$ (2.0 mL) was added to **23** (5.0 g, 0.036 mol) in EtOH (10 mL) and benzene (100 mL). The reaction mixture was heated at reflux (10 h, Dean−Stark trap), cooled, washed (water, 5% $NaHCO_3$, and sat. brine), dried, and

concentrated to a solid, which was chromatographed (10% EtOAc/hexane) to give ethyl ester **24** (5.65 g, 94%) as a white powder, mp 71−73 °C, which was used without further purification.

A reported procedure for 4-bromo-3-hydroxybenzoic acid[108] was modified to substantially improve the yield of **25**. To a stirred solution of **24** (332 mg, 2.0 mmol) in glacial HOAc (2.0 mL) was slowly added Br_2 (320 mg, 2 mmol) in HOAc (1.0 mL) with stirring at room temperature. After stirring for 6 h, additional Br_2 (90 mg, 0.56 mmol) in HOAc (0.3 mL) was added, and stirring was continued (14 h). Ether (50 mL) was added, and the organic layer was washed (water, 5% $NaHCO_3$, and sat. brine), dried, and concentrated to an oil. Chromatography (8% EtOAc/8% CH_2Cl_2/hexane) gave **25** as a white powder (260 mg, 53%), mp 90→92 °C. TLC (17% EtOAc/hexanes) R_f 0.47. FT-IR ($CHCl_3$) 3388, 1695, cm^{-1}. ^1H NMR δ 1.39 (t, J = 7.2 Hz, 3H, CH_3), 4.37 (q, J = 7.2 Hz, 2H, OCH_2), 5.75 (s, 1H, OH), 7.48 (d, J = 8.1 Hz, 1H, 6-ArH), 7.55 (d, J = 8.1 Hz, 1H, 5-ArH), 7.68 ppm (s, 1H, 2-ArH).

Ethyl 4-Bromo-3-benzyloxybenzoate (26). To a suspension of **25** (4.5 g, 18.4 mmol) and K_2CO_3 (4.1 g, 30 mmol) in acetone (150 mL) under Ar was added benzyl bromide (3.4 g, 20 mmol). The mixture was heated at reflux for 15 h, concentrated, then diluted with CH_2Cl_2 (100 mL), washed (water, 1 N HCl, and brine), and dried. Concentration and chromatography (5% EtOAc/hexane) afforded 5.2 g (84%) of **26** as a white powder, mp 50−52 °C. TLC (20% CH_2Cl_2/hexane) R_f 0.35. FT-IR ($CHCl_3$) 1722 cm^{-1}. ^1H NMR δ 1.39 (t, J = 7.2 Hz, 3H, CH_3), 4.37 (q, J = 7.2 Hz, 2H, OCH_2), 5.21 (s, 2H, OCH_2Ph), 7.39 (m, 3H, ArH), 7.50 (m, 3H, ArH), 7.63 ppm (m, 2H, ArH). MALDI−FTMS (HRMS) calcd $C_{16}H_{15}BrNaO_3$ [MNa^+] 357.0097, found 357.0093.

4-Bromo-3-benzyloxybenzyl Alcohol (27). To **26** (3.35 g, 10 mmol) dissolved in CH_2Cl_2 (25 mL) and cooled under Ar in a dry ice−acetone bath was slowly added 20 mL of 1.0 M DIBAL (20 mmol) in hexanes with stirring. After 2 h, the stirred reaction mixture was diluted with 1 N HCl (20 mL) and CH_2Cl_2 (50 mL), and stirring was continued for 0.5 h. The organic layer was washed and dried. Concentration and chromatography (9% EtOAc/hexane) afforded 2.78 g (91%) of **27** as a white solid, mp 73−75 °C. TLC (9% EtOAc/hexane) R_f 0.17. FT-IR (powder) 3383 cm^{-1}. ^1H NMR δ 4.63 (d, J = 5.7 Hz, 2H, $ArCH_2O$), 5.16 (s, 2H, OCH_2Ph), 6.83 (d, J = 8.1 Hz, 1H, 6-ArH), 7.00 (s, 1H, 2-ArH), 7.33−7.54 (m, 5H, ArH), 7.53 ppm (d, 1H, 5-ArH). MALDI−FTMS (HRMS) calcd $C_{14}H_{13}BrNaO_2$ [MNa^+] 314.9991, found 314.9998.

Ethyl (*E*)-4-Bromo-3-benzyloxycinnamate (29). To a stirred solution of **27** (2.77 g, 10 mmol) in CH_2Cl_2 (30 mL) cooled in an ice bath was slowly added PCC (3.23 g, 15 mmol). This mixture was stirred for 5 h at room temperature before Et_2O (50 mL) was added. Filtration and concentration gave the 3-benzyloxy-4-bromobenzaldehyde (**28**) as a white powder, which was used in the next step without further purification.

To triethyl phosphonoacetate (0.33 g, 1.5 mmol) dissolved in anhydrous Et_2O (10 mL) then cooled in a dry ice−acetone bath was added 1.5 mL of 0.91 M $KN(SiMe_3)_2$ (1.35 mmol) in THF under Ar with stirring, which was continued for 0.5 h. Next, **28** (0.24 g, 0.83 mmol) in Et_2O (10 mL) was slowly added to the solution with cooling in the dry ice−acetone bath. After stirring for 1 h more, the mixture was allowed to warm to ambient temperature, stirred overnight, poured into water (50 mL) containing HOAc (1.0 mL), and extracted into Et_2O (20 mL). The extract was washed, dried, and concentrated. Chromatography (5% EtOAc/hexane) of the residue afforded 0.28 g (91%) of **29** as a white solid, mp 45−48 °C. TLC (9% EtOAc/hexane) R_f 0.67. FT-IR ($CHCl_3$) 1711, 1640 cm^{-1}. ^1H NMR δ 1.33 (t, J = 7.2 Hz, 3H, CH_3), 4.26 (q, J = 6.9 Hz, 2H, CH_2), 5.18 (s, 2H, CH_2Ph), 6.39 (d, J = 15.9 Hz, 1H, ArCH=C), 7.01 (d, J = 8.4 Hz, 1H, 6-ArH), 7.06 (s, 1H, 2-ArH), 7.33−7.50 (m, 5H, ArH), 7.57 (d, J = 8.4 Hz, 1H, 5-ArH), 7.58 ppm (d, J = 15.9 Hz, 1H, C=$CHCO_2$). MALDI−FTMS (HRMS) calcd $C_{18}H_{18}BrO_3$ [MH^+] 361.0434, found 361.0437.

Ethyl (*E*)-4-Bromo-3-hydroxycinnamate (30). A solution of **29** (260 mg, 0.72 mmol) in CH_2Cl_2 (5 mL) and 1.0 M BBr_3 (1.5 mmol) in CH_2Cl_2 (1.5 mL) was stirred at −78 °C under Ar for 2 h, then diluted with water (10 mL) and CH_2Cl_2 (20 mL). The organic phase was washed, dried, and concentrated. Flash chromatography (10% EtOAc/hexane) gave **30** as a white powder (180 mg, 92%), mp 135−137 °C. TLC (9% EtOAc/hexanes) R_f 0.25. FT-IR ($CHCl_3$) 3328, 1678 cm^{-1}. ^1H NMR δ 1.34 (t, J = 6.9 Hz, 3H, CH_3), 4.27 (q, J = 7.2 Hz, 2H, OCH_2), 5.62 (s, 1H, OH), 6.42 (d, J = 15.9 Hz, 1H, ArCH=C), 6.98 (d, J = 8.4 Hz, 1H, 6-ArH), 7.18 (s, 1H, 2-ArH), 7.48 (d, J = 8.1 Hz, 1H, 5-ArH), 7.58 ppm (d, J = 15.9 Hz, 1H, C=$CHCO_2$). MALDI−FTMS (HRMS) calcd $C_{11}H_{12}BrO_3$ [MH^+] 270.9970, found 270.9971.

Ethyl (*E*)-4-Bromo-3-(3′-*tert*-butoxycarboxamidopropoxy)cinnamate (31). A suspension of **30** (320 mg, 1.18 mmol) and K_2CO_3 (500 mg, 3.62 mmol) in acetone (50 mL) containing 3-(*tert*-butoxycarboxamido)propyl bromide (**33**) (480 mg, 1.98 mmol) was heated at reflux under Ar for 20 h, then concentrated. The residue was extracted with CH_2Cl_2, and the extract was washed (water, 1 N HCl, and brine) and dried. Concentration and chromatography (10% EtOAc/hexane) of the residue afforded 410 mg (81%) of **31** as a white powder, mp 65−67 °C. TLC (17% EtOAc/hexane) R_f 0.30. FT-IR 3425, 2980, 1706 cm^{-1}. ^1H NMR δ 1.34 (t, J = 7.2 Hz, 3H, CH_3), 1.44 (s, 9H, $OC(CH_3)_3$), 2.07 (t, J = 6.0 Hz, 2H, 2′-CH_2), 3.40 (q, J = 5.7 Hz, 2H, 3′-CH_2N), 4.13 (t, J = 5.7 Hz, 2H, 1′-CH_2O), 4.26 (q, J = 7.2 Hz, 2H, OCH_2), 5.22 (s, 1H, NH), 6.47 (d, J = 15.9 Hz, 1H, ArCH=C), 7.00 (s, 1H, 2-ArH), 7.01 (d, J = 6.3 Hz, 1H, 6-ArH), 7.54 (d, J = 8.7 Hz, 1H, 5-ArH), 7.60 ppm (d, J = 15.9 Hz, 1H, C=$CHCO_2$). MALDI−FTMS (HRMS) calcd $C_{19}H_{26}BrNNaO_5$ [MNa^+] 450.0886, found 450.0889.

3-Bromo-1-(*tert*-butoxycarbonyl)propylamine (33). A reported procedure was applied[109] to 3-bromopropylamine hydrobromide (**32**) (4.4 g, 20 mmol), Et_3N (3.0 mL, 20 mmol), and di-(*tert*-butyl)dicarbonate (5.5 g, 25 mmol) in CH_2Cl_2 (20 mL) to give after workup and chromatography (5% EtOAc/hexane) 3.95 g (83%) of **33** as a colorless liquid. TLC (17% EtOAc/hexane) R_f 0.61. FT-IR (film) 3399, 1678 cm^{-1}. ^1H NMR δ 1.45 (s, 9H, $OC(CH_3)_3$), 2.05 (m, 2H, 2-CH_2), 3.28 (q, J = 6.3 Hz, 2H, 1-CH_2N), 3.45 (t, J = 6.3 Hz, 2H, 3-CH_2Br), 4.66 ppm (s, 1H, NH).

Ethyl (*E*)-4-[3′-(1-Adamantyl)-4′-benzyloxyphenyl]-3-[(3′-*tert*-butoxycarboxamido)propoxy]cinnamate (38). To **31** (321 mg, 0.75 mmol), 3-(1-adamantyl)-4-benzyloxyphenylboronic acid[5] (**37**) (362 mg, 1.0 mmol), and $Pd(PPh_3)_4$ (60 mg, 0.052 mmol) in DME (5 mL) was added under Ar with stirring 2.0 M aq Na_2CO_3 (1.0 mL). The reaction mixture was heated at reflux for 20 h, cooled to room temperature, then extracted (EtOAc). The extract was washed, dried, and concentrated. Flash chromatography (EtOAc/hexane) of the residue gave **38** as a yellow powder (410 mg, 83%), mp 73−75 °C, which was used without further purification in the deprotection steps to give **10** and **14**. TLC (20% EtOAc/hexane) R_f 0.30. FT-IR 3366, 1711 cm^{-1}. ^1H NMR δ 1.35 (t, J = 6.9 Hz, 3H, CH_3), 1.43 (s, 9H, $OC(CH_3)_3$), 1.72 (s, 6H, $AdCH_2$), 1.95 (m, 2H, 2′-CH_2), 2.04 (s, 3H, AdCH), 2.17 (s, 6H, $AdCH_2$), 3.24 (d, J = 5.4 Hz, 2H, 3′-CH_2N), 4.03 (t, J = 5.7 Hz, 2H, 1′-CH_2O), 4.28 (q, J = 6.6 Hz, 2H, OCH_2), 4.55 (s, 1H, NH), 5.16 (s, 2H, OCH_2Ph), 6.45 (d, J = 15.9 Hz, 1H, ArCH=C), 7.00 (d, J = 8.7 Hz, 1H, 5′-ArH), 7.11 (s, 1H, 2-ArH), 7.20 (d, J = 7.8 Hz, 1H, 6′-ArH), 7.34−7.45 (m, 5H, ArH), 7.51 (s, 1H, 2′-ArH), 7.53 (d, J = 7.2 Hz, 2H, 5,6-ArH), 7.68 ppm (d, J = 15.9 Hz, 1H, C=$CHCO_2$). MALDI−FAB calcd $C_{42}H_{52}NO_6$ [MH^+] 664.8, found 664.8.

Ethyl (*E*)-4-[3′-(1-Adamantyl)-4′-benzyloxyphenyl]-3-(3′-acetamidopropoxy)cinnamate (40). To a mixture of **38** (400 mg, 0.6 mmol) in EtOH (10 mL) was added concentrated HCl (1.0 mL). This mixture was heated at reflux for 1 h, then concentrated. The residue containing the primary amine **39** was sequentially treated with CH_2Cl_2 (20 mL), pyridine (1.0 mL), and Ac_2O (1.0 mL) and stirred overnight at room temperature before being washed, dried ($MgSO_4$), and concentrated. Flash chromatography (EtOAc/hexane) gave **40** as a white powder (280 mg, 77%), mp 80−82 °C. TLC (67% EtOAc/hexane) R_f 0.28. FT-IR 3293, 1716 cm^{-1}. ^1H NMR δ 1.35 (t, J = 7.2 Hz, 3H, CH_3), 1.45 (s, 2H, 2′-CH_2), 1.72 (s, 6H,

$AdCH_2$), 2.04 (s, 6H, AdCH and $COCH_3$), 2.15 (s, 6H, $AdCH_2$), 3.37 (q, J = 5.4 Hz, 2H, 3′-CH_2N), 4.12 (t, J = 5.1 Hz, 2H, 1′-CH_2O), 4.28 (q, J = 7.2 Hz, 2H, OCH_2), 5.15 (s, 2H, OCH_2Ph), 5.67 (s, 1H, NH), 6.45 (d, J = 16.2 Hz, 1H, ArCH=C), 7.00 (d, J = 7.8 Hz, 1H, 5′-ArH), 7.09 (s, 1H, 2′-ArH), 7.22 (d, J = 7.8 Hz, 1H, ArH), 7.26–7.42 (m, 5H, ArH), 7.45 (d, 1H, J = 6.9 Hz, 1H, ArH), 7.49 (s, 1H, 2-ArH), 7.50 (d, J = 8.1 Hz, 1H, ArH), 7.69 ppm (d, J = 16.2 Hz, 1H, C=$CHCO_2$). MALDI–FTMS (HRMS) calcd $C_{39}H_{45}NNaO_5$ (MNa^+) 630.3190, found 630.3172.

Ethyl (*E*)-4-[3′-(1-Adamantyl)-4′-hydroxyphenyl]-3-(3′-acetamidopropoxy)cinnamate (41). A solution of **40** (303 mg, 0.5 mmol) and 1.0 M BBr_3 (1.5 mmol) in CH_2Cl_2 (1.5 mL) and CH_2Cl_2 (5 mL) was stirred at −78 °C under Ar for 2 h, then diluted with water (10 mL) and CH_2Cl_2 (20 mL). The organic phase was washed, dried, and concentrated. Flash chromatography (EtOAc/hexane) gave **41** as an off-white powder (226 mg, 77%), mp 110–113 °C. TLC (67% EtOAc/hexane) R_f 0.20. FT-IR 3408, 1706, 1637 cm^{-1}. ^1H NMR δ 1.35 (t, J = 6.9 Hz, 3H, CH_3), 1.44 (s, 2H, 2′-CH_2), 1.77 (s, 6H, $AdCH_2$), 2.04 (s, 3H, AdCH). 2.08 (s, 3H, $COCH_3$), 2.14 (s, 6H, $AdCH_2$), 3.38 (q, J = 5.4 Hz, 2H, 3′-CH_2N), 4.13 (t, J = 6.3 Hz, 2H, 1′-CH_2O), 4.27 (q, J = 7.2 Hz, 2H, OCH_2), 5.81 (s, 1H, NH), 6.30 (s, 1H, OH), 6.44 (d, J = 15.9 Hz, 1H, ArCH=C), 6.75 (d, J = 8.1 Hz, 1H, 5′-ArH), 7.09 (s, 1H, 2′-ArH), 7.20 (d, J = 7.5 Hz, 1H, ArH), 7.26 (d, J = 8.1 Hz, 1H, ArH), 7.33 (d, J = 8.1 Hz, 1H, ArH), 7.40 (s, 1H, 2-ArH), 7.68 ppm (d, J = 15.9 Hz, 1H, C=$CHCO_2$). MALDI–TFMS (HRMS) calcd $C_{32}H_{40}NO_5$ (MH^+) 518.2906, found 518.2892.

(*E*)-4-[3′-(1-Adamantyl)-4′-hydroxyphenyl]-3-(3′-acetamidopropoxy)cinnamic Acid (10). To a suspension of **41** (190 mg, 0.387 mmol) in MeOH (10 mL) was added NaOH (100 mg, 2.5 mmol). The mixture was stirred at reflux temperature under Ar for 1 h, cooled to room temperature, acidified (1 N HCl), and extracted (EtOAc). The extract was washed, dried ($MgSO_4$), and concentrated to afford **10** as an off-white powder (170 mg, 94%), mp 195–199 °C. FT-IR (powder) 3400, 1691, 1632 cm^{-1}. ^1H NMR (DMSO-$^2H_6$) δ 1.73 (s, 6H, $AdCH_2$), 1.77 (s, 3H, $COCH_3$), 1.78 (m, 2H, 2′-CH_2), 2.03 (s, 3H, AdCH), 2.10 (s, 6H, $AdCH_2$), 3.17 (d, J = 5.4 Hz, 2H, 3′-CH_2N), 4.06 (broad s, 2H, 3′-CH_2O), 6.63 (d, J = 15.9 Hz, 1H, ArCH=C), 6.80 (d, J = 8.1 Hz, 1H, 5′-ArH), 7.21 (d, J = 8.7 Hz, 1H, ArH), 7.29 (s, 3H, ArH and 2′-ArH), 7.37 (s, 1H, 2-ArH), 7.61 (d, J = 15.9 Hz, 1H, C=$CHCO_2$), 7.86 (s, 1H, NH), 9.41 ppm (s, 1H, OH). MALDI–FTMS (HRMS) calcd $C_{30}H_{35}NNaO_5$ [MNa^+] 512.2407, found 512.2402.

Ethyl (*E*)-4-[3′-(1-Adamantyl)-4′-hydroxyphenyl]-3-(3′-aminopropoxy)cinnamate (43). A solution of **38** (500 mg, 0.75 mmol) and 1.0 M BBr_3 (1.5 mmol) in CH_2Cl_2 (1.5 mL) and CH_2Cl_2 (20 mL) was stirred at −78 °C under Ar for 2 h, then diluted with water (10 mL) and CH_2Cl_2 (20 mL). The organic phase was washed, dried, and concentrated to give ethyl (*E*)-4-[3′-(1-adamantyl)-4′-hydroxyphenyl]-3-(3′-*tert*-butoxycarboxamido)propoxycinnamate (**42**) as a pale-yellow solid. The solid in EtOH (20 mL) containing concentrated HCl (1.5 mL) was heated at reflux under Ar for 2 h. The solution was concentrated before dilution with MeOH (20 mL). $NaHCO_3$ (200 mg) was added, and this mixture was stirred for 1 h under Ar, then concentrated. Flash chromatography (9% MeOH/CH_2Cl_2) gave **43** as a white solid (278 mg, 78%), mp 181–183 °C. TLC (9% MeOH/CH_2Cl_2) R_f 0.62. FT-IR 3244, 1706, 1632 cm^{-1}. ^1H NMR δ 1.34 (t, J = 7.2 Hz, 3H, CH_3), 1.76 (s, 6H, $AdCH_2$), 1.94 (m, 2H, 2′-CH_2), 2.05 (s, 3H, AdCH), 2.15 (s, 6H, $AdCH_2$), 2.85 (m, 2H, 3′-CH_2N), 3.74 (s, 2H, NH_2), 4.09 (s, 2H, 3′-CH_2O), 4.28 (q, J = 7.5 Hz, 2H, OCH_2), 5.71 (s, 1H, OH), 6.43 (d, J = 15.9 Hz, 1H, ArCH=C), 6.62 (d, J = 7.8 Hz, 1H, 5′-ArH), 7.08 (s, 1H, 2-ArH), 7.17 (d, J = 7.2 Hz, 1H, ArH), 7.20 (d, J = 8.4 Hz, 1H, ArH), 7.30 (s, 1H, 2′-ArH), 7.32 (d, J = 7.5 Hz, 1H, ArH), 7.68 ppm (d, J = 15.9 Hz, 1H, C=$CHCO_2$). MALDI–FTMS (HRMS) calcd $C_{30}H_{38}NO_4$ [MH^+] 476.2795, found 476.2790.

(*E*)-4-[3′-(1-Adamantyl)-4′-hydroxyphenyl]-3-(3′-aminopropoxy)cinnamic Acid (14). To a suspension of **43** (260 mg, 0.547 mmol) in MeOH (10 mL) was added NaOH (100 mg, 2.5 mmol) in water (1.0 mL). The reaction mixture was stirred at reflux temperature under Ar for 1 h, cooled to room temperature, acidified (1 N HCl), and concentrated. The resultant solid was diluted with water (5 mL) and Et_2O (10 mL), then stirred for 1 h, filtered, and dried under vacuum to give **14** as an off-white powder (236 mg, 89%), mp 238–240 °C. FT-IR 3381, 1686 cm^{-1}. ^1H NMR (CD_3OD) δ 1.87 (s, 6H, $AdCH_2$), 2.11 (s, 3H, AdCH), 2.13 (m, 2H, 2′-CH_2), 2.24 (s, 6H, $AdCH_2$), 3.08 (t, J = 7.5 Hz, 2H, 3′-CH_2N), 4.20 (t, J = 6.0 Hz, 2H, 1′-CH_2O), 6.56 (d, J = 16.2 Hz, 1H, ArCH=C), 6.81 (d, J = 8.4 Hz, 1H, 5′-ArH), 7.23 (d, J = 8.4 Hz, 1H, 6′-ArH), 7.30 (d, J = 8.4 Hz, 2H, ArH), 7.33 (s, 2H, 2,2′-ArH), 7.73 ppm (d, J = 16.2 Hz, 1H, C=$CHCO_2$). MALDI–FTMS (HRMS) calcd $C_{28}H_{34}NO_4$ (MH^+) 448.2482, found 448.2488.

Ethyl 5-Chloro-6-hydroxy-2-naphthalenecarboxylate (46). A suspension of **44** (4.90 g, 26.0 mmol), in EtOH (25 mL) was treated with concentrated H_2SO_4 (1.0 g), stirred for 5 days, then heated at reflux for 1 h to complete esterification. After removal of EtOH at reduced pressure, the ethyl ester **45** was isolated by extraction (EtOAc), followed by washing (2 × 5% $NaHCO_3$ and sat. brine) and drying ($MgSO_4$). Concentration and crystallization afforded **45** (4.81 g, 85%), mp 109–110 °C. TLC (EtOAc) R_f 0.83. ^1H NMR (400 MHz) δ 1.47 (t, J = 7.0 Hz, 3H, CH_3), 4.47 (q, J = 7.0 Hz, 2H, CH_2), 6.13 (s, 1H, OH), 7.19 (dd, J = 8.8 Hz, J = 2.4 Hz, 1H, 7-NapH), 7.20 (s, 1H, 5-NapH), 7.70 (d, J = 8.5 Hz, 1H, 8-NapH), 7.87 (d, J = 8.3 Hz, 1H, 4-NapH), 8.01 (dd, J = 8.6 Hz, J = 1.8 Hz, 1H, 3-NapH), 8.54 ppm (d, J = 0.8 Hz, 1H, 1-NapH). Anal. ($C_{13}H_{12}O_3$) C, H. MALDI–FTMS (HRMS) calcd $C_{13}H_{13}O_3$ (MH^+) 217.0859, found 217.0861.

α-Chlorination of **45** was conducted by modifying a reported procedure.[59] To a solution of **45** (3.62 g, 16.7 mmol) in glacial HOAc (32 mL) was added sulfuryl chloride (2.27 g, 16.8 mmol). The mixture heated for 2.5 h at 70 °C, then stirred at room temperature for 36 h. Concentration, ice-bath cooling, and filtration afforded **46** as white crystals (2.60 g, 62%), mp 139–142 °C. TLC (20% EtOAc/benzene) R_f 0.61. ^1H NMR (400 MHz) δ 1.45 (t, J = 5.4 Hz, 3H, CH_3), 4.44 (q, J = 5.4 Hz, 2H, CH_2), 6.16 (s, 1H, OH), 7.32 (d, J = 8.8 Hz, 1H, 7-NapH), 7.82 (d, J = 8.8 Hz, 1H, 8-NapH), 8.07 (d, J = 8.8 Hz, 1H, 4-NapH), 8.15 (dd, J = 8.8 Hz, J = 1.6 Hz, 1H, 3-NapH), 8.54 ppm (s, 1H, 1-NapH). Anal. ($C_{13}H_{11}ClO_3$) C, H. MALDI–FTMS (HRMS) calcd $C_{13}H_{12}ClO_3$ (MH^+) 251.0469, found 251.0473.

Ethyl 6-[3′-(1-Adamantyl)-4′-benzyloxyphenyl]-5-chloro-2-naphthalenecarboxylate (48). To **46** (2.05 g, 8.18 mmol) and pyridine (2.0 mL, 25 mmol) dissolved in CH_2Cl_2 (55 mL) and cooled in an ice bath was added over a 5-min period trifluoromethanesulfonic anhydride (1.7 mL, 10.1 mmol). The reaction mixture was allowed to warm to room temperature, stirred for 18 h, washed (2 × H_2O, 10% HCl, and sat. brine), then dried ($MgSO_4$). Concentration afforded ethyl 5-chloro-6-trifluoromethanesulfonyloxy-2-naphthalenecarboxylate (**47**) as white crystals (2.43 g, 78%), mp 99–100 °C. TLC (25% EtOAc/hexane) R_f 0.80, which was used without further purification in the following step. ^1H NMR δ 1.47 (t, J = 6.9 Hz, 3H, CH_3), 4.47 (d, J = 6.8 Hz, 2H, CH_2), 7.52 (d, J = 8.9 Hz, 1H, 7-NapH), 7.97 (d, J = 9.0 Hz, 1H, 8-NapH), 8.27 (d, J = 8.7 Hz, 1H, 4-NapH), 8.37 (d, J = 8.8 Hz, 1H, 3-NapH), 8.64 ppm (s, 1H, 1-NapH).

To a solution of arylboronic acid **37** (500 mg, 1.38 mmol), triflate **47** (524 mg, 1.37 mmol), $Pd(PPh_3)_4$ (165 mg, 0.143 mmol), and LiCl (114 mg, 2.69 mmol) in dimethoxyethane (12 mL) under Ar was added 2.0 M aq Na_2CO_3 (1.4 mL). The reaction mixture was heated at reflux (18 h), diluted (EtOAc and sat. brine), and extracted (CH_2Cl_2). The organic extract was dried ($MgSO_4$) and concentrated. Flash chromatography (5% EtOAc/hexane) of the residue and concentration provided **48** as white crystals (420 mg, 56%), mp 177–179 °C. TLC (10% EtOAc/hexane) R_f 0.37. FT-IR (KBr) 1716 cm^{-1}. ^1H NMR (400 MHz) δ 1.47 (t, J = 6.0 Hz, 3H, CH_3), 1.74 (s, 6, $AdCH_2$), 2.05 (s, 3H, AdH), 2.20 (s, 6H, $AdCH_2$), 4.46 (q, J = 7.0 Hz, 2H, OCH_2), 5.20 (s, 2, $CHPh_2$), 7.06 (d, J = 8.8 Hz, 1H, 5-ArH), 7.3–7.4 (m, 2, ArH), 7.4–7.5 (m, 3, ArH), 7.5–7.6 (m, 3, ArH and 7-NapH), 7.90 (d, J = 8.0 Hz, 1H, 8-NapH), 8.20 (dd, J =

8.8 Hz, J = 1.6 Hz, 1H, 3-NapH), 8.44 (d, J = 8.8 Hz, 1H, 4-NapH), 8.62 ppm (d, J = 1.6 Hz, 1H, 1-NapH). MALDI–FTMS (HRMS) calcd $C_{36}H_{36}ClO_2$ (MH^+) 550.2275, found 550.2285.

Ethyl 6-[3′-(1-Adamantyl)-4′-hydroxyphenyl]-5-chloro-2-naphthalenecarboxylate (49). To **48** (170 mg, 0.31 mmol) dissolved in CH_2Cl_2 (30 mL) and cooled in a dry ice–EtOH bath was added 1.0 M BBr_3 (900 mmol) in CH_2Cl_2 (0.90 mL) over a 2-min period. After being stirred at this temperature for 1 h, the mixture was diluted with cold H_2O (10 mL) and allowed to warm to room temperature. The organic layer was separated, dried ($MgSO_4$), and concentrated to give **49** as white crystals (101 mg, 71%), mp 256–260 °C. TLC (toluene) R_f 0.26. ^1H NMR (300 MHz, $CDCl_3$) δ 1.47 (t, J = 7.0 Hz, 3H, CH_3), 1.80 (s, 6H, $AdCH_2$), 2.10 (s, 3H, AdCH), 2.18 (s, 6H, $AdCH_2$), 4.47 (q, J = 7 Hz, 2H, CH_2), 4.91 (s, 1H, OH), 5.30 (s, 2H, CH_2), 6.77 (d, J = 7.3 Hz, 1H, 5′-ArH), 7.38 (s, 1H, 2′-ArH), 7.54 (d, J = 8.1 Hz, 2H, 7-NapH and 6′-ArH), 7.90 (d, J = 9.6 Hz, 1H, 8-NapH), 8.19 (d, J = 9.0 Hz, 1H, 4-NapH), 8.44 (d, J = 9.0 Hz, 1H, 3-NapH), 8.62 ppm (s, 1H, 1-NapH). MALDI–FTMS (HRMS) calcd $C_{29}H_{30}ClO_2$ (MH^+) 460.1805, found 460.1798.

6-[3′-(1-Adamantyl)-4′-hydroxyphenyl]-5-chloro-2-naphthalenecarboxylic Acid (2). A suspension of **49** (230 mg, 0.50 mmol) in 1.0 M NaOH in 75% aq EtOH (5 mL) was heated at reflux for 40 min, cooled, acidified (10% HCl), then extracted (EtOAc). The extract was washed (sat. brine), dried ($MgSO_4$), and concentrated to give **2** as a white powder (205 mg, 95%), mp 282–284 °C (dec). TLC (5% MeOH/$CHCl_3$) R_f 0.26. FT-IR 2983, 1640 cm^{-1}. ^1H NMR (300 MHz, d_6-DMSO) δ 1.74 (s, 6H, $AdCH_2$), 2.05 (s, 3H, AdCH), 2.16 (s, 6H, $AdCH_2$), 6.91 (d, J = 8.1 Hz, 1H, 5′-ArH), 7.24 (d, J = 8.5 Hz, 1H, 6′-ArH), 7.27 (s, 1H, 2′-ArH), 7.62 (d, J = 8.4 Hz, 1H, 7-NapH), 8.16 (d, J = 8.5 Hz, 2H, 4,8-NapH), 8.37 (d, J = 9.1 Hz, 1H, 3-NapH), 8.68 (s, 1H, 1-NapH), 9.62 ppm (s, 1H, OH). MALDI–FTMS (HRMS) calcd $C_{27}H_{26}ClO_2$ (MH^+) 432.1492, found 432.1502.

Computational Studies. Generation of an RARγ LBD Model for Docking and Simulations. An all-H representation of the RARγ LBD was generated using the XLEAP module of AMBER6[110] and the 9-*cis*-RA (**5**)-bound holo-RARγ LBD crystal structure[65] (PDB entry 3LBD). The initial all-atom model was energy-minimized with a small number of steps (100 steepest descents plus 1900 conjugate-gradient) to remove large initial repulsions in atomic positions as evaluated by the AMBER force-field compared to crystal structure contacts.

Short molecular dynamics (MD) equilibration of the model at constant temperature was performed to provide additional structure relaxation and establish reasonable hydrogen-bonding patterns in the vicinity of the LBP. The model was equilibrated at 300 K with decreasing harmonic constraints over a 20-ps time interval using a 1-femtosecond integration time-step followed by a 70-ps unconstrained equilibration. All bonds involving hydrogens were constrained using SHAKE.[111] The model was then converted to a polar-H representation using AMBER41 for energy-based docking using AUTODOCK 3.0.[112]

Energy-Based Docking. Energy-based docking of flexible AHPN (**1**), 5-Cl-AHPN (**2**), 3-Cl-AHPC (**9**), 3-A-AHPC (**10**), and AHPC (**11**) in the rigid RARγ model was performed using the LGA[113] approach embodied in AUTODOCK 3.0. The LGA docking parameters were: mutation rate, 0.02; crossover rate, 0.80; maximum number of generations, 2.7×10^4; elitism, 1; and local search frequency, 0.06. The lowest energy-binding mode was investigated in short exploratory dynamics employing AMBER6 and an all-atom representation to examine differential ligand effects on RARγ.[114] Charge parametrization for all ligands was derived from restrained electrostatic potential fits derived from DFT computations at ligand optimized geometries.[115]

MD Model Equilibration. MD equilibrations of the all-atom model representations of AHPN (**1**), 5-Cl-AHPN (**2**), 3-A-AHPC (**10**), and AHPC (**11**) docked to the RARγ LBD at constant temperature were performed using a 1-fs integration time-step with constraint of all bonds involving hydrogens employing SHAKE. Coordinates were saved every 0.250 ps for subsequent analysis. The nonbonded pair list was updated every 10 steps. A radial screened dielectric constant (D = r) was employed. Production dynamics was performed for 300 ps to make initial probes of the different potential effects of ligand groups on receptor conformation in the neighborhood of the LBP. To permit a critical comparison of the dynamics of AHPC and 3-A-AHPC in the RARγ LBD with reasonable damping of surface fluctuations, following the identification of low-energy docking modes, the docked lowest-energy conformations of the RARγ LBD–AHPC and 3-A-AHPC complexes were solvated within a large box comprised of 4014 waters and having the initial dimensions of 70 Å × 60 Å × 60 Å. After an initial short 50-ps equilibration at constant volume and a 100-ps equilibration at constant pressure, the system was subjected to 300 ps of production dynamics at 300 K. Periodic boundary conditions were employed with a particle-mesh Ewald summation to provide realistic boundary forces and eliminate the distorting effects of potential truncation.

Density Functional Theory (DFT) Exploration of Inter-ring Torsional Potential Surfaces. AHPN (**1**), 5-Cl-AHPN (**2**), 3-Cl-AHPC (**9**), 3-A-AHPC (**10**), and AHPC (**11**) torsional relaxed potential surfaces were computed using the nonlocal B3LYP DFT functional and a 6-31G** basis set. Optimizations employed Jaguar 4.1 (Schrodinger), default self-consistent field (SCF), and geometric convergence criteria. Unconstrained geometry optimization was performed at each of the parametrically varied torsional angles.

Biology. Reagents. *trans*-RA (**4**) and tryspin-TPCK were purchased from Sigma, and [11,12-$^3H_2$]9-*cis*-retinoic acid (43 Ci/mmol) from Amersham. 4-(5′,6′,7′,8′-Tetrahydro-5′,5′,8′,8′-tetramethyl-2′-anthracenyl)benzoic acid (TTAB, **21**)[71] and the 2-substituted 1,3-dithiolane **22**[70] were synthesized as previously described, as were [5,5′-$^3H_2$]6-[3′-(1-adamantyl)-4′-hydroxyphenyl]-2-naphthalenecarboxylic acid, AHPN (**1**), (*E*)-4-[3′-(1-adamantyl)-4′-hydroxyphenyl]-3-chlorocinnamic acid (3-Cl-AHPC, **9**), and 9-*cis*-RA (**5**).[4,39,40,116,117]

AHPN Analogues. Both agonists and antagonists were dissolved in Me_2SO prior to addition to media. The final concentration of Me_2SO was 0.1% for cancer and leukemia cells. All experiments were conducted in triplicate.

Radioligand Binding and DPSA. DPSA studies using [^{35}S]RARγ and LBD competition radioligand-binding experiments were conducted using bacterially expressed RARs (as GST-fusion proteins) and $(His)_6$–RXRα as described.[70]

GST-Pulldown Assays. Experiments were performed as previously described using GST-p300 1–450 or GST-NCoR 2110–2453 fusion proteins and [^{35}S]methionine-labeled hRARγ LBD prepared by in vitro translation.[70]

Plasmids. Expression vectors for RARγ, RXRα, and the reporter gene $(TREpal)_2$-*tk*-CAT have been described.[118]

Receptor Transcriptional Activation in Cotranfected Cells. CV-1 cells were routinely maintained in DMEM, supplemented with 10% fetal calf serum (FCS), 100 units/mL of penicillin, and 100 μg/mL of streptomycin. For transfection assays, cells were seeded at 1.0×10^5 cells/mL in 24-well plates for 16–24 h before transfection. Cells were then transfected using the calcium chloride precipitation method[119] with either $(TREpal)_2$-*tk*-CAT (200 μg) alone or with the RARγ vector (100 μg) or RXRα vector (20 μg). Cells were cotransfected with β-galactosidase (β-gal) expression vector (pCH 110, Amersham Biosciences) and carrier DNA (pBluescript, Stratagene) to a final concentration of 1000 μg/well. Following transfection for 20 h, the medium was changed to DMEM containing 5% charcoal-stripped FCS, and cells were treated for 24 h with an AHPN analogue or retinoid. Chloramphenicol acetyl transferase (CAT) activity was normalized to β-gal activity to standardize for transfection efficiency.

Cell Lines. Retinoid-resistant MDA-MB-231 and MDA-MB-468 breast cancer and H292 lung cancer and retinoid-sensitive H460 lung and LNCaP prostate cancer cell lines were obtained from the American Type Cell Collection. Retinoid-resistant HR-60R leukemia cells were a gift from Dr. Stephen Collins

(University of Washington, Seattle, WA). Cells were cultured as described below.

Cell Proliferation. MDA-MB-468 cells (1.0×10^5 cells) were seeded in DMEM/F12 medium (Invitrogen Life Technologies) supplemented with 5% fetal bovine serum and 25 μg per mL of gentamicin in Petri dishes or 6-well plates. After 24 h, 3-A-AHPC (**10**) (2.0×10^{-6} M final concentration) and/or 3-Cl-AHPC (**9**) (0.5×10^{-6} M) or vehicle alone were added. Cells were harvested at the times indicated in the figures, and living cell numbers were assessed using a commercial colorimetric assay for the mitochondrial dehydrogenase cleavage of water-soluble 3-(4,5-dimethylthiazol-2-yl)-2,5-diphenyltetrazolium bromide (Sigma-Aldrich) according to the manufacturer's directions. H460 and H292 lung cancer and LNCaP prostate cancer cell lines were grown in RPMI 1640 supplemented with 10% FCS.

Apoptosis. At 24 h after seeding with 1.0×10^5 MDA-MB-468 cells, agonist (0.5×10^{-6} M final concentration) or antagonist (2.0×10^{-6} M) alone or the combination was added, and incubations were continued for 48 or 72 h. Cells were then harvested, and the relative number of apoptotic cells was assessed after fixing and acridine orange staining by counting 200-cell fields for the presence of nuclear fragmentation as previously described.[3]

H460 cells (5×10^5) were treated with 1.0×10^{-6} M 5-Cl-AHPN (**2**) or 3-Cl-AHPC (**9**) alone or combined with $1.0 \times 10^{-}$,[6] $2.5 \times 10^{-}$,[6] or 5.0×10^{-6} M 3-A-AHPC (**10**). After 36 h, cells were trypsinized, then washed with phosphate-buffered saline (PBS, pH 7.4). After fixation with 3.7% paraformaldehyde, cells were washed (PBS) and stained with 4,6-diamidino-2-phenylindole (DAPI, 50 μg/mL) to visualize nuclei by fluorescent microscopy.[38] Cells displaying nuclear morphology characteristic of apoptosis were scored in samples of at least 600 cells. Apoptosis (%) was expressed as the ratio of apoptotic cells to total cells $\times$ 100.

Western Blotting. MDA-MB-468 cells (1.0×10^5) were treated for 72 h with a proapoptotic AHPN (0.5×10^{-6} M final concentration) or antagonist **3** (2.0×10^{-6} M) alone or combined. Cells were lysed, and Western blots were performed on the lysates using anti-p21$^{WAF1/CIP1}$ antibody (Transduction Laboratories) and β-actin as the loading control as previously described.[4]

RNA Preparation and Northern Blotting. Total RNA samples were prepared by the guanidine hydrochloride/ultracentrifugation method.[119] Total RNA (30 μg) from cancer cells treated with or without 1.0×10^{-6} M 5-Cl-AHPN (**2**) alone or combined with 1.0×10^{-6} M or 5.0×10^{-6} M 3-A-AHPC (**10**) for 4 h was fractionated on 1% agarose gels. The fractionated RNA was transferred to nylon filters and probed with ^{32}P-labeled TR3 LBD cDNA.[118] Ethidium bromide-stained ribosomal RNA was used as the loading control.

Ligand Binding. Nuclear extracts were prepared from HL-60R cells (1.0×10^5) as we previously described.[4] [5,5′-^{3}H$_2$]-AHPN[4] (10×10^{-9} M, 150 000 dpm) was added to the nuclear extracts in the presence and absence of 20×10^{-6} M nonlabeled AHPN (**1**) or 3-A-AHPC (**10**) or vehicle alone. After a 90-min incubation at 22 °C, free ligand was separated from bound ligand on a 0.5-cm $\times$ 4.0-cm column of fine-mesh G25 Sephadex (Pharmacia) by elution with binding buffer.[4] The bound fraction was counted as we described.[4]

Acknowledgment. These studies were supported by NCI grant P01 CA51993 (M.I.D., M.L., J.A.F., and X.Z.), California Breast Cancer Research Program grant 8WB-017 (M.I.D., D.H.L., X.Z.), and California Tobacco-Related Diseases Research Program grants 6RT-0212A (M.I.D.) and 11RT-0081 (X.Z., M.I.D.). N.B.-S. was supported by a postdoctoral fellowship from the California Breast Cancer Research Program. D.L.H. acknowledges the NSF supercomputer grant award MCB030032 at the Pittsburgh Computer Center. Special thanks go to Cynthia Cook and Helen Hansen for their help with preparing this manuscript.

Appendix

Acromyns and/or code numbers for 6-[3′-(1-adamantyl)-4′-hydroxyphenyl)]-2-naphthalenecarboxylic acid, its analogues, and retinoids are listed in the legend for Figure 1. Other abbreviations are 1-Ad, 1-adamantyl; 3-A, 3-(3′-acetamidopropyloxy); Bcl-2, diffuse B-cell lymphoma cytoprotective protein; CAT, chloramphenicol acetyl transferase; CPK, Corey–Pauling–Kortum; CV-1, African green monkey kidney cell line; DAPI, 4,6-diamidino-2-phenylindole; DPSA, differential protease sensitivity assay; DTF, density functional theory; FCS, fetal calf serum; GST, glutathione *S*-transferase; LBD, ligand-binding domain; LGA, Larmarkian Genetic Algorithm; LBP, ligand-binding pocket; NCoR, nuclear receptor corepressor protein; p21$^{WAF/CIP1}$, 21-kDa wild-type p53-activated fragment 1 or cyclin-dependent kinase-2-interacting protein; p300, an acetyl transferase and transcriptional coactivator of nuclear receptors; PBS, phosphate-buffered saline, pH 7.4; RA, retinoic acid; RAR, retinoic acid receptor; RXR, retinoid X receptor; TPCK-trypsin, bovine pancreas trypsin treated with *N*-(*p*-tosyl)-L-phenylanlanine chloromethyl ketone; TREpal, palindromic RAR- and RXR-responsive element; *tk*, thymidine kinase promoter; TTN, 5,6,7,8-tetrahydro-5,5,8,8-tetramethyl-2-naphthalene.

Supporting Information Available: Elemental analyses for compounds **45** and **46**. This material is available free of charge via the Internet at http://pubs.acs.org.

References

(1) Bernard, B. A.; Bernardon, J. M.; Delescluse, C.; Martin, B.; Lenoir, M. C.; Maignan, J.; Charpentier, B.; Pilgrim, W. R.; Reichert, U.; Shroot, B. Identification of synthetic retinoids with selectivity for human nuclear retinoic acid receptor gamma. *Biochem. Biophys. Res. Commun.* **1992**, *186*, 977–983.

(2) Shao, Z.-M.; Dawson, M. I.; Li, X. S.; Rishi, A. K.; Sheikh, M. S.; Han, Q. X.; Ordonez, J. V.; Shroot, B.; Fontana, J. A. p53 independent G_0/G_1 arrest and apoptosis induced by a novel retinoid in human breast cancer cells. *Oncogene* **1995**, *11*, 493–504.

(3) Li, X.-S.; Rishi, A. K.; Shao, Z. M.; Dawson, M. I.; Jong, L.; Shroot, B.; Reichert, U.; Ordonez, J.; Fontana, J. A. Posttranscriptional regulation of p21$^{WAF1/CIP1}$ expression in human breast carcinoma cells. *Cancer Res.* **1996**, *56*, 5055–5062.

(4) Fontana, J. A.; Dawson, M. I.; Leid, M.; Rishi, A. K.; Zhang, Y.; Hsu, C.-A.; Lu, J. S.; Peterson, V. J.; Jong, L.; Hobbs, P.; Chao, W.-R.; Shroot, B.; Reichert, U. Identification of a unique binding protein specific for a novel retinoid inducing cellular apoptosis. *Int. J. Cancer* **2000**, *86*, 474–479.

(5) Dawson, M. I.; Hobbs, P. D.; Peterson, V. J.; Leid, M.; Lange, C. W.; Feng, K. C.; Chen, G.; Gu, J.; Li, H.; Kolluri, S. K.; Zhang, X.; Zhang, Y.; Fontana, J. A. Apoptosis induction in cancer cells by a novel analogue of 6-[3-(1-adamantyl)-4-hydroxyphenyl]-2-naphthalenecarboxylic acid lacking retinoid receptor transcriptional activation activity. *Cancer Res.* **2001**, *61*, 4723–4730.

(6) Mangelsdorf, D. J.; Umesono, K.; Evans, R. M. The retinoid receptors. In *The Retinoids: Biology, Chemistry, and Medicine*; Sporn, M. B., Roberts, A. B., Goodman, D. S., Eds.; Raven Press: New York, 1994; pp 319–349.

(7) Dawson, M. I.; Chao, W. R.; Pine, P.; Jong, L.; Hobbs, P. D.; Rudd, C. K.; Quick, T. C.; Niles, R. M.; Zhang, X.-K.; Lombardo, A.; Ely, K. R.; Shroot, B.; Fontana, J. A. Correlation of retinoid binding affinity to RARα with retinoid inhibition of growth of estrogen receptor-positive MCF-7 mammary carcinoma cells. *Cancer Res.* **1995**, *55*, 4446–4451.

(8) Fitzgerald, P.; Teng, M.; Chandraratna, R. A. S.; Heyman, R. A.; Allegretto, E. A. Retinoic acid receptor α expression correlates with retinoid-induced growth inhibition of human breast cancer cells regardless of estrogen receptor status. *Cancer Res.* **1997**, *57*, 2642–2650.

(9) Chao, W. R.; Hobbs, P. D.; Jong, L.; Zhang, X.-K.; Zheng, Y.; Wu, Q.; Shroot, B.; Dawson, M. I. Effects of receptor class- and subtype-selective retinoids and an apoptosis-inducing retinoid on the adherent growth of the NIH:OVCAR-3 ovarian cancer cell line in culture. *Cancer Lett.* **1997**, *115*, 1–7.

(10) Li, H.; Kolluri, S. K.; Gu, J.; Dawson, M. I.; Cao, X.; Hobbs, P. D.; Lin, B.; Chen, G.; Lu, J.; Lin, F.; Xie, Z.; Fontana, J. A.; Reed, J. C.; Zhang, X. Cytochrome c release and apoptosis induced by mitochondrial targeting of nuclear orphan receptor TR3. *Science* **2000**, *289*, 1159−1164.

(11) Milbrandt, J. Nerve growth factor induces a gene homologous to the glucocorticoid receptor gene. *Neuron* **1988**, *1*, 183−188.

(12) Chang, C.; Kokontis, J. Identification of a new member of the steroid receptor super-family by cloning and sequence analysis. *Biochem. Biophys. Res. Commun.* **1988**, *155*, 971−977.

(13) Hazel, T. G.; Nathans, D.; Lau, L. F. A gene inducible by serum growth factors encodes a member of the steroid and thyroid hormone receptor superfamily. *Proc. Natl. Acad. Sci. U.S.A.* **1988**, *85*, 8444−8448.

(14) Leid, M.; Kastner, P.; Lyons, R.; Nakshatri, H.; Saunders: M.; Zacharewski, T.; Chen, J.-Y.; Staub, A.; Garnier, J.-M.; Mader, S.; Chambon, P. Purification, cloning, and RXR identity of the HeLa cell factor with which RAR or TR heterodimerizes to bind target sequences efficiently. *Cell* **1992**, *68*, 377−395.

(15) Green, D. R.; Reed, J. C. Mitochondria and apoptosis. *Science* **1998**, *281*, 1309−1312.

(16) Lin, B.; Kolluri, S. K.; Lin, F.; Liu, W.; Han, Y. H.; Cao, X.; Dawson, M. I.; Reed, J. C.; Zhang, X.-K. Conversion of Bcl-2 from protector to killer by interaction with nuclear orphan receptor Nur77/TR3. *Cell* **2004**, *116*, 527−540.

(17) Armstrong, R. B.; Ashenfelter, K. O.; Eckhoff, C.; Levin, A. A.; Shapiro, S. S. General and reproductive toxicology of retinoids. In *The Retinoids: Biology, Chemistry, and Medicine*; Sporn, M. B., Roberts, A. B., Goodman, D. S., Eds.; Raven Press: New York, 1994; pp 545−572.

(18) Graf, N.; Riesinger, P.; Reinhard, H. Retinoids in the treatment of acute promyelocytic leukemia. Review of the literature. *Klin. Padiatr.* **1995**, *207*, 43−47.

(19) Selleri, C.; Pane, F.; Notaro, R.; Catalano, L.; Santoro, L. E.; Luciano, L.; Frigeri, F.; Salvatore, F.; Rotoli, B. All-*trans*-retinoic acid (ATRA) responsive skin relapses of acute promyelocytic leukaemia followed by ATRA-induced *pseudotumour cerebri*. *Br. J. Haematol.* **1996**, *92*, 937−940.

(20) De Botton, S.; Dombret, H.; Sanz, M.; Miguel, J. S.; Caillot, D.; Zittoun, R.; Gardembas, M.; Stamatoulas, A.; Conde, E.; Guerci, A.; Gardin, C.; Geiser, K.; Makhoul, D. C.; Reman, O.; de la Serna, J.; Lefrere, F.; Chomienne, C.; Chastang, C.; Degos, L.; Fenaux, P. Incidence, clinical features, and outcome of all *trans*-retinoic acid syndrome in 413 cases of newly diagnosed acute promyelocytic leukemia. The European APL Group. *Blood* **1998**, *92*, 2712−2718.

(21) Levi, I.; Raanani, P.; Shalmon, B.; Schiby-Brilliant, R.; Ben-Bassat, I. Acute neutrophilic dermatosis induced by all-*trans*-retinoic acid treatment for acute promyelocytic leukemia. *Leuk. Lymphoma* **1999**, *34*, 401−404.

(22) Wu, W.; Sun, G.; Zhou, R.; Li, X.; Shen, Z.; Wang, Z. The relationship between the levels of granulocyte colony-stimulating factor and leukocytosis induced by all-trans retinoic acid in acute promyelocytic leukemia. *Chin. Med. J. (Engl.)* **1999**, *112*, 1085−1087.

(23) Tommasino, C.; De Felice, L.; Colombo, S.; Salaris, D.; Capocasa, T.; Giudici, D. Retinoic acid syndrome. Severe respiratory insufficiency treated with CPAP. *Minerva Anestesiol.* **2000**, *66*, 555−559.

(24) Duvic, M.; Hymes, K.; Heald, P.; Breneman, D.; Martin, A. G.; Myskowski, P.; Crowley, C.; Yocum, R. C. Bexarotene is effective and safe for treatment of refractory advanced-stage cutaneous T-cell lymphoma: Multinational phase II−III trial results. *J. Clin. Oncol.* **2001**, *19*, 2456−2471.

(25) Martín del Pozo, M.; Cisneros de la Fuente, E.; Solano, F.; Martín, M. L.; de la Serna, J. The retinoic acid syndrome, a complication of acute promyelocytic leukemia therapy. *An. Med. Intern.* **2001**, *18*, 195−200.

(26) Goncalves, A.; Camerlo, J.; Bun, H.; Gravis, G.; Genre, D.; Bertucci, F.; Resbeut, M.; Pech-Gourg, F.; Durand, A.; Maraninchi, D.; Viens, P. Phase II study of a combination of cisplatin, all-*trans*-retinoic acid and interferon-α in squamous cell carcinoma: Clinical results and pharmacokinetics. *Anticancer Res.* **2001**, *21*, 1431−1437.

(27) Khuri, F. R.; Rigas, J. R.; Figlin, R. A.; Gralla, R. J.; Shin, D. M.; Munden, R.; Fox, N.; Huyghe, M. R.; Kean, Y.; Reich, S. D.; Hong, W.-K. Multi-institutional Phase I/II trial of oral bexarotene in combination with cisplatin and vinorelbine in previously untreated patients with advanced nonsmall-cell lung cancer. *J. Clin. Oncol.* **2001**, *19*, 2626−2637.

(28) Park, C. J.; Bae, Y. D.; Choi, J. Y.; Heo, P. S.; Lee, K. S.; Park, Y. S.; Lee, J. A. Sweet's syndrome during the treatment of acute promyelocytic leukemia with all-trans retinoic acid. *Korean J. Intern. Med.* **2001**, *16*, 218−221.

(29) Shin, D. M.; Glisson, B. S.; Khuri, F. R.; Clifford, J. L.; Clayman, G.; Benner, S. E.; Forastiere, A. A.; Ginsberg, L.; Liu, D.; Lee, J. J.; Myers, J.; Goepfert, H.; Lotan, R.; Hong, W. K.; Lippman, S. M. Phase II and biologic study of interferon α, retinoic acid, and cisplatin in advanced squamous skin cancer. *J. Clin. Oncol.* **2002**, *20*, 364−370.

(30) Standeven, A. M.; Teng, M.; Chandraratna, R. A. S. Lack of involvement of retinoic acid receptor α in retinoid-induced skin irritation in hairless mice. *Toxicol. Lett.* **1997**, *92*, 231−240.

(31) Iulianella, A.; Lohnes, D. Contribution of retinoic acid receptor γ to retinoid-induced craniofacial and axial defects. *Dev. Dyn.* **1997**, *209*, 92−104.

(32) Look, J.; Landwehr, J.; Bauer, F.; Hoffmann, A. S.; Bluethmann, H.; LeMotte, P. Marked resistance of RARγ-deficient mice to the toxic effects of retinoic acid. *Am. J. Physiol.* **1995**, *269*, E91-E98.

(33) Reczek, P. R.; Ostrowski, J.; Yu, K. L.; Chen, S.; Hammer, L.; Roalsvig, T.; Starrett, J. E., Jr.; Driscoll, J. P.; Whiting, G.; Spinazze, P. G. Role of retinoic acid receptor γ in the Rhino mouse and rabbit irritation models of retinoid activity. *Skin Pharmacol.* **1995**, *8*, 292−299.

(34) Sheikh, M. S.; Shao, Z.-M.; Li, X.-S.; Dawson, M. I.; Jetten, A. M.; Wu, S.; Conley, B. A.; Garcia, M.; Rochefort, H.; Fontana, J. A. Retinoid-resistant estrogen receptor-negative human breast carcinoma cells transfected with retinoic acid receptor-α acquire sensitivity to growth inhibition by retinoids. *J. Biol. Chem.* **1994**, *269*, 21440−21447.

(35) Swisshelm, K.; Ryan, K.; Lee, X.; Tsou, H. C.; Peacocke, M.; Sager, R. Down-regulation of retinoic acid receptor β in mammary carcinoma cell lines and its up-regulation in senescing normal mammary epithelial cells. *Cell Growth Differ.* **1994**, *5*, 133−141.

(36) Li, X.-S.; Shao, Z.-M.; Sheikh, M. S.; Eiseman, J. L.; Sentz, D.; Jetten, A. M.; Chen, J.-C.; Dawson, M. I.; Aisner, S.; Rishi, A. K.; Fontana, J. A. Retinoic acid nuclear receptor β (RARβ) inhibits breast carcinoma anchorage independent growth. *J. Cell. Physiol.* **1995**, *165*, 449−458.

(37) Lotan, R.; Xu, X. C.; Lippman, S. M.; Ro, J. Y.; Lee, J. S.; Lee, J. J.; Hong, W.-K. Suppression of retinoic acid receptor-β in premalignant oral lesions and its up-regulation by isotretinoin. *New Engl. J. Med.* **1995**, *332*, 1405−1410.

(38) Liu, Y.; Lee, M.-O.; Wang, H.-G.; Li, Y.; Hashimoto, Y.; Klaus, M.; Reed, J. C.; Zhang, X. RARβ mediates the growth-inhibitory effect of retinoic acid by promoting apoptosis in human breast cancer cells. *Mol. Cell. Biol.* **1996**, *16*, 1138−1149.

(39) Zhang, Y.; Dawson, M. I.; Mohammad, R.; Rishi, A. K.; Farhana, L.; Feng, K. C.; Leid, M.; Peterson, V.; Zhang, X.-K.; Edelstein, M.; Eilander, D.; Biggar, S.; Wall, N.; Reichert, U.; Fontana, J. A. Induction of apoptosis of human B-CLL and ALL cells by a novel retinoid and its nonretinoidal analogue. *Blood* **2002**, *100*, 2917−2925.

(40) Zhang, Y.; Dawson, M. I.; Ning, Y.; Polin, L.; Parchment, R. E.; Corbett, T.; Mohamed, A. N.; Feng, K. C.; Farhana, L.; Rishi, A. K.; Hogge, D.; Leid, M.; Peterson, V. J.; Zhang, X.-K.; Mohammad, R.; Lu, J. S.; Willman, C.; VanBuren, E.; Biggar, S.; Edelstein, M.; Eilender, D.; Fontana, J. A. Induction of apoptosis in retinoid-refractory acute myelogenous leukemia by a novel AHPN analogue. *Blood* **2003**, *102*, 3743−3752.

(41) Schiff, L. J.; Okamura, W. H.; Dawson, M. I.; Hobbs, P. D. Structure-biological activity relationships of new synthetic retinoids on epithelial differentiation of cultured hamster trachea. In *Chemistry and Biology of Synthetic Retinoids*; Dawson, M. I., Okamura, W. H., Eds.; CRC Press: Boca Rotan, 1990; pp 302−363.

(42) Dawson, M. I.; Chan, R. L.-S.; Derdzinski, K.; Hobbs, P. D.; Chao, W.-R.; Schiff, L. J. Synthesis and pharmacological activity of 6-[(*E*)-2-(2,6,6-trimethyl-1-cyclohexen-1-yl)ethen-1-yl]-and 6-(1,2,3,4-tetrahydro-1,1,4,4-tetramethyl-6-naphthyl)-2-naphthalenecarboxylic acids. *J. Med. Chem.* **1983**, *26*, 1653−1656.

(43) Schiff, L. J.; Moore, S. J.; Dawson, M. I.; Hobbs, P. D.; Chan, R. L.-S.; Derdzinski, K. Biological activity of aromatic retinoid acid analogues in hamster tracheal organ culture. In *In Vitro Models of Respiratory Epithelium*; Schiff, L. J., Ed.; CRC Press: Boca Raton, FL, 1986; pp 51−83.

(44) Cincinelli, R.; Dallavalle, S.; Merlini, L.; Penco, S.; Pisano, C.; Carminati, P.; Giannini, G.; Vesci, L.; Gaetano, C.; Illy, B.; Zuco, V.; Supino, R.; Zunino, F. A novel atypical retinoid endowed with proapoptotic and antitumor activity. *J. Med. Chem.* **2003**, *46*, 909−912.

(45) Dawson, M. I.; Chao, W.-R.; Hobbs, P. D.; Delair, T. The inihibitory effects of retinoids on the induction of ornithine decarboxylase and the promotion of tumors in mouse epidermis. In *Chemistry and Biology of Synthetic Retinoids*; Dawson, M. I., Okamura, W. H., Eds.; CRC Press: Boca Rotan, 1990; pp 385−466.

(46) Dawson, M. I.; Park, J.-H.; Chen, G.; Chao, W.; Dousman, L.; Waleh, N.; Hobbs, P. D.; Jong, L.; Toll, L.; Zhang, X.; Gu, J.; Agadir, A.; Merchant, J. L.; Bai, L.; Verma, A. K.; Thacher, S. M.; Chandraratna, R. A. S.; Shroot, B.; Hill, D. L. Retinoic acid

(RA) receptor transcriptional activation correlates with inhibition of 12-*O*-tetradecanoylphorbol-13-acetate-induced ornithine decarboxylase (ODC) activity by retinoids: A potential role for *trans*-RA-induced ZBP-89 in ODC inhibition. *Int. J. Cancer* **2001**, *91*, 8–21.

(47) Dawson, M. I.; Hobbs, P. D.; Stein, R. B.; Berger, T. S.; Heyman, R. A. Interaction of retinoids with retinoic nuclear receptor isoforms. In *Retinoids: New Trends in Research and Clinical Applications*; Livrea, M. A., Packer, L., Eds.; Marcel Dekker: New York, 1992; pp 205–221.

(48) Lehmann, J. M.; Dawson, M. I.; Hobbs, P. D.; Husmann, M.; Pfahl, M. Identification of retinoids with nuclear receptor subtype-selective activities. *Cancer Res.* **1991**, *51*, 4804–4809.

(49) Dawson, M. I.; Zhang, X.; Hobbs, P. D.; Jong, L. Synthetic retinoids and their usefulness in biology and medicine. In *Vitamin A and Retinoids: An Update of Biological Aspects and Clinical Applications*; Livrea, M. A., Ed.; Birkhäuser Verlag: Basel, Switzerland, 2000; pp 161–196.

(50) Lehmann, J. M.; Jong, L.; Fanjul, A.; Cameron, J. F.; Liu, X. P.; Haefner, P.; Dawson, M. I.; Pfahl, M. A novel class of retinoids, selective for retinoid X receptor response pathways. *Science* **1992**, *258*, 1944–1946.

(51) Dawson, M. I.; Jong, L.; Hobbs, P. D.; Cameron, J. F.; Chao, W.-R.; Pfahl, M.; Lee, M.-O.; Shroot, B. Conformational effects on retinoid receptor selectivity. 2. Effects of retinoid bridging group on retinoid X receptor activity and selectivity. *J. Med. Chem.* **1995**, *38*, 3368–3383.

(52) Dawson, M. I.; Cameron, J. F.; Hobbs, P. D.; Jong, L.; Pfahl, M.; Zhang, X.; Lehmann, J. M. (SRI International and The Burnham Institute, formerly La Jolla Cancer Research Foundation). Bridged bicyclic aromatic compounds and their use in modulating gene expression of retinoid receptors. U.S. Patent 5,837,725, 1998.

(53) Dawson, M. I.; Hobbs, P. D.; Jong, L.; Xiao, D.; Chao, W.-R.; Pan, C.; Zhang, X.-K. sp2-bridged diaryl retinoids: Effects of bridge-region substitution on retinoid X receptor (RXR) selectivity. *Bioorg. Med. Chem. Lett.* **2000**, *10*, 1307–1310.

(54) Dawson, M. I.; Zhang, X.-K. Discovery and design of retinoic acid receptor and retinoid X receptor class- and subtype-selective synthetic analogues of all-*trans*-retinoic acid and 9-*cis*-retinoic acid. *Curr. Med. Chem.* **2002**, *9*, 623–637.

(55) Boehm, M. F.; Zhang, L.; Zhi, L.; McClurg, M. R.; Berger, E.; Wagoner, M.; Mais, D. E.; Suto, C. M.; Davies, J. A.; Heyman, R. A.; Nadzan, A. M. Design and synthesis of potent retinoid X receptor selective ligands that induce apoptosis in leukemia cells. *J. Med. Chem.* **1995**, *38*, 3146–3155.

(56) Beard, R. L.; Colon, D. F.; Song, T. K.; Davies, P. J.; Kochhar, D. M.; Chandraratna, R. A. S. Synthesis and structure–activity relationships of retinoid X receptor selective diaryl sulfide analogues of retinoic acid. *J. Med. Chem.* **1996**, *39*, 3556–3563.

(57) Dawson, M. I.; Chao, W. R.; Hobbs, P. D.; Zhang, X.-K. Effects of *trans*-retinoic acid, 9-*cis*-retinoic acid, 1α,25-(dihydroxy)-vitamin D_3 and a novel apoptosis-inducing retinoid on breast cancer and endothelial cell growth. *Cancer Lett.* **1998**, *133*, 1–8.

(58) Robertson, K. A.; Emami, B.; Collins, S. J. Retinoic acid-resistant HL-60R cells harbor a point mutation in the retinoic acid receptor ligand-binding domain that confers dominant negative activity. *Blood* **1992**, *80*, 1885–1889.

(59) Ota, E.; Shimozawa, J. T. Substitution reactions of phenanthrols. XII. Conversion of phenanthrols to the corresponding chloro- and bromophenanthrenes and their dipole moment measurements. *Nippon Kagaku Kaishi* **1987**, *4*, 757–761.

(60) Dawson, M. I.; Cavasotto, C. N.; Hobbs, P. D.; Jong, L.; Feng, K.-C.; Lui, H.; Abagyan, R.; Zhang, X. Synthesis and biological activity of an RXR antagonist. Presented at the 93rd Annual AACR National Meeting, San Francisco, CA, 2002.

(61) Brzozowski, A. M.; Pike, A. C.; Dauter, Z.; Hubbard, R. E.; Bonn, T.; Engstrom, O.; Ohman, L.; Greene, G. L.; Gustafsson, J.-A.; Carlquist, M. Molecular basis of agonism and antagonism in the oestrogen receptor. *Nature* **1997**, *389*, 753–758.

(62) Pike, A. C.; Brzozowski, A. M.; Hubbard, R. E.; Bonn, T.; Thorsell, A. G.; Engstrom, O.; Ljunggren, J.; Gustafsson, J. A.; Carlquist, M. Structure of the ligand-binding domain of oestrogen receptor β in the presence of a partial agonist and a full antagonist. *EMBO J.* **1999**, *18*, 4608–4618.

(63) Delabre, K.; Guiochon-Mantel, A.; Milgrom, E. In vivo evidence against the existence of antiprogestins disrupting receptor binding to DNA. *Proc. Natl. Acad. Sci. U.S.A.* **1993**, *90*, 4421–4425.

(64) Brand, C.; Ségard, P.; Plouvier, P.; Formstecher, P.; Danzé, P. M.; Lefebvre, P. Selective alteration of gene expression in response to natural and synthetic retinoids. *BMC Pharmacol.* **2002**, *2*, 13.

(65) Klaholz, B. P.; Renaud, J. P.; Mitschler, A.; Zusi, C.; Chambon, P.; Gronemeyer, H.; Moras, D. Conformational adaptation of agonists to the human nuclear receptor RARγ. *Nat. Struct. Biol.* **1998**, *5*, 199–202.

(66) Apfel, C.; Bauer, F.; Crettaz, M.; Forni, L.; Kamber, M.; Kaufmann, F.; LeMotte, P.; Pirson, W.; Klaus, M. A retinoic acid receptor α antagonist selectively counteracts retinoic acid effects. *Proc. Natl. Acad. Sci. U.S.A.* **1992**, *89*, 7129–7133.

(67) Lala, D. S.; Mukherjee, R.; Schulman, I. G.; Koch, S. S.; Dardashti, L. J.; Nadzan, A. M.; Croston, G. E.; Evans, R. M.; Heyman, R. A. Activation of specific RXR heterodimers by an antagonist of RXR homodimers. *Nature* **1996**, *383*, 450–453.

(68) Arulmozhiraja, S.; Selvin, P. C.; Fujii, T. Structures, potential energy curves, and torsional barrier heights for selected polychlorinated biphenyls: A density functional theory study. *J. Phys. Chem. A* **2002**, *106*, 1765–1769.

(69) Arulmozhiraja, S.; Fujii, T. Torsional barrier, ionization potential, and electron affinity of biphenyl—A theoretical study. *J. Chem. Phys.* **2001**, *115*, 10589–10594.

(70) Peterson, V. J.; Barofsky, E.; Deinzer, M. L.; Dawson, M. I.; Feng, K. C.; Zhang, X.-K.; Madduru, M. R.; Leid, M. Mass-spectrometric analysis of agonist-induced retinoic acid receptor γ conformational change. *Biochem. J.* **2002**, *362*, 173–181.

(71) Dawson, M. I.; Hobbs, P. D.; Derdzinski, K. A.; Chao, W.-R.; Frenking, G.; Loew, G. H.; Jetten, A. M.; Napoli, J. L.; Williams, J. B.; Sani, B. P.; Wille, J. J., Jr.; Schiff, L. J. Effect of structural modifications in the C7–C11 region of the retinoid skeleton on biological activity in a series of aromatic retinoids. *J. Med. Chem.* **1989**, *32*, 1504–1517.

(72) Nielsen, L. L.; Dell, J.; Maxwell, E.; Armstrong, L.; Maneval, D.; Catino, J. J. Efficacy of p53 adenovirus-mediated gene therapy against human breast cancer xenografts. *Cancer Gene Ther.* **1997**, *4*, 129–138.

(73) Sheikh, M. S.; Li, X.-S.; Chen, J. C.; Shao, Z. M.; Ordonez, J. V.; Fontana, J. A. Mechanisms of regulation of WAF1/Cip1 gene expression in human breast carcinoma: Role of p53-dependent and independent signal transduction pathways. *Oncogene* **1994**, *9*, 3407–3415.

(74) Xinarianos, G.; Liloglou, T.; Prime, W.; Sourvinos, G.; Karachristos, A.; Gosney, J. R.; Spandidos, D. A.; Field, J. K. p53 status correlates with the differential expression of the DNA mismatch repair protein MSH2 in nonsmall cell lung carcinoma. *Int. J. Cancer* **2002**, *101*, 248–252.

(75) Campling, B. G.; el-Deiry, W. S. Clinical implications of p53 mutations in lung cancer. *Methods Mol. Med.* **2003**, *75*, 53–77.

(76) Zhang, Y.; Huang, Y.; Rishi, A. K.; Sheikh, M. S.; Shroot, B.; Reichert, U.; Dawson, M. I.; Poirer, G.; Fontana, J. A. Activation of the p38 and JNK/SAPK mitogen-activated protein kinase pathways during apoptosis is mediated by a novel retinoid. *Exp. Cell Res.* **1999**, *247*, 233–240.

(77) Li, Y.; Lin, B.; Agadir, A.; Liu, R.; Dawson, M. I.; Reed, J. C.; Fontana, J. A.; Bost, F.; Hobbs, P. D.; Zheng, Y.; Chen, G.-Q.; Shroot, B.; Mercola, D.; Zhang, X.-K. Molecular determinants of AHPN (CD437)-induced growth arrest and apoptosis in human lung cancer cell lines. *Mol. Cell. Biol.* **1998**, *18*, 4719–4731.

(78) White, E. Life, death, and the pursuit of apoptosis. *Genes Dev.* **1996**, *10*, 1–15.

(79) Green, D.; Kroemer, G. The central executioners of apoptosis: Caspases or mitochondria? *Trends Cell. Biol.* **1998**, *8*, 267–271.

(80) Hsu, C. K. A.; Rishi, A. K.; Li, X.-S.; Dawson, M. I.; Reichert, U.; Shroot, B.; Fontana, J. A. Bcl-X_L expression and its down-regulation by a novel retinoid in breast carcinoma cells. *Exp. Cell Res.* **1997**, *232*, 17–24.

(81) Fanjul, A. N.; Piedrafita, F. J.; Al-Shamma, H.; Pfahl, M. Apoptosis induction and potent antiestrogen receptor-negative breast cancer activity *in vivo* by a retinoid antagonist. *Cancer Res.* **1998**, *58*, 4607–4610.

(82) Rishi, A. K.; Sun, R. J.; Gao, Y.; Hsu, C. K.; Gerald, T. M.; Saeed Sheikh, M.; Dawson, M. I.; Reichert, U.; Shroot, B.; Fornace, A. J., Jr.; Brewer, G.; Fontana, J. A. Posttranscriptional regulation of the DNA damage-inducible gadd45 gene in human breast carcinoma cells exposed to a novel retinoid CD437. *Nucleic Acids Res.* **1999**, *27*, 3111–3119.

(83) Lu, X. P.; Fanjul, A.; Picard, N.; Pfahl, M.; Rungta, D.; Nared-Hood, K.; Carter, B.; Piedrafita, J.; Tang, S.; Fabbrizio, E. Novel retinoid-related molecules as apoptosis inducers and effective inhibitors of human lung cancer cells in vivo. *Nat. Med.* **1997**, *3*, 686–690.

(84) Sun, S.-Y.; Yue, P.; Shroot, B.; Hong, W. K.; Lotan, R. Implication of c-Myc in apoptosis induced by the retinoid CD437 in human lung carcinoma cells. *Oncogene* **1999**, *18*, 3894–3901.

(85) Sun, S.-Y.; Yue, P.; Wu, G. S.; El-Deiry, W. S.; Shroot, B.; Hong, W. K.; Lotan, R. Implication of p53 in growth arrest and apoptosis induced by the synthetic retinoid CD437 in human lung cancer cells. *Cancer Res.* **1999**, *59*, 2829–2833.

(86) Sun, S.-Y.; Yue, P.; Chen, X.; Hong, W. K.; Lotan, R. The synthetic retinoid CD437 selectively induces apoptosis in human lung cancer cells while sparing normal human lung epithelial cells. *Cancer Res.* **2002**, *62*, 2430–2436.

(87) Hsu, C. A.; Rishi, A. K.; Li, X.-S.; Gerald, T. M.; Dawson, M. I.; Schiffer, C.; Reichert, U.; Shroot, B.; Poirer, G. C.; Fontana, J. A. Retinoid induced apoptosis in leukemia cells through a retinoic acid nuclear receptor-independent pathway. *Blood* **1997**, *89*, 4470−4479.

(88) Giannì, M.; de Thé, H. In acute promyelocytic leukemia NB4 cells, the synthetic retinoid CD437 induces contemporaneously apoptosis, a caspase-3-mediated degradation of PML/RARα protein and the PML retargeting on PML-nuclear bodies. *Leukemia* **1999**, *13*, 739−749.

(89) Mologni, L.; Ponzanelli, I.; Bresciani, F.; Sardiello, G.; Bergamaschi, D.; Gianni, M.; Reichert, U.; Rambaldi, A.; Terao, M.; Garattini, E. The novel synthetic retinoid 6-[3-adamantyl-4-hydroxyphenyl]-2-naphthalenecarboxylic acid (CD437) causes apoptosis in acute promyelocytic leukemia cells through rapid activation of caspases. *Blood* **1999**, *93*, 1045−1061.

(90) Oridate, N.; Higuchi, M.; Suzuki, S.; Shroot, B.; Hong, W.-K.; Lotan, R. Rapid induction of apoptosis in human C33A cervical carcinoma cells by the synthetic retinoid 6-[3-(1-adamantyl)-hydroxyphenyl]-2-naphthalenecarboxylic acid (CD437). *Int. J. Cancer* **1997**, *70*, 484−487.

(91) Wan, X.; Duncan, M. D.; Nass, P.; Harmon, J. W. Synthetic retinoid CD437 induces apoptosis of esophageal squamous HET-1A cells through the caspase-3-dependent pathway. *Anticancer Res.* **2001**, *21*, 2657−2663.

(92) Adachi, H.; Adams, A.; Hughes, F. M.; Zhang, J.; Cidlowski, J. A.; Jetten, A. M. Induction of apoptosis by the novel retinoid AHPN in human T-cell lymphoma cells involves caspase-dependent and independent pathways. *Cell Death Differ.* **1998**, *5*, 973−983.

(93) Schadendorf, D.; Worm, M.; Jurgovsky, K.; Dippel, E.; Reichert, U.; Czarnetzki, B. M. Effects of various synthetic retinoids on proliferation and immunophenotype of human melanoma cells in vitro. *Recent Results Cancer Res.* **1995**, *139*, 183−193.

(94) Schadendorf, D.; Kern, M. A.; Artuc, M.; Pahl, H. L.; Rosenbach, T.; Fichtner, I.; Nurnberg, W.; Stuting, S.; von Stebut, E.; Worm, M.; Makki, A.; Jurgovsky, K.; Kolde, G.; Henz, B. M. Treatment of melanoma cells with the synthetic retinoid CD437 induces apoptosis via activation of AP-1 *in vitro*, and causes growth inhibition in xenografts in vivo. *J. Cell Biol.* **1996**, *135*, 1889−1898.

(95) Meister, B.; Fink, F. M.; Hittmair, A.; Marth, C.; Widschwendter, M. Antiproliferative activity and apoptosis induced by retinoic acid receptor-γ selectively binding retinoids in neuroblastoma. *Anticancer Res.* **1998**, *18*, 1777−1786.

(96) Langdon, S. P.; Rabiasz, G. J.; Ritchie, A. A.; Reichert, U.; Buchan, P.; Miller, W. R.; Smyth, J. F. Growth-inhibitory effects of the synthetic retinoid CD437 against ovarian carcinoma models in vitro and in vivo. *Cancer Chemother. Pharmacol.* **1998**, *42*, 429−432.

(97) Holmes, W. F.; Soprano, D. R.; Soprano, K. J. Comparison of the mechanism of induction of apoptosis in ovarian carcinoma cells by the conformationally restricted synthetic retinoids CD437 and 4-HPR. *J. Cell Biochem.* **2003**, *89*, 262−278.

(98) Holmes, W. F.; Soprano, D. R.; Soprano, K. J. Elucidation of molecular events mediating induction of apoptosis by synthetic retinoids using a CD437-resistant ovarian carcinoma cell line. *J. Biol. Chem.* **2002**, *277*, 45408−45419.

(99) Hsu, J. Y.; Pfahl, M. ET-1 expression and growth inhibition of prostate cancer cells: A retinoid target with novel specificity. *Cancer Res.* **1998**, *58*, 4817−4822.

(100) Liang, J. Y.; Fontana, J. A.; Rao, J. N.; Ordonez, J. V.; Dawson, M. I.; Shroot, B.; Wilber, J. F.; Feng, P. Synthetic retinoid CD437 induces S-phase arrest and apoptosis in human prostate cancer cells LNCaP and PC-3. *Prostate* **1999**, *38*, 228−236.

(101) Lu, X. P.; Fanjul, A.; Picard, N.; Shroot, B.; Pfahl, M. A selective retinoid with high activity against an androgen-resistant prostate cancer cell type. *Int. J. Cancer* **1999**, *80*, 272−278.

(102) Ponzanelli, I.; Gianni, M.; Giavazzi, R.; Garofalo, A.; Nicoletti, I.; Reichert, U.; Erba, E.; Rambaldi, A.; Terao, M.; Garattini, E. Isolation and characterization of an acute promyelocytic leukemia cell line selectively resistant to the novel antileukemic and apoptogenic retinoid 6-[3-adamantyl-4-hydroxyphenyl]-2-naphthalenecarboxylic acid. *Blood* **2000**, *95*, 2672−2682.

(103) Lovat, P. E.; Ranalli, M.; Bernassola, F.; Tilby, M.; Malcolm, A. J.; Pearson, A. D.; Piacentini, M.; Melino, G.; Redfern, C. P. Synergistic induction of apoptosis of neuroblastoma by fenretinide or CD437 in combination with chemotherapeutic drugs. *Int. J. Cancer* **2000**, *88*, 977−985.

(104) Lovat, P. E.; Ranalli, M.; Bernassola, F.; Tilby, M.; Malcolm, A. J.; Pearson, A. D.; Piacentini, M.; Melino, G.; Redfern, C. P. Distinct properties of fenretinide and CD437 lead to synergistic responses with chemotherapeutic reagents. *Med. Pediatr. Oncol.* **2000**, *35*, 663−668.

(105) Costantini, P.; Jacotot, E.; Decaudin, D.; Kroemer, G. Mitochondrion as a novel target of anticancer chemotherapy. *J. Natl. Cancer Inst.* **2000**, *92*, 1042−1053.

(106) Marchetti, P.; Mortier, L.; Beauvillain, V.; Formstecher, P. Are mitochondria targets of anticancer drugs responsible for apoptosis? *Ann. Biol. Clin. (Paris)* **2002**, *60*, 391−403.

(107) Buehler, C. A.; Harris, J. O.; Shacklett, C.; Block, B. P. The action of formaldehyde on *m*-hydroxybenzoic acid. II. *J. Am. Chem. Soc.* **1946**, *68*, 574−577.

(108) Kelly, K. G.; Ellenbogen, L. Histidine decarboxylase inhibiting 4-bromo-3-hydroxy-hippuric acid. Ger. Patent 2,062,611, 1971.

(109) Barrow, J. C.; Nantermet, P. G.; Selnick, H. G.; Glass, K. L.; Rittle, K. E.; Gilbert, K. F.; Steele, T. G.; Homnick, C. F.; Freidinger, R. M.; Ransom, R. W.; Kling, P.; Reiss, D.; Broten, T. P.; Schorn, T. W.; Chang, R. S.; O'Malley, S. S.; Olah, T. V.; Ellis, J. D.; Barrish, A.; Kassahun, K.; Leppert, P.; Nagarathnam, D.; Forray, C. In vitro and in vivo evaluation of dihydropyrimidinone C-5 amides as potent and selective α_{1A} receptor antagonists for the treatment of benign prostatic hyperplasia. *J. Med. Chem.* **2000**, *43*, 2703−2718.

(110) Case, D. A.; Pearlman, D. A.; Caldwell, J. W.; Cheatham, T. E., III.; Ross, W. S.; Simmerling, C. L.; Darden, T. A.; Merz, K. M.; Stanton, R. V.; Cheng, A. L.; Vicent, J. J.; Crowley, M.; Tsui, V.; Radmer, R. J.; Duan, Y.; Pitera, J.; Massova, I.; Seibel, G. L.; Singh, U. C.; Weiner, P. K.; Kollman, P. A. *AMBER6*. University of California, San Francisco, 1999.

(111) Ciccotti, G.; Ryckaert, J. P. Molecular dynamics simulation of rigid molecules. *Comput. Phys. Rep.* **1986**, *3*, 345.

(112) Goodsell, D. S.; Morris, G. M.; Olson, A. J. Automated docking of flexible ligands: Applications of AutoDock. *J. Mol. Recognit.* **1996**, *9*, 1−5.

(113) Morris, G. M.; Goodsell, D. S.; Halliday, R. S.; Huey, R.; Hart, W. E.; Belew, R. K.; Olson, A. J. Automated docking using a Lamarckian genetic algorithm and an empirical binding free energy function. *J. Comput. Chem.* **1998**, *19*, 1639−1662.

(114) Cornell, W. D.; Cieplak, P.; Bayly, C. I.; Gould, I. R.; Merz, K. M., Jr.; Ferguson, D. M.; Spellmeyer, D. C.; Fox, T.; Caldwell, J. W.; Kollman, P. A. A second generation force field for the simulation of proteins, nucleic acids, and organic molecules. *J. Am. Chem. Soc.* **1995**, *117*, 5179−5197.

(115) Bayly, C. I.; Cieplak, P.; Cornell, W. D.; Kollman, P. A. A well-behaved electrostatic potential based method using charge restraints for deriving atomic charges: The RESP model. *J. Phys. Chem.* **1993**, *97*, 10269−10280.

(116) Charpentier, B.; Bernardon, J. M.; Eustache, J.; Millois, C.; Martin, B.; Michel, S.; Shroot, B. Synthesis, structure-affinity relationships, and biological activities of ligands binding to retinoic acid receptor subtypes. *J. Med. Chem.* **1995**, *38*, 4993−5006.

(117) Sakashita, A.; Kizaki, M.; Pakkala, S.; Schiller, G.; Tsuruoka, N.; Tomosaki, R.; Cameron, J. F.; Dawson, M. I.; Koeffler, H. P. 9-*cis*-retinoic acid: Effects on normal and leukemic hematopoiesis in vitro. *Blood* **1993**, *81*, 1009−1016.

(118) Zhang, X.-K.; Hoffmann, B.; Tran, P. B.; Graupner, G.; Pfahl, M. Retinoid X receptor is an auxiliary protein for thyroid hormone and retinoic acid receptors. *Nature* **1992**, *355*, 441−446.

(119) Wu, Q.; Dawson, M. I.; Zheng, Y.; Hobbs, P. D.; Agadir, A.; Jong, L.; Li, Y.; Liu, R.; Lin, B.; Zhang, X.-K. Inhibition of *trans*-retinoic acid-resistant human breast cancer cell growth by retinoid X receptor-selective retinoids. *Mol. Cell. Biol.* **1997**, *17*, 6598−6608.

JM030524K